VOYAGER

DESIGN STUDIES

Volume Four: Orbiter-Bus Design
Part One

VOYAGER DESIGN STUDIES ·

Volume IV: Orbiter - Bus Design

Part I

Avco RAD-TR-63-34

15 October 1963

FOREWORD

The Voyager Design Study final report is divided into six volumes, for convenience in handling. A brief description of the contents of each volume is listed below.

Volume I -- Summary

A completely self-contained synopsis of the entire study.

Volume II -- Scientific Mission Analysis

Mission analysis, evolution of the Voyager program, and science payload.

Volume III -- Systems Analysis

Mission and system tradeoff studies; trajectory analysis; orbit and landing site selection; reliability; sterilization

Volume IV -- Orbiter-Bus System Design

Engineering and design details of the orbiter-bus

Volume V -- Lander System Design

Engineering and design details of the lander.

Volume VI -- Development Plan

Proposed development plan, schedules, costs, problem areas.

TABLE OF CONTENTS

TABLE OF CONTENTS (Cont'd)

TABLE OF CONTENTS (Concl'd)

LIST OF TABLES

LIST OF FIGURES

LIST OF FIGURES (Cont'd)

LIST OF FIGURES (Cont'd)

LIST OF FIGURES (Cont'd)

LIST OF FIGURES (Concl'd)

ACKNOWLEDGMENTS

SUMMARY

This report presents the results of a 6-month conceptual design study conducted by Avco Research and Advanced Development Division for the National Aeronautics and Space Administration. The objectives of the study were the synthesis of a conceptual design of an unmanned spacecraft to perform scientific orbiter-lander missions to Mars and Venus during planetary opportunities from 1969 to 1975, and the formulation of a plan delineating the development program leading to first launch during the Mars 1969 opportunity.

The basic approach makes use of a 6000- to 7000-pound orbiter-lander; tradeoff studies were conducted to determine the payload and mission capabilities with smaller and larger spacecraft. The orbiter-lander was selected as yielding the maximum in scientific value short of manned exploration. The lander separates from the orbiter-bus and descends to the planet surface by parachute, where it makes atmospheric and surface measurements and conducts a variety of scientific experiments. The information obtained is relayed to Earth via the orbiter-bus which meanwhile is placed in a planetocentric orbit. The orbiter-bus collects scientific data in transit and maps the planet while in orbit. The lifetime of both orbiter-bus and lander is 6 months for the Mars missions. For Venus, the orbiter life is also 6 months, but the lander life is only 10 to 20 hours because of the hostile environment. A small capsule was designed for Venus, in addition to the lander, to conduct atmospheric measurements after entering from orbit; the capsule does not survive landing. Landers and capsules would be sterilized to avoid contamination of the planets, but the orbiter-bus would be placed on a trajectory which would ensure that it would remain above the sensible atmosphere for at least 50 years; thus, no sterilization would be required. The development plan shows that to obtain the scientific value desired, two spacecraft should be scheduled for each launch opportunity and hardware development should begin in 1964 to meet the 1969 launch date for Mars.

1. DESIGN STUDY

1.1 Mission Goals

The orbiter-bus has been designed to achieve two primary mission goals: (1) to gather scientific data about the surface and atmospheric characteristics of Mars and Venus while in a bound orbit about these planets; and (2) to serve as a bus to guide the lander to the neighborhood of the plenet and then as a stable platform from which to release the lander towards the planet. The secondary mission goal of the orbiter-bus is to perform scientific measurements in the interplanetary environment. A detailed discussion of the type of scientific data to be collected and the lander orientation accuracy requirements are presented in volumes II, Scientific Mission Analysis, and III, Systems Analysis.

1.2 Design Goals

The orbiter-bus design has been channeled so that the reference configuration (the Mars orbiter-bus) can, with small modification, accommodate the following: (1) missions to Venus, for which the total radiation energy flux is considerably greater due to both the closer proximity to the Sun and higher albedo of this planet, and to satisfy significantly different look-angle requirements than for a Mars mission; (2) to satisfy the varying look-angle requirements for four launch opportunities towards Mars and four launch opportunities towards Venus; (3) alterations in scientific instruments for two planets, and although not considered for this conceptual study, changes in scientific instruments from launch opportunity to launch opportunity: (4) to serve as both an orbiter and a bus allowing maximum utilization of systems so that a proven vehicle can be used over a broader spectrum of space missions; (5) two landers so that a greater probability of achievement of lander mission goals can be anticipated. In 1971, when the transfer trajectory energy requirements and planetary approach energy are at their minimum for Mars, sufficient weight will be available to launch two landers and inject a vehicle into orbit about Mars. Also, by 1975 the scientific measurement goals of the orbiter could be expected to be satisfied and it would no longer be necessary to include an orbiter. In this case, the orbiter-bus would serve only as a bus for the two landers.

1.3 Design Constraints

Achievement of the mission goals and design goals are limited by the multiple constraints placed on design. The constraints include allowable orbiter-bus weight, allowable shroud envelope, booster launch environment, DSIF performance, and the requirements of maintaining the planets in a sterile condition relative to Earth contaminents.

The allowable orbiter-bus weight is dependent upon the results of a tradeoff which considers: (1) the weight that the booster can place on an interplanetary trajectory; (2) the propulsion requirements for interplanetary trajectory corrections and for orbital injection; and (3) the weight allocated to the lander.

The shroud envelope sets the characteristic dimension of the spacecraft. Orbiter-bus utilization of this envelope must be satisfied in conjunction with the requirements to mate the spacecraft to the booster transition section, and attachment of the lander, which must be located so that it can be released from the orbiter-bus. The large dimension (approximately 20 feet) of the transition section of the S-VI stage permitted the use of fixed or nondeployable solar cell panels with the attendant benefit of a structure which is removed from the central structural elements of the spacecraft so that it can serve as an external mount for the gimballed, high-gain Earth antennas, and gimballed, planetary scientific instrumentation package.

The static and dynamic loads experienced during launch determine the structure that the spacecraft must have so that the large systems, that is, the lander the propulsion system, and solar panels will be supported. The launch loads and the subsequent stress levels also influence the design and/or selection of components.

DSIF performance effects the design of the orbiter-bus in two ways; guidance and communications. The tracking accuracies of the DSIF prescribe the precision to which the trajectory can be determined. With this information the magnitude and direction of midcourse and terminal velocity corrections can be established. It has been found that to achieve the required orbital injection accuracies and lander impact accuracies, an on-board guidance system is required to improve DSIF tracking capability near the target planet. The second influence of the DSIF is its performance as the ground communications link to receive data transmitted from the orbiter-bus. The DSIF also provides for ground control of the orbiter-bus through an on-board omni-antenna system in the event of failure of the stabilization and control system to maintain the proper orientation.

Finally, the requirements of sterilization have been approached from the viewpoint of using the guidance system to bias the trajectory so that the probability of not contaminating the planets is satisfied. The other course of action

that could have been selected would have been to sterilize the orbiter-bus according to the procedures that have been established for the lander and discussed in volume III, Systems Analysis. It was felt that the attendant problems of development of components to withstand heat sterilization and the expense of sterile assembly should be avoided if the trajectory bias necessary, based on the anticipated performance of guidance systems, would not restrict the mission goals. This work is also reported upon in volume III, Systems Analysis. It appears a guidance bias to satisfy sterilization requirements is a practical approach. This guidance restriction is reflected in selection of a 1,700-km periapsis, which incorporates 200-km, 3-σ guidance accuracy. Some of the system calculations presented are based on 1500 km, the lower allowable limit of the periapsis.

1.4 Orbiter-Bus Design Configuration

The reference design - the Mars orbiter-bus with a single lander - and modification to a Venus orbiter-bus are shown in figures 1 and 2. From these figures it should be noted that:

1. The lander is located on top of the orbiter-bus so that the design will accommodate two landers. It is not possible to mount two landers (of larger dimension than the present 7-foot diameter) on the bottom due to interference with the shroud envelope.

2. The lander is located opposite the solar cells so as to allow for a more uniform temperature distribution and to facilitate the use of a passive thermal-control system. The only energy source for the temperature control of the orbiter-bus is the sun, whereas the energy source for the lander could be the energy dissipated from the radioisotope thermoelectric generator plus solar energy. If the lander were on the same side as the solar cells, then the lander would have both an internal energy source and an external energy source, and so complicate the thermal control of the orbiter-bus.

3. A common structural junction of orbiter-bus, lander, and spacecraft adapter is employed so that the lander loads do not pass through the orbiter-bus. This design feature, plus mounting the lander on the top with respect to the launch loads so that the orbiter-bus will experience tension loads during launch, allows for a minimum-weight structural design of the orbiter-bus. This weight saving in the orbiter-bus structure is magnified by the saving in propulsion for orbital injection.

4. Solar panels are rigid, which removes the requirement of deployment of solar cell panels, serves as a mounting structure for the scientific gimbal and communication antennas, and allows full 360-degree choice of clock-angle location to satisfy the varying look-angle requirements.
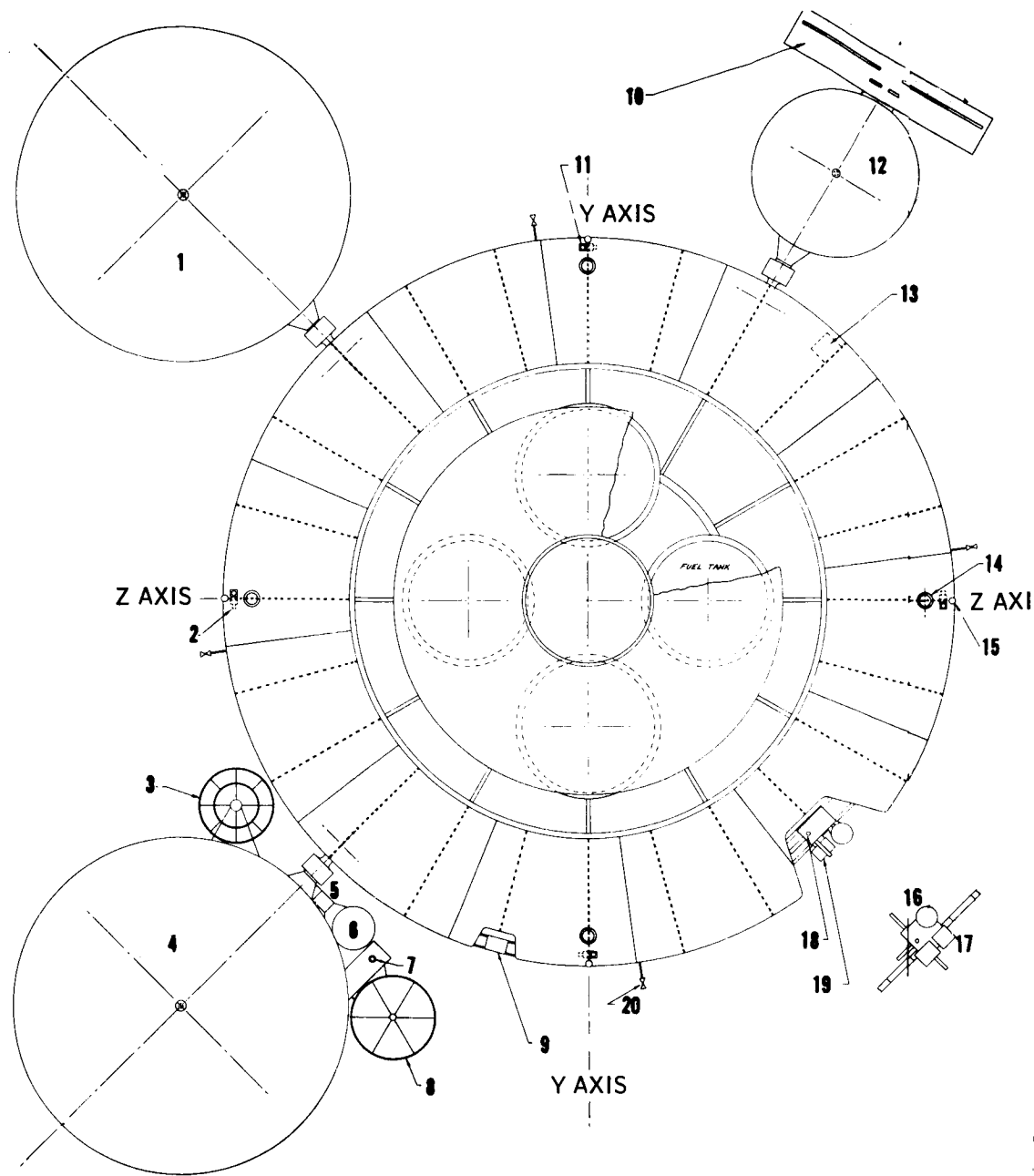
1. 8' DIA. ANTENNA DEPLOYED
2. ATTITUDE CONTROL JETS
3. RELAY ANTENNA
4. 8' DIA. ANTENNA MICROWAVE MAPPING
5. IRRADIOMETER
6. IRSPECTROMETER
7. ANTENNA - LANDER COMMAND
8. 2' DIA. ANTENNA RADIOMETRIC MAPPING
9. MAGNETOMETER

10. BI-STATIC RADAR DI-POL
11. ATTITUDE CONTROL JET
12. 4' DIA. ANTENNA DEPLO
13. AUXILIARY STAR TRACKI
14. VERNIER ROCKETS 4 EQI
15. ACQUISITION SUN SENSC
16. ION CHAMBER
17. COSMIC DUST DETECTOF
18. MICROMETEROID DETEC

63-8966

Figure 2 VEN

30

21 7 22 23

78°

31

25

30

32

X AXIS

SECTION C-C

26

27

4

5

40

39

28 29

33 A

34

38

37

36

35

A

54

55

56

VIEW A-A

— = 10 INCHES
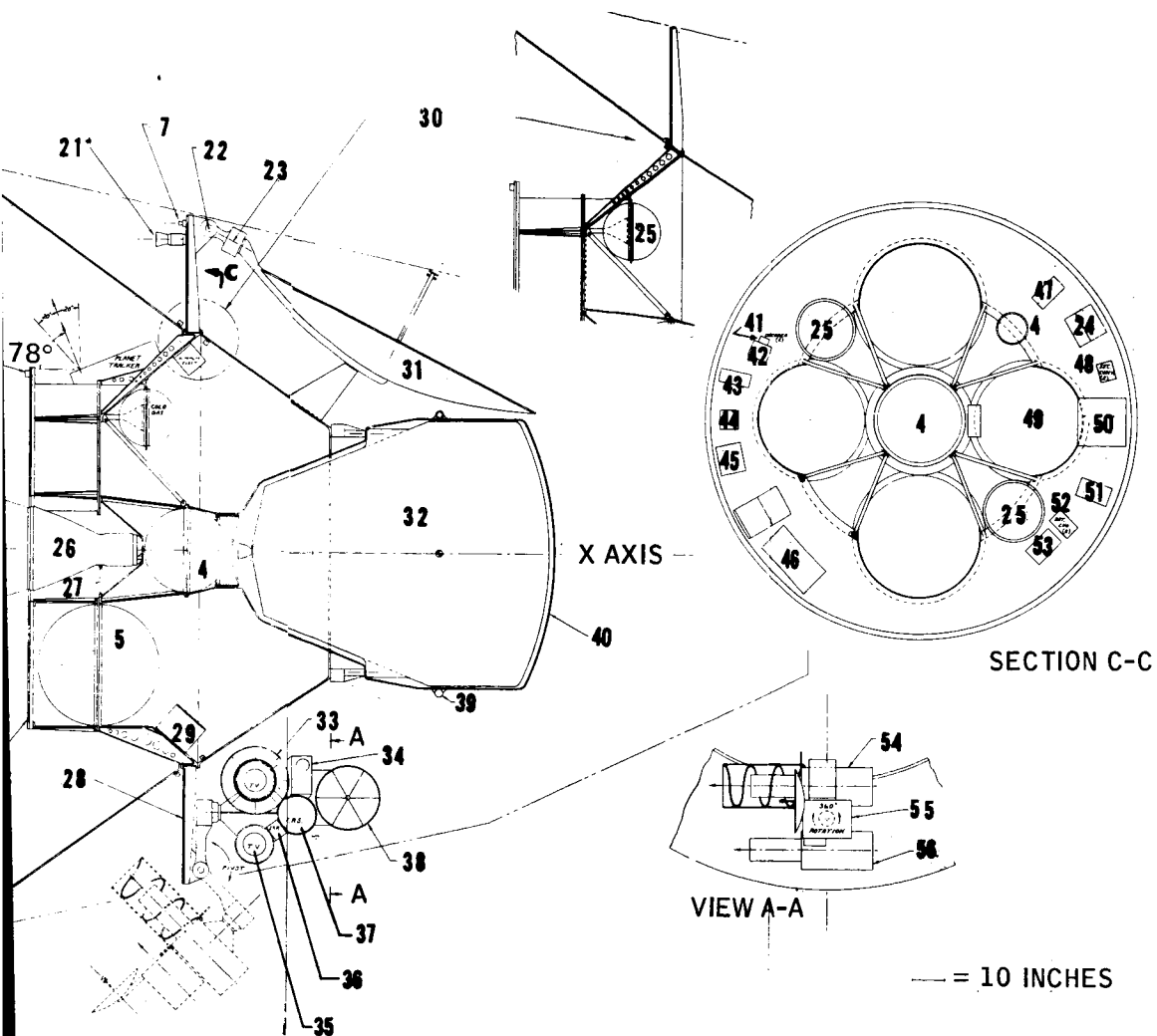
T DETECTOR
E SUN SENSOR
CKETS

XIS
ELECT.

T ENGINE

ARRAY DISCS
TOTAL APPROX.
RDER
DESIGN
OWED

NNA
ZON SENSOR

ER
ETER

38. ANTENNA – LANDER COMMAND
    AND ALTIMETER
39. SPIN ROCKETS
40. STERILIZATION SHIELD
41. DECODER (2)
42. VHF RECEIVER (2)
43. TRANSPONDER (2)
44. VHF TRANSMITTER (2)
45. MULTIPLEX CONTROL (2)
46. DIGITAL COMPUTER
47. PRIM. CONV. (2)
48. SEC. CONV. (2)
49. INERTIAL SENSORS
50. MAPPING RECORDER (2)
51. S-BAND TRANSMITTER (2)
52. BAT. CHG. (2)
53. BATTERY 5 X 6 X 10
54. HIGH RESOLUTION TV
55. I. R. SPECTROMETER
56. LOW RESOLUTION TV

IGN--MARS ORBITER-BUS

Y AXIS

240
DIA

Y AXIS

Z AXIS

Z AXIS   X AXIS

Ċ OF CANOPUS SENSOR

90°

Y AXIS
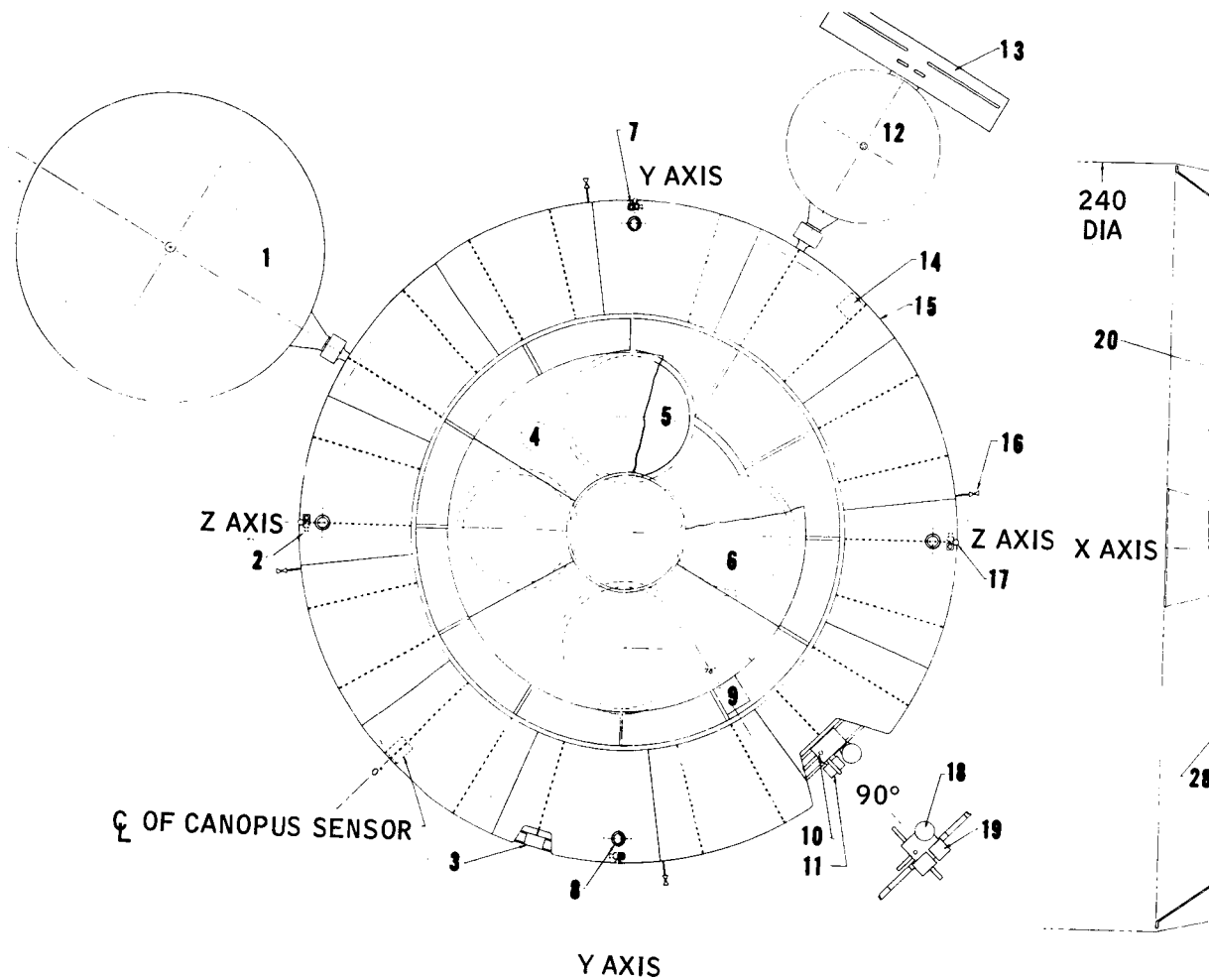
1. 8' DIA. ANTENNA DEPLOYED
2. 4 ATTITUDE CONTROL JETS
3. MAGNETOMETER
4. PRESSURANT TANK
5. OXIDIZER TANK
6. FUEL TANK
7. ATTITUDE CONTROL JETS
8. VERNIER ROCKETS 4 EQUALLY SPACED
9. PLANET TRACKER
10. MICROMETEROID DETECTOR
11. PARTICLE FLUX DETECTOR
12. 4' DIA. ANTENNA DEPLOYED
13. BI-STATIC RADAR DI-POLE
14. AUXILIARY STAR TRACKER
15. O.D. OF SOLAR CELL DISC
16. OMNI-DIRECTIONAL COMMAND ANTENNA
    4 EQUALLY SPACED
17. ACQUISITION SUN SENSOR
    4 EQUALLY SPACED
18. ION CHAMBER

19. COSMIC DUS
20. LIMIT CYCLI
21. VERNIER RO
22. PIVOT AXIS
23. ROTATION A
24. AUTOPILOT
25. COLD GAS
26. MAIN ROCKE
27. 4 STRUTS
28. SOLAR CELL
    200 SQ. FT.
29. RELAY RECO
30. ALTERNATE
31. ANTENNA ST
32. LANDER
33. RELAY ANTE
34. PLANET HOR
35. TV
36. IRRADIOMETI
37. IRSPECTROM

Figure 1 REFERENCE DES

240
DIA

14

25

21

X AXIS

22   **23**   **24**   X AXIS

26

21

27

$\longmapsto$ = 10 INCHES

LE
S
YED
ER
UALLY SPACED
R 4 EQUALLY SPACED

R

TOR

US ORBITER-BUS

1.5 Characteristics of Orbiter-Bus Systems

A summary of the characteristics and performance of the orbiter-bus systems for the Mars and Venus designs are presented in table 1.

1.6 Orbiter-Bus Weight Table

A summary (table 2) of the weight breakdowns of both the Mars and Venus orbiter-bus follows:

1.7 Introductory Remarks

The sections that follow describe in detail the systems which, under the design constraints, will satisfy the mission goals and the design goals. The reference systems are presented and/or other systems that were discarded or that could be considered if their continued development bears out the anticipated performance claims.

Section 2, Scientific Payload, section 3, Communications, section 4, Power Supply, can be considered a description of the payload of the orbiter-bus. The object of the orbiter-bus in the narrower sense is to carry scientific instruments to the planets and to perform measurements. In the larger sense, the objectives are to return to Earth information about the planets.

Section 5, Guidance, describes the techniques for directing the orbiter-bus along its interplanetary trajectory and guiding the orbiter-bus into a bound orbit about Mars and Venus. Stabilization and Control, section 6, describes the system that will establish the spacecraft orientation and maintain the vehicle's orientation to satisfy the communications, propulsion, power supply, and scientific payload systems. Section 7, Propulsion System, presents the method of obtaining velocity increments to alter the trajectory and satisfy the guidance systems and also the velocity decrement to inject the orbiter-bus into a bound orbit. The preceding sections, plus section 8, Materials, section 9, Thermal Control, and section 10, Structure, are integrated into a vehicle design in section 11, Design. In the design section are described the evolution of the configuration and also the modifications that are necessary for the reference design (the single-lander Mars orbiter-bus) to achieve the many design goals.

TABLE 1

CHARACTERISTICS AND PERFORMANCE OF ORBITER-BUS SYSTEM

System	Mars Orbiter-Bus	Venus Orbiter-Bus
Scientific Instruments	Particle flux detector, ion chamber, cosmis dust detector, micrometeoroid detector, bi-static, radar, magnetometer, infrared radiometer, infrared spectrometer.	
	Optical mapping; two sets of optics, 85-inch and 33-inch focal length. Resolution: 250 meters continuous mapping and 40 meters discrete pictures.	X-band, 8-foot parabolic antenna, range resolution-150 meters, surface resolution - 1,500 meters. X-band radiometer, 8-foot parabolic antenna; K_u-band radiometer, 2-foot parabolic antenna; extended microwave spectrometer.
Communication	In transit, 35-w, S-band, 4-foot parabolic antenna; in orbit, 120-w, S-band, 8-foot parabolic antenna; VHF command receiver, helix antenna; S-band command receiver, omniantenna	Same except for 70-w transmitter in orbit system.
Power Supply	Solar cells, 182 square feet effective area; nickel cadmium batteries.	Solar cells, 68 square feet effective area; nickel cadmium batteries.
Guidance	DSIF plus optical-inertial using accelerometers, planet tracker, horizon scanner, computer.	
Stabilization and Control	Sun-Canopus reference, nitrogen cold gas, limit cycle ± 0.1 degrees, using Sun sensor, star tracker, and gas bearing gyros.	

TABLE 1 (Concl'd)

System	Mars Orbiter-Bus	Venus Orbiter-Bus
Propulsion	Hyperbolic propellant: mixed oxides of nitrogen-oxidizer and mixture of monomethyhydrazene plus hydrazene-fuel; 327 Isp; helium pressurant expulsion; 2,500 to 1,500-pound main thrust chamber; four 60 to 36-pound thrust chambers for vector control.	
Thermal Control	Passive system	
Structure	Aluminum monocoque	

TABLE 2

MARS-VENUS WEIGHT BREAKDOWN

	Mars Orbiter-Bus	Venus Orbiter-Bus
Scientific Payload		
Particle flux detector	2.5 pounds	2.5 pounds
Ion chamber	1.3	1.3
Cosmic dust detector	2.5	2.5
Micrometeoroid detector	8.0	8.0
Bi-static radar	8.0	8.0
Magnetometer	5.0	5.0
Infrared radiometer	3.0	3.0
Infrared spectrometer	29.0	29.0
Extended microwave spectrometer	--	35.0
Microwave radiometer	--	24.0
Radar electronics	--	32.0
X-band radar and radiometric mapping antenna K_u-band radiometric Mapping antenna	--	30.0
Optical mapping	76.0	--
Total	135.3 pounds	180.3 pounds
Communications		
Multiplexing and encoding	76 pounds	54 pounds
Transmission and reception	133	127
Antennas	54	51
Cabling and plumbing	20	20
Total	283 pounds	252 pounds
Power Supply		
Solar panel	243 pounds	81 pounds
Batteries	176	88
Power conditioning	42	25
Total	461 pounds	194 pounds

TABLE 2 (Concl'd)

	Mars Orbiter-Bus	Venus Orbiter-Bus
Guidance		
Auxiliary star tracker	9 pounds	9 pounds
Planet tracker	35	35
Planet horizon scanner	12	12
Accelerometer and electronics	6	6
Digital computer, Input/output and power supply	49	49
Total	111 pounds	111 pounds
Stabilization and Control		
Sensors	9 pounds	9 pounds
Electronics	13	13
Reaction system*	53	53
Total	75 pounds	75 pounds
Propulsion		
Burnout weight**	460 pounds	460 pounds
Structures*	324 pounds	324 pounds
Grand Total	1,849 pounds	1,596 pounds

* The cold-gas requirement for Venus will in general be lower than for Mars because of the shorter flight times.

** Tankage can contain up to 3,400 pounds of propellant.

*** The structural weight is increased by 50 percent to allow for fittings, bracketry, and so forth.

2. SCIENTIFIC PAYLOAD

2.1 Interplanetary Measurements

The Mars and Venus orbiter-bus has been designed to incorporate scientific instruments that would allow for the measurements of phenomena in interplanetary space. The objectives of these measurements are to obtain fundamental scientific data, and also to monitor the external influences acting on the spacecraft so that its performance can be evaluated. The instruments to accomplish these goals are representative of the minimum measurements that would be required. These include:

Instrument *	Weight (pounds)
Particle flux detector	2.5
Ion chamber	1.3
Cosmic dust detector	2.5
Micrometeoroid detector	8.0
Bistatic radar	8.0
Magnetometer	5.0

from *the prescribed list of instruments furnished by NASA.

The particle flux detector and ion chamber will monitor the high-energy particles in interplanetary space. Both the cosmic dust and micrometeoroid detectors will measure the distribution of particles in space. The bistatic radar experiment is designed to measure the electron density in interplanetary space by the technique of measuring the attenuation of an electromagnetic signal sent from Earth. Investigation of interplanetary magnetic fields will be performed by the magnetometer.

2.2 Planetary Measurements

Scientific instruments that are used in planetary orbit that are common to both the Mars and Venus orbiter-bus include some of the same instruments used during the interplanetary transit; these are the micrometeoroid detector, magnetometer, and bistatic radar, which in this application is used to measure the attenuation characteristics of the planetary atmosphere. An infrared radiometer (3 pounds) will be used to map the surface of Mars and map the clouds of Venus. The infrared spectrometer (29 pounds) will be used to determine the

constituents in the atmospheres of Mars and Venus.

The optical mapping system (76 pounds) will be used exclusively for the Mars orbiter-bus; the microwave mapping, active radar mapping, and an extended microwave spectrometer will be used exclusively for the Venus orbiter-bus. The Venus mapping system weighs 86 pounds. of which 24 pounds is the microwave radiometer, 32 pounds is the radar electronics, and 30 pounds is the antenna system. Both of these systems dominate the design and selection of the data-handling, communications, and power-supply subsystems, and will be expanded upon in the following sections. All of the scientific instruments for planetary measurements except the radar electronics, mapping antennas, and optical mapping system have been drawn from the prescribed list of instruments furnished by NASA.

2. 3 Mass Orbiter Optical Mapping System

1. <u>Technical approach.</u>

   a. <u>General system considerations.</u>

   1) <u>Orbit selection.</u> During the system-analysis phase of the study, considerable attention was paid to the task of orbit selection. The weight penalties associated with achieving near circular orbits made it desirable to select a quite eccentric orbit for the mapping task. Originally, it was decided to map only in the region near periapsis and consequently demands were placed on the orbit geometry. This problem is discussed in some detail in the system analysis volume. In essence, there exists an adverse interaction between the length of time in sun light and the orbit inclination. It is extremely desirable to obtain a near polar orbit to maximize the probability of mapping at all planet latitudes. Orbit precession for near 90 degrees inclination is very rapid making the time that periapsis is in a sunlit region quite small. Rather than accept an orbit, the inclination of which precluded the possibility of polar mapping, it was decided to design a mapping system with reasonable capability at all altitudes. The orbit selected for mapping system synthesis has an inclination of 90 degrees, a periapsis of 1500 km, and apoapsis of 10,000 km.

   2) <u>Limitations of orbital mapping.</u> "Mapping" is a very broad term, with many meanings, from the crudest charting by dimensional vectors to sophisticated projections with contour lines fully descriptive of variations in height or depth. The considerable altitudes of our orbit, the power limitations upon communications, and the absence of any ground control from the planet itself, combine to limit us to the production of what is called an uncontrolled mosaic. Because of the considerable altitudes, vertical sighting yields substantially true planimetric projection.

An optical system can form a plane image, on board the orbiter, of any portion of the planet surface toward which it is directed. It can be made to bring to a common focus all the luminous radiations, visible and invisible, which leave the planet and are not absorbed, or otherwise modified, by the planet's atmosphere, or such atmospheric effects as clouds, dusts, and particles. But a plane image on board the orbiter is in itself useful to us only as a potential source of information upon which we may hope to draw. The image, as far as it goes, represents a sort of perfection. But we cannot by any means whatever preserve for our use on Earth the full content of the optical observation. If it were possible to make photographic records and recover them, we could do very well; and the limitations on data gathering imposed, for example, by the size of the silver grains, or the imperfect panchromatism of the emulsion, or the differential wavelength absorption by the gelatine, would be easy to put up with. If we could process photographs on board and transmit their content by the highly developed techniques of facsimile communication, we could do very well with the results, especially if the scale of our photographs were large. But considerations of weight and power exclude any such approach, and we are forced to limit the size of our optical image to little more than a square inch and to dissect it, for transmission, into a very limited number of rather coarse elementary units about any one of which we can say no more than that it is on the whole most fairly represented by some one of a limited number of grays.

2) <u>Selected mode of operation</u>. Ability to record views of the planet from any point in the orbit has been considered a basic requirement, and it is considered desirable for eventual compilation to make all views cover the same field area, with constant resolution and as nearly as possible uniform quality. Since the altitude varies from 1500 km to 10,000 km, the most convenient way to maintain an equal field of view with a constant raster would be to have an optical system of continuously variable focal length covering a range from minimum to maximum in the ratio of 1500/10,000 = 3/20, and maintaining the size of the image of a constant area unchanged with changing altitude. This could be achieved with a "Zoom" lens system; but the necessary mechanical motions would be troublesome to maintain reliably in space, and the problem of achromatization over the whole wavelength range of the S-20 photocathode is so severe that Avco RAD considers it unwise to use any refractive system. The degree of "Zoom" required is too great to be achieved electronically by operations upon the electron-optics of any standard image tube.

Therefore, instead of a single camera system with continuous variation of focal length and a constant-raster, Avco RAD proposes to provide two complete camera systems, with two different fixed focal lengths: one to be used for mapping at the lower altitudes and the other for mapping at the higher altitudes. Each system is to have a raster which is variable with altitude over a range of

$$\sqrt{\frac{10,000}{1,500}} = \sqrt{\frac{20}{3}} = 2.5820;$$ and the focal lengths of the two systems are to differ in this same ratio.

-13-

Between the two points at which the altitude has the value of the geometric mean between periapsis and apoapsis, there are on one side a region of lower altitudes, with a minimum at periapsis and, on the other side, a region of higher altitudes with a maximum at apoapsis. These regions are dealt with, for mapping purposes, by the shorter and longer focus systems respectively. The geometric mean altitude, h_M, is reached a short distance beyond the latus rectum of the orbital ellipse, in the direction of the apoapsis.

The use of two independent cameras has the advantage that if for any reason one of them should fail, the other can at once take over and operate throughout the orbit, instead of only through its normal part. This is a useful measure of insurance.

4) <u>System weights.</u> The weights of the two camera systems will be, as now envisaged, substantially equal. The quartz elements for each will weigh about 12. 3 pounds. The image orthicon, deflection, focus, and alignment coils will weigh about 10. 5 pounds (with aluminum-wound focus coil): and the electronics are estimated at 15 pounds per camera. The two systems together will weigh 2 (12. 3 + 10. 5 + 15) = 75. 6 pounds.

b. <u>Resolution and determination of focal length.</u>

1) <u>Strip mapping.</u> The degree of resolution which can be achieved is by no means an independent variable. Compilation or bridging of the final mosaic is strongly dependent from the swath width. The problem is not primarily optical. The basic limitation is the image tube. A picture of good quality can be made up of 233 x 233 elements regardless of the size of the planet area to which each element corresponds. If this unit area is 37. 5 meters on each side, the view will cover a field 8. 74 km , or 5.4 miles square. This would warrant mapping at a scale of 1/750, 000, which is quite good; but at that scale, one such view would occupy only 0. 21 inch^2. With minimum side lap, at least 3600 passes (perfectly arranged) would be needed to fill in an equatorial zone, and they would take over 42 months of orbiting, at the lowest estimate. In the absence of any ground control, very serious difficulty would be expected in matching up such small areas into a mosaic except when well-marked features are present.

It is clear that resolution for mapping purposes cannot be pushed too far. A reasonably large area must be covered by each view, and the resolution is then fixed by the properties of the image tube. In six months of orbiting, we expect to make about 520 passes. If we take 21, 000 km as the circumference of Mars, add one-third for side lap, and divide by 520, we get 53 km as a width of swath which would be appropriate. If we consider 233 lines (at any line density) as the limit of image-tube performance, we arrive at a resolution unit of about 53/233 or 0. 23 km. For safety and convenience, we fix on 0. 25 km as a good working value for our resolution.

The reason for choosing 233 lines to make up the image is perhaps not immediately clear, since 233 lines per target inch is by no means the limit of the usefulness of a good image orthicon. As will be made plain below, we have to increase the number of lines per target inch, the line density, over a range of 2.582 to 1. If our lowest line density is 233, the one-inch square target image will be 233 lines high. If our highest line density is 2.582 x 233 ≈ 600

lines per target inch our image is only $\frac{233}{600}$ = 0.388 inch high and we are, in

fact, nearing the limit of what can be asked of an image orthicon operating under automatic controls.

It remains to determine what the focal lengths shall be. The constant field

of view is to be 233 by 0.25 km square. At $h_M = 1500 \times \sqrt{\frac{20}{3}}$ km = 3873 km,

the image at the photocathode should be $\frac{9}{7} \times 233 \times \frac{1}{600}$ inches square. (The

image at the photocathode of an image orthicon is $\frac{9}{7}$ larger each way than the

target image.)

$$F_1 = 1500 \sqrt{\frac{20}{3}} \times \frac{9}{7} \times \frac{233}{600} \times \frac{1}{233 \times 0.25} = 33.20$$

$$F_2 = F_1 \sqrt{\frac{20}{3}} = 85.71$$

$$\frac{9 \times 233}{7 \times 600}$$

PHOTOCATHODE I

F_I

$1500 \times \sqrt{\frac{20}{3}}$

$$\frac{233}{4}$$
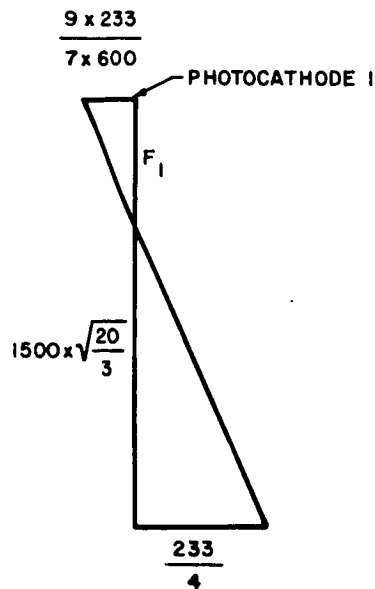
63-9321

Determination of Focal Length

-15-

In general terms, $F_1 = \sqrt{h_A \cdot h_P} \times \dfrac{\text{photocathode dia.}}{\text{target dia.}} \times \dfrac{\text{lines per scan}}{\text{max. line}}$

$$\times \frac{1}{\text{lines per scan} \times \text{width of resolution unit}}$$

$$= \sqrt{h_A \cdot h_P} \times \frac{\text{photocathode dia}}{\text{target dia.}} \times \frac{1}{\substack{\text{max. line density} \\ \text{x width of} \\ \text{resolution unit}}}$$

and $F_2 = h_A \times \dfrac{\text{photocathode dia.}}{\text{target dia.}} \times \dfrac{1}{\substack{\text{max. line density x width of} \\ \text{resolution unit}}}$

2) <u>High-Resolution Operation.</u> The term "edge" is used to identify a change in luminance of one resolution unit relative to the resolution unit last observed. In digitalizing the output from the scanning operation, a 6-bit word is recorded to describe the relative lightness or darkness of each of 233^2 units, and whenever there is a change in the descriptive word, it implies the presence of what is called an "edge." Advantage is taken of these easily counted changes to distinguish scenes with a high expectancy of significance from scenes with a high expectancy of monotony.

Whenever the orbiter is in the region of lower altitudes, and the mapping views are being taken by the shorter-focus camera system, an edge detector counts the number of edges in each frame. Whenever this number exceeds by any considerable amount the normal expectancy, it is to be taken as an indication that the view then in sight contains an amount of detail which may justify making a high-resolution record of it with the longer-focus camera. This operation will normally be limited to moderately low altitudes (never greater than h_M), and will, of course, be predicated on the availability of bits for the extra communication involved, as shown by a continuous calculation. If views with exceptionally high edge counts are not numerous enough to use up all the bits available, in any orbit, for these discrete high-resolution views, shots will be made at random in the neighborhood of the lowest altitude from which an illuminated area on the planet is visible. It is clear that when the planet-surface is visible only from altitude greater than $h_M = 3873$ km, the longer-focus camera will be in use for mapping, and no separate views of higher resolution can be obtained.

The change-over at mean altitude to or from the long-focus system will be so arranged that the shorter-focus system is never used at altitudes higher than h_M. As the altitude increases and passes the value of h_M, the longer-focus system takes over. As the altitude decreases and reaches h_M, the shorter-focus system takes over.

In the event of any malfunction in either system which makes it output unreliable, that system will be completely deactivated and the other system will begin continuous operation.

When the 85.71 inch system is used for single shots, a 600-line raster fills the target and the resolution is $\frac{9}{7}$, the ratio of photocathode diameter to target diameter, times h/F (lines per target height), or $9h/7 \times 85.71 \times 600 = 2.5 \times 10^{-5}$. At h_P this amounts to 37.5 meter resolution over a 22.5 km-square/ and at h_M to 96.8 - meter resolution over a 58 km-square field. These values represent useful additions to the 250-meter resolution, 58 km-square field, which is standard for mapping. The 600-line raster at h_M gives a higher resolution than the 233 line mapping raster but probably somewhat inferior picture quality.

Each discrete view, with 600 x 600 elements, requires about 6.6 times as many bits for transmission as a 233 x 233-element mapping picture. It is expected that 4.5 kilobits per second will be available for 75 percent of each orbiting period, or about 89.1 megabits in all. Mapping pictures are to be taken at approximately $4/5 \times 233 / 1/4 = 46.6$ km intervals, to provide about 20 percent forward lap, so in the 10,500 km half-circumference of Mars we may take as many as 225 mapping pictures. These will require $225 \times 233^2 \times 6 = 73.32$ megabits, leaving a balance of about 15.68 megabits. Since one high-resolution view requires 6×600^2 bits, or 2.16 megabits, there will always be enough bits to transmit at least seven of these discrete views in addition to routine mapping.

The bit balance may be somewhat greater than this. The cameras are continuously exposing and scanning, at fixed time intervals. Views may be read into the tape recorder from an exposure made at the beginning of any of these time intervals. The length of the interval is to be 2.2 seconds, sufficient to make an exposure and then to read out the 233 x 233 = 54,289 picture elements at a rate of 25,000 elements per second.

One discrete, high-resolution picture is valuable, and it may be felt that a series of abutting or overlapping high-resolution pictures from the lowest possible altitude would probably be more valuable still. At 1500 km altitude, the 85.71-inch focal length system covers a field 22.5 km-square. For an abutting field, the travel should be 22.5 km, which, at 2.5 km per second, would take only 9.0 seconds. To clear the target of 600^2 picture elements in 9.0 seconds, we should have to read out at the rate of 40,000 picture elements per second instead of 25,000 as planned. This means an increase from $6 \times 25,000 = 150,000$ bits per second to $6 \times 40,000 = 240,000$ bits per second into the recorder, and to obtain any overlap this increase would have to be greater still. This may prove to be feasible. If provision were made for reading out 50,000 picture elements instead of 25,000, the exposure cycle interval could be reduced from 2.2 to 1.1 seconds, with some advantage in the way of more uniform forward lap.

During the intervals between recorded exposures, the cyclic operation of the cameras allows continuous monitoring of the control voltages and up-dating of exposure-duration. When it is found that the exposure must be so long that that blurring of the image will become serious, the series of exposures will be discontinued until a region of sufficient illumination again comes into view. The criterion for tolerable blurring may be defined as some distance in terms of the resolution unit, (perhaps ten percent) and the maximum permissible exposure duration may be taken as the time during which the system will move through the tolerable distance. This time will, of course, be an elliptic function of the altitude, but may be computed with sufficient exactness on the basis of the data available.

The moment at which an exposure should ideally be recorded is determined as that at which the time integral of the suborbital velocity since the last recorded exposure reaches a preset value corresponding to suborbital travel of 46.6 km. The moment at which the exposure will in fact be recorded is the first beginning of a 2.2-second interval which occurs after the preset value of the integral is reached. This could result in a retardation of any exposure by any amount up to 2.2 seconds. This can never correspond to more than 5.5 km of travel, or to a reduction of forward lap to 10.6 percent, which is tolerable. This reduction in overlap, often repeated, may very well increase appreciably the number of bits available for extra high-resolution views. A running account of the balance between bits used and reserved bits which can be called for will prevent the waste of any potentially useful bits except when the sunlit portion of the planet lies entirely on the apoapsis side of the geometric mean altitudes.

    3)   Performance Characteristics.

        a)   The area on the planet represented by the scanned image from either camera is constant and consists of 233 x 233 resolution units, each 1/4 x 1/4 km. The area per view is therefore 58.25 x 58.25 km-square = 3393 km-square=54,289 x (1/16 km-square).

        b)   The resolution unit of $1/4 \times 1/4 = 1/16$ km^2 is "resolved" in the sense that it corresponds to one of 54,289 areas on the image-tube target the charge upon which is assessed individually during read-out.

        c)   Calculations are based on the assumption of a 1500 x 10,000 km orbit, but can quite readily be scaled to any other.

        d)   Forward lap of one recorded view over the preceding will lie between 20 and 10 percent; i.e., the travel between successive recorded views will be between 46.6 and 52.4 km as measured on the suborbital track.

e) The raster of the shorter-focus camera is to vary from a line density of 233 to one of 600 lines per target inch between $h_p \approx 1504$ and $h_M = 3873$ km, according to $D_1 = 0.155$ (h) (strictly 0.15492 (h)) lines per target inch. After h = 3873 km, the longer-focus camera takes over, and the line density of the shorter-focus system remains at 600 lines per target inch until h begins to decrease.

f) The raster of the longer-focus camera is to vary from a line density of 233 to one of 600 lines per target inch between $h_M \simeq 3883$ and $h_A = 10,000$ km according to $D_2 = 0.060$ (h) lines per target inch. Whenever the shorter-focus camera is in use (i. e., whenever the altitude is less than 3883 km), the line density of the longer-focus camera is to remain constant at 600 lines per target inch in readiness for single, high-resolution exposures.

g) In normal mapping use, the image to be scanned and recorded will always consist of a square 233 lines high. But since the line density varies with altitude the image on the target will vary in height inversely with altitude.

h) The image formed at the target by the shorter-focus (F_1) system at $h_M = 3873$ will be $233/D_1 = 233/3873$ x 1.5492 = 0.3883 inch square. The image formed by the longer-focus (F_2) system at h = 3883 will be $233/D_2 = 233/3883$ x 0.06 = 1.000 inch square.

i) Since these two images represent the same area, d^2, d = 3873 x 0.3883/ F_1 = 3883/F_2. Therefore, F_2/F_1 = 3883/3873 x 0.3883 =

$$2.582 = \frac{h_M}{h_p} = \frac{h_A}{h_M} = \sqrt{\frac{20}{3}} .$$

j) The image at the photocathode, as formed by the optical system, is 9/7 larger (measured diagonally) than the target image, so

$$F_1 = \frac{9}{7} \times \frac{3873}{600 \times 0.25} = 33.20 \text{ inches} ; \quad F_2 = F_1 \sqrt{\frac{20}{3}} = 85.71 \text{ inches.}$$

k) The luminance of the Martian surface, assuming a mean distance from the sun of 1.524 AU and an albedo of 0.15, is estimated at

$B_\theta = 872 \cos \theta$ millilamberts, or $810 \cos \theta$ foot lamberts, for values of $0 < \theta < 90°$,

where θ is the phase angle, i. e., the sun-planet orbiter angle.

l) The maximum photocathode illumination using an F/5 system with reflection losses of 19 percent is expected to be about 6 foot candles.

m) With maximum exposure times of 10 milliseconds (corresponding to a movement during exposure of 25 meters at maximum velocity; that is, ten percent of a resolution unit), it is expected that useful data can be gathered even when $\cos \theta$ is of the order of 10^{-6}. This should make it possible to make mapping pictures over very nearly half the planet circumference at each pass.

n) The selection of viewing positions, to provide 10 to 20 percent overlapping of each picture by the next, is controlled by a computation of suborbital velocity. Exposure-duration is continuously computed in the intervals between recorded views.

o) View data are recorded on tape for transmission at any desired rate or time. (All data recorded will be transmitted within one orbital period from the moment of recording.) Each of 233^2 picture elements is represented in the record by a six-bit word, but by the use of Roberts' modulation, using pseudo-random noise, quality equivalent to eight bit-per-element PCM is achieved.

p) On the low-altitude side of the geometric-mean altitude, h_M, the 33.20-inch system does the mapping and the 85.71-inch system remains in readiness with a 600 line raster of 600 lines per target inch. An edge-count comparator observes the edge content of the field at 2.2-second intervals, or less. Any abnormally high count raises the presumption that the region in sight is worth examining closely, so the 85.71-inch system operates in the high-resolution mode to produce a picture of an area 0.015 h square with a resolution of $2.5 h \times 10^{-5}$. At periapsis, when $h_p = 1500$ km, this means an area 22.5 km square and resolution of 37.5 meters. At $h_M = 3873$ km, the area is 58 km-square and the resolution about 97 meters.

q) Pointing accuracy ($3-\sigma$) of the camera-mount axis will be 0.5 degree, total excursion. In general, attitude control will limit the rates of rotation (pitch and roll) to 10 microradians per second, and the limit-cycle magnitude to 6 minutes of arc in all.

No provision is made for the control of "yaw," the rotation of the orbiter about any axis approaching a radius vector from Mars. It is not expected that this motion will be of any great amplitude, but in any case its effect upon vertical viewing will be limited to a displacement of the image relative to the orbital plane. Since the amount of the rotation will always be known, and communicated at the time of each live exposure, any displacement of the frame outlines with respect to the suborbital track will be calculable by the compilers of the mapping data.

r) The scale used for maps based on these views can properly be fixed by representing the linear resolution unit by a measure comparable

with the smallest linear dimension readily appreciated, at reading distance, by the normal eye. If this is taken to be 50 microns, the map scale becomes 50 microns/0.25 km, or 1/5,000,000. A Martian globe to this scale would measure about 52-1/2 inches in diameter. A terrestrial globe to this scale would measure about 101 inches in diameter.

c.   Photogrammetric Considerations.

1)   Stereometric measurements. Vertical viewing from high altitudes is almost perfectly equivalent to planimetric projection. It makes the distance to the object the shortest possible and gives maximum magnification, and therefore provides for the best possible resolution of planimetric features. It reduces displacement effects due to relief to a minimum; but unfortunately it also yields a very minimum of information about relief.

2)   Oblique viewing is almost universally employed for mapping large areas of Earth by aerial photography: but the case is entirely different:

Earth	Mars
a. The images are formed on photographic film with high resolution.	a. For the mapping of Mars we have to use TV techniques, with no more than a few hundred lines of resolution. A 9-inch square photographic film capable of resolving 40-50 lines per mm can yield easily 10^8 picture elements, whereas 10^6 is considerably more than can be realized by automatic TV in space as the art stands today.
b. The altitude from which the photographs are made is maintained quite constant.	b. The altitudes from Mars in the elliptical orbit under consideration vary by a factor of 20/3.
c. The altitudes used for mapping flights on Earth are generally 40,000 feet or less.	c. The lowest altitude from Mars is expected to be 1500 km or about 5 million feet: more than a hundred times the usual altitudes for mapping Earth. And the maximum altitude is more than six times as great as the lowest.

The total disparity of the Mars-mapping problem from aerial mapping of Earth is emphasized here because it is dangerously tempting to think that techniques useful above Earth can necessarily be adapted for use above Mars. In particular the techniques used above Earth for stereometric measurements are so highly developed, so brilliantly successful, and so extremely desirable that it is with the greatest reluctance that one faces the conclusion that they are almost universally inapplicable on Mars.

For example "Trimetrogon" camera, largely used for large-scale terrestrial mapping, has a field of 74°, or 1.292 radians. From apoapsis, the entire disk of Mars subtends an angle of 0.666 radians, and so would fill only a small part of the Trimetrogon field of view.

It is of some interest to consider under what conditions useful topography might be achieved. If the base, the distance between the positions of the orbiter from which the paired views are to be taken, is equal to the altitude of the orbiter (i.e., $B/H = 1$) then $\tan\left(\dfrac{\theta}{2}\right) = \dfrac{B}{2H} = 0.500$, $\tan\dfrac{(\theta + \Delta\theta)}{2} = \dfrac{B}{2(H - \Delta h)}$, and for minimum discernible Δh, $\Delta\theta = 0.00014$ radian.

$$\tan\left(\frac{\theta + \Delta\theta}{2}\right) = \frac{0.50007}{0.999965} = \frac{H}{2(H - \Delta h)}$$

$$\Delta h_{min} = \frac{0.000175}{1.00014} \cdot H \quad .$$

If $H = 1500$ km, $\Delta h_{min} = 262$ meters.

Figure 3 gives the base/height ratio required for significant stereo effect.
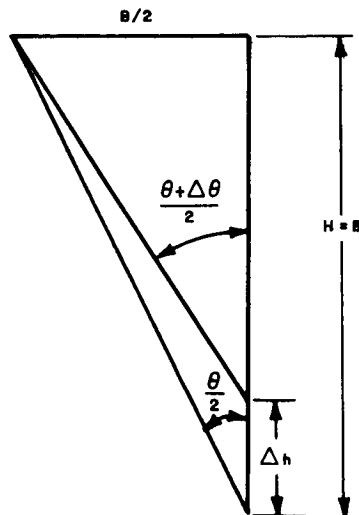
Figure 3 BASE/HEIGHT RATIO REQUIRED FOR SIGNIFICANT STEREO EFFECT

It should be possible, by the above calculation, to distinguish the increment, $\Delta h = 262$ meters, of relief or object height, even from an altitude of 1500 km, provided the base is equal to the altitude. The angle $2\left(\dfrac{\theta}{2}\right)$ is about 53 degrees in this case; and if $\Delta h = \dfrac{0.262}{1500} \cdot H\Delta\left(\dfrac{\theta}{2}\right) \simeq 14.4$ seconds, so $\Delta\theta \simeq 30$ seconds, the usually accepted minimum discernible value of stereo angular parallax. (C. M. Aschenbrenner's formula for $\Delta h_{min} = \dfrac{1}{2.5\,\Theta MR}$ where R is the resolving power in lines per millimeter, $\Theta = B/H$, and $M = F/H = \dfrac{85 \text{ in.}}{12 \text{ in.}} \times \dfrac{1}{5\times10^6 \text{ft}} =$

1.4×10^6. Substituting $\Delta H = 262$ meters $= 860$ feet and $B/H = 1$, we obtain $R = 33$. This value of R, the required resolving power, would not be much too high for a 600-line raster with a one-inch target.) But so long a base as 1500 km is difficult to obtain reliably, and to maintain $B = H$ symmetrically about apoapsis, at 10,000 km, is not a practical possibility.

If we could point our long-focus camera about 26-1/2 degrees ahead and take a picture, and then point the camera 26-1/2 degrees astern; and then after 10 minutes, or longer, take another picture when the same planet area came in view, we should probably be able to distinguish planes separated by about a quarter of a kilometer: or if not a quarter, then a half. It is not every 10- or 20-mile square of territory that exhibits a change of altitude of even 250 meters, 820 feet; but we might find some such in the right places to have their pictures taken. But the difficulty of calculating the exact timing of the second shot of a stereo pair (and it must be very exact, or there will be no overlap) with the added difficulties caused by inevitable small changes in attitude and pointing, means paying a prodigious price for a highly improbable advantage.

The conclusion that stereo techniques cannot be employed usefully from the very high altitudes of an appreciably eccentric orbit has not been reached without earnest effort to find means to adapt them. Eminent authorities in this field have been consulted and have concurred. It may be possible, at some considerable cost, to achieve the evidence necessary to draw on the map of Mars contour lines to indicate changes in relief of the order of 3000 feet. Radar mapping could probably produce results of comparable (or better) resolution with even higher reliability.

2) Overlap. In mapping from relatively low altitudes above Earth, it is possible to obtain stereo relief from vertical views provided that the successive views overlap sufficiently. (The least contour-interval which can be plotted accurately is generally taken as not less than 0.083 percent of the flight altitude.) The overlapping of views in the direction of the flight path (the "forward lap") must never be less than 50 percent for full stereo coverage. The limits usually adopted are 55 to 65 percent. Between 10 and 40 percent of side lap is considered best in mapping Earth from the air.

The main significance of these overlaps is stereometric. It is true that with high values of overlap, no object is ever imaged very far from the center of one view or another, and planimetrically that is an advantage at the relatively low altitudes used for Earth mapping, but not of great importance for our purposes. It is true also that generous overlapping increases the probability that clearly recognizable features will be common to successive views, which greatly facilities compilation.

This consideration is important because of the complete lack of ground control, and the risk of jeopardizing our orientation. But the orbiter attitude angles will be known for each exposure, and the intersection of the orbital plane with the field of view can be calculated with some precision, and errors due to faulty bridging should not be a serious problem.

The very high degree of redundancy which is useful for mapping Earth is not worth its cost in communications capacity in the Martian application. Instead of overlaps of 50 percent, our purposes will be adequately served by 20 percent or less, and the number of bits needed for transmission with equal modulation is reduced by 37.5 percent, and this allows the use of a gray scale with 64 instead of 16 steps.

3) Platform stability and sighting. The two camera systems are to be mounted together on a two-gimbal mount by means of which their common axis may be pointed along a radius vector from the planet center, by controls relative to the inertially-stabilized orbiter platform, one axis of which is continuously directed toward the Sun. The accuracy of pointing will have a 3-σ maximum value of 0.5 degree, or 8.73 milliradians, total excursion. (The field angles of the cameras vary between 38.83 milliradians at periapsis to 5.83 milliradians at apoapsis.)

What matters in compiling the mapping data is not so much having an angular error as knowing what the error is. Provisions will therefore be made for recording with each exposure the magnitudes of the angles of the camera axis relative to the orbiter platform.

What matters in making the pictures for mapping is not the amount of angular deviation of the camera axis but the rate. If the angles are all known at the moment of exposure, it makes very little difference, photogrammetrically, where

the axis lies, within the bounds of its six-minute-of-arc limit cycle, provided its attitude is reasonably constant. By reasonably constant we mean that it is changing only slowly, and is not so far different from what its attitude was when the previous exposure was made that the compiler risks losing the continuity between exposures, provided by the planned overlap, on which his bridging depends. The maximum angular velocity of the camera axis about any axis will be 10 microradians per second. The most unfavorable case occurs at apoapsis when the time between exposures may be as long as 35 km/0.33 km sec^{-1} = 106 seconds. In so long a time, the "hitch" or "roll" angles might change as much as 1.06 milliradians; less than four minutes of arc, and less than one fifth of the angular field of the corresponding camera. This is not of an order to cause any difficulty in data reduction.

4) <u>Framing control.</u> A computer function equivalent to a sort of suborbital odometer will be provided. This will begin integration of suborbital distance at the instant of each exposure which is to be recorded, and when the integrated distance reaches the value of (100-20)/100 x 233/4 = 46.6 km, a picture may be recorded, provided the scene is bright enough to make a useful picture without exceeding the present maximum exposure. This question is asked and answered in every "dry" exposure between recorded shots. If the light is adequate and the minimum distance has been traveled, the next exposure will be "live," and the scan output will be recorded for transmission.

5) <u>Field-size control.</u> To minimize the difficulties of compilation, scale, resolution, and coverage of the mapping views are maintained uniform from one end of the orbit to the other, with the one very minor exception that the ratio of the focal lengths of the two optical systems may very well differ by a very small amount from its intended value. This would require only a small constant adjustment of scale.

With a constant focal length, the primary image of an area of constant size becomes smaller as the altitude increases. But the output from the image tube depends not on the size of the optical image but on the size of the scanning raster. If the line density of the raster varies, like the height of the optical image, inversely as the altitude, the 233 lines on the target which determine the portion of the electron-optical image to be scanned, will always correspond to 233 x 1/4 km on the planet.

When the focal length is changed, as it is every time the orbiter passes through the mean altitude, the relation between the raster size and the electron-optical image size is maintained unchanged, so there is no change of scale. It is to be expected that the picture quality will be best when the line density is least, as it is in the regions of periapsis and just above the mean altitude.

6) <u>Color capability.</u> It is well known that for most of the time the atmosphere of Mars is largely impenetrable by light of wavelengths below

about 4500A, and photographs by blue or violet light generally show little or no surface detail. But from time to time this phenomenon ceases, and the planet surface is seen clearly in short-wavelength light. There is no general agreement among astrophysicists on the reasons for the veiling effect or for its occasional suspension. Whether some sort of Rayleigh scattering begins abruptly at about 4500A, or some form of molecular absorption is responsible, it is probable that picture quality might often be improved by filtering. The universal use of a minus-blue filter, however, would block off a very sensitive region of the image-orthicon photocathode and render the instrument incapable of distinguishing between the presence and absence of the veiling effect in the Martian atmosphere.

Any single color filter could readily be embodied in the optical systems under consideration. If necessary, one filter could be so mounted as to be introduced or withdrawn at will; but changing filters is hardly compatible with economy of space or the maintenance of perfect collimation. It is only outside the system, in the full aperture of the incoming beam, that alternate filters could be introduced, if the most reliable spacing of the optical components is to be preserved. Moving parts in the optical systems should be avoided; and if the very desirable goal of color-separation pictures were to be pursued, a three-camera system at least, would be required, each camera having its own fixed response (or pair of responses, if negative branches in the sensitivity curves have to be taken into account).

The S-20 ("tri-alkali") photocathode is highly sensitive throughout the visual range, and well below and above it. From about 3200 to about 7800A it is the most sensitive detector known; and it is more than probable that the Martian surface will reflect radiation below 4000A and above 6850A, that is, in wavelength regions to which the human eye is not responsive.

For true visual color, if it were desired to know how the planet would look to a human observer, the observing system must follow the pattern of the human eye. Quite grave distortions of visual truth might well result from adding to the "blue" image the effect of radiation of wavelengths below, say, 4100A, to which the eye is blind, or from adding to the "red" image the effect of radiation above 6850A, which forms no part of the visual record. It would be necessary to make the "blue" system cut off signal from the ultraviolet end of the Martian spectrum, and to throw out from the "red" system any signal strength due to the near infrared. Since we should not wish to waste this potentially valuable information, two more cameras would be needed; making five in all. Though this would be most valuable, it is not compatible with the limitations upon the present orbiter.

Experience in high-altitude aerial photography of Earth indicates that color information is of marginal value. This is due both to the color-selective scattering properties of the atmosphere as well as to the lack of pronounced coloration

on a large enough scale to give interesting detail when viewed from far away. For this reason, full color transmission is not planned, although it could be included. If the bit rate permitted, and additional optics could be added, the red and blue records imaged by separate lenses on the same single target with the "white" light record. When color is wanted, the whole tripartite image would be scanned, to be reconstructed on Earth by optical superposition, first obtaining the green record by white-minus-red-minus-blue. When mono-chrome is wanted, only the "white" image would be scanned.

It is felt that considerations of weight and power make it unwise to attempt in the present design to obtain full color separation pictures; and by way of consolation it is argued that the coarseness of the achievable resolution and the very large amount of intervening atmosphere would very likely cause each view to be not very far from monochromatic. Since, however, it can be predicted confidently that there will be variations in the dominant tonality of different views as the result of variations in atmospheric conditions and in the constitu-tion of the surface area viewed, it is considered that steps should be taken to obtain some indication of the wavelength-energy relations prevailing at each observation.

To accomplish this, a very narrow line made up of five (or more) filters is to be embodied in the image orthicon face plate within the area occupied by the highest-altitude view. As long as the face-plate illumination is strong enough to cause any signal to be obtained from any of the filtered regions, some indication of the color of the field will be obtained. This device is in effect a five- (or more)-color spectrometer of very narrow angle, with a rather coarse read-out.

63-9249
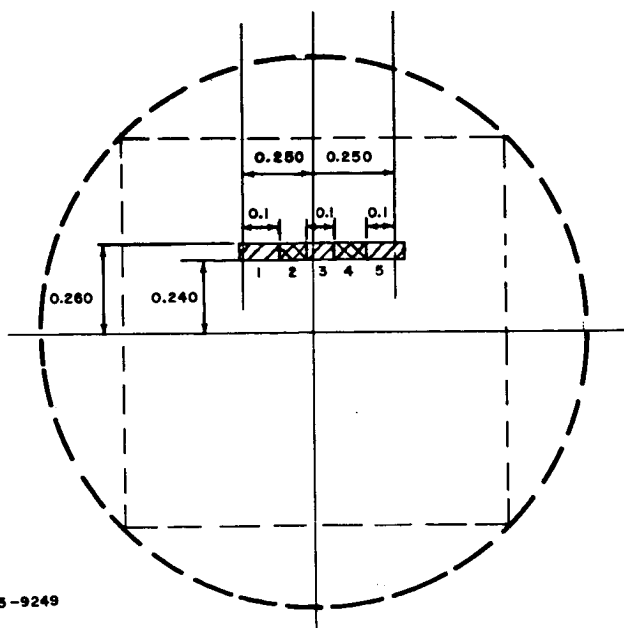
Figure 4 FIVE-COLOR FILTER

-27-

Five filters are shown in the sketch (figure 4). It is intended that one should cut off wavelengths above about 4250A and another, wavelengths below about 6500A. The other three filters cover the visible spectrum in such steps as 4000 to 4900, 4800 to 6000, and 5800 to 6850A. The filters should be inlaid in the image orthicon face plate so as to be as near as possible to the photo-cathode layer, and the face plate surfaces worked optically flat after the inlay medium is hard.

d. Communications considerations.

1) Bit rate versus resolution. For planimetric mapping without reference to color, using a square format 233 lines high and a gray scale of 2^6 = 64 steps, the basic bit requirement is 233^2 x 6 = 325, 734/bits per exposure. To these must be added a word for each of three angles, one for time, and one for altitude, but the total bits needed per exposure will not exceed 325, 850.

The content of each exposure must be read out in something less than the minimum time between exposures, and at appropriate moments the read-out is recorded for later transmission to Earth. Recording at the rate of 150 kilobits per second, or 25, 000 six-bit words, each representing one picture element, gives a 2. 2 second interval between exposures.

The number of mapping exposures per orbit to be recorded for transmission will not exceed 3332, the radius of Mars in km, times $\pi/\dfrac{(100-20)}{100}$ 233 x 0. 25 = 225; so the total number of bits required for mapping will not exceed 225 x 325, 850 = 73. 32 megabits out of the 89 megabits for transmission available in each orbital period, leaving a bit balance sufficient for the transmission of seven high-resolution shots with 360, 000 six-bit picture elements apiece. We get 1/4 km resolution for all our mapping pictures, and 2. 5 h x 10^{-5} km resolution for our discrete views. This is the use which it is proposed to make of the expected supply of bits for transmission. But what elements of compromise does it contain? Could we get better resolution if we could have more bits?

More bits alone would not help out. We cannot safely push the line density of the automatically controlled image orthicons beyond 233 $\sqrt{\dfrac{20}{3}}$ = 600 lines per target inch. And we should be most reluctant to make our mapping swath much narrower. But certainly, if we could command unlimited bits, and also unlimited storage capacity and recording speed, we could use the long-focus camera continuously from h_M through periapsis to h_M on the other side, to produce a narrow high-resolution strip picture made up of overlapping views. Without any overlapping, this would require about 304 views and resolution

The remaining requirements are the following:

1. Nominal resolvable ground resolution   0.25 km

2. Equivalent focal lengths

     a. Short-focal length   33.20 inches

     b. Long focal length   85.71 inches

3. Relative apertures

     a. Shorter focal length   F/5.0

     b. Longer focal length   F/12.9

4. Spectral range   S-20 phosphor

5. Wavelength range   3000 to 8000 A

The S-20 phosphor exhibits a peak response at about 4200A and has an optically useful spectral range from 3000 to 8000A. Since it is believed that a very appreciable part of the radiation from Mars lies outside the visual range, it is considered wise to eliminate chromatic aberration as a problem by using reflection optics; but a possible refractive system has been worked out, and is described below.

The resolution requirement for the optical system is dictated by the requirement of 600 TV lines per target height or approximately 20 TV lines per millimeter. To be conservative, this number of optical lines may be taken as the required resolution for the optical system. The half-angular field of view for the 33.20-inch system will be 0.027 radian. The 85.71-inch system is to have a half-angular field of 0.0105 radian.

With this information, then, the optical system requirements are completely determined. The short focal length system, operating at a relative aperture of F/5.0, must cover a full 3.11-degree angular field over a spectral range of 3000 to 8000. The long focal length system must cover a full angular field of 1.20 degrees operating at a relative aperture of F/12.9, or faster. The image performance level is taken as 20 lines/mm for both systems; about twice the minimum requirements.

Based on these values, the simplest refractor configuration capable of satisfying all the requirements for the 33.20-inch focal length system seems to be a conventional triplet design (see figure 5), composed of all spherical refracting interfaces. (A two-lens doublet construction would have too much field curvature.) Since all surfaces are spherical there are no complicated production problems and full quality control is guaranteed. But a refractor is undesirable.

would vary from 97 meters to 37.5 meters and back again. But it would take 656 megabits; roughly seven times the number at our disposal.

The uncompensated change of picture size with resulting changes in both scale and coverage with altitude would make interpretation very inconvenient, and the timing of the exposures would present some difficulty. However, we should certainly wish to use the maximum line density throughout. So either optical or electron-optical "zoom" would have to be introduced to keep the field area constant by increasing the magnification with altitude. System complexity would be much increased, but the region over which higher resolution could be obtained would be somewhat extended at an enormous increase in bits used.

Or again, if unlimited bits were available, we could use a very long-focus camera - say 9 or 10 meters, giving a field approximately 5 km square, with resolution of perhaps 8 meters. A picture of so small an area would be almost meaningless unless it formed part of a cluster of adjacent views, and coverage equal to that of the mapping system proposed and require not less than 144 times as many pictures and 6.6 times as many bits per picture; an increase of 890 times in all.

These extreme cases are mentioned only to emphasize that, although along with minimum picture width and maximum focal length, the supply of bits does contribute to the limitation of the resolution which can be achieved, the crux of the matter is the image tube; its ability to go on delivering signals of adequate amplitude as the target is scanned with closer and closer-spaced rasters. The information is all there, at least as far as the photocathode; but to get it out, and to Earth, needs more than just additional bits; it needs at least an entirely new type of image tube.

2. Subsystem description

a. Optical system. This program demands reliability from the optical system under extended operational life and adverse environmental conditions. Components and assemblies must be insensitive even to radical temperature changes. The simplest type of optical system consistent with the image quality required must be selected. No extraordinary demands should be made as regards materials or manufacture.

1) System configurations. The system requirements are quite specific. The optics package must perform mapping functions at altitudes ranging from a minimum of 1500 km to a maximum of 10,000 km from the Martian surface. Therefore, it is obvious that either a variable-power optical system, or two or more separate systems must be used. The latter choice is preferable because of the mechanical difficulties implicit in changing optical components in order to effect a change in optical power. Also, two separate optical units provide extra assurance in case one instrument should give out.

ULTRA-VIOLET TRIPLET

(a)

DIAM 6.75"

DIAM 4.75"

DIAM 6.75

8.68"

-117.30"

42.90"

-8.53"

-10.66"

7.03"

0.74"

0.30"

0.78"

3.97"

5.02"
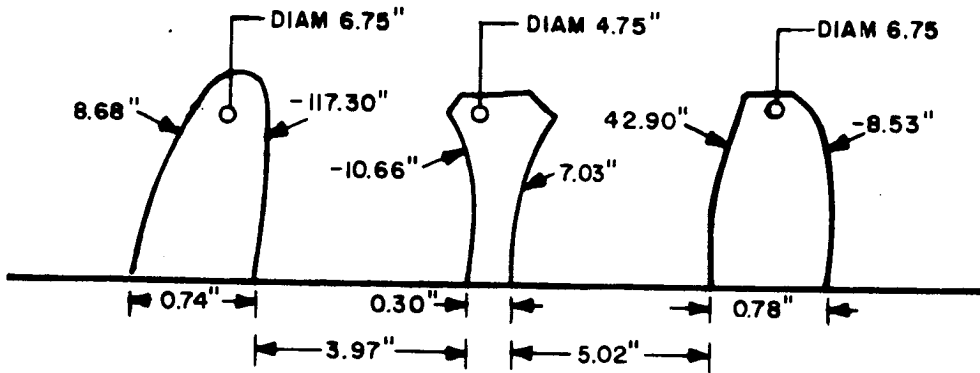
APERTURE FOCAL LENGTH	32.23 "
BACK FOCAL DISTANCE	27.01 "
RELATIVE APERATURE	F/5.0

(b)

LONG FOCAL-LENGTH SYSTEM

-60.733"

7 "

21.08 "

28.841"

21.22"

21.01"
TO I.D
TARGET
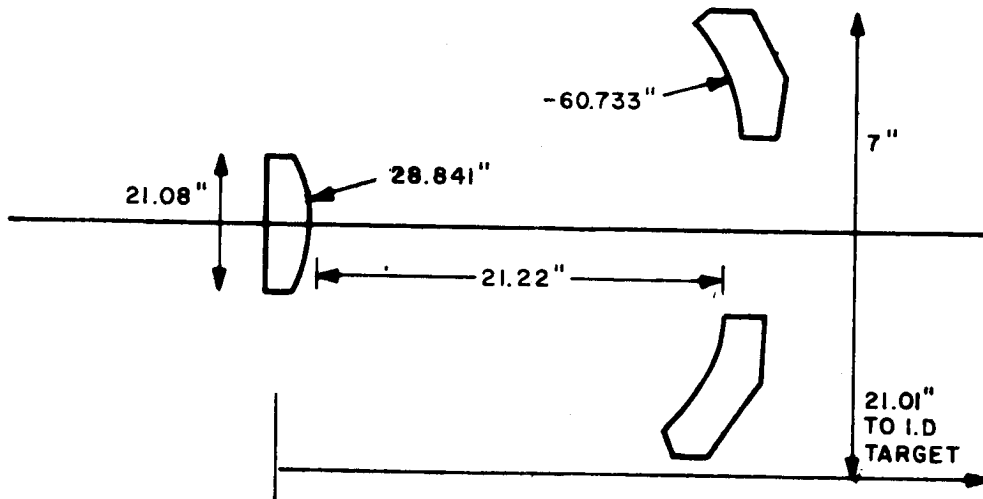
63-9278

Figure 5 ULTRAVIOLET TRIPLET

-31-

Alternate solutions were explored. A Cassegrain telescope is unsuitable because it cannot cover the large field angle required. Coma, field curvature, and astigmatism degrade the image badly from about 0.80 degrees off-axis. The conventional Maksutov system, consisting of a spherical primary mirror and a meniscus correcting lens, was unsuitable for the 85.71-inch system because of its length, and for the 33.20-inch because of its inherent field curvature and the large field angles required.

To reduce the length of the long-focus system and to minimize the weight of supporting members, it is necessary to use a high telephoto ratio. This can be achieved neatly with systems of the Cassegrainian type, and the 1.2-degree field angle is not too large. The relatively low speed of F/12.9 permits straightforward optical production, and if, in the final design, a little extra weight can be tolerated, this speed can be increased, perhaps to F/8, without risk.

2)   Short-focal-length system.

a)   Triplet. Glasses were selected for high-ultraviolet transmission characteristics as well as their optical dispersions. Advanced automatic design procedures and electronic computer equipment were used to develop a preliminary system shown in figure 5. The performance characteristics of this lens are shown in the attached plots of energy concentration as a function of blur circle radius   (figures 6 and 7). The system resolution requirement of 20 lines per mm means 20 dark lines of width of (0.5/20) mm, and 20 spaces of width of (0.5/20) mm. Therefore W = 0.5/20 = 0.0250 mm, or 2W = blur circle diameter = 0.050 mm (.0020 inch). Now, for low-contrast ground resolution it is necessary that a minimum of 50 percent of the energy be used to determine limiting resolution values. On this basis the resolution obtained from the graphs is as follows:

Total Field Angle = 3.30 Degrees

Wavelength	Blur circle diameter	Resolution (lens)
4359	0.0008 inch	50 lines/mm
5461	0.0008 inch	50 lines/mm

This refractive system is capable of putting substantially 100 percent of the available energy within the required blur circle diameter in a fully optimized version. It is seen that its resolution exceeds the minimal requirement by a factor of 2.5 over the full range of field angles called for. Nevertheless, because of the wide range of wavelengths over which the S-20 phosphor is sensitive, and the unknown factors in the reflectivity of Mars, it seems prudent to provide for operation over the widest range possible, and the simple triplet system performance is found inadequate at the extremes of the wavelength range.
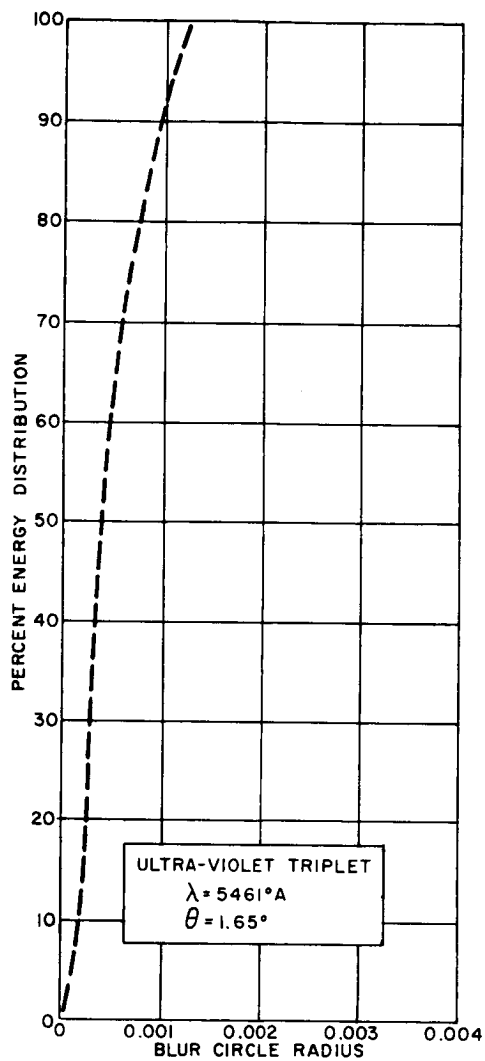
Figure 6 ENERGY DISTRIBUTION VERSUS BLUR CIRCLE RADIUS FOR
ULTRAVIOLET TRIPLET AT λ = 5471A

62-9282

-33-
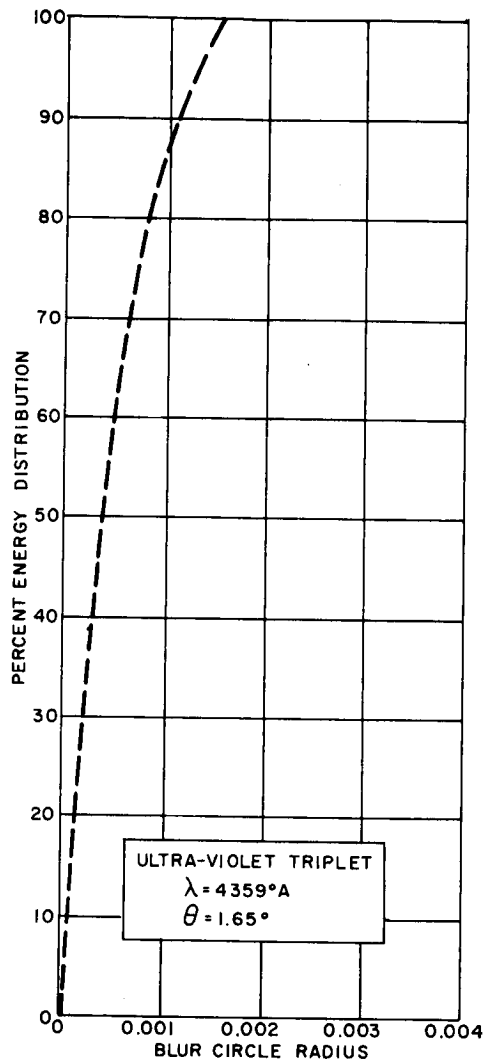
62-9283

Figure 7 ENERGY DISTRIBUTION VERSUS BLUR CIRCLE RADIUS FOR
ULTRAVIOLET TRIPLET AT λ = 4359A

-34-

b) Schmidt-Cassegrain: Flat-field anastigmat. A computa-
tion program was carried out for this system, and the results establish the
basic feasibility of this system configuration for the short-focal length system
over the complete spectral range of sensitivity for the S-20 phosphor. The de-
sign specifications of an F/4 system are contained in figure 8. Design for F/4
was carried out to insure that the final system will yield at least F/5 perform-
ance. This was done with no significant penalty in overall system design param-
eters. The energy distribution diagram, figure 9, shows that resolution will
be acceptable.

3) Long focal length system - Cassegrain type.
Cassegrain, the primary mirror is an exact paraboloid and the secondary mirror
is an exact convex hyperboloid. However, making the secondary hyperbolic is
difficult, and its mounting is very exacting. If this secondary can be made pre-
cisely spherical, and so readily controlled, then the system is straight-
forward.   This is done in the so-called "Dall-Kirkham" system by "un-
dercorrection" of the basic sphere of the primary mirror in terms of para-
bolization. This undercorrection balances out the spherical aberration contributed
by the spherical-surface secondary. This undercorrection causes the primary
mirror surface to assume a figure, intermediate between sphere and paraboloid,
which is very nearly a true ellipsoid. This means that during manufacture the
primary mirror can be tested as an ellipsoid with foci at specified points, and
so the quality can be controlled. The resulting mirror system presents no
manufacturing problem and can readily be made to yield diffraction-limited per-
formance. A long-focus Dall-Kirkham of aperture F/10 is shown in figure 10.

Such a system was designed, consisting of an ellipsoidal primary mirror
of 7.0-inch diameter and a secondary mirror of 2.1 inches diameter. As the
primary mirror is only F/4.4 it is very easily figured and possesses no strong
zonal characteristics. The system is compact, measuring approximately 25
inches overall. Spot diagram and energy distribution plots (figure 11) indicate
the high-performance capability of this system.

4) Construction and testing. Because of the extreme variation in
thermal environment it is very desirable to use low-expansion materials for
both the optical elements and the mount-support structure. Therefore, quartz
will be used for the mirror elements and quartz tubing, honed to match the
mirror diameter, will be used as the basic mount structure. Also, the second-
ary mirror will actually be evaporated directly upon a low-power, full-diameter
meniscus shell. This procedure will assure precision centering of both com-
ponents as well as air-space control.

The Schmidt-Cassegrain type of system, when designed on the lines of
J. G. Baker's flat-field anastigmats (ref. 1), is capable of performing at an
extremely high level of image quality over a very broad spectral range. The
two focal lengths of the mirrors are made precisely equal in order to provide
a zero Petzval sum and, therefore, an inherently flat field condition. The three
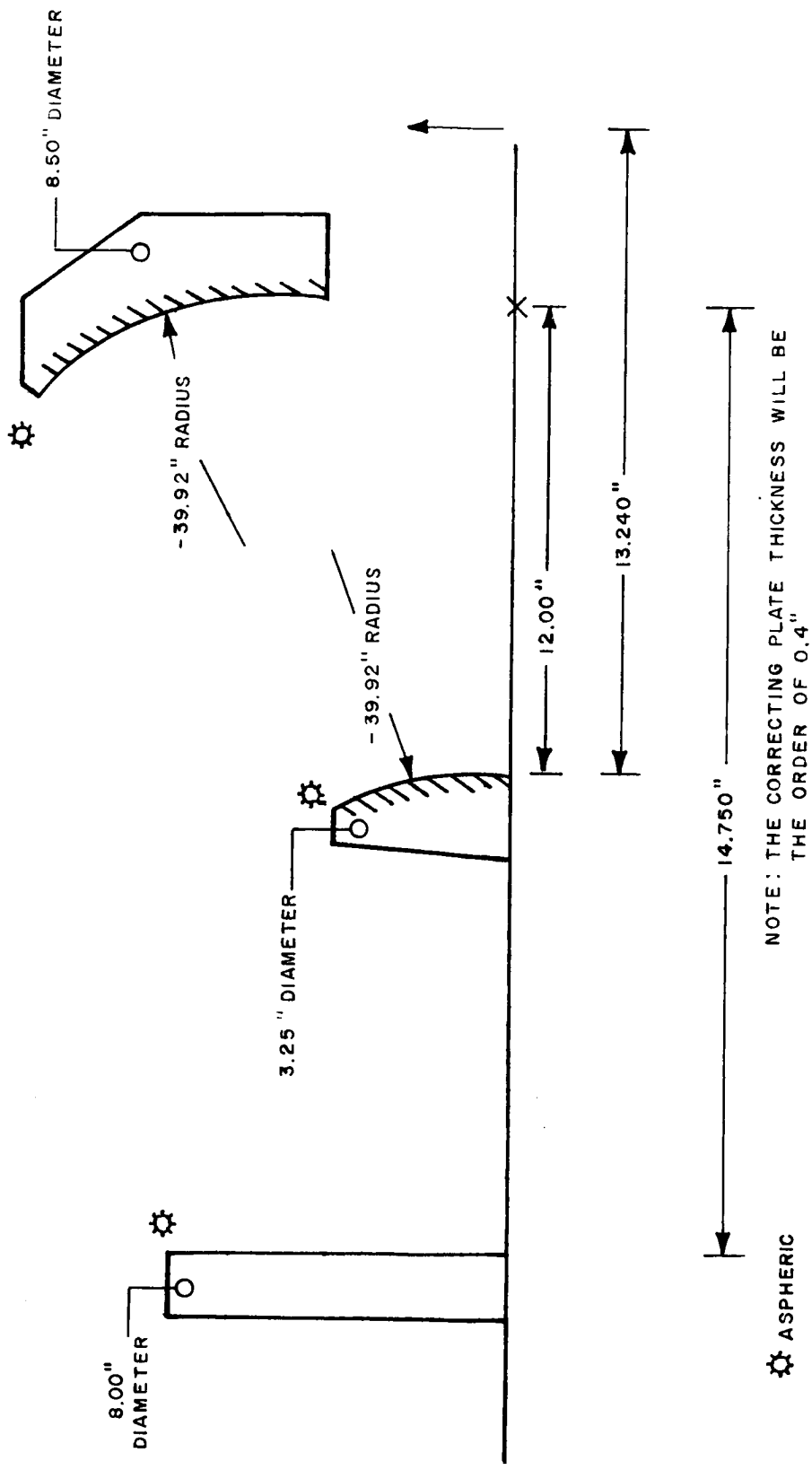
Figure 8 SCHMIDT-CASSEGRAIN: FLAT-FIELD ANASTIGMAT

8.50" DIAMETER

-39.92" RADIUS

-39.92" RADIUS

3.25" DIAMETER

8.00" DIAMETER

12.00"

13.240"

14.750"

NOTE: THE CORRECTING PLATE THICKNESS WILL BE THE ORDER OF 0.4"

✿ ASPHERIC

63-9279

-36-
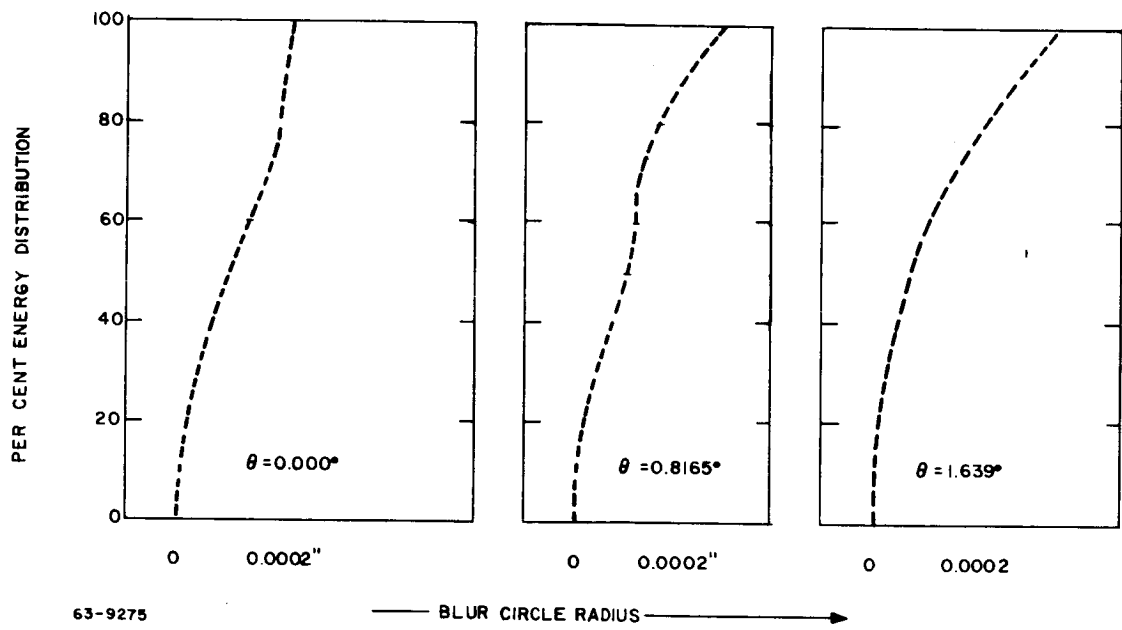
Figure 9 ENERGY DISTRIBUTION VERSUS BLUR CIRCLE RADIUS FOR
FLAT-FIELD ANASTIGMAT

DIA. .7"

RAD. 60.733"

21.22"

25.01"

RAD. 28.841"

DIA. 2.108"
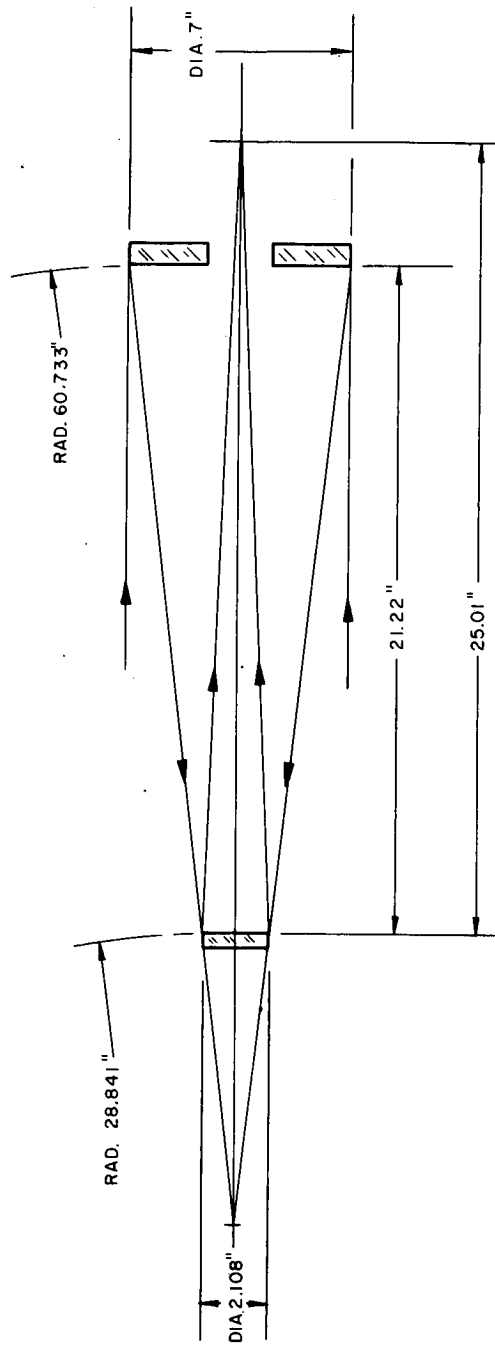
Figure 10 LONG-FOCUS DALL-KIRKHAM

63-10273

-38-
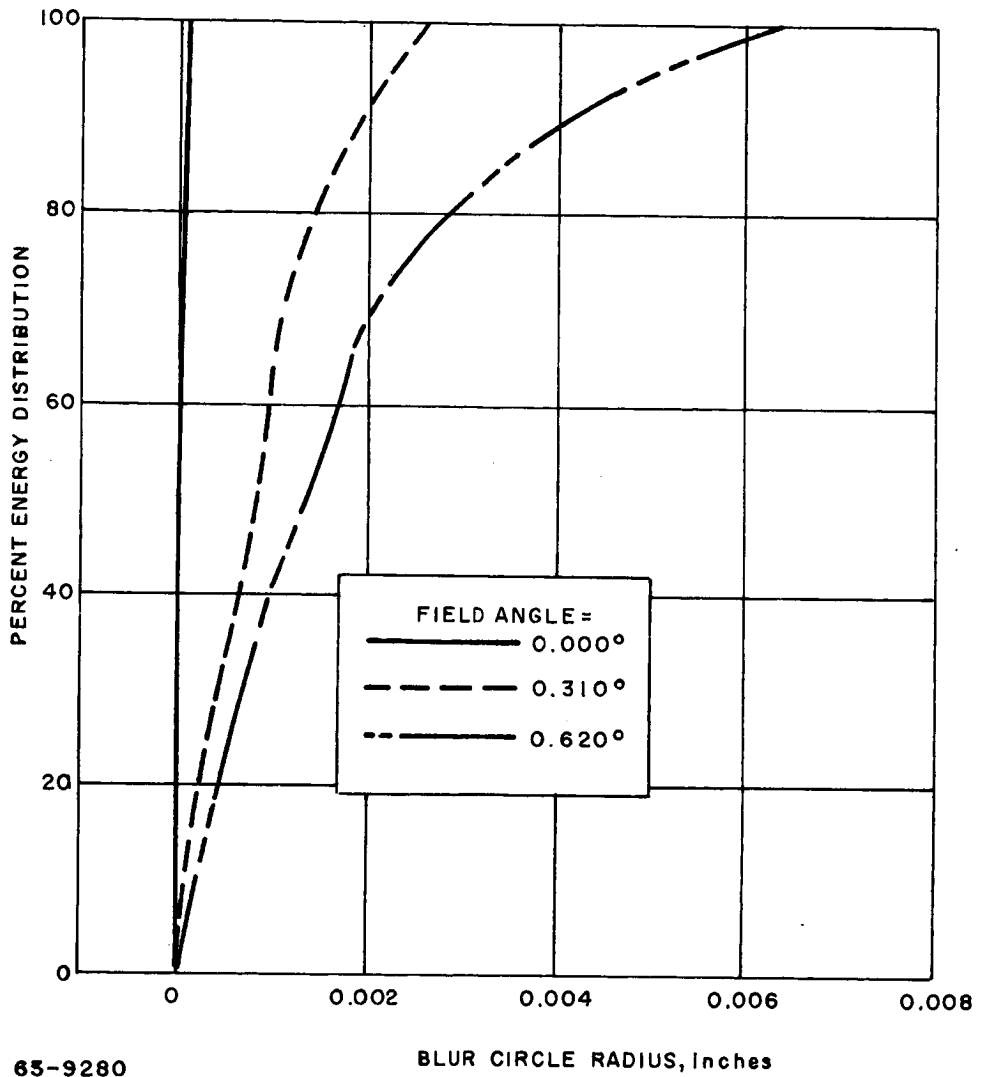
Figure 11 ENERGY DISTRIBUTION VERSUS BLUR CIRCLE RADIUS FOR
LONG-FOCUS DALL-KIRKHAM

residual aberrations of spherical aberration, coma, and astigmatism may then be removed by very weak figuring in the primary and secondary mirrors, and a mild aspheric in the correcting plate.

The image quality, as shown by spot diagrams, remains essentially uniform across the entire image. During the final figuring of the correcting plate, the skilled optician will produce a diffraction-limited system on axis, which means that the fabricated system is capable of an even higher performance level than indicated by the geometrical ray plots.

Another slight variation of this design, and one which permits direct quality control of the individual components, is the use of a precisely spherical secondary. In this case, no optical figuring of its surface profile is required. Then, the concave primary assumes a more oblate figure and may be independently tested as shown below.

In this testing procedure the primary mirror is given a null testing technique which insures that the figuring is precisely accurate to a given value of asphericity with respect to a sphere (fig. 12). Then the complete system, primary mirror, secondary mirror, and correcting plate may be mounted and tested as a unit. Since the primary and secondary surfaces are already correct, this allows the optician to figure the aspheric on the correcting plate to an exact profile by null-testing the entire optical system as a complete unit. Since the theoretical design indicates that diffraction-limited quality on axis is to be expected from this physical configuration, the optician will be able to secure image quality perfection using this absolute null-testing method.

The ellipsoidal primary figure on the 85.71-inch modified Cassegrain may also be figured by a similar absolute null-testing technique.

b. Image tube. The reasons for preferring image orthicons to any other image tube are numerous and compelling, the most important being that short exposures are indispensable for good resolution, unless some system for compensating image motion is introduced, and in any noncircular orbit that is a serious complication. The extremely high light-sensitivity of the image orthicon is important because it allows the use of exposure times so short as to minimize blurring of the image by movement of the camera axis during exposure as a result of forward movement in orbit and rotations about control axes. It is also important because it requires exposure of only moderate length under conditions of minimum illumination.

The extremely short exposure times required under conditions of maximum illumination exclude the use of any mechanical shutter (which would in any case be undesirable) and the image orthicon is readily shuttered electronically by a negative-going pulse applied to the photocathode. The duration of the pulse is very easily varied, substantially without limit, and its rise time can be made incomparably shorter than the mechanical equivalent.

OBLATE
SURFACE

TESTING
SPHERE
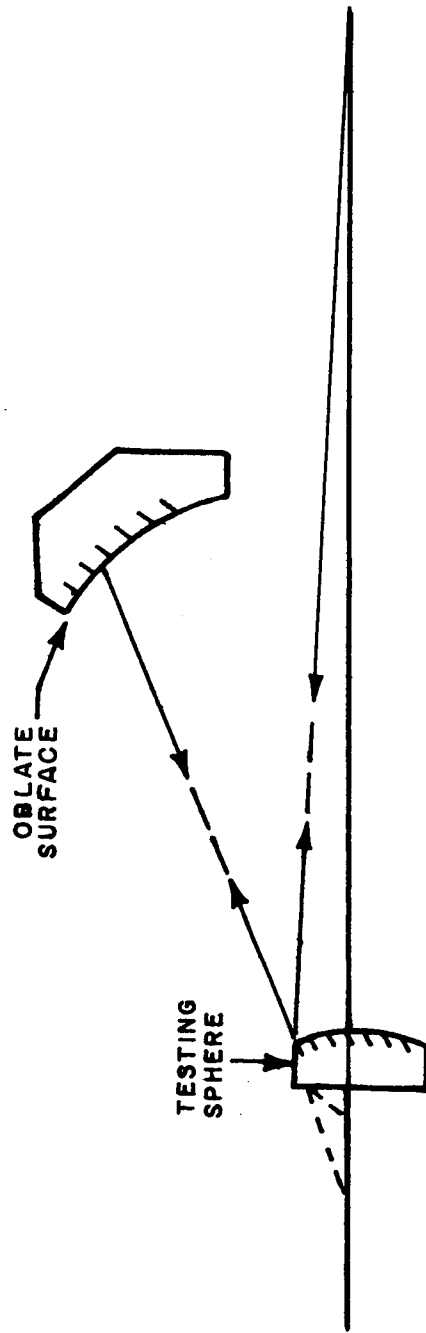
63-9273

Figure 12 OPTICAL TEST APPARATUS

-41-

Although a good image orthicon is capable of resolving 2000 lines, or more, the amplitude response becomes insufficient for our purposes at some much lower density. The maximum line density which it is proposed to use is 600 lines per target inch, and $600/M = 232.4$ or approximately 233. Between h_P, the altitude at periapsis and h_M, the geometric-mean altitude of $1500M = 10,000/M = 3873$ km, the raster of the shorter-focus system is to change in density, proportionally to altitude, from 233 lines per target inch to 600 lines per target inch; but it is to consist always of 233 lines for data purposes. In exactly the same way, the raster of the longer focus system is to change in density, proportionally to altitude, between h_M and h_A, the altitude at apoapsis, from 233 lines per target inch to 600 lines per target inch, and is also to consist always of 233 lines for data purposes.

c.   Electronic subsystem summary.

1)   System block diagram. The basic block diagram of the TV mapping system is shown in figure 13. There are two independent image orthicon cameras, each comprising a clock pulse generator, timing generator, raster generator, camera tube and optical assembly, and video amplifier. Scanning is at a rate of one frame in 2.2 seconds. Both video signals go to the camera-select control, where the signal from the appropriate camera is chosen according to altitude. The altitude also controls the raster size so that the map scale remains constant at all altitudes. Automatic controls are provided to insure correct image orthicon operation under various conditions of temperature and scene illumination.

The picture recording control selects individual frames for recording when the brightness is adequate and when a suitable ground distance has been covered since the previous recording to obtain about 20 percent overlap. The control operates by enabling the video gate and turning on the tape recorder for one frame period. At periapsis about one frame in 10 is recorded, and at apoapsis, about 1 in 70.

Note that the analog video information is added to pseudo-random noise before digital conversion to prevent contouring. A 34-db signal-to-noise ratio picture results. Tape recording is digital, so that on playback, direct transmission from the tape to the transmitter is possible.

The command system may be used to make fine adjustments in I.O. operation or to override the normal picture recording sequence in various ways. Provision is made in certain cases to record automatically extra pictures with the long focal length lens at those lower altitudes at which the shorter lens is normally used. This is accomplished by means of the complex scene detector, which counts edges, or sharp transition points. When the number of such edges in any frame recorded with the short lens exceeds a threshold, an extra picture is recorded from the long focal length lens.

-42-
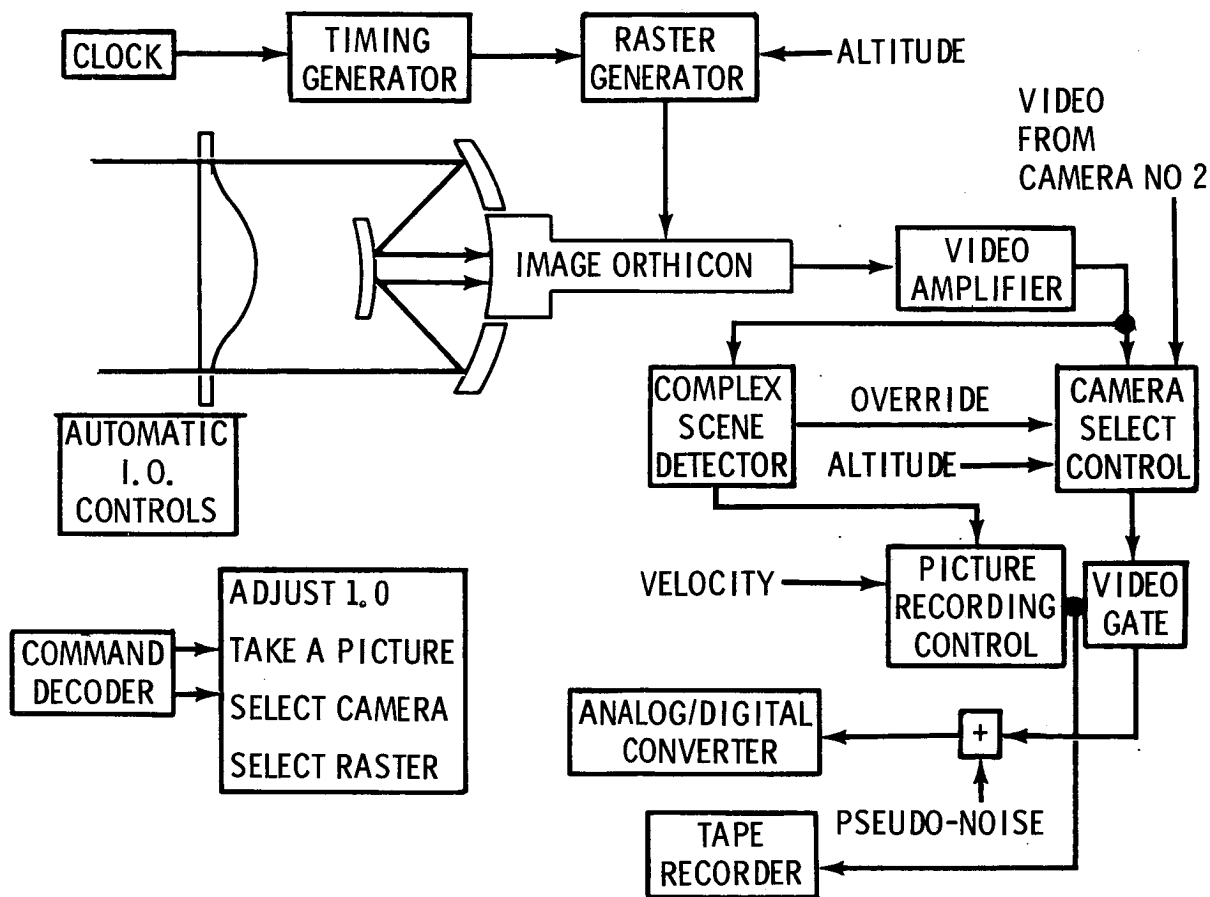
Figure 13 BASIC TELEVISION CIRCUIT

63-8648

The modulation method is six-bits-per-element PCM, employing pseudo-random noise to obtain a continuous tone scale. The signal-to-noise ratio is about 48:1 amplitude of 34 db and the performance in the presence of channel noise is very good. The digital technique permits multiplexing of telemetry data on the same transmitter and also permits an emergency mode of very slow transmission with no adjustments to the TV system other than change of clock frequency. It also allows a change in the TV system parameters during the development period without circuit design changes.

The picture-taking operation is entirely automatic. As long as the illumination is adequate, pictures will be taken with about 20-percent overlap, under control of the on-board altimeter and speedometer. Raster dimensions are set and a camera is selected to produce constant-quality, constant-scale images at all altitudes. No commands are needed unless it is desired to override some of the automatic controls or if a different camera or image scale is desired than originally planned.

A very small portion of each exposure is viewed through five overlapping wavelength filters, as shown in figure 14.

2) Scanning the image orthicon. The swath may be taken as 180 degrees in length, or 10,500 km. Resolution is to be 0.25 km per picture element; but with 20 percent overlap between pictures, this becomes effectively 0.2 km, so the swath has an effective length of 52,500 picture elements. If each view is 233 elements wide, there will be 12,232,500 picture elements in the swath. At a data rate of 4500 bits per second with an assumed duty cycle of 75 percent, 88.8 megabits could be transmitted per orbit, sufficient to describe 14,800,000 picture elements, or 2,567,500 x 6 = 15,405,000 bits to use in other applications. If higher data rates were available, then a wider swath might be covered, and the mission duration reduced; but, this would call either for a higher-resolution camera tube, or for a more complicated camera-pointing routine so that pictures could be taken side-by-side.

The choice of 233 scanning lines, while somewhat arbitrary, is based on the desire that the quality of the final maps be determined by the data rate and not by the camera-tube performance. While image orthicons have been reported to have resolved some thousands of lines, the response of even the very high quality 4-1/2-inch studio types such as the General Electric image orthicon no. 7389a is only some 56 percent of its peak value at 400 lines in the 4 x 3 format (465 lines in square format) under carefully controlled conditions. In space applications it would be unreasonable to expect better performance than that. It is well known that image quality is largely a function of the amplitude response at the middle line frequencies, rather than simply the resolution, or cutoff line frequency. Indeed, this is one of the principal reasons for the superior quality of image orthicon pictures compared to vidicon pictures, since the two have comparable resolution limits.

-44-
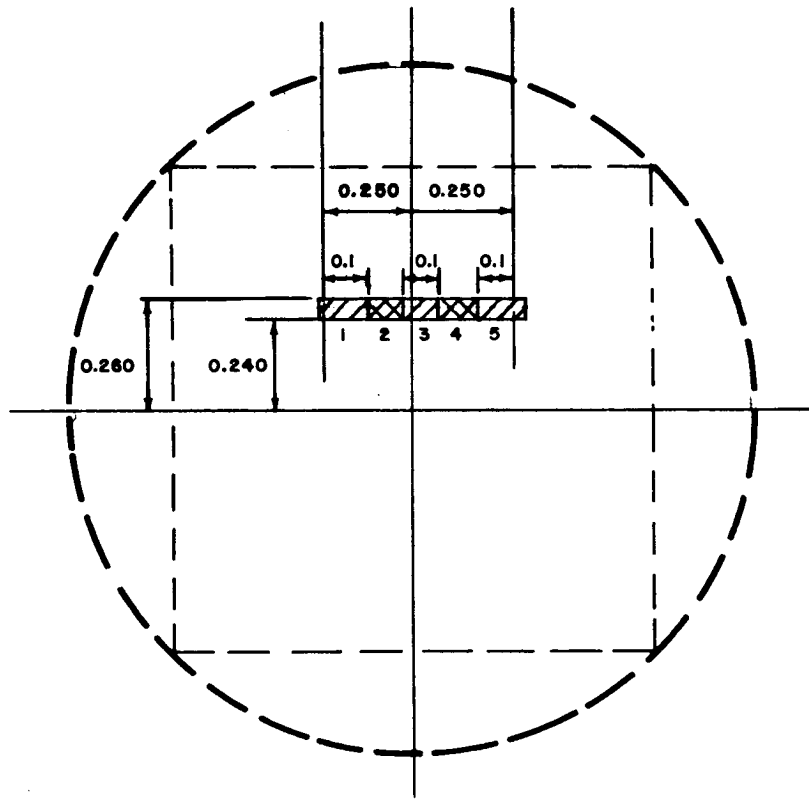
Figure 14 FIVE-COLOR FILTER

63-9249

The amplitude response can be improved somewhat by equalization, but this is done easily only in the horizontal direction, and then only at some sacrifice in signal-to-noise ratio. So, it seems best to limit the line density to a value at which the response is not too small at the upper end of the video band. We have chosen not to exceed 600 lines in square format. If, during the development of the camera system, experience under conditions of extended periods of "hands-off" operation indicates that this number should be changed, it will be reconsidered. No design changes will be needed, as a simple change in logic will change the raster.

3) <u>Time sequence considerations.</u> Once the decision to use tape buffering of the video data has been made, considerable flexibility is available in the choice of the scanning rate. At one extreme we might scan at the slowest possible rate, so that recording on the tape would be essentially continuous. For an assumed data rate of 3000 bits/sec, this would be 500 picture elements per second. On the other hand, very high speed scanning is also possible. We have chosen 25,000 picture elements/sec, a rate which is low enough so that low-power sweeps suffice, but high enough so that at periapsis, only about one in ten pictures will be recorded. At apoapsis, where the suborbital velocity is much lower, about one frame in 70 will be used. The reason for this procedure is so that automatic correction of exposure and focus can be achieved with time constants several frames in length, thus keeping these adjustments essentially constant during each frame that is recorded, but permitting smooth control, especially during transit of the terminator.

The procedure for selecting frames to be recorded is to integrate a smoothed analog voltage proportional to suborbital velocity. The next frame following the time when a preset level is exceeded will be recorded, and the integrator discharged. This will result, at worst, in variation of the overlap between 20 and 10 percent.

4) <u>Circuit design philosophy.</u> As far as possible, circuit techniques will be digital. Even where this results in a moderate increase in the transistor count, reliability is increased because such circuits are individually more reliable than analog circuits. In addition, lower power operation is feasible and certain conveniences, both in design and operation, result. One such convenience is the ability to operate on direct coupled, element-by-element basis. Thus, for an emergency mode of operation in which direct transmission is attempted at very low bandwidths, only the clock rate need be changed, and no other adjustments are called for. In addition, changes in raster size and line density , both automatically and by command, are very simple, as in the achievement of highly linear sweeps.

5) <u>Description of the block diagram.</u> Figure 15 shows the proposed design in functional block diagram form.
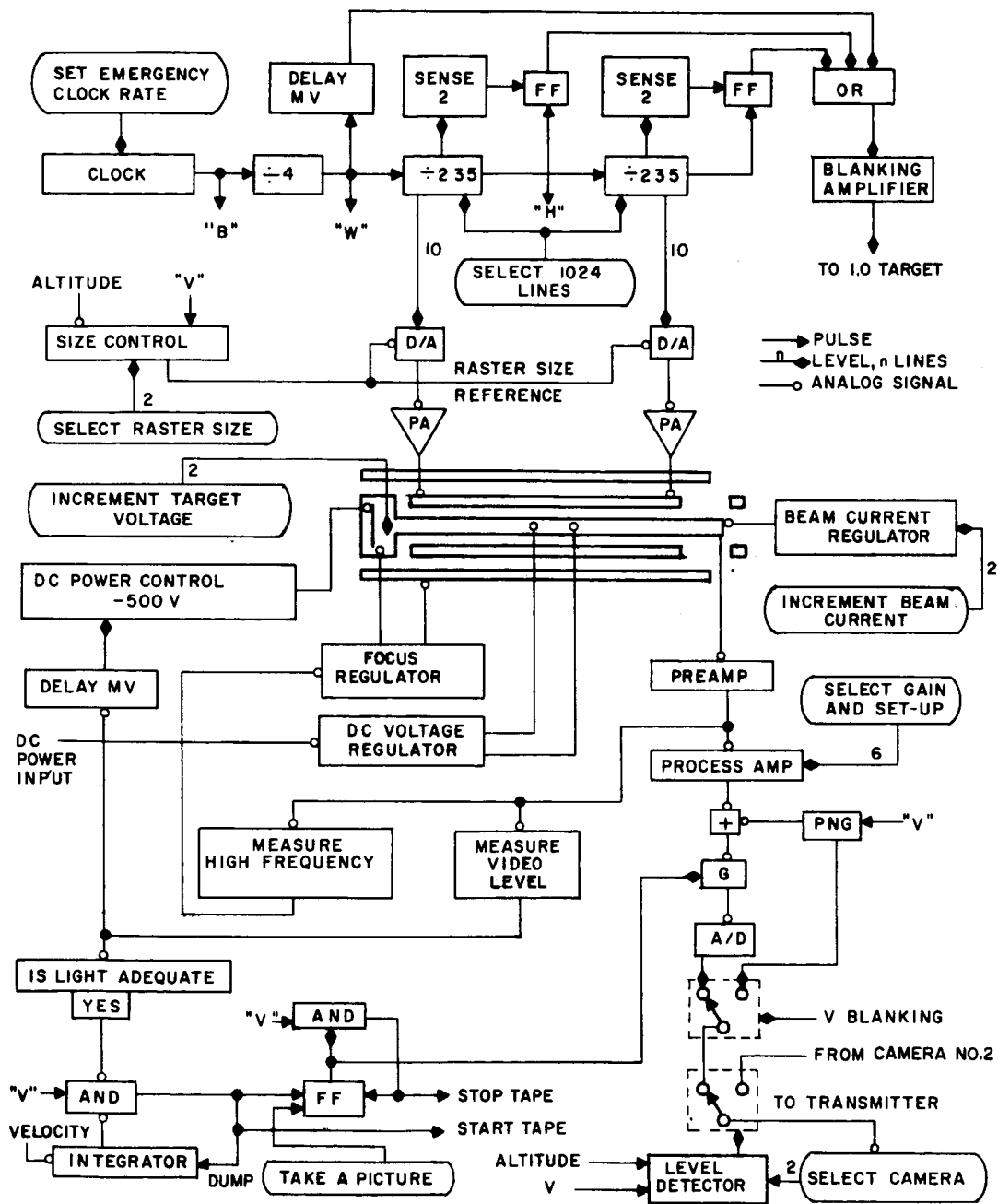
Figure 15 TELEVISION CIRCUITS SCHEMATIC

The scanning generator, a multivibrator clock generator, normally operating at 100 kc, times the entire system. On command, a much lower rate is available for the emergency mode. The clock frequency (B) is divided by 4 for word frequency (W), by N for horizontal frequency (H), and by N again for vertical (V). All dividers are binary, and the last two are adjustable, on command, from the normal 235 to 1024 in order to obtain a very high density raster. Since gates are also provided to detect the second step after reset, which is used to generate the horizontal and vertical blanking waveforms, which are OR'd for application to the target of the image orthicon, by the blanking amplifier. Note that element blanking, as well as line and frame blanking, is used. This permits a change in clock rate with no other adjustments since the beam-time-on per element is constant. Figure 16 shows details of the timing generators, using the horizontal divider as an example.

While analog integrator circuits could be used to generate sawtooth waveforms from the H and V pulse trains, recent experience with digital circuits has been so satisfactory that they are planned for this application. The method is to regard the state of the divider chain as a ten-digit binary number and to convert this to analog form in a resistance ladder, as shown in figure 17. The switches are saturated transistors controlled by the divider stages. The reference voltage for the ladder gives proportional control of sweep size, and is inversely proportional to the altitudes. This is accomplished by a nonlinear circuit using biased diodes in the usual manner. Note that the altitude at the beginning of the vertical sweep (at the time the exposure is made) must be held in a sample-hold circuit triggered by V. Ground command will permit selection of the largest or smallest raster, or a size appropriate for 1024 lines, rather than the automatically selected size.

The sweep amplifiers will be of the complementary type, as shown in figure 18. A bridge circuit as in (a) will be used if only one power supply is available, and a push-pull circuit, as in (b), if both negative and positive supplies can be used. In either case, a resistor R in series with the deflection coil is used to sense the current to supply a feedback signal.

6) Camera controls. Image orthicons require power supplies of -400 to -650 volts for the photocathode and 1200 to 1800 volts for the anode, with all intermediate voltages derived from these by means of a divider. Although tube-to-tube differences require adjustments in a large number of the electrode voltages and coil currents, it appears that satisfactory unattended operation may be achieved by presetting almost all of these to fixed values. In this category fall the photocathode voltage (during exposure) the electron multiplier voltages, G2, 3, and 5, the alignment coil current, and probably the target voltage as well. The beam current is controlled to a preset value by sensing the cathode current and adjusting G1 as needed. If more elaborate controls prove desirable, they can be developed along known lines.
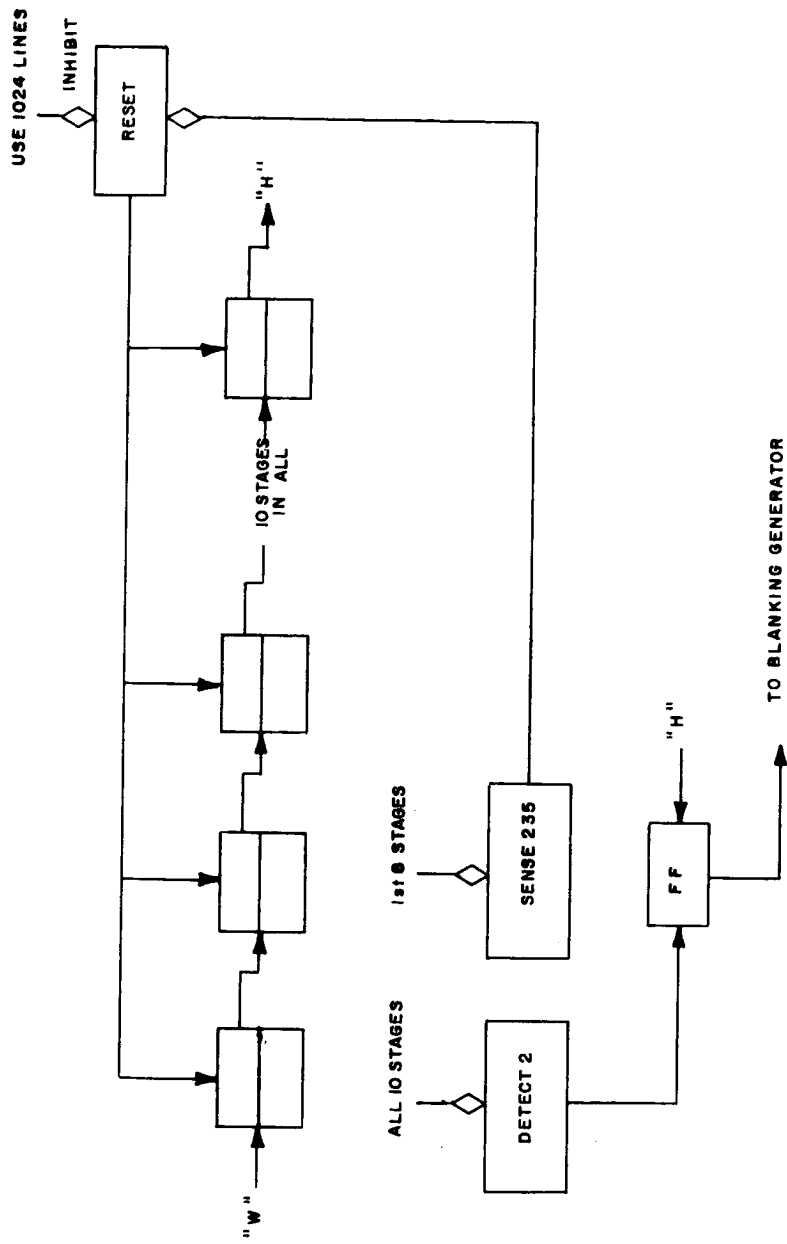
Figure 16 HORIZONTAL-DEFLECTION TIMING GENERATOR

63-9259

-49-
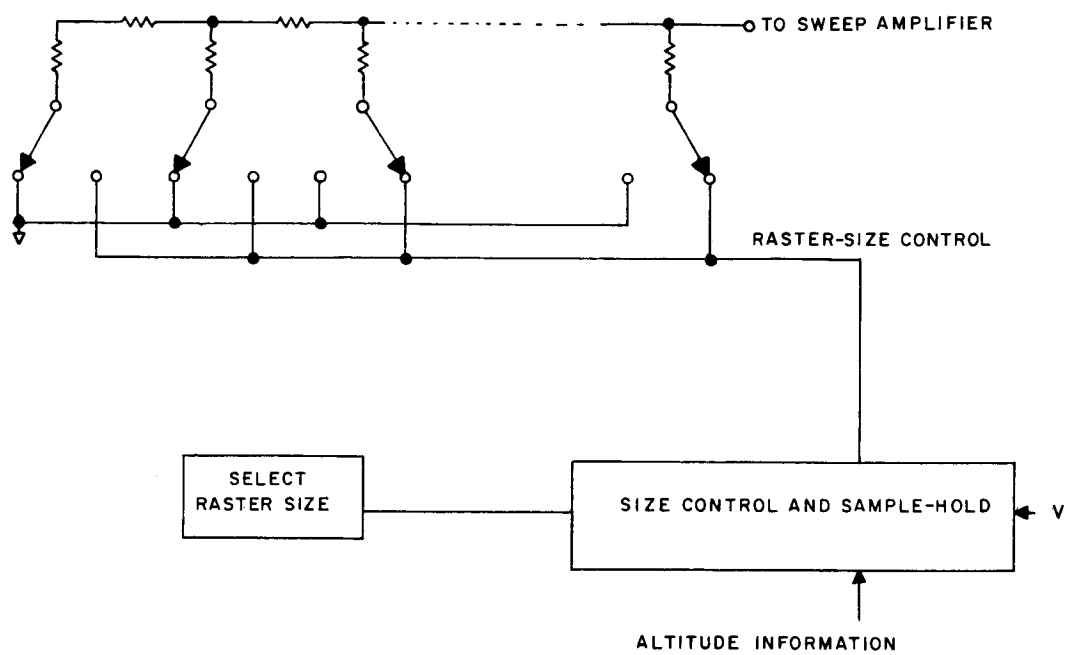
Figure 17 SWEEP AMPLIFIER
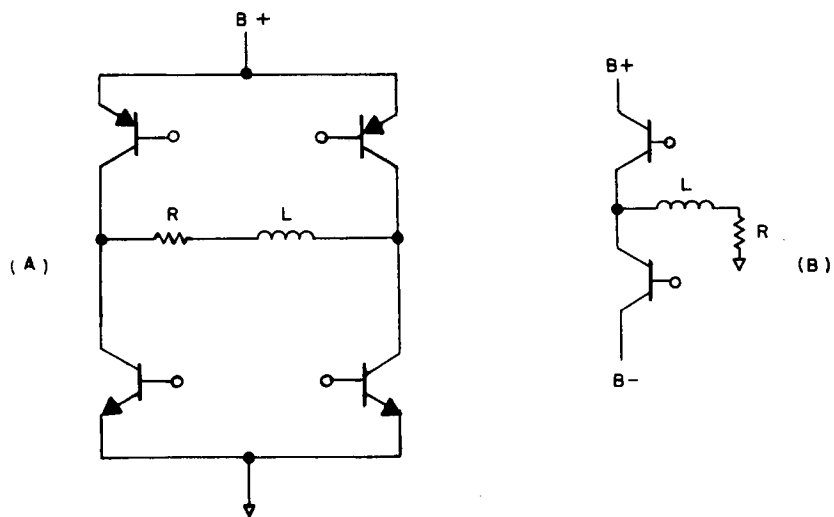
Figure 18 SAW-TOOTH GENERATOR

Since the focus depends on the tube temperature, and this cannot be precisely predicted or controlled in space (as in a studio camera it can be by adjusting the flow of cooling air), it will be necessary to adjust G4, G6, and the current in the focus coil. It is planned to do this by means of a hunting-type servo system in which all three are perturbed by a small ac signal, the resulting change in the energy of the high-frequency portion of the video signal is determined by a phase detector, and appropriate adjustment can be a fraction of a frame.

7) Video controls. The exposure time will be controlled by turning the photocathode on for an appropriate interval by starting and stopping the oscillator in the converter power supply. The control signal is derived by measuring the peak-to-peak video voltage over several frames. Since, in the image orthicon, modulation is by means of depleting the return beam, the blanking signal is applied to the target, causing the entire beam to be returned to the multiplier. Thus, black corresponds to maximum anode current, and it is the difference between this and the current corresponding to peak white which controls the exposure. For general purposes this is a completely satisfactory technique. However, there may be certain types of terrain in which the interesting details are of low contrast in some particular portion of the grey scale. For such scenes it may be desirable to "stretch" a portion of the grey scale to fill the input range of the analog-digital converter. A ground-controllable process amplifier having eight choices of "set-up" and eight of incremental gain will be supplied for this purpose. The process amplifier will also include aperture correction, which, of course, must be a function of the picture element spacing.

The video preamplifier presents no especially difficult problems. The image orthicon current may be expected to be about 0.1 microamp which is smaller than the value attained at normal scanning rates by the ratio of normal bandwidth to Voyager bandwidth. Thus, an input impedance of 250 kilohms which gives an input voltage of 1/40 v, will result in a value of Johnson noise just equal to the shot noise already in the signal. However, most of the total noise is amplified image orthicon beam noise, and can be expected to be much higher. Therefore, an input impedance even lower than 250 K can be used without penalty.

Note that at the highest altitude used with each lens, only about 15 percent of the image-tube target area is scanned. Thus, for equal photocathode illumination, only 15 percent of the lowest-altitude signal would be obtained. The automatic exposure control is expected to handle this variation very easily.

8) Pseudo-noise generator. In the Roberts technique, random noise is added to the analog video signal before quantizing and subtracted at the receiver after decoding. Since both noise waveforms must be identical, the "noise" must be a long deterministic sequence which seems to be random.

Such sequences are easily generated by shift registers in which the input is a logical function of the previous state. Since an N-bit register has 2^N states, rather short registers can generate long sequences. In this case the sequence should be somewhat longer than one frame. Since $2^{16} > 233 \times 233$, 16 stages will do.

A subsidiary advantage of the availability of the pseudo-noise generator is the opportunity to use it to generate "uniquely decipherable" synchronization signals. It is planned to transmit the pseudo-noise during the vertical blanking interval. On earth, synchronous detection using majority logic will be used to detect the start of each frame even if a few bits are in error. Since random sequences are essentially never found in natural video, it is highly unlikely that video will ever be mistaken for synch. In the case of horizontal synch, in which the transmitted pseudo-noise is only 6 bits in length, there is substantial opportunity for this to happen. In that case, a flywheel type of synchronization, similar to that used in TV receivers, is appropriate.

9) <u>Picture-sequence control.</u> Pictures are to be taken whenever the light is adequate and when sufficient distance has elapsed since the previous recording. The first is accomplished by means of a level detector, the input to which is the amplitude of the video signal. When this amplitude falls some preset amount below full scale, which implies that the maximum exposure time is being used, the output of the level detector inhibits the AND gate which controls the tape recorder start signal. The second requirement is met by means of a similar level control acting on the output of an analog integrator which operates on suborbital velocity information. The AND gate is inhibited until the required distance is exceeded, at which time, the next following V pulse sets a control flip-flop and also discharges the integrator. This gated pulse also starts the tape recorder. The next V pulse stops the tape. The FF output level also opens the gate which passes the analog-plus-pseudo-noise video to the Voyager A/D converter. Note that if some time is needed to start the tape recorder, a pulse train in advance of the V pulses can be derived.

Camera selection is accomplished by means of a level detector operating on the altitude signal, but changeable only coincident with a synch pulse. Since both cameras operate all the time, the only operation called for is to switch one signal or the other to the transmitter. A command is provided to select any one camera regardless of the altitude.

10) <u>Command system.</u> In addition to the previously mentioned commands, it is desirable to have incremental control of beam current and target voltage, since these are the principal controls used in studio cameras. Such incremental controls can be accomplished either with a solenoid-operated potentiometer or an up-down counter plus D/A converter. The latter has been used in the weight-power estimate, but a final decision will be made during the development period. Note that the estimates include the command registers and circuits necessary to carry out the controls, but not the command decoders themselves.

11) <u>Automatic focal length selection for detailed pictures.</u> It is desirable to take some high-resolution pictures in addition to the regular relatively low-resolution mapping pictures. To accomplish this automatically we can use the system of figure 19.

In this procedure, the analog video signal passes to an edge detector. This is a circuit which produces a pulse at each picture element where the instantaneous amplitude of the high-frequency portion of the video signal exceeds a threshold. These edge pulses are counted on a per-frame basis only when the short focal length lens is being used. When the number of such pulses exceeds a preset number in any one frame, the vertical synchronization pulse next following produces a signal which lasts just one frame. This signal is fed to the camera-select control, overriding it and causing a high-resolution picture to be recorded. The TV system then goes back to its normal operation.

Associated with the incorporation of this feature into the system are 6 analog transistors, 180 mw, and 36 digital transitors 360 mw/540 mw total additional power.

2.4 Venus Orbiter Microwave Mapping System

1. <u>Objectives.</u> The objectives of the mapping system are to determine topographical features, reflection characteristics of the surface, and radiation maps of surface emissions. This section treats only the radar mapping portion of the radar-radiometric mapping system. However, antenna considerations of the mapping system do include both the radiometric and radar. The microwave radiometer was selected from the list of scientific instruments furnished by NASA. Other possible mapping objectives are the determination of the depolarization characteristics of the surface to provide information for evaluating surface roughness, and near limb Brewster angle measurements.

The basic design of the radar is influenced by a number of factors in addition to the obvious restrictions imposed by power, weight, and reliability considerations. Combination radar and radiometer mapping should provide for simultaneous operation to allow for correlation of radar and radiometer measurements. Another factor is the maximum data rate allowed for transmission of radar and radiometer data. It should be noted that although radar mapping may be accomplished only on the order of 50 percent of the orbital period due to ellipticity of the orbit, data can be transmitted during the entire orbital period (excluding occultation time). However, a large increase in overall data capacity can be achieved only at the expense of providing extremely high data-storage capacity in the system.

2. <u>System description.</u> The radar system proposed here is an X-band pulsed radar capable of operating simultaneously with a fixed frequency
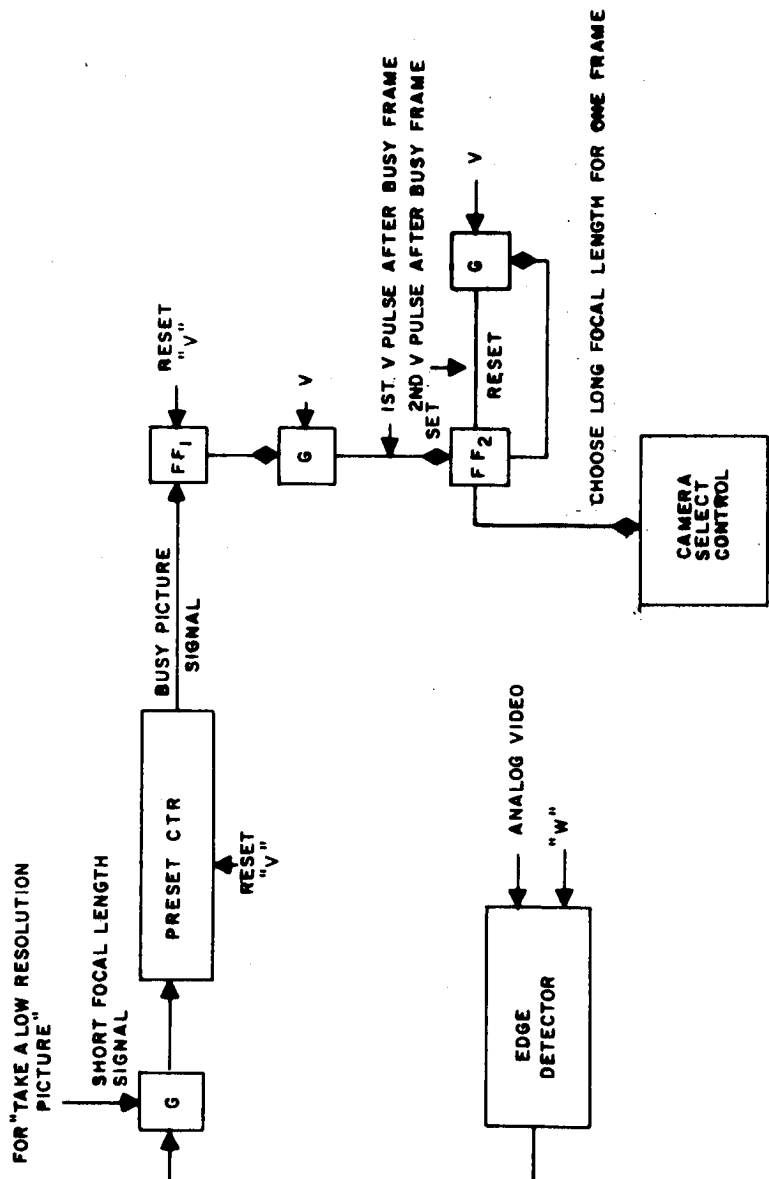
Figure 19 EDGE-COMPARATOR CIRCUIT

63-9287

-54-

radiometer operating at X- and Ku bands through a single 8-foot diameter antenna. The radar operates at a nominal 9500 mc; the X-band radiometer operates at a nominal 8500 mc. X-band was selected for the radar on the basis of available information on the atmospheric transmission characteristics of the planet Venus (Section B3a). The antenna is scanned in a two-way raster-type pattern (i.e., no flyback) with raster lines normal to the ground track. The radar beamwidth is slightly less than 1 degree.

For purposes of this study, a number of parameters were selected somewhat arbitrarily; further study is required to determine the final values. A one-microsecond pulse width was selected to provide a range resolution capability of approximately 0.15 km (500 feet). A pulse repetition frequency (prf) of 3000 pulses per second was selected to provide a high duty cycle and a correspondingly low ratio of peak-to-average power. A 15-kw peak (45 watts average) output power was used in the performance calculations. A nominal prf of 3000 provides an unambiguous range of 50 km or more than five times the height of Mt. Everest. (For comparison, a prf of 30 pulses per second or less must be used to provide unambiguous range at the maximum mapping altitude of 4000 km.) The prf may be varied to prevent blind spots and to resolve range ambiguities.

The proposed radar provides the following measurements. At small scan angles (up to several beamwidths off vertical), data will be obtained on the minimum and maximum ranges, corresponding to the highest and lowest surfaces detectable by the radar; this is termed contour mapping. Data will also be collected on the signal level of the received pulse integrated over parts of the range interval between the minimum and maximum ranges detected. At angles exceeding several beamwidths of vertical (depending on altitude), the range difference between the near and far edges (3-db points) of the beam exceeds the range resolution of 0.15 km, and accurate contour mapping is no longer realizable. Under these conditions the signal level of the received pulse is integrated over a range gated increment of the received pulse. This is termed area mapping. Signal level measurements are quantized in terms of 8 "grey levels" or amplitude levels. Video integration is used at all times to achieve adequate signal-to-noise values with the assumed transmitter power of 15 kw peak, 45 watts average.

Depolarization measurements can be readily provided by using parallel receiver channels and gating and integrating circuits, or by switching the outputs of the direct and cross-polarized channels to a single receiver. Further study is required to determine if the cross polarization measurements should be made.

Two scan patterns are planned for radar mapping (figure 20). The wide angle (area mapping) scan provides area mapping over the scan coverage described below. The contour mapping scan provides contour mapping, combined

-55-

RADAR MAPPING ZONE
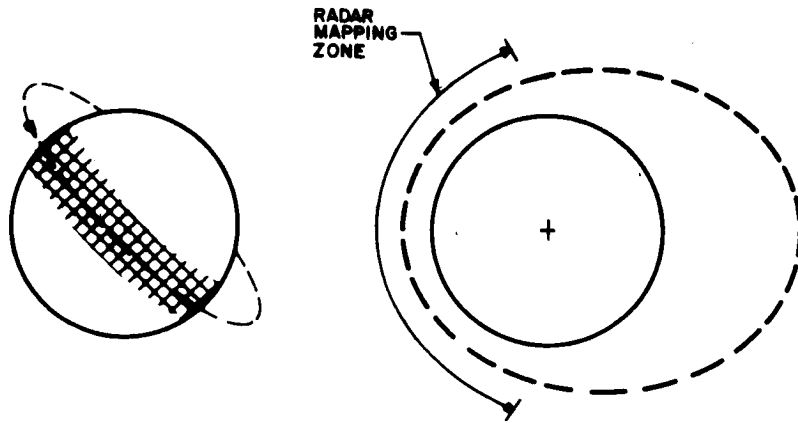
TYPICAL MAPPING SCAN

TYPICAL VOYAGER ORBIT
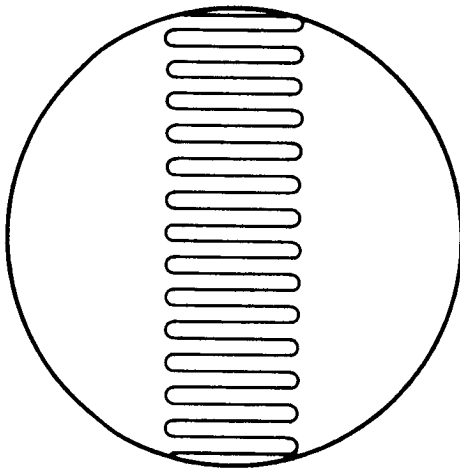
AREA MAPPING SCAN
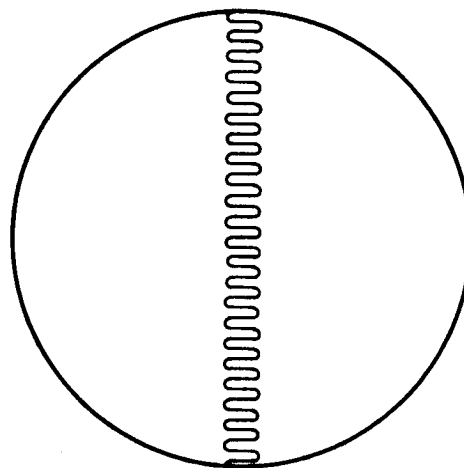
CONTOUR MAPPING SCAN

63—9262

(NOT TO SCALE)

Figure 20 ANTENNA SCAN PATTERNS

with a signal level measurement capability, at scan angles near 0 degree, together with a capability for improved surface resolution due to the slower scan rate. Details of the scan patterns and the scanning system are given below.

The area mapping scan would provide an "area" map of a belt varying from 3000 km wide at 4000 km altitude to 540 km wide at 1000 km altitude, if the scan limits were held constant. In practice, scan limits will be reduced with increasing altitude to achieve a more uniform scan coverage or constant belt width.

The contour mapping scan limits are varied from approximately ± 1.5 degrees at 4000 km altitude to ± 9 degrees at 1000 km; the resulting scan pattern on the surface is shown in figure 20. In the contour mapping mode, the antenna motion represents a compromise between maximum data rate, surface resolution, minimum detectable area, and other factors.

The proposed mapping routine consists of alternately mapping with the wide angle scan for a single orbit, followed by three or four orbits mapping with the contour mapping scan. This process is then repeated, until Brewster angle measurements are desired. These measurements can be made by extending the wide angle scan limit until the beam approaches the limb or the desired angle. The mapping routine described here (excluding the Brewster angle measurement) provides a high resolution contour map, together with a series of wide angle "area-reflectivity" maps.

3. Performance characteristics. Radar performance is considered in terms of the two general cases: 1) contour mapping at scan angles near zero degrees, and 2) area mapping (or signal-level measurements) at larger scan angles. For the first case, figure 21 shows minimum detectable area versus transmitter power for various values of altitude, telemetry bit rate, and data fineness (or number of bits per data point).

The curves are based on integration to achieve a signal-to-noise ratio of 13.5 db and therefore the results apply principally to the contour mapping mode. Note that for a fixed bit rate (corresponding to a fixed integration time), the minimum detectable area decreases with increasing transmitter power, as might be expected. Also, the figure shows that for a fixed minimum detectable area, lower bit rates result in decreased power requirements due to the longer integration times. The graphs of figure 21 are based on the assumption that the signal-to-noise ratio varies directly as $\sqrt{n}$ where n is the number of pulses integrated; this is a conservative assumption. Emphasis is placed on minimum detectable area so that the contour map will indicate as accurately as possible the highest and lowest points within each resolution area. The effects on mapping accuracy of varying pulse width, prf, range gate width, etc., are still under investigation. A more detailed discussion of the effects of integration on signal-to-noise ratio area resolution, etc., are given below.
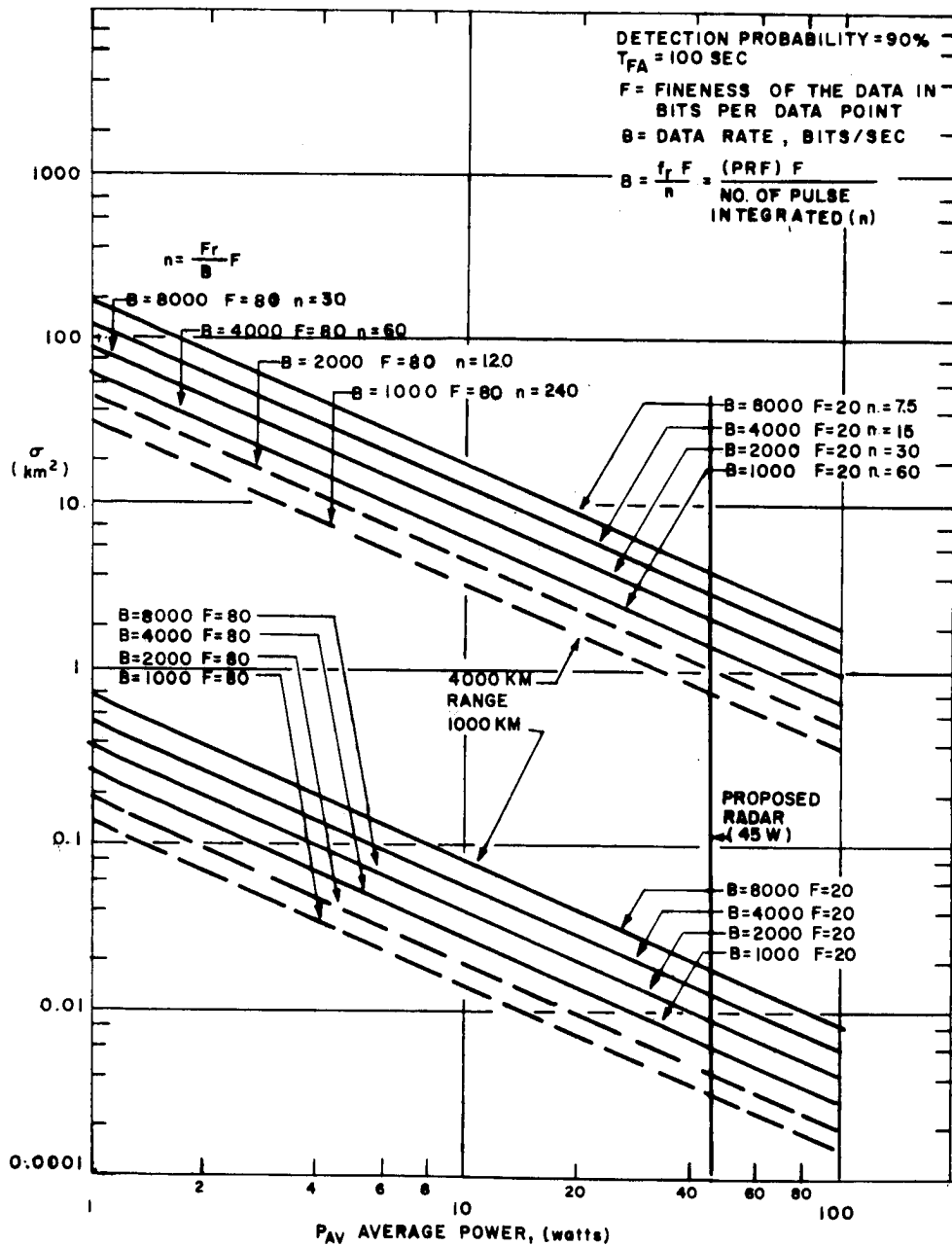
Figure 21 MINIMUM DETECTABLE RADAR CROSS SECTION σ VERSUS AVERAGE POWER

63-9263

-58-

Radar performance in the area mapping mode is best described somewhat differently, because the emphasis is not on detection of a minimum detectable area. The performance (minimum detectable area) shown in figure 21 is based on an "integrated" signal-to-noise ratio of 13.5 db, which corresponds to a probability of detection of 90 percent and a false alarm time of 100 seconds. An integrated signal-to-noise ratio of 21.3 db is required to provide the 8 grey levels for area mapping. Figure 22 shows area mapping performance in terms of transmitter average power versus scan angle for various values of range gate width, pulses integrated and telemetry bit rate. In this case the radar area is based on pulse width, beamwidth, and scan angle. Note that the data rates are relatively low; for the area mapping case, radar performance may be considered as power-limited. Current investigations are directed toward optimizing radar parameters, including pulse width, prf, range gate width and integration period, and angular scan limits.

Proceeding from the relationships indicated in figures 21 and 22, a basic approach to the design of the range-gated integrators and the tracker/programmer can be described. Assuming that contour mapping is the primary goal, values for transmitter power and minimum detectable area can be selected after the maximum telemetry rate is established. Using this value for transmitter power and considering the area mapping mode, the 21.3 db signal-to-noise ratio required for 8 grey levels can be achieved by various combinations of range gate widths and integration times. In this case, both range gate width and integration time influence the surface resolution obtained at moderate and larger scan angles off vertical. A proper choice of values leads to good surface resolution capability. If further study shows that the integration times for the contour mapping and area mapping modes are significantly different, variable integrators may be used as indicated in the radar block diagram. The integration constant required for best performance may also vary with the scan angle and altitude. The feasibility of providing such features requires further study.

a. <u>Selection of wavelength.</u> In one respect, the radar frequency should be as high as possible. For a given antenna size, a high frequency means a small beamwidth and, consequently, more detail in the radar map. Of course, the frequency selected must be such that radar components are readily available and that atmospheric attenuation is not too great. Of particular concern may be the recently reported possibility of a band of hydrocarbon surrounding the planet. Published works have been consulted to establish the current knowledge of the total atmosphere. The prime reference has been Edward Glaser (ref. 2) reporting the work of Chandra and Srivastava (ref. 3). The former states that an X-band signal would be attenuated by only 0.037 db in the atmosphere of Venus. Thus the current evidence, the necessity for good resolutions, and the knowledge that signals from Venus or its shell have been received at 2388 mc led to the choice of X-band (10 gc) for the radar frequency. Additional experiments and expansion of the atmospheric knowledge may indicate that the radar frequency should be modified.

n = NUMBER OF PULSES INTEGRATED

σ = $\sigma_o A_i$

σ_o = 0.1

A_i = $R B r \frac{c}{2}$ sec

BW = 0.0141 RADIAN

f_r = 3000 seconds^{-1}

$(S/N)_1$ = 21.3 db (8 LEVELS)

λ = 3 CM

T_{sys} = 1570°K

A_e = 2.81 M^2

r = 1 μSEC

a = GRAZING ANGLE

$P_{AV} = \frac{(S/N)_1}{\sqrt{mn}} \ Q^1 R^3 \cos a$

$m = \frac{GATE\ WIDTH}{PULSE\ WIDTH}$

$Q' = Q \frac{f_r}{\sigma_o B r \frac{c}{2}}$

$Q = \frac{\lambda^2 k T_{sys} 4\pi}{A_e^2}$

RANGE GATE = 15 μSEC
n = 83
B = 722

RANGE GATE = 30 μSEC
n = 83
B = 722

RANGE GATE = 15 μSEC
n = 415
B = 145

RANGE GATE = 15 μSEC
n = 830
B = 72

RANGE GATE = 15 μSEC
n = 1660
B = 36

RANGE GATE = 30 μSEC
n = 1660
BIT RATE B
B = 36 BITS/SEC

F = 20 BITS PER DATA POINT

$B = \frac{f_r F}{n}$

P_{AV}, watts

ψ, degrees

Figure 22 AVERAGE POWER P_{AV} VERSUS LOOK ANGLE ψ
ALTITUDE = 4000 KM

-60-

b. Radar resolution. At scan angles near zero, the surface resolution is determined primarily by the spacecraft altitude and antenna beamwidth. Other factors are pulse width, scan angle, scan rate, range gate width, and integration time.

The 8-foot antenna considered here provides a basic resolution (beamwidth) of slightly less than one degree. Corresponding resolution on the planet surface is approximately 15 km and 60 km at altitudes of 1000 and 4000 km respectively (for vertical incidence). The use of video integration tends to degrade surface resolution due to motion of the antenna during the integration process. For example, using a typical area mapping scan where the antenna moves one beamwidth on the surface (corresponding to 830 pulses transmitted) and an integration time of 27 milliseconds (corresponding to an antenna motion of approximately 1/10 beamwidth, the beam is "smeared" to 1.1 degrees. However, this degradation is more than offset by the sampling of the video integrator output at 27 millisecond intervals. This provides data points at intervals of 1/10 beamwidth (or approximately 6 km at 4000 km altitude) on the surface. Thus locations of unusual features might be determined to within 1/10 beamwidth. Therefore, at scan angles near zero, surface resolutions (normal to the surface track vector) of the order of 1.5 km and 6 km at altitudes of 1000 km and 4000 km respectively might be achieved. Resolution parallel to the surface vector would be one beamwidth, providing a rectangular resolution area. Increasing the scan speed to provide more scans per unit time could provide more uniform (approaching a square) resolution areas of approximately 5 km^2 and 19 km^2 at 1000 km and 4000 km altitudes respectively. This surface resolution would be improved by using a longer range gate, a slower scan speed, a shorter integration time, or a longer pulse width; however, the choice of these parameters is, of course, influenced by other performance considerations.

At larger scan angles, the use of range gating provides a control on "lateral" resolution (normal to the surface track vector). The beamwidth and altitude still govern the azimuth resolution (in the direction of spacecraft travel), except as noted above. The lateral resolution at a given altitude and scan angle is controlled primarily by the range gate width and the integration time, assuming transmitter power is fixed. The effect of range gating is to divide the elliptical shape of the beam (at the surface at larger scan angles) into near-rectangular sections whose lateral dimension (corresponding to range) is controlled by the range gate width. The effect of integration time is as indicated above, to blur or lengthen the beam shape in the range dimension.

Since both range gate width and integration time are used to improve the signal-to-noise ratio, either or both may be changed to improve the resolution. In general, the best resolution is achieved when the range gate width (projected on the surface) and the "blur distance" due to antenna motion during the integration time are approximately equal. These values are a function of scan angle and of the required signal-to-noise ratio. The graph of figure 22 shows

performance in terms of range gates of 15 and 30 μ seconds, and various values of integration time. The use of a range gate of 30 μ seconds and an integration time corresponding to integration of 83 pulses results in a lateral surface resolution of approximately 0.2 beamwidth. Using the proposed transmitter power (45 watts) allows scanning only to about ±17 degrees for this case. Achieving good resolution at greater scan angles requires a wider range gate and a longer integration time. In general, resolution capabilities should not degrade far beyond this value for a maximum scan angle of 20 degrees.

c. <u>Performance versus scan angle.</u> The principal effect of scanning at larger angles off the vertical is the change in the type of mapping information available. As noted above, accurate contour mapping is possible only at small scan angles. Figure 23 shows the effect of changing scan angle on ΔR, the range between the near and far edges (3-db points) of the beam, at an altitude of 4000 km. Figures 24 and 25 show additional detail. The radar has no means for determining surface contour variations with the range interval ΔR. On this basis, the two mapping modes (contour mapping and area mapping) described above are used.

A second effect of varying the scan angle is to increase range; however, this effect is small compared to the increase in range to variation of altitude due to orbit ellipticity. For a fixed orbital altitude, the effect of increasing range (due to increased scan angle) is to require a wider range gate or longer integration time in order to provide adequate signal-to-noise ratio for 8 grey level mapping. As noted above, the surface resolution should not exceed 0.3 to 0.4 degree if integration time and range gate width are carefully selected.

d. <u>Performance versus system weight.</u> The usual method of improving the overall performance of a well designed radar is to increase transmitter power, assuming antenna size is fixed. In this application performance can be defined in terms of achieving the desired signal-to-noise ratio (13.5 db for contour mapping and 21.3 db for area mapping) for a given value of target area σ, or a given resolution capability. In figure 21 the change in transmitter power with changing target area is shown explicitly. In figure 22 area mapping performance is indicated in terms of transmitter power required (at any given scan angle) to achieve a desired resolution capability, defined in terms of range gate width and integration time. (See section b, above, for a discussion of surface resolution versus range gate width and integration time.) Note that in the case of figure 22 "effective" target area can be related to range gate width and indirectly to integration time.

In either the contour mapping mode or the area mapping mode, increased performance requires increased transmitter power, and this is the principal factor in increased system weight. It is assumed here that additional range gated integrators will not be required. The exact effect of increasing transmitter power cannot be readily determined; however, a rule-of-thumb which is
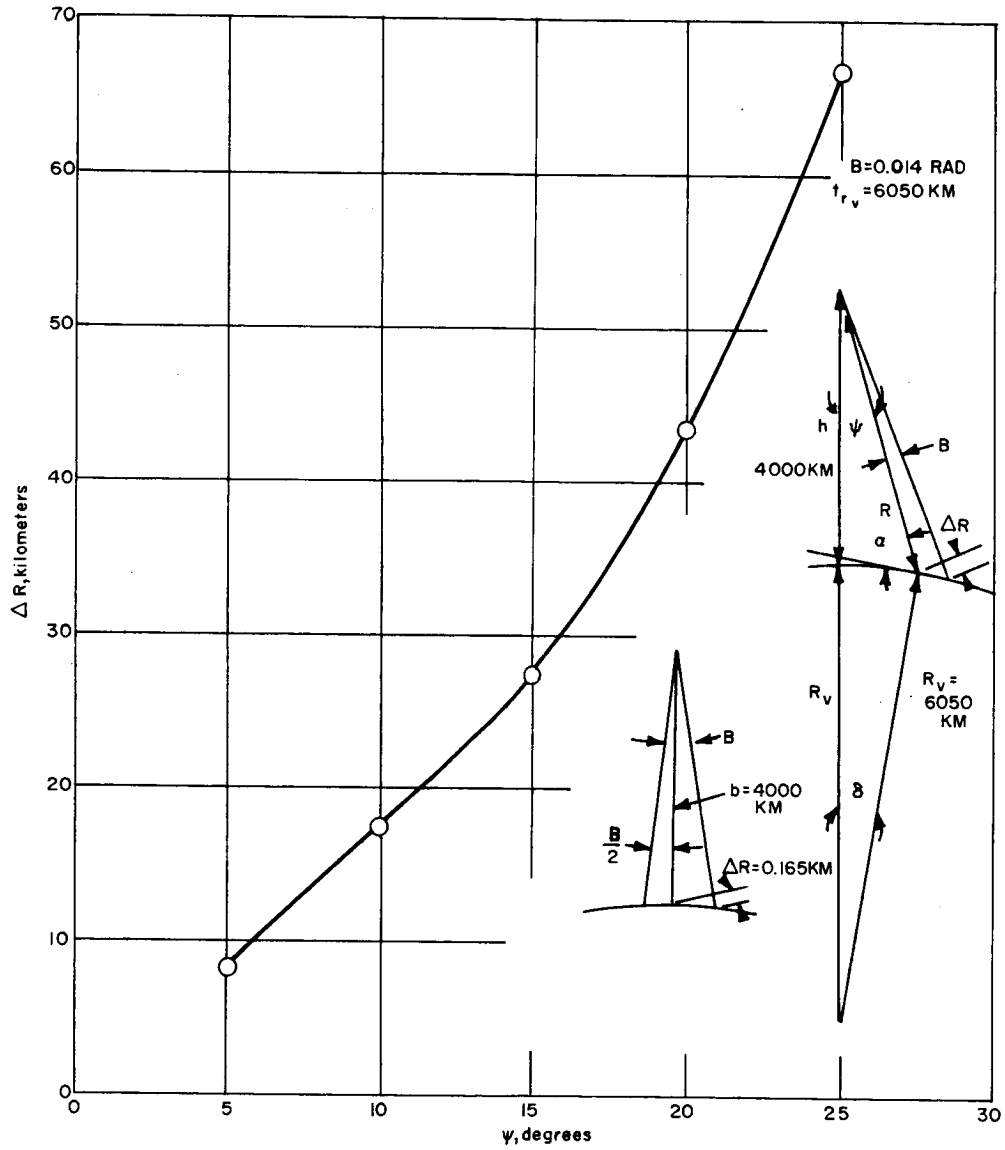
Figure 23 ΔR VERSUS ψ (h = 4000 KM AND ψ = 5 TO 25 DEGREES)

63-9265

-63-

ΔR (km)

10

9

8

7

6

5

4

3

2

1

0   5   10   15   20   25   26   27

Ψ degrees

h = 1000 km

$\psi + \frac{B}{2}$ Ψ   B

ΔR

R_V $R_V = 6050$ KM

ACTUAL LOOK ANGLE
$= \Psi + \frac{B}{2} = 8.5 + \frac{0.8}{2} = 8.9°$ FOR

ΔR = 2.5 KM

Figure 24 ΔR VERSUS ψ (ALTITUDE = 1000 KM)

-64-

Figure 25 ΔR VERSUS ψ OR ϵ (ALTITUDE = 4000 KM)

63-9267

-65-
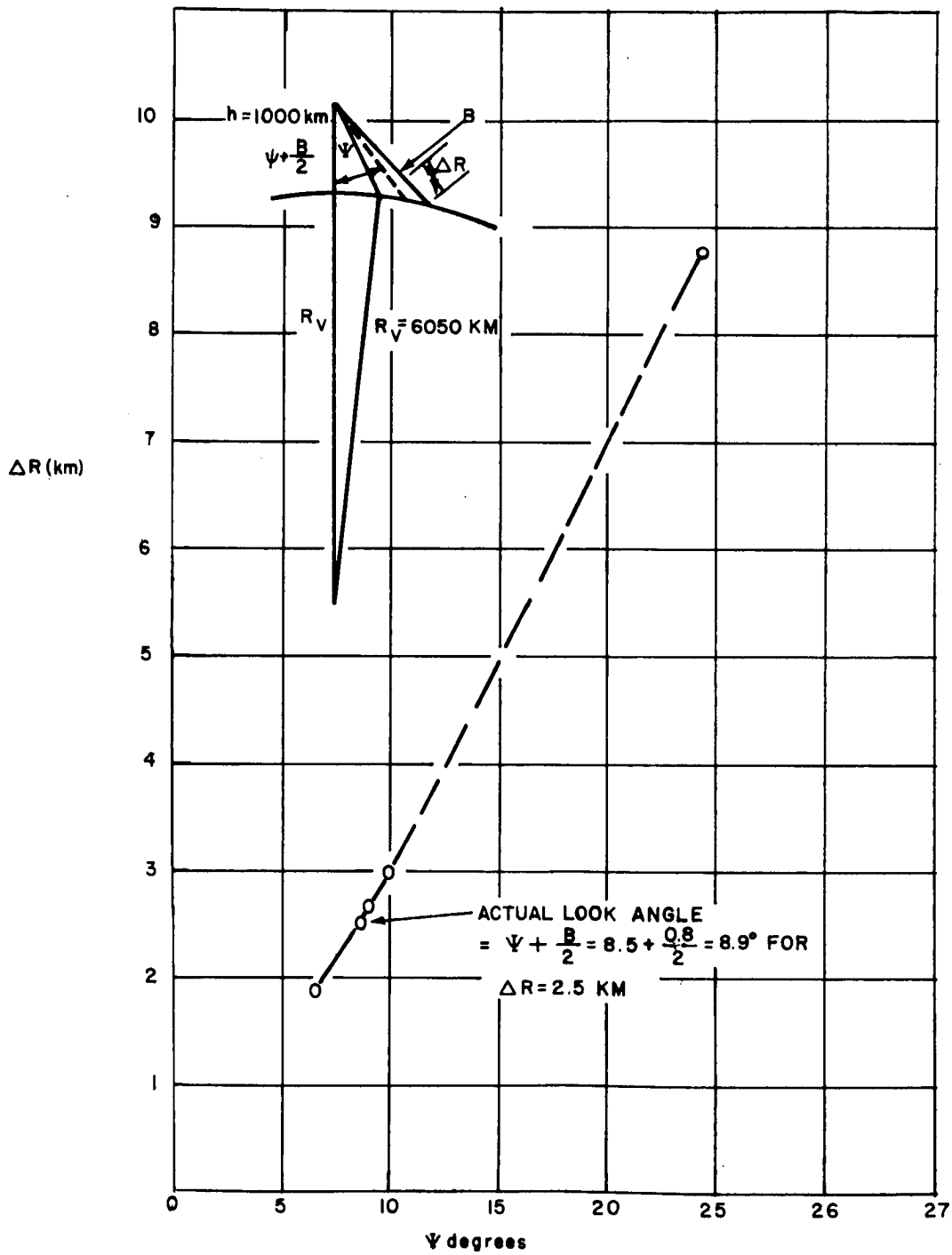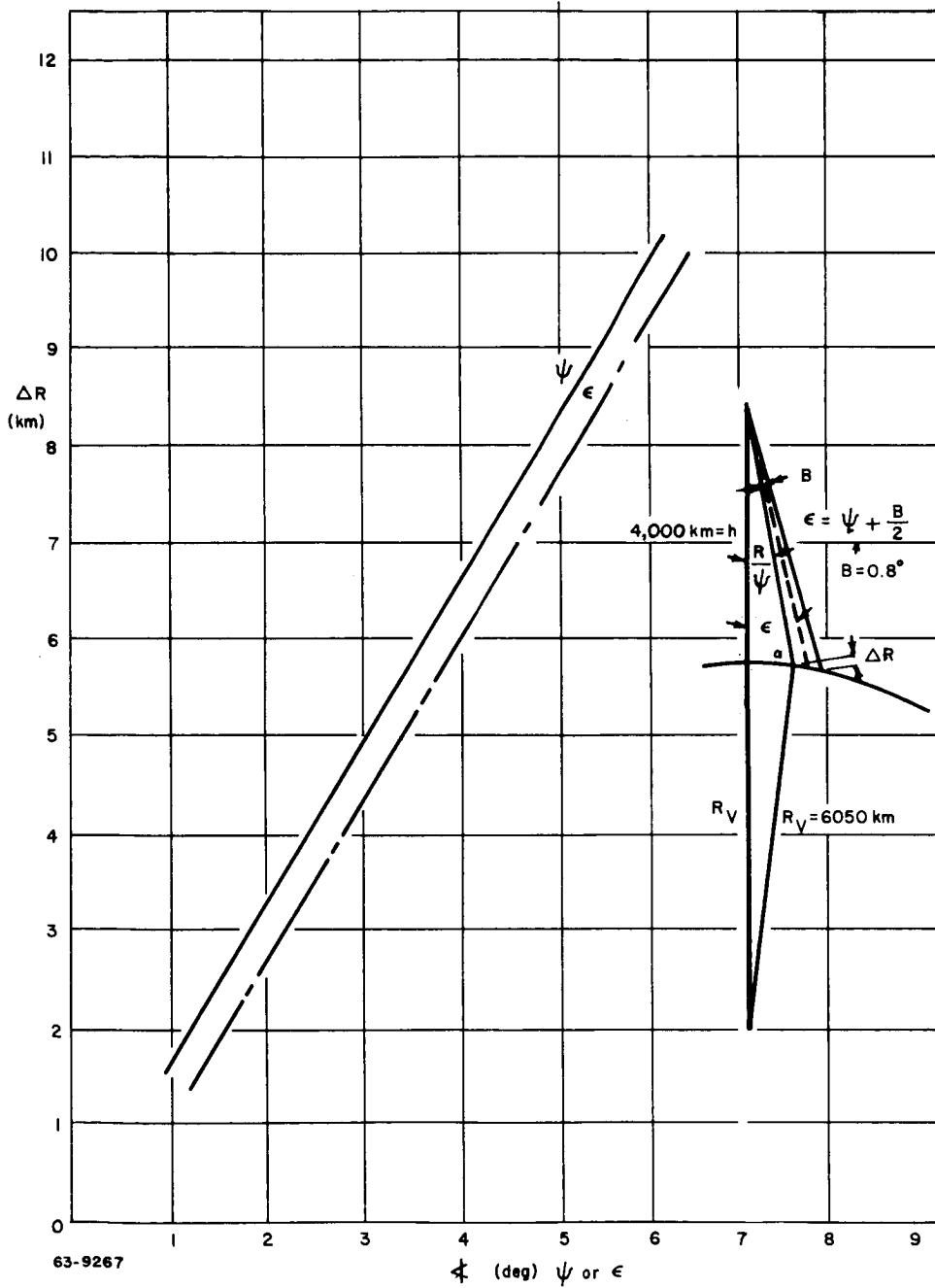
used is that modulation weight varies directly as peak power in kw, and output stage weight varies directly as the square root of peak power in kw.

    e.   <u>Alternative systems.</u> An alternative system configuration that was studied is FM/CW radar. Its possibilities are still under investigation. Sidelooking radar mapping techniques were also investigated. The results indicated that the latter correlation technique might be used to provide improved surface resolution along the direction of the surface track vector, if provision were made to eliminate the merging of the doppler-broadened spectral lines in the received waveform. Further study is required to determine the advantages of these correlation techniques over other methods of obtaining improved surface resolution.

Sidelooking radar as a mapping techniques provides two resolution parameters, namely doppler filter bandwidth (along the velocity vector) and pulse width (in the direction normal to the velocity vector). Varying the pulse width allows one to change the resolution in one dimension without physically altering the antenna. Under specified conditions the other resolution dimension can be altered without physically altering the antenna by varying the doppler filter bandwidth. The necessary and sufficient condition required to perform this is that $2f_d < f_r$ where f_d is the doppler frequency, and f_r is the radar prf. Thus the returns can be plotted in a three-dimensional space of power, time, and doppler frequency.

The high prf required by the inequality given in the preceding paragraph is necessary to prevent merging of doppler components of adjacent spectral lines. This requirement for high prf is incompatible with the low prf required to avoid range ambiguities. One approach to this problem is to use a wide open receiver (no doppler filters); the performance characteristics of such a system were investigated and found to be generally similar to those of a scanning type radar.

One notable exception to the above is the relatively poor lateral resolution capability (resolution normal to the velocity vector) of the sidelooking technique when looking vertically downward. Lateral resolution varies directly as the pulse width and may be extremely poor at vertical incidence when using long pulses. Another disadvantage associated with the sidelooking technique is the inability to distinguish between mountains at larger scan angles (off vertical) and sea-level returns at smaller scan angles when both arrive in the same range interval. For example, a 30,000-ft mountain at seven degrees off vertical may appear at approximately the same range as sea-level return from directly below the spacecraft.

Considering the foregoing, conventional sidelooking radar mapping techniques appear to be unsuited for planetary mapping missions; the deficiencies are inherent in some cases.

4. <u>Subsystem descriptions.</u> A block diagram of the mapping radar is shown in figure 26. Pulses formed in the pulse-forming network are triggered by the prf selector at a nominal rate of 3000 pps. The tracker programmer provides inputs to the prf selector to prevent eclipsing or to allow range ambiguity resolution. The pfn generates one-microsecond pulses which are amplified to provide drive for the modulator. The output of the magnetron at a frequency of 9500 mc is fed to the antenna through the microwave circuits shown in figure 27. The nominal output power is 15 kw peak, 45 watts average. The radar antenna is a mechanically scanned 8-ft paraboloidal dish; details of antenna construction and the scanning technique are discussed below. Primary power is estimated at 175W; weight and volume (exclusive of antenna systems) are 32 lb and 4.5 ft^3; antenna and drive mechanism is estimated at 30 lb.

The received signal passes through a preselector filter to the tunnel diode autodyne converter. A receiver noise figure of 6 db was used in the performance calculations. A reference signal may be fed into the preselector to permit system calibration using a known noise or signal level. The bandwidth of the IF circuits is a nominal 1 mc; the IF amplifier gain is linear over a range of 40 db. The output of the video amplifier is fed to the range-gated video integrators, where the noncoherent integration is used to provide acceptable signal-to-noise ratios.

a. <u>The range-gated video integrators.</u> The range-gated video integrators and associated circuits are key units in the mapping operation and will be discussed in more detail. The range-gated video integrating circuits are required to achieve adequate signal-to-noise levels for the contour mapping and for the radar area measurements. The integrators are connected in parallel to the output of the video amplifier. The range gates are controlled by the tracker programmer to provide leading-edge and trailing-edge tracking of the received pulse for minimum and maximum range measurement (contour mapping), and also to allow integration over any desired part of the received pulse for signal level measurements.

In the contour mapping mode, a stack of five range-gated filters is used to bracket or track the leading edge of the received pulse, and a similar stack is used to track the trailing edge, in a manner similar to conventional leading-edge tracking. Each of these range gates is one microsecond wide. Range is measured to an accuracy of approximately 0.15 km, corresponding to one microsecond, by the conventional measurement of time from the last "main bang."

The tracker/programmer provides a number of functions, including the following: (1) it acts as a tracking loop to control the location of the range gates for leading and trailing edge tracking; (2) it controls the locations and widths of gates in radar area measuring; (3) it controls the integration time by controlling the sampler switch; (4) it controls the time constant of the integrator if a variable time constant integrator is used; (5) it controls insertion of the receiver calibration signal; and (6) it also controls the prf to prevent blind spots and
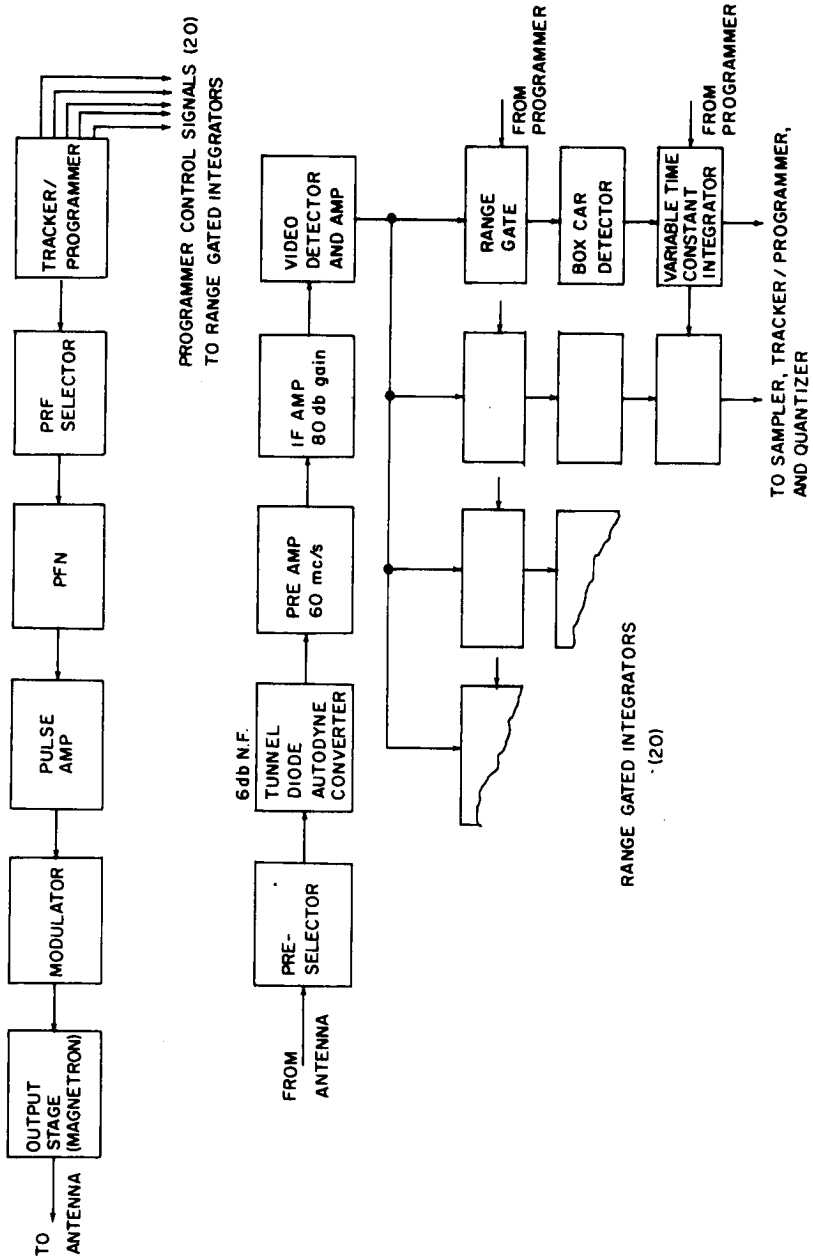
Figure 26 VOYAGER RADAR BLOCK DIAGRAM

-68-

63-9268

ORBITAL ROTATION
AXIS

SCAN
AXIS

SPACECRAFT
VELOCITY
VECTOR

TO
PLANET

SIDE VIEW

SCAN
AXIS

ORBITAL
ROTATION

AXIS

SPACE-
CRAFT
STRUCTURE

TO
PLANET

FRONT VIEW

ORBITAL
ROTATION
AXIS

SCAN
AXIS

SPACECRAFT
STRUCTURE

BOTTOM VIEW

NOTE:

SCAN AND ROTATION AXES
WILL BE LOCATED TO
REDUCE REACTION EFFECTS OF
ANTENNA MOTION
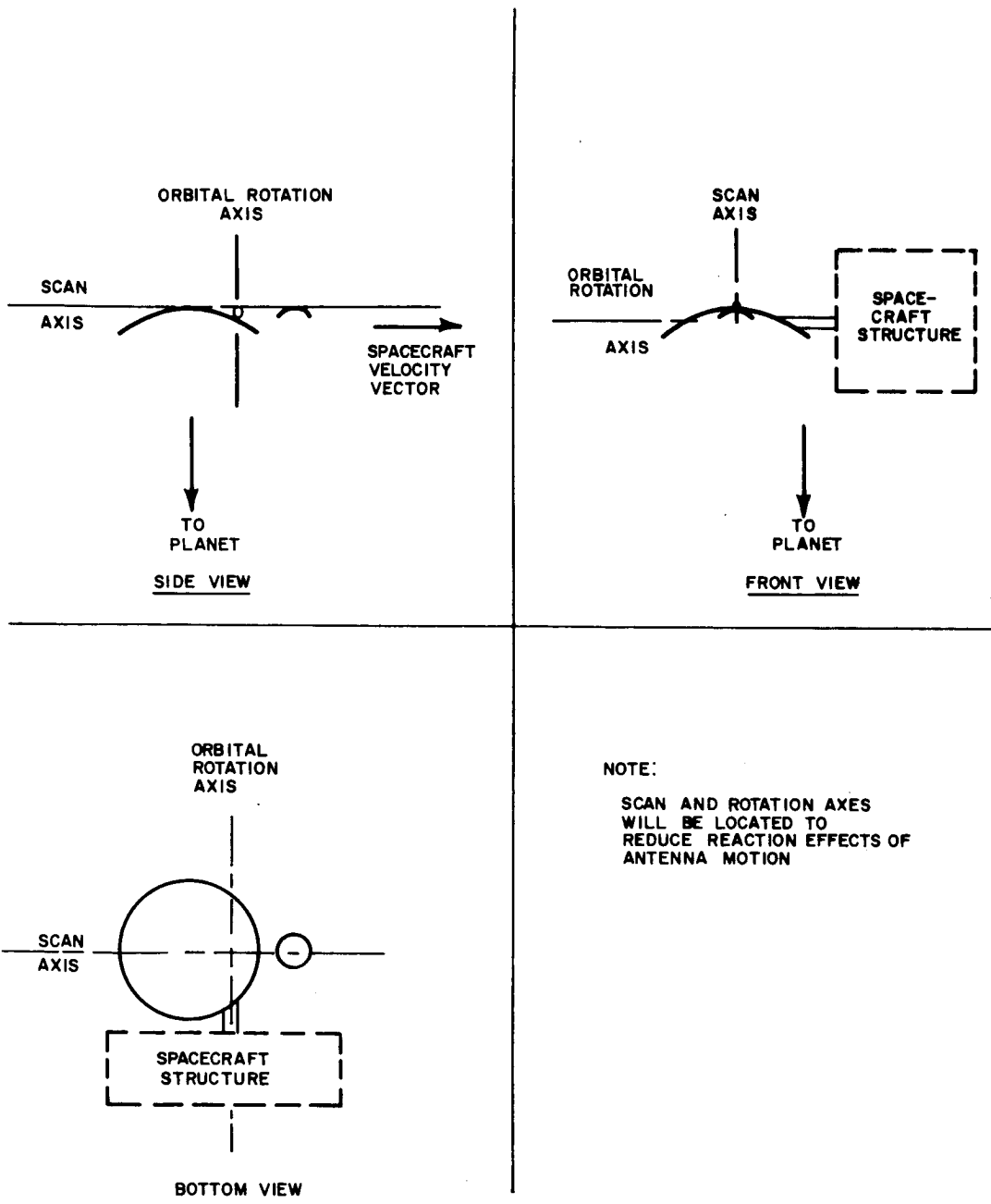
63-9269

Figure 27 ANTENNA CONFIGURATION

resolve range ambiguities. When a part of a received pulse is gated to an integrator channel, the signal is fed to the box-car detector whose output is applied to the integrator. After the integrator has received the proper number of range-gated pulses (corresponding to the integration time), the sampler obtains an analog output from the integrator, and successively from all other integrators in operation. If leading edge tracking is being performed, the output may or may not exceed the threshold. The tracker programmer compares the outputs of the five tracking channels and adjusts the locations of the range gates so that the middle channel occupies the range position where the target was detected on the previous sampling cycle. When radar area measurements are being made, the sampler outputs are directed to the tracker for ranging purposes, and to an analog-to-digital converter or quantizer prior to transmission to the storage or the telemetry unit.

The interval between the leading and trailing edges of the received pulse (the length of the pulse) is determined by the range between the nearest and most distant areas detected. Ten additional range-gated integrators are used to provide radar area (combined area-reflectivity) measurements over this range interval between the leading and trailing edges. The number to be used represents a compromise between considerations of equipment weight and maximum telemetry and the desire for providing good range resolution through a large number of range gated units. Each of these ten units operates on a 10 microsecond or 1.5 km range gate in the contour mapping mode. This provides a capability for ten measurements of signal level over an altitude range of approximately 15 km.

In the area mapping mode, all twenty range-gated integrators are used for radar area measurements in a manner similar to that indicated in the previous paragraph, except that each unit may be gated "on" for up to approximately 16 microsecond or 2.4 km. The twenty range gates then "cover" the interpulse period (a nominal 333 microseconds) between main bangs. As the antenna approaches the wide-angle scan limit, the returned pulse is "stretched" due to the extended area within the beam (for a scan angle of 20 degrees at 4000 km altitude, the returned pulse is 290 microseconds long). It should be noted that this pulse stretching characteristic sets an upper limit on scan angle for a given prf, since overlapping of the received pulses is undesirable.

The time constant of the integrators is based on the number of pulses to be integrated. This value can in turn be related to the prf and the angular scan rate to determine the amount of antenna motion (or beam smearing) during integration. The disadvantage of lower surface resolution due to beam smearing (or integration) must be weighed against the improved range performance (in terms of minimum detectable area) resulting from integration. A third factor influencing integration time is the maximum allowable telemetry rate. Reducing the integration time reduces the beam smearing but increases the number of measurements per unit time; the maximum allowable telemetry rate tends to

set an upper limit on the measurements per unit time, and a lower limit on integration time. Integration time, in turn, strongly influences map fidelity; good map fidelity requires that the minimum detectable area be as small as practicable (indicating a longer integration time).

        b.   <u>Antenna configuration and scanning characteristics.</u> The antenna configuration proposed for the mapping system has two parabolic dishes, each independently gimballed to scan across the planet normal to the ground track (see figure 28). A 2-ft diameter dish is used for radiometric mapping at 4 and 8 mm. An 8-ft diameter dish is used for radiometric mapping at 1.5 and 3 cm and for radar mapping at 3 cm. The 8-ft antenna is capable of receiving two orthogonal polarizations; coax-fed log-periodic feeds are used for broadband operation. The smaller antenna may use a log periodic feed or a modified horn. The microwave signal separation circuits associated with the antennas is shown in figure 27.

        The antennas are gimballed and driven independently on the scan axes to allow the smaller antenna to scan to the limit of the planet while the larger antenna is scanning over a smaller angle, mapping the surface. If feasible, the scans will be in opposite directions and synchronized so that the reaction torques about the scan axes will tend to cancel.

        The antenna scan patterns are shown pictorially in figure 29. This scan pattern is achieved by moving the dish as shown in figure 30. This represents a desirable scan pattern for wide angle mapping. The scan angle for the larger antenna will be adjusted periodically to allow scanning to the horizon for Brewster angle measurements; also the scan angle during radar mapping may be adjusted for altitude and received data variations in order to maximize radar mapping information. The feasibility of counterscanning (in opposite directions) the two antennas under these conditions requires further investigation.

        The weight of the entire antenna assembly, including drive mechanisms is estimated at 30 pounds. This does not include provision for special fixtures for protection against the stress environment during launch or for reaction control devices. The final antenna design will represent a compromise between a heavier antenna capable of withstanding the launch environment without special fixtures, and an extremely light antenna which tends to minimize drive power requirements and guidance and attitude control problems after launch.

        Other types of antenna configurations investigated for this application included various electronic and low-inertia scanning systems, and also systems which are sometimes referred to as "signal-processing" antennas. Most of the electronic scan and low inertia scanning systems were rejected because of the difficulties imposed by the combined requirements for dual polarization and broad-band operation. It should be noted that some of these scanning techniques would receive serious consideration if the requirement for broadband operation were dropped. The investigation of other antennas (Mills Cross, synthetic
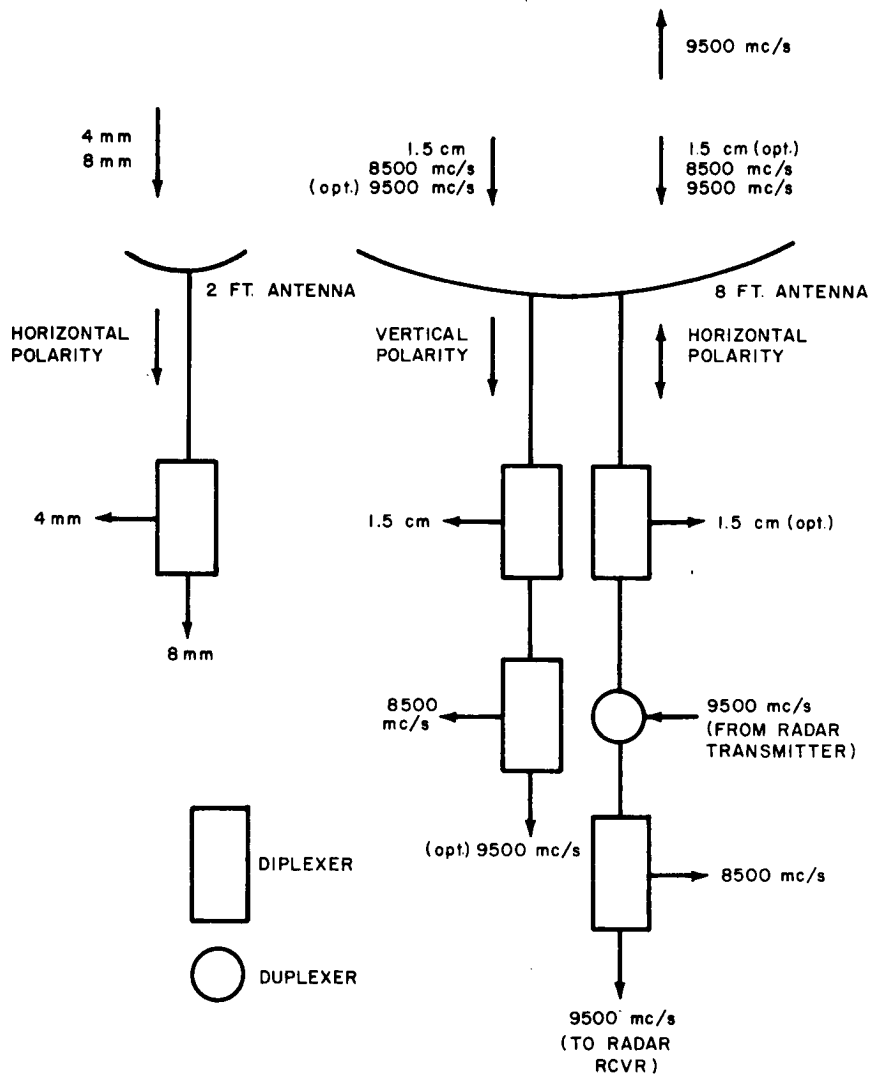
Figure 28 MICROWAVE SIGNAL SEPARATION CIRCUITRY
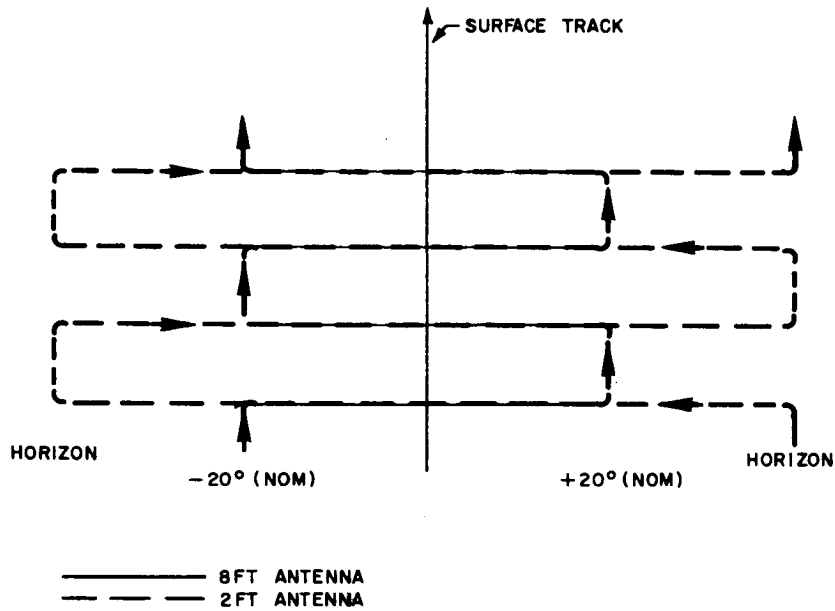
NOTES:
(1) LINES INDICATE LOCATIONS OF CENTER OF BEAMS ON PLANET SURFACE
(2) ANTENNA MOTION PROVIDES NEAR-UNIFORM ILLUMINATION FOR 3 CM BEAM
(3) FIGURE SHOWS COUNTER SCANNING MOTION OF DISHES

63-9271

Figure 29 MAPPING ANTENNA TYPICAL SCAN PATTERN (WIDE-ANGLE SCAN)

-73-

MOTION ABOUT SCAN AXIS

TIME ——→
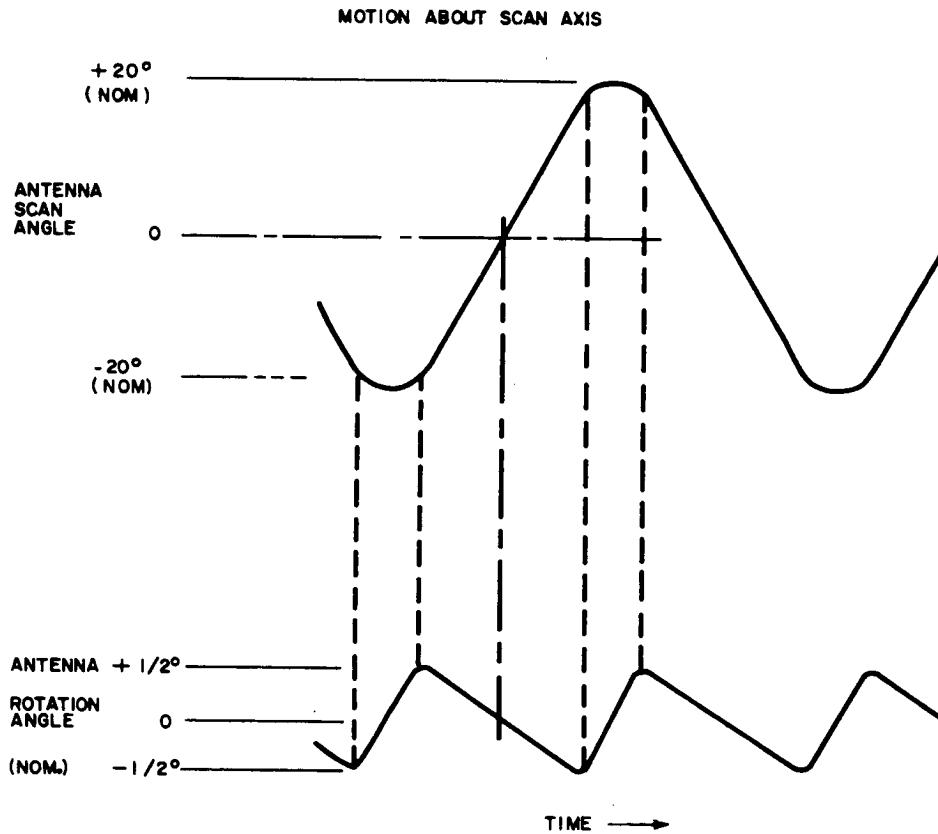
MOTION ABOUT ABOUT ORBITAL ROTATION AXIS
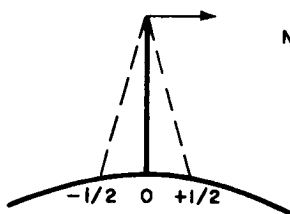
NOTE:

AN ADDITIONAL ROTATION (FROM + TO − ANGLE)
ABOUT THE ORBITAL ROTATION AXIS IS
REQUIRED (FOR PLANETOCENTRIC ATTITUDE
POSITIONING OF ANTENNA PLATFORM) AS THE
VEHICLE ORBITS THE PLANET

63-9272

Figure 30 ANTENNA BEAM POSITIONING VERSUS TIME

aperture antennas, etc.) indicated that increased performance (better surface resolution) was usually obtained at the expense of decreased sensitivity and a significant increase in on-board data processing equipment. In general, the comments above regarding dual polarization and broadband operation also apply to this class of antenna systems.

3. COMMUNICATIONS

PART I -- MARS ORBITER

3. 1 Communication System Requirements

The Mars orbiter-bus communications system monitors and transmits to Earth scientific and engineering data acquired during the transit and orbital phases of the mission. It also receives commands from Earth at any time, aids the DSIF in obtaining range measurements, and acts as a relay station for the Mars lander.

The operational life of the Mars orbiter-bus is approximately 15 months, 10 of which are spent in transit, the remainder in mapping the planet surface. During the in-transit phase, the orbiter -bus and lander (the spacecraft) are attached to each other. After injection into orbit, several maneuvers will be made to place the spacecraft on a near-miss trajectory with Mars. During these maneuvers, the guidance and control system performance and the response of the orbiter-bus is transmitted to DSIF. Throughout the in-transit phase, the engineering status of the spacecraft must be determined.

At a distance of approximately one million kilometers from Mars, the lander will be separated from the orbiter. After separation the orbiter-bus must be capable of receiving data transmitted from the lander. As the orbiter-bus nears the planet, final maneuvers will occur to place the orbiter-bus in an elliptical orbit around Mars. This orbit will have a 1700-km periapsis and a 10, 000-km apoapsis. While in orbit, the orbiter-bus must map the planet surface and be capable of receiving data from the lander.

Communication System General Description

1. <u>General Description.</u> The Mars orbiter-bus communications system will transmit all data required during the orbital phase through either of two highly directional S-band communication links. The main communication link consists of a steerable 8-foot parabolic antenna and a 120-watt transmitter. This system is used primarily to transmit the mapping data acquired during the orbital phase. At a transmitted bit rate of approximately 4600 bits/sec, a worst case data performance margin of +2. 19 db can be expected at a worst case range of 3.6×10^8 km.

The secondary communication link consists of a steerable 4-foot parabolic antenna and a 35-watt transmitter. This system is used primarily to transmit

the guidance and control and engineering status data acquired in transit. At a transmitted bit rate of 300 bits/sec a worst case data performance margin of +4.58 db can be expected at a range of 3.6×10^8 km.

These two links serve as redundant backups to each other, however, with the 4-foot parabola, a reduced amount of mapping data will be transmitted.

Each of these links will contain coherent transponders to aid the DSIF in making range measurements. They will also include command receivers to receive commands from Earth.

Commands normally will be received through a separate command system. This system consists of an antenna subsystem providing isotropic coverage and doubly redundant command receivers. While in the orbital phase when the orbiter-bus is at or near periapsis, commands cannot be received due to the high rate of change of doppler. During a large part of the orbital period, however, the rate of change of doppler is low enough for the command receiver to operate properly.

While in transit, maneuver exercises will be transmitted in real time. During the long intervals between maneuvers, engineering data will be stored periodically for transmission to the DSIF on command.

The data transmitted by the lander after separation and again after landing will be received through a VHF pulsed linear chirped receiving system. This system will include a 65-degree helix antenna and a pulsed linear chirped receiver having a pulse compression gain in signal to noise ratio of +20db.

An S-band radar altimeter will be used by the orbiter to control the focusing, picture-size and picture-sampling rate of the mapping equipment. At orbit altitudes less than 1800 km, this altimeter will transmit bursts of 5 pulses which, if received by the lander, will signal the lander to begin transmitting its stored scientific data.

Three tape recorders will be used to store the data acquired by the orbiter, two for mapping data and one for recording the received data from the lander and the scientific and engineering status data from the orbiter. The two mapping recorders alternately will store and play out data on each orbit. The total mapping data acquired during one orbit will be stored in one tape recorder. During the next orbit, this stored data will be transmitted to Earth while the second recorder is storing mapping data.

The multiplexing equipment on board the orbiter will be similar to, but less complex than, the equipment used in the lander.

The main source of power for the orbiter equipment will be a solar panel array having an area of 182 square feet. The power available from this array

is approximately 728 watts. While in orbit, the orbiter may pass through the Mars-sun umbra region. To provide power in this region, storage batteries will be used and subsequently recharged when the orbiter is again in the sun-lit region.

To satisfy the high reliability figure required of the orbiter, the communication system will be 100 percent redundant. All redundancies in the communication system will be passive, except for the command systems associated with the omni-directional antenna..

The total weight, volume, and power consumption of orbiter-bus communication system components are listed in tables 3 and 4. Parameters for the data transmission equipment is broken out of table 3 and presented in table 4.

A simplified block diagram of an orbiter communication system which will meet all of the requirements stated in section 1 is shown in figure 31. Two direct link communication systems were selected for the orbiter; one to be used in transit, the other to be used while in orbit.

3.3 Detailed Description of In-Transit Communication Link

The communication link parameters associated with this phase are listed in table 5. The range indicated in this table is the maximum range that can be expected as determined for the launch opportunities listed in table 6.

The data monitored in transit is primarily engineering status measurements which can be sampled at relatively slow rates and stored for periodic playout. Using a multiplexing scheme similar to, but less complex than the lander multiplexing system, a transmitted bit rate of 300 bits/sec was determined as adequate for playing out stored in-transit data. The accuracy of these measurements will be 5 percent for most data and 1 percent for selected measurements. A 9-bit analog-to-digital converter will be used; the 5 most significant bits used for data channels requiring 5-percent accuracy, and 2 adjacent channels used for the 5 most significant bits and 4 least significant bits, respectively, for data requiring 1 percent accuracy. The details of sampling and recording are discussed in the lander entry and descent section. At 300 bits/sec, a worst case performance margin of +4.58 db can be expected using a 35 watt S-band transmitter. The carrier and synchronization power required by this system, as in the lander direct link system, are negligible. In the following sections, several important parameters of the in-transit system are evaluated. First, the diameter of the antenna which yields minimum communications system weight is found. Use of a 4-foot antenna instead of the calculated 5.8 feet is shown to lead to a negligible weight penalty. In the section on the transponder, the first factor of interest is the noise figure. Next follows the determination of the internal frequencies. Of primary interest is the specification of the carrier-phase,

SOLAR PANELS → POWER CONDITIONING EQUIPMENT

BATTERY

CENTRAL PROGRAMMER AND SEQUENCER

TV CAMERA

MULTIPLEXER/ENCODER

SCIENCE AND ENGINEERING DATA

MAPPING RECORDER NUMBER 1

MAPPING RECORDER NUMBER 2

RELAY RECORDER
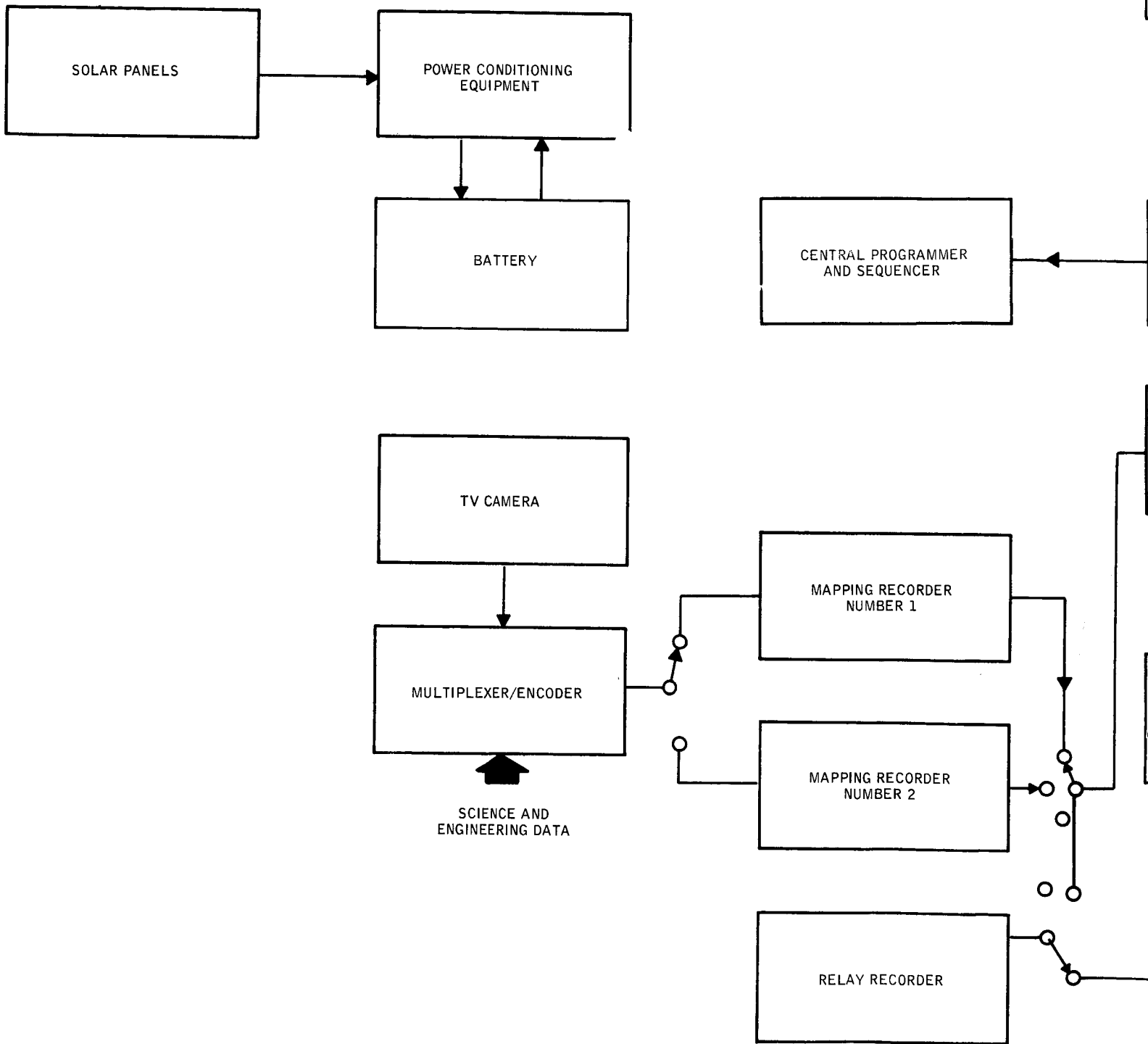
63-9237

Figure 31 COMMUNICATION SYSTE

| 4-FOOT ANTENNA DRIVE | ← | ANTENNA CONTROL | → | 8-FOOT ANTENNA DRIVE |

```
┌─────────────────────┐      ┌─────────────────────┐      ┌─────────────────────┐
│ 4-FOOT ANTENNA DRIVE │ ◄─── │   ANTENNA CONTROL    │ ───► │ 8-FOOT ANTENNA DRIVE │
└─────────────────────┘      └─────────────────────┘      └─────────────────────┘

                             ┌─────────────────────┐      ┌─────────────────────┐
                             │  COMMAND RECEIVER    │ ◄─── │       S-BAND         │
                             │   COHERENT PSK       │      │ OMNIDIRECTIONAL      │
                             │                      │      │     ANTENNA          │
                             └─────────────────────┘      └─────────────────────┘
┌─────────────────────┐
│  COMMAND DECODER    │ ◄──
│                     │ ◄──  ┌─────────────────────┐      ┌─────────────────────┐
└─────────────────────┘      │      20 WATT         │ ───► │                      │
                             │ S-BAND TRANSPONDER   │      │ 8-FOOT PARABOLIC     │
                             │      RANGING         │ ◄─── │     ANTENNA          │
┌─────────────────────┐      └─────────────────────┘      └─────────────────────┘
│  S-BAND MODULATOR   │
│                     │      ┌─────────────────────┐      ┌─────────────────────┐
└─────────────────────┘      │      35 WATT         │ ───► │                      │
                             │ S-BAND TRANSPONDER   │      │ 4 FOOT PARABOLIC     │
                             │      RANGING         │ ◄─── │     ANTENNA          │
                             └─────────────────────┘      └─────────────────────┘

┌─────────────────────┐      ┌─────────────────────┐      ┌─────────────────────┐
│ COMMAND GENERATOR   │ ◄─── │  ALTIMETER/COMPUTER  │ ◄─── │    S-BAND ANTENNA    │
│                     │ ───► │                      │ ───► │                      │
└─────────────────────┘      └─────────────────────┘      └─────────────────────┘
                                       │
                                       ▼
                                    CAMERA

                             ┌─────────────────────┐      ┌─────────────────────┐
                      ◄───    │   VHF RECEIVER       │ ◄─── │        VHF           │
                             │  (LINEAR CHIRP)      │      │  HELIX ANTENNA       │
                             └─────────────────────┘      └─────────────────────┘
```

M BLOCK DIAGRAM

TABLE 3

MARS ORBITER (COMMUNICATIONS)
SUBSYSTEM--WEIGHTS, VOLUMES, AND POWER CONSUMPTIONS

Major Subsystem	Redundancy	Volume (cubic inches)	Weight (pounds)	Power Consumed (watts)
Eight-foot antenna (with drive)	0	--	29.6	--
Four-foot antenna (with drive)	0	--	14.8	--
Antenna driver amplifier	1	288	10.0	--
120-watt S-band power amplifier (with special power supply)	0	275	16.0	240
35-watt S-band power amplifier (with special power supply)	0	180	10.0	70
S-band transponder	Double redundant each parabola (2 parabolas)	1200	40.0	20
S-band command receiver	Double redundant each 2π steradians (4π steradians)	800	28.0	
Command decoder	1 (active)	22	2.0	12
Multiplexer - encoder	1	300	18.0	3
Subcarrier modulator + P. N. generators	1	80	4.0	3
VHF receiver	1	300	13.0	3
S-band altimeter	1	160	12.0	80
Command generator	1	20	2.0	2
Mars mapping recorder No. 1	0	1300	19.0	6
Mars mapping recorder No. 2	0	1300	19.0	6
Mars relay recorder	0	1150	16.0	6
S-band omni-antenna system	0	--	4.0	--
S-band altimeter integrated antenna	0	--	3.0	--
VHF helix antenna	0	--	2.5	--
Cabling and Plumbing	0	--	20.0	--
Totals		.7375	282.6	507

TABLE 4

DATA TRANSMISSION EQUIPMENT
WEIGHT, VOLUMES, AND POWER CONSUMPTIONS

Major Subsystem	Volume (cubic inches)	Weight (pounds)	Power Consumed (watts)
120-watt S-band power amplifier (with special power suppy)	275	16.0	240
35-watt S-band power amplifier (with special power supply)	180	10.0	70
S-band transponder	1200	40.0	20
Multiplexer-encoder	300	18.0	3
Subcarrier modulator plus P. N. generators	80	4.0	3
VHF receiver	300	13.0	3
Mars mapping recorder No. 1	1300	19.0	6
Mars mapping recorder No. 2	1150	16.0	6
Total	4785	136.0	351

TABLE 5

IN-TRANSIT TELECOMMUNICATIONS DESIGN CONTROL CHART

PROJECT: VOYAGER
CHANNEL: MARS ORBITER TO PSIF
MODE: IN-TRANSIT (4-FOOT PARABOLA)

No.	Parameter		Nominal Value	Tolerance	Worst Value
1.	Total transmitter power	35 watts	+45.44 dbm	+0.0 db -0.5 db	+44.94 dbm
2	Transmitting circuit loss	with diplexer	-1.0 db	+0.0 db -0.5 db	-1.5 db
3	Transmitting antenna gain	4-foot diameter	+26.65 db	±0.46 db	+26.19 db
4	Transmitting antenna pointing loss		-0.2 db	±0.2 db	-0.4 db
5	Space loss = 32.46 +20 log F + 20 log R F 2300 mc, R 3.6 x 10^8 km		-270.83 db	---	-270.83 db
6	Polarization loss		-0.0 db	+0.0 db -0.08 db	-0.08 db
7	Receiving antenna gain		+61.0 db	+0.0 db -0.5 db	+60.5 db
8	Receiving antenna pointing loss		---	---	---
9	Receiving circuit loss		-0.1 db	maximum	-0.1 db
10	Net circuit loss		-184.48 db	+0.66 db -1.74 db	-186.22 db
11	Total received power		-139.04 dbm	+0.66 db -2.24 db	-141.28 dbm
12	Receiver noise spectral density (N/B) T system 50°K NF		-181.43 dbm	±0.7 db	-180.73 dbm
Carrier Performance					
13	Carrier modulation loss				
14	Received carrier power		negligible		
15	Carrier APC noise BW ($2B_{LO}$)				
	Carrier track (1-way)				
16	Threshold SNR in $2B_{LO}$				
17	Threshold carrier power				
18	Performance margin				

TABLE 5 (Concl'd)

No.	Parameter		Nominal Value	Tolerance	Worst Value
	Carrier - Track (2-way)				
19	Threshold SNR in $2B_{LO}$				
20	Threshold carrier power				
21	Performance margin				
	Carrier - telemetry				
22	Threshold SNR in $2B_{LO}$				
23	Threshold carrier power		negligible		
24	Performance margin		corresponds to subcarrier SNR degradation of 1.5 db		+ 3db
Subcarrier Performance					
	Data channel				
25	Bit rate (1/t)	300 bps	+ 24.77 db	---	+ 24.77 db
26	Required ST/N/B	1×10^{-3}	(6.8 + 1.5) db	+1.8 db / -0.10 db	+ 10.1 db
27	Threshold subcarrier power		-147.76	±1.9db	-145.86 db
28	Modulation loss				
29	Received data subcarrier power		-139.04 dbm	+0.66 db / -2.24 db	-141.28 dbm
30	Performance margin		+ 8.72 db	+2.56 db / -4.14 db	+4.58 db
	Synchronization Channel				
31	Sync APC noise BW ($2B_{LO}$)				
32	Threshold SNR in $2B_{LO}$				
33	Threshold subcarrier power		negligible		
34	Modulation loss				
35	Received sync subcarrier power				
36	Performance margin				

TABLE 6

EARTH-TO-PLANET RANGES AS A FUNCTION OF MARS AND VENUS OPPORTUNITIES

Arrival Date Period	Worst Case Encounter Range		Worst Case Encounter plus 30-Day Range		Worst Case Encounter plus 150-Day Range	
	AU	KM	AU	KM	AU	KM
MARS						
14 Oct. -2 Dec.* (69)	1.38	207×10^6	1.58	237×10^6	2.37	356×10^6
28 Nov. -31 Dec.* (71)	1.19	179×10^6	1.47	220×10^6	2.40	360×10^6
4 Feb.* 27 Mar. (73)	1.97	296×10^6	1.73	260×10^6	0.88	132×10^6
VENUS						
7 Dec. -23 Dec.* (70)	0.47	70.5×10^6			1.49	224×10^6
18 Sept. -3 Oct.* (72)	0.97	145×10^6			1.68	252×10^6
7 Apr.* -20 Apr. (73)	1.73	260×10^6			1.19	179×10^6
11 Oct. -31 Oct.* (75)	0.63	94.5×10^6			1.53	230×10^6

*Worst Launch Date

locked-loop characteristics, particular emphasis being given to capture and tracking ranges in the presence of doppler and doppler rate of change. Analyses are performed not only for the transit case but also for the far more stringent requirements encountered in orbit. Particular emphasis was given to determining carrier threshold required during receipt of commands via the omnidirectional antenna system. It is clearly established that a problem of data reception from either the 4- or 8-foot dishes at the DSIF presents no difficulty.

The next objective is to obtain the threshold requirements of the PN synchronous loop. First, a bandwidth and command-word rate are obtained which are compatible with the length requirements, and in addition do not lead to unduly long code-acquisition times. It is established that a PN sync threshold can be obtained which will yield the required high probability of maintaining lock in this loop during a command. Lastly, various command-error-detection techniques were examined. The method using a parity check bit for each information bit was found to satisfy all probability requirements. The threshold for the command data for the resultant bit-error probability was evaluated. All of the above threshold requirements were used to complete the values in the command link design control chart.

The ranging subsystem, and its associated problems, are discussed. The system characteristics of the command demodulator and detector, and the command decoder are detailed. A comparative analysis of the synchronous loop lock characteristics for the Mariner R and proposed Voyager schemes is performed. The spectrum of the received command is examined.

It was decided to use the amplitron for all S-band power amplifiers because of its high efficiency at the powers required. Other factors influencing this decision are availability and reliability performance. The specific technical characteristics of the S-band power amplifiers are discussed in detail.

1. <u>Determination of optimum antenna diameter</u>. Scientific data will be gathered for approximately four days and then played out in approximately two hours.

<div align="center">

Constant Power Loading

</div>

Command transponder	20 watts	
Command decoder	11 watts	
		(maneuvers neglected)
Guidance and control complex	12 watts	
Scientific instruments	5 watts	
Recorder	6 watts	
Multiplexing	3 watts	
	Total 57 watts	

Transmission ower Requirements

Transmitter (eff.= 0.50) $2 P_T$

Drivers   20 watts
                              Total $\overline{20 + 2\, P_T \text{ watts}}$.

Figure 32 gives the in-transit power profile.
Based on figure 32,

$$\text{Battery WH} = \left[\frac{77 + 2\,P_T}{0.85} - P_S\right]\ 2$$

$$= 181 + 4.71\ P_T - 2.0\ P_S\quad.\tag{1}$$

$$\text{Discharge rate} = \frac{10}{2} = 5\,; \text{capacity factor} = 0.785\quad.$$

$$\text{Battery Weight} = \frac{WH}{6.4 \times 0.785} = \frac{WH}{5.03}$$

$$= 36 + 0.94\ P_T - 0.4\ P_S\quad.\tag{2}$$

Also with a battery recharge efficiency of 0.8

$$0.85\left(P_S - \frac{57}{0.85}\right)\ \times\ 96\ =\ \frac{181 + 4.71\ P_T - 2.0\ P_S}{0.8}\quad.$$

Thus, $5.9\ P_T = 84.0\ P_S - 5696$

$$P_T = 14.25\ P_S - 965\tag{3}$$

$$P_S = 0.07\ P_T + 62.8$$

$$\text{weight of solar cells} = 0.3\ P_S\tag{5}$$

$$\text{weight of antenna} = 3.7D\quad.\tag{6}$$
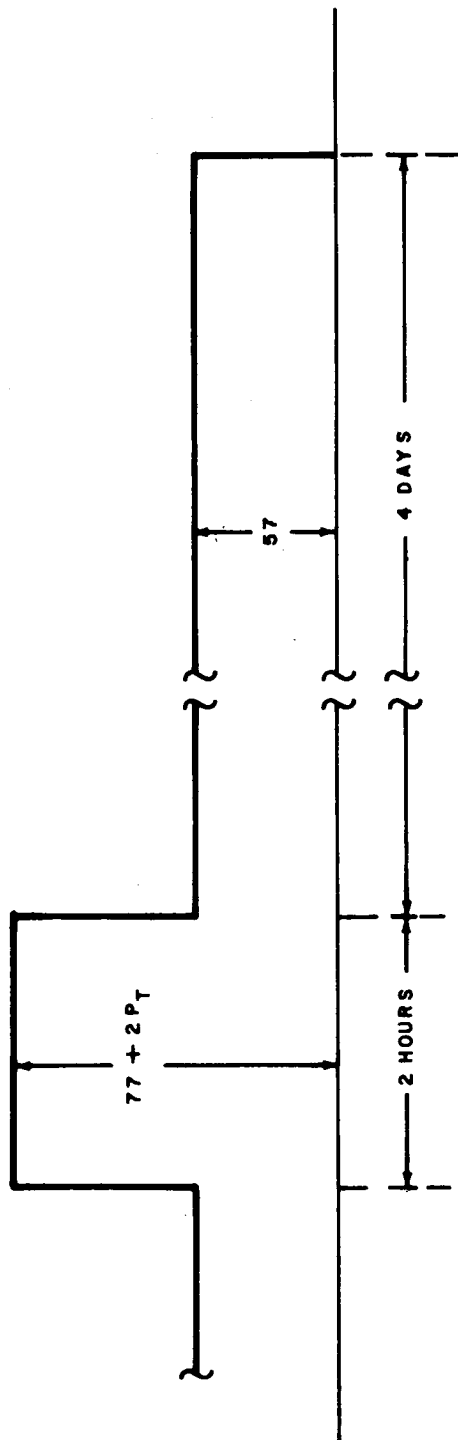
Figure 32 INTRANSIT POWER PROFILE

63-9674

-86-

Total variable weight

$$= 36 + 0.94\ P_T - 0.4\ P_S + 0.3\ P_S + 3.7\,D$$

$$= 0.933\ P_T + 29.7 + 3.7\,D \quad.$$

From general control chart included in the discussion of the Mars lander antenna optimization,

$$P_T = \frac{BR^2}{1.19 \times 10^5 \times D^{1.875}} \quad.$$

Total variable weight

$$= \frac{0.933\ BR^2}{1.19 \times 10^5 \times D^{1.875}} + 29.7 + 3.7\,D \quad.$$

For minimum weight

$$\frac{1.875 \times 0.933 \times BR^2}{1.19 \times 10^5 \times D_{opt}^{2.875}} = 3.7$$

$$D_{opt}^{2.875} = 3.98\ BR^2 \times 10^{-6} \quad. \tag{7}$$

Minimum weight obtained from D_{opt} is

$$= \frac{0.933\ BR^2\ D_{opt}}{1.19 \times 10^5 \times 3.98 \times 10^{-6}\ BR^2} + 29.7 + 3.7\ D_{opt}$$

$$= 5.67\ D_{opt} + 29.7 \quad. \tag{8}$$

The weight penalty incurred in using a nonoptimum D is

$$
= \frac{0.933 \ BR^2}{1.19 \times 10^5 \times D^{1.875}} + 29.7 + 3.7D - 5.67 \ D_{opt} - 29.7
$$

$$
= D \left[1.97 \left(\frac{D_{opt}}{D} \right)^{2.875} + 3.7 - 5.67 \left(\frac{D_{opt}}{D} \right) \right] .
$$

Considering

$$
B = 300 \text{ bits/sec}
$$

and

$$
R = 360 \times 10^6 \text{ km} .
$$

$$
D_{opt}^{2.875} = 3.98 \ BR^2 \times 10^{-6}
$$

$$
D_{opt} = 5.78 \text{ feet} .
$$

Weight penalty for 4-foot antenna

$$
= 4 \left[1.97 \left(\frac{5.78}{4} \right)^{2.875} + 3.7 - 5.67 \left(\frac{5.78}{4} \right) \right]
$$

$$
= 4.7 \text{ pounds} .
$$

2. Transponder Subsystem

a. General requirements. One of the primary functions of the tele-
communications system on board the Mars orbiter is to provide a coherent trans-
ponder capability in order that position and motion can be accurately determined.
Simultaneous measurements are made at the DSIF of doppler frequency shift,
phase shift of both carrier and range code, and apparent angle of arrival. The
receiving portion of the transponder is also used to receive commands from the
DSIF.

The associated subsystems must operate reliably for extremely long periods,
exceeding 450 days in the case of the Mars orbiter. Reliable carrier lock in
orbit must be achieved in the presence of high values of doppler and doppler
rates, the values of which are not known initially.

b.   General description. The transponder (figure 33) regenerates the input carrier signal by means of phase lock techniques, shifts its frequency and retransmits it, after stripping off the incoming modulation and replacing it with the telemetry or ranging sidebands. The extremely narrow noise band-width permits the loop to track the carrier and none of the modulation. (Acquisition problems resulting from the high doppler frequencies involved and the small noise bandwidths are avoided by frequency adjustments at the Earth transmitter.) Use of multiples of the voltage-control oscillator (VCO) frequency at the mixer local oscillators keeps the signal centered in the pass-band of the IF amplifiers. If the quadrature detector indicates that the loop is not in lock, the transmitting channel switches from the noisy VCO signal to the more stable source.

The preselector has two functions: (1) it protects the receiver from strong off frequency signals when the spacecraft is near the Earth, and (2) it, along with the diplexer, offers protection against the transponder's own transmitted signal. For the tunnel diode RF amplifier, a noise figure of 4. 25 db and gain of 18 db were selected. The first IF is 47-13/16 mc. The mixer-preamplifier has a noise figure of 8 db and a gain of 20 db which includes the mixer loss. Excluding the preamplifiers the first IF amplifier has a gain which is varied by the AGC over a range of 105 db with the maximum gain being 62 db. The band-width of this amplifier is 3. 5 mc to accommodate the ranging signal which is amplified at 47-13/16 mc before being routed to the ranging channel. Doing all of the automatic gain control in the first IF amplifier removes the need of gain tracking in both the second IF amplifier and the ranging channel amplifier. The second IF amplifier, which operates at 4-25/32 mc, has a bandwidth of 3 kc (crystal filter) and a fixed gain of 50 db. The AGC holds the output of this amplifier to -6 dbm (± 1 db). The transponder noise figure (including the pre-selector but not the diplexer) is 4. 4 db.

In the transmitter channel, the phase modulation occurs at 71-23/32 mc. To provide a maximum deviation of ±4 radians at the antenna the maximum deviation at the modulator will be ± 1/8 radian. To obtain greater efficiency, power amplification will take place at 573-3/4 mc. The efficiency of the output multiplier will be about 25 percent so the amplifier output will have to be 5 watts to give the required 1. 2-watt S-band output.

Certain transponders use the same antenna for transmission and reception, so biplexers will be required. They will introduce about 1. 5 db of attenuation and provide 60-db isolation to the receiver. The preselector should provide an additional 80-db isolation.

For a 120-watt transmitter, the leakage power level at the receiver input is 50. 8 - 140 =89. 2 dbm which can be eliminated by the RF and IF amplifier tuning since it is 180 mc away from the receiver frequency.

TO RANGING
SUBSYSTEM

```
                                        ┌─────────────┐
                                        │  ISOLATION  │
                                        │  AMPLIFIER  │
                                        └─────────────┘

        ┌──────────┐              ┌──────────────┐
        │   AGC    │◄─────────────│     AGC      │◄──────
        │   LOOP   │              │  AMPLIFIER   │
        │  FILTER  │              └──────────────┘
        └──────────┘
```

INPUT

2113–5/16
MC

```
┌──────────────┐   ┌─────────────┐   ┌──────────────┐   ┌──────────────┐        ┌──────────────┐
│  PRESELECTOR │   │ RF AMP N.F. │   │ MIXER–PREAMP │   │   IF AMP     │   ⊗    │   IF AMP     │◄──
│     BW =     │─► │   3.8 DB    │─► │  BW = 3.5 MC │─► │ f = 47–13/16 │─►      │ f₀ = 4–25/32 │
│     8 MC     │   │             │   │              │   │     MC       │        │     MC       │
└──────────────┘   └─────────────┘   └──────────────┘   └──────────────┘        └──────────────┘
```

$$\begin{bmatrix} \text{INPUT} & 221 \\ \text{OUTPUT} & 240 \end{bmatrix}$$

```
                              ┌──────────────┐
                              │     X48      │◄──────────
                              └──────────────┘
```

OUTPUT

2295 MC
1.20 WATTS

```
        ┌──────────┐   ┌──────────────┐   ┌──────┐   ┌──────────────────┐   ┌──────┐
◄───────│    X4    │◄──│  POWER AMP   │◄──│  X8  │◄──│ PHASE MODULATOR  │◄──│  X5  │
        │          │   │  573.75 MC   │   │      │   │   + 1/8 RAD      │   │      │
        └──────────┘   └──────────────┘   └──────┘   │   CAPABILITY     │   └──────┘
                                                     └──────────────────┘
                                                            ▲
```

TELEMETRY.
RANGING.
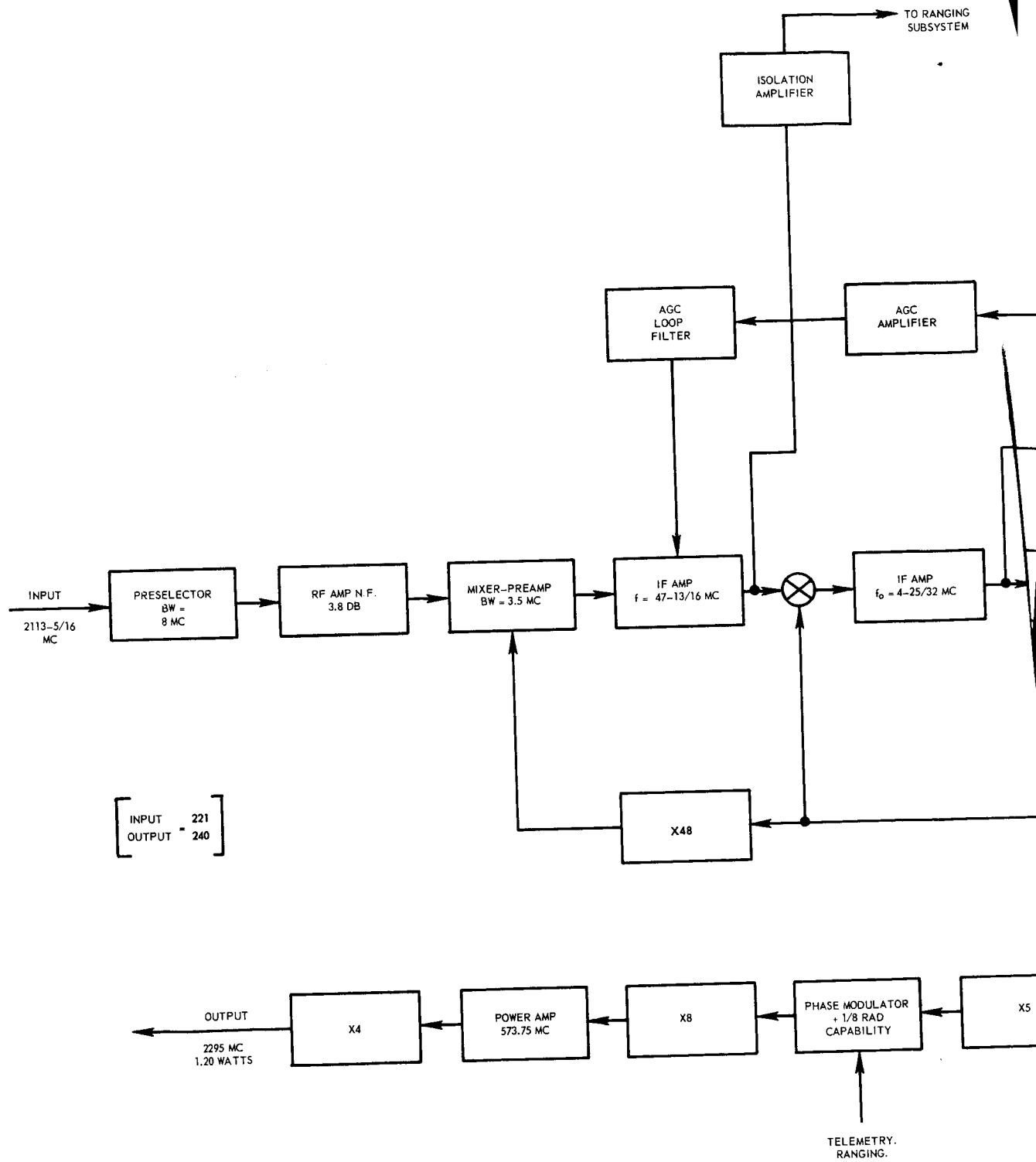
Figure 33 TRANSPONDER BL

TO COMMAND DETECTOR
AND DEMODULATOR
(SPACECRAFT)

OR

TO DATA
DETECTOR
(DSIF)

ISOLATION
AMPLIFIER

$\pi/2$

LIMITER

LOOP
FILTER

VCO
14–11/32 MC

X1/3

LIMITER

X3

OSC.
14–11/32MC
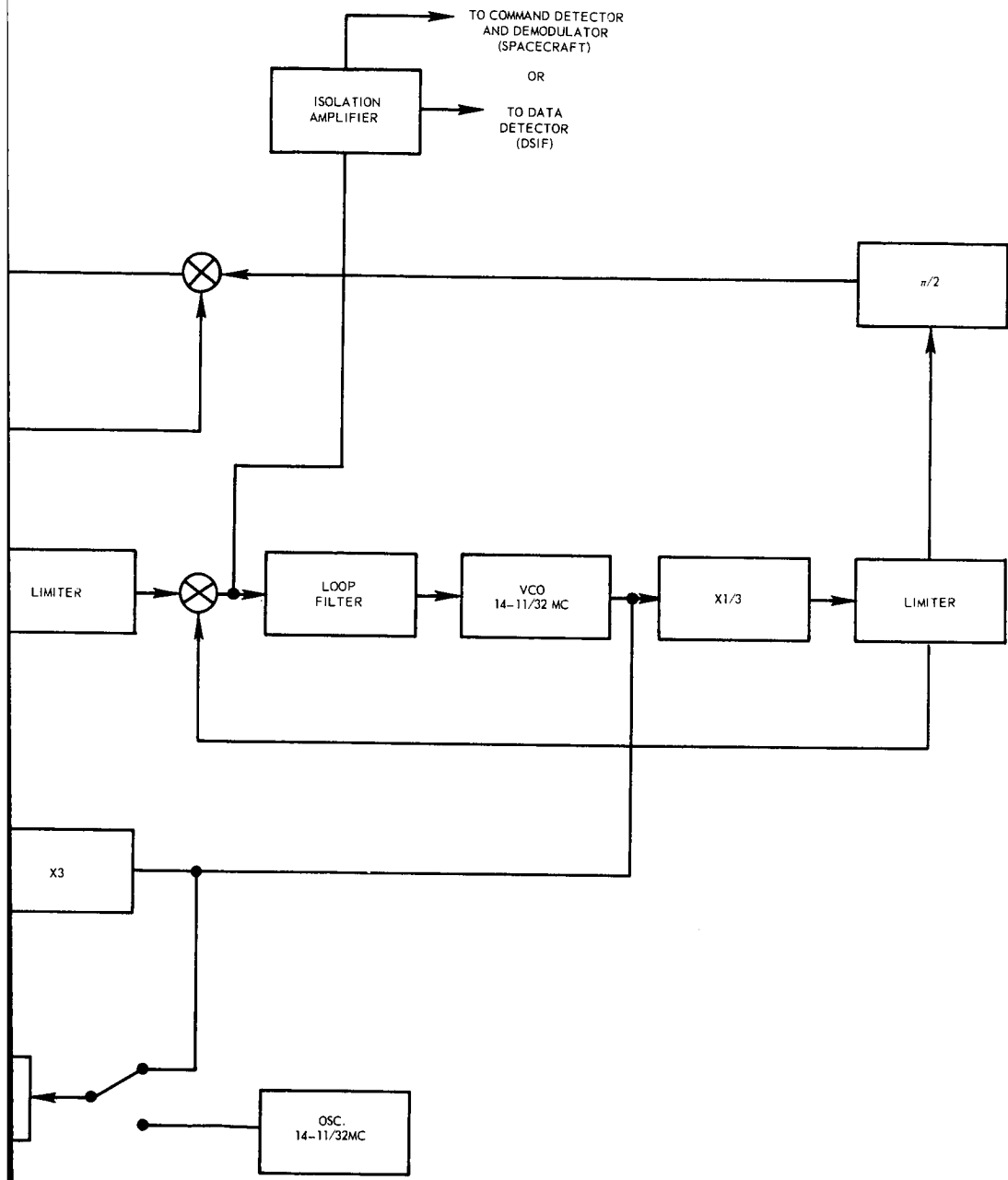
DIAGRAM

Integrated circuitry is planned where possible for the transponder. The anticipated weight and volume are 10 db in 300 in.[3] For a 1.20-watt output, a 20-watt input will be required.

c. Determination of transponder internal frequencies. It was given that DSIF requires the received signal to transmitted signal frequency ratio to be 221/240. The pair 2295 mc and 2113-5/16 were used in designing the S-band transponder. It is not a simple matter to select a set of IF's and multipliers which will give the desired transponder input and output frequencies. The loop of figure 34 was used for establishing the various frequency restrictions. The blocks A, B, C and D are multipliers.

The VCO frequency, f, will be assumed less than 10 mc, and to get started some general assumptions have to be made. Upper bounds of 10 mc for the VCO frequency and 80 mc for the modulator input will be taken. This means that A and D must be quite large. To prevent distortion, it was felt that D should be a power of 2. An obvious first guess for D would therefore be 32. Three equations now can be written.

$$IF_iL - B_f = f . \tag{9}$$

(Notice that if this equation does not lead to a satisfactory solution, it can be re-written as $Bf - IF_i = f$.)

$$CDF = 2295 \text{ mc and} \tag{10}$$

$$2113-5/16 - Af = (IF)_i . \tag{11}$$

Combining equations (9), (10), and (11) gives

$$A + B + 1 = \left[29 \ \frac{7}{15}\right] C \tag{12}$$

from which it can be seen that C must be a multiple of 15, since A, B, and C can only be integers.

This is the only choice for C that will give a reasonable VCO frequency. For the value of D, which was assumed, is C=15. This fixes f at 4-25/32 mc. From equation (12)

$$A + B = 441 .$$

To keep the first IF frequency (IF), in the vicinity of 50 to 60 mc, B must be under 15. Different values of B were tried in an effort to find one that was a factor of A. This led to B = 9 and A = 432 = 48 x 9. These are the numbers that were used in the transponder of figure 31.

d. Transponder noise figure. Noise figure of a 2.2-kmc germanium tunnel-diode (TD) amplifier is 4.25 db. This includes the (necessary) circulator,
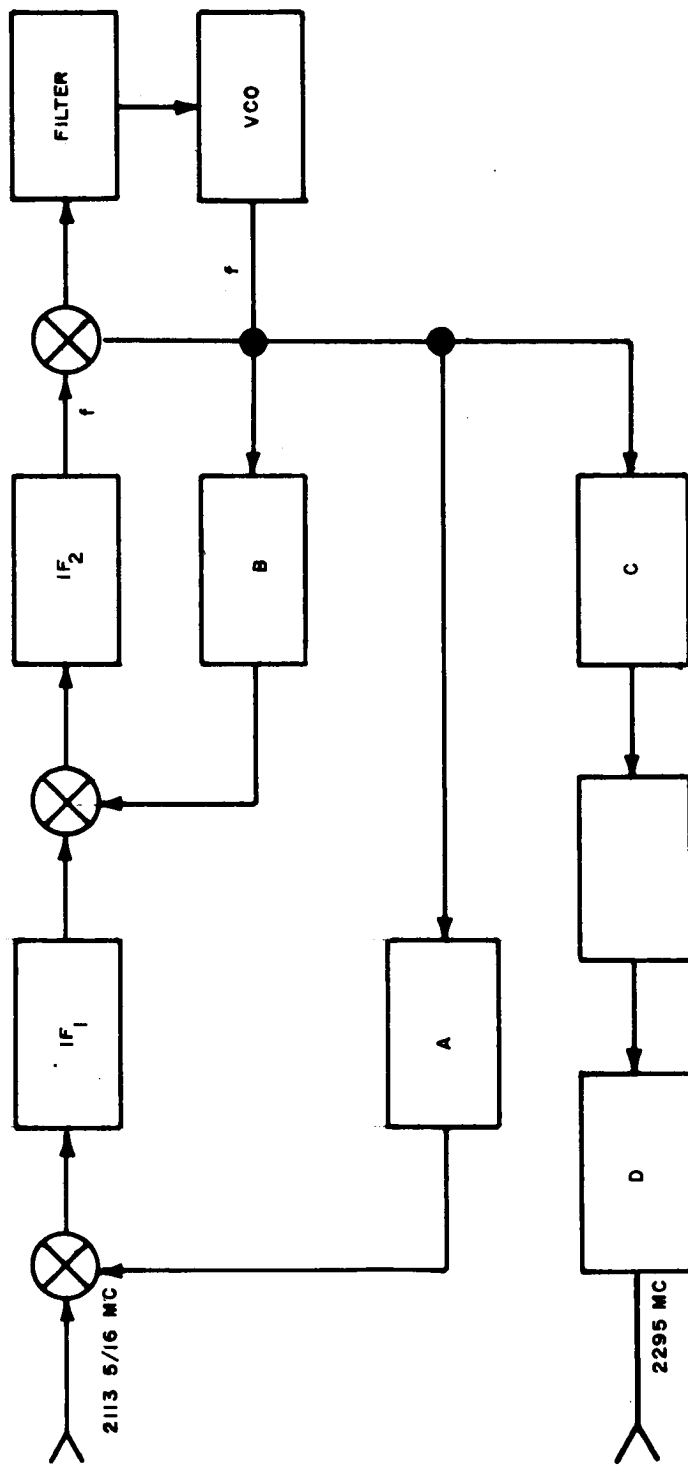
Figure 34 MODEL LOOP

63-9676

-92-

but does not include degradation due to following IF amplifier. The gain of the TD amplifier can be as high as 18 db for a one-stage amplifier. The degradation due to a mixer and IF amplifier with 8-db combined noise figure now can be computed:

$$F_{12} = F_1 + \frac{F_2 - 1}{G} = 2.67 + \frac{6.3 - 1}{63} = 2.75 = 4.4 \text{ db} .$$

Thus a germanium TD amplifier can be expected to provide a system noise figure of 4.5 db (of course, neglecting elements ahead of the amplifier, such as antenna and lines). Noise figure variations over the bandwidth would not exceed ± 0.5 db.

The germanium TD amplifier will have this noise figure over an ambient range of -10°C to + 65°C. (Lower limit caused by the circulator.) Weight of TD amplifier, including circulator, is 8 ounces.

Phase distortion is much better than 10 degrees. The noise figure referred to holds over many megacycles of bandwidth.

Better results can be achieved with a galium antimonide diode. However, it is temperature sensitive and would require control within 5 to 10 degrees.

It is well to note that tunnel-diode amplifiers work by majority carrier conduction and are, therefore, not very susceptible to radiation damage.

    e.   **The carrier phase locked loop.** The criteria which determine the performance required of the carrier-phase locked-loop are a function, not only of the phase of the mission, but also of what is being received. During transit, neither doppler nor doppler rate of change is considered a problem since they are both highly predictable. In addition, the DSIF will have no difficulty in compensating for them. However, the doppler and rate of change of doppler in orbit are of a high magnitude and go through cyclic variations. Under these conditions, it will be shown that it is necessary to sweep the DSIF carrier frequency in order to achieve lock in the orbiter loop. It is the objective of this section to determine the required thresholds for the loop for the various modes of transmission.

    1)   Selection of orbiter loop noise bandwidth. During one orbit of Mars, the doppler frequency will change by approximately ± 17 kc. The greatest rate of change of doppler will be about 36 cps/sec. The greatest doppler change during any 2000-second period (time for one round trip between Earth and vehicle) will be about 20 kc.

    Assume that there is no a priori information regarding doppler, yet carrier lock must be achieved in the vehicle while it is in orbit. Then the carrier loop

must be at least a second order type to get the largest capture range for a given noise bandwidth. Jafees and Rechtin (ref. 4) show that the optimum damping ratio is

$$\zeta = 0.71 \; . \tag{13}$$

We chose the loop natural frequency W_n (all values referred to here are threshold values) from an empirical formula given by Frazier and Page (ref. 5):

$$R \approx 0.22 \; W_n^2 \; . \tag{14}$$

R in equation (14) is the maximum rate of change of signal frequency if the loop is to acquire the signal 9 times out of 10. Certain constants which are negligible in this case have been deleted from the original expression. This is justifiable. The output signal-to-noise ratio (S/N) is above 6 db. Equation (13) is based on experiment and is said to hold with good accuracy for $\zeta > 0.5$.

It will appear shortly that the signal cannot be acquired without sweeping the Earth oscillator; hence the sweep rate must be added to the doppler rate to get R. When the damping ratio has a value given by equation (13) the loop noise threshold bandwidth $(2B_L)_{th}$ is given by

$$(2B_L)_{th} = \frac{3\sqrt{2}}{4} \; W_n \quad \text{(in cps)} \; . \tag{15}$$

We might choose R only slightly larger than the maximum doppler rate, but the permitted sweep rate then is so slow that an inordinate time is required for acquisition. A reasonable compromise appears to be to sweep at a rate equal to the maximum doppler rate, so that R is double the maximum doppler rate:

$$R = 72 \; \text{cps/sec} \; . \tag{16}$$

The required 34-kc doppler range then is swept in 940 seconds. Equations (14), (15) and (16) result in

$$W_n = 18 \; \text{rad/sec} \; ; \tag{17}$$

and

$$(2B_L)_{th} = 19 \text{ cps} .$$

In the system calculations $(2B_L)_{th}$ is taken as $(2B_L)_{th} = 20 \text{ cps}$. (18)

2) <u>Derivation of capture and tracking ranges</u>. At this point, the fact will be demonstrated that the capture range is very limited, and the Earth oscillator must be swept. When the signal and local oscillator are stationary in frequency, and when $W_n/K \ll 1$ as will certainly be the case here, Viterbi (ref. 6) gives as an upper limit for the frequency difference permitting capture in the absence of noise

$$\Omega = 2\sqrt{\zeta W_n K} \quad \text{rads/sec} . \tag{19}$$

The loop gain is given by

$$K = 2\pi K_D \ KVM \text{ rad/sec} \tag{20}$$

where

$$K_D = \text{phase detector constant}$$

$$K_V = \text{VCO constant}$$

and

$$M = \text{multiplying factor} .$$

For the transponder

$$M = \frac{\text{received frequency}}{\text{VCO frequency}}$$
$$= \frac{2113 - 5/16}{14 - 11/32}$$
$$= 147 - 1/3 . \tag{21}$$

For K_D and K_V we take the following Mariner values

$$K_D = 1.072 \times 10^{-2} \text{ volts/deg} \tag{22}$$

and

$$K_V = 120 \text{ cps/volt} \tag{23}$$

whence

$$K = 2\pi \left(360 \frac{\text{deg}}{\text{cycle}} \right) (1.072 \times 10^{-2})(120)(147\text{-}1/3)$$

$$= 429,000 \text{ rads/sec} . \tag{24}$$

The best possible capture range is

$$\Omega = 2 \sqrt{(0.71)(18)(429,000)}$$

$$= 4670 \text{ rads/sec}$$

$$= 743 \text{ cps} . \tag{25}$$

For such a situation, the Earth oscillator must be swept in order to cause capture in the orbiter phase loop.

Once the orbit has been computed, it is possible to program the transmitted frequency so it will cancel most of the doppler shift when it arrives at the vehicle. However, accurate doppler data are needed in order to establish the orbit. In this critical period, if tracking must be performed via the omnidirectional antenna for some reason, the foregoing assumptions are all justified. The Earth transmitter must be swept over the full doppler range. This may be done once per roundtrip interval, following which the frequency is held fixed. The Earth station then waits for the return signal, which carries with it a telemetered indication of lock and frequency offset, among other things. With this information, the offset may be reduced.

The approximate hold in range is

$$\frac{429,000}{2} = 68.3 \text{ kc/s} . \tag{26}$$

3) <u>Derivation of loop time constants</u>. Using the optimum filter for a second order loop as derived by Jaffee and Rechtin(ref. 7) the transfer function for the loop of figure 35 becomes,
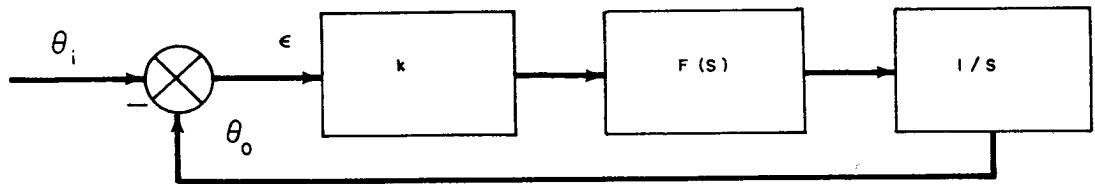
63 – 9677

Figure 35 PHASE LOCK LOOP

$$H(s) = \frac{1 + \frac{3}{4B_L} s}{1 + \frac{3}{4B_L} s + \frac{9}{32B_L^2} s^2}$$
(27)

where the noise bandwidth, $2B_L$, is defined by

$$2B_L = \frac{1}{2\pi i} \int_{-i\infty}^{+i\infty} |H(s)|^2 \, ds \quad .$$
(28)

For a practical filter transfer function such as

$$F(s) = \frac{1 + T_2 s}{1 + T_1 s} \quad ,$$
(29)

the loop transfer function would be

$$H(s) = \frac{1 + T_2 s}{1 + \left(\frac{1}{k} + T_2\right) s + \left(\frac{T_1}{k}\right) s^2} \quad .$$
(30)

Using equation (30) in equation (28) and evaluating the integral from the table on page 369 of ref. (8) the noise bandwidth is found to be

$$2B_L = \frac{T_2^2 + \frac{(T_1)}{k}}{2 \frac{(T_1)}{k} (1/k + T_2)} \quad .$$
(31)

Comparison of equations (27) and (30) shows that, for large k (RADS)

$$T_2 = \frac{3}{4B_L}$$
(32)

(33)

For the transponder $2B_L$ = 20 cps so T_2 = 0.075 second and T_1 = 1210 seconds.

4) Variation of transponder noise bandwidth as a function of input S/N ratio.

The presence of the limiter at the phase-detector input causes the loop gain to vary with the input signal-to-noise ratio. This variation of loop gain causes the noise bandwidth to vary, becoming wider for a large (S/N) in or large loop gain. The relationship between noise bandwidth $(2B_L)$, and loop gain k, will be derived first. For $T_2 >> 1/k$ equation (31) can be written approximately as

$$2B_L = \frac{kT_2}{2T_1} + \frac{1}{2T_2} \tag{34}$$

and

$$2B_L - \frac{1}{2T_2} = \frac{T_2}{(2T_1)k} \cdot \tag{35}$$

We can then write

$$\frac{2B_L - \frac{1}{2T_2}}{2B_{L_{th}} - \frac{1}{2T_2}} = \frac{k}{k_{th}} \tag{36}$$

where the subscript th identifies the threshold values.

From equation (32)

$$T_2 = \frac{3}{4B_{L_{th}}} \tag{37}$$

or

$$\frac{1}{2T_2} = \frac{2B_{L_{th}}}{3} \tag{38}$$

Then from equation (36),

$$2B_L = \frac{k}{k_{th}} \left[2B_{L_{th}} - \frac{2B_{L_{th}}}{3} \right] + \frac{2B_{L_{th}}}{3} \tag{39}$$

$$(2B_L) = (2B_{L_{th}}) \; 1/3 \left[1 + 2\frac{k}{k_{th}} \right] \cdot \tag{40}$$

The phase detector gain, K_d, is proportional to signal amplitude. The signal amplitude is kept constant at the limiter input so the limiter output equals the

limiter supression factor, a, times the constant input signal. Therefore, $K_d \sim a$

$$a^2 = \frac{S_a}{P_a} = \frac{S_a}{S_a + N_a} = \frac{1}{1 + \left(\frac{N_a}{S_a}\right)} \cdot \tag{41}$$

(See figure 36) $[(S/N)_b]$ = 0.00 db. In the transponder the loop bandwidth = 20 cps while the bandwidth at the loop input is

$$3 kc \cdot \text{So } (S/N)_b = \left(\frac{20}{3000}\right)\left(\frac{S}{N}\right)_a = \frac{1}{150} \times 1 \tag{42}$$

or -21.76 db. Since the limiter output always is within 3db of its input, the input signal to noise ratio for the threshold condition is such that the following approximation is valid.

$$\left(\frac{N}{S}\right)_a = \frac{4}{\pi} \left(\frac{N}{S}\right) \text{ in (ref. 9).} \tag{43}$$

So from equation (41)

$$a_{th} = \left[\frac{1}{1 + \frac{4}{\pi}\left(\frac{N}{S}\right)_{in\ th}}\right]^{1/2} \cdot \tag{44}$$

For $(S/N)_{in}$ less than -10 db this equation will hold.

$$a = \left[\frac{1}{1 + \frac{4}{\pi}\left(\frac{N}{S}\right)_{in}}\right]^{1/2} \cdot \tag{45}$$

Then

$$\frac{K_d}{K_{d_{th}}} = \frac{a}{a_{th}} = \left[\frac{1 + \frac{4}{\pi}\left(\frac{N}{S}\right)_{in\ th}}{1 + \frac{4}{\pi}\left(\frac{N}{S}\right)_{in}}\right]^{1/2} \cdot \tag{46}$$

The only factor of loop gain, k, that varies with $(S/N)_{in}$ is K_d so

$$\frac{k}{k_{th}} = \frac{K_d}{K_{d_{th}}}$$

and the above equation

can be used to compute the change in $2B_L$ as $(S/N)_{in}$ varies.

-100-
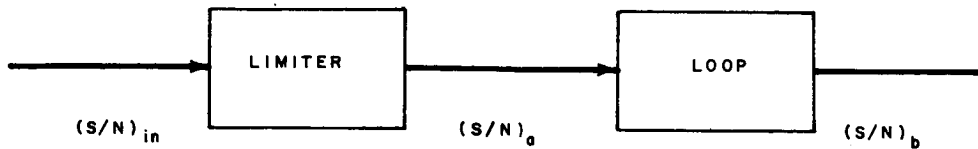
63-9678

Figure 36 LOOP SIGNAL-TO-NOISE RELATIONSHIPS

2B_LT VERSUS SNR

2B_L = TWO SIDED OUTPUT
NOISE BANDWIDTH
(IN CPS)

T = MEAN TIME FOR
PHASE ERROR TO
REACH 90° (IN
SECONDS)

SNR = LOOP OUTPUT
SNR (DB)

63-9679
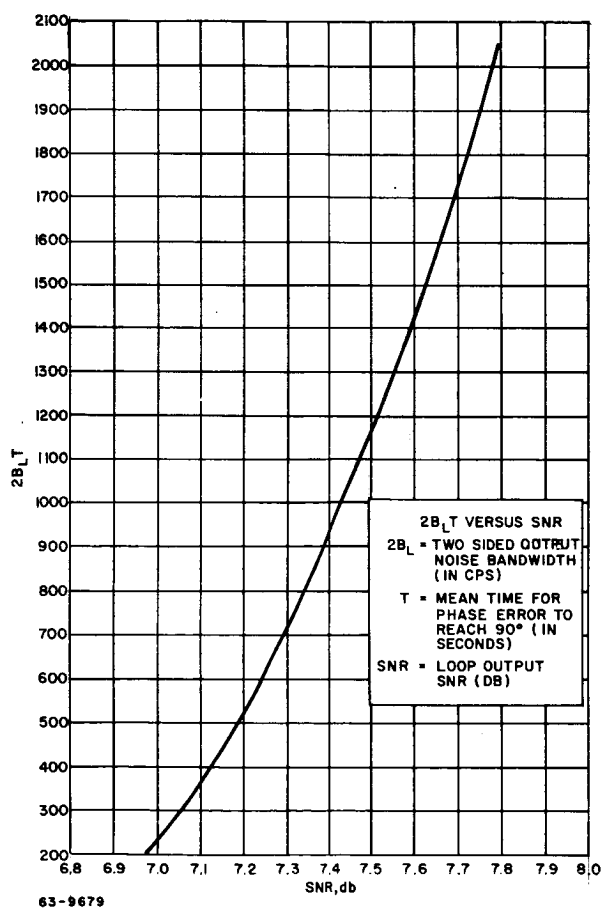
Figure 37 2B_LT VERSUS SIGNAL-TO-NOISE

The loop is considered to be operating at its threshold when the signal-to-noise ratio in the bandwidth $2B_L$ is one. Since the predetection bandwidth is 3 Kc, the threshold $\left(\dfrac{N}{S}\right)$ at the limiter input is $\left(\dfrac{3000}{20}\right)(1) = 150$ from which

$$\frac{k}{k_{th}} = \left[\frac{1 + \dfrac{4}{\pi}\,(150)}{1 + \dfrac{4}{\pi}\left(\dfrac{N}{S}\right)_{in}}\right]^{1/2} \simeq [1 + 4/\pi\,(150)]^{1/2} = 13.8 \tag{47}$$

and from equation (40) $2B_L = (2B_L)_{th}$ (9.25)= 190.4 cps for large input signal-to-noise ratio.

5) <u>Derivation of carrier loop thresholds</u>. In order for the communication link to be useful, the carrier loop must not only lock, but it must also stay in lock long enough to permit accomplishment of the function for which the link is being used. These functions are: (1) transmission of commands from the DSIF to spacecraft, (2) transmission of data from spacecraft to DSIF, (3) two-way coherent measurement of doppler, and (4) coherent ranging.

The accomplishment of cases (2), (3), and (4) in orbit will be shown possible only by use of the high-gain antenna. In this circumstance, there is little problem in meeting the carrier threshold requirements. In transit, the high-gain antenna will be used in any case, since it will be so frequently required for the transmission of data.

Case (1) is of interest both in transit and orbital conditions.

a) <u>Orbiter carrier loop threshold during receipt of commands</u>. If we assume that about 60 seconds are required for PN code locking (63 PN bits per PN word, and 1-cps synchronizing loop bandwidth) and 40 seconds more are allocated to command reception, lock must then be maintained with reasonable probability for 100 seconds.

Loss of lock must be defined, and it is difficult to do so. Our definition will be that lock is lost when the instantaneous phase error becomes equal to or greater than 90 degrees; this is satisfying not only because at this point the gain of the phase detector (hence, the restoring force in the loop) goes to zero, but because even if the loop returns to the locked condition some of the command data will have been lost. When the carrier phase error is 90 degrees, the subcarriers vanish.

Viterbi (ref. 10) gives an expression for the mean time to reach an arbitrary phase error, starting from zero, for a first-order loop, and indicates that for large SNR the same expression holds roughly true for a second-order loop. Solving this expression for 90-degree phase error results in the graph of figure 37. Defining threshold SNR as that which will result in a 90-degree

phase error once in 100 seconds, we find that for $2B_L$ = 20 cps, the loop SNR must be 7.8 db.

Some experimental results given by Weaver (ref. 11) and figure 38 indicate that second order effects in practical circuits may cause the theoretical figure to be degraded. He has measured the SNR required in order for the probability to be 10 percent that phase error will exceed 90 degrees. Since number of independent samples, or time, is not a parameter in his results, they only can have meaning for each independent sample of the loop output. These occur at a rate of approximately $2B_L$ per second.

If the average phase error is zero, as is the case when the loop filter contains an ideal integrator, and if a limiter is incorporated, Weaver's results indicate that when the loop SNR is about 5 db, the probability is 10 percent that any one independent sample of the output will have a phase error of 90 degrees or more.

We wish to find the SNR required for a cumulative probability of 50 percent that 90 degrees will be exceeded over a period of 100 seconds, that is, over a total of 2 x 100 x B_L independent samples. The cumulative probability P_{cum} is given by

$$P_{cum} = 1 - (1 - p)^{200\,B_L} \tag{48}$$

where p is the probability for one sample hence

$$p = 1 - (1 - P_{cum})^{1/200\,B_L} \quad .$$

In the case P_{cum} is 0.5, n is 2000, and

$$p = 2.5 \times 10^{-4} \quad , \tag{49}$$

Now, the approximation that the probability density function of phase is normal must be made. Then, in the phase error distribution for 5 db SNR, the probability is 10 percent that a 90-degree error is exceeded; hence, the rms value of the distribution must be 55 degrees. In order to narrow the distribution so that the probability is 2.5 x 10^{-4} that 90 degrees is exceeded, the new rms value must be 25 degrees. The noise power must therefore be reduced about 4 times, or 6 db, below the value given by Weaver. The required SNR at threshold is therefore approximately 11 db.

There is a 3.3-db spread between these two definitions of threshold, and in the absence of better information the more pessimistic should be chosen.
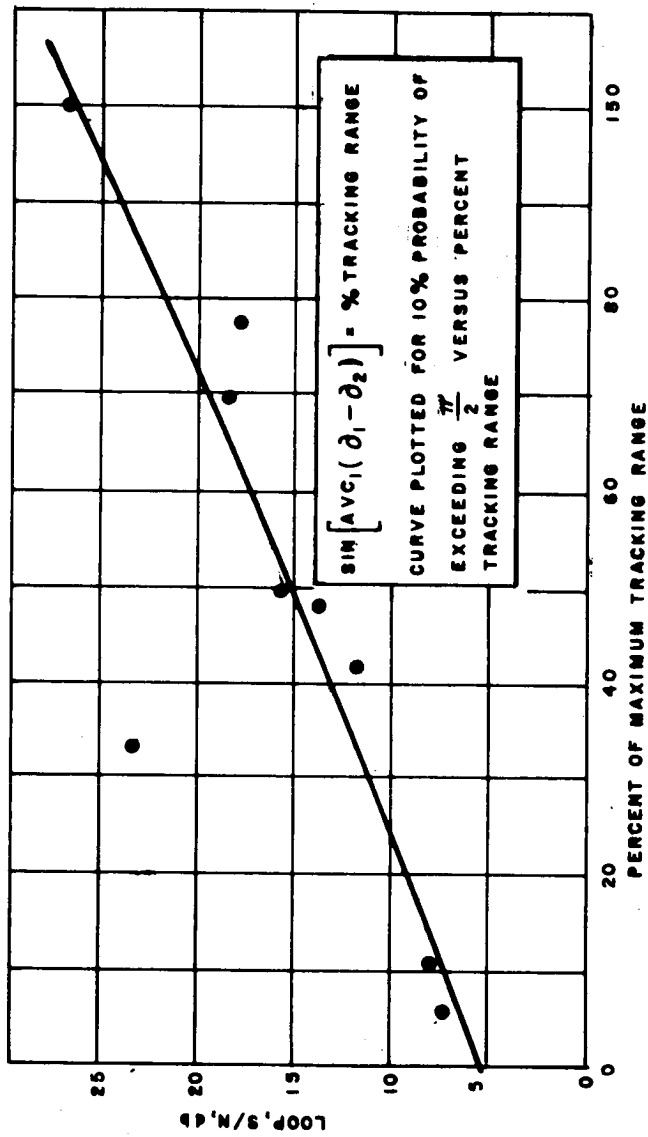
Figure 38 MEASURED THRESHOLDS WITH LIMITING

-104-

If the loop does not contain a high gain integrator, there will be mean phase error due to the doppler offset. The steady-state phase error is

$$\theta = \sin^{-1} \frac{D}{K} = \sin^{-1} \frac{17,000 \times 2\pi}{429,000} = \sin^{-1} (0.25) = 14.5 \text{ degrees} \qquad (50)$$

where

$$D = \text{doppler shift (rad/sec) and } K = \text{loop gain.}$$

Weaver's results indicate that the threshold is thereby raised 2.5 db above the value it has when the offset is zero. The incorporation of a high-gain integrator eliminates this steady-state offset and the required increase in threshold SNR. It seems essential therefore that a high-gain integrator be incorporated in the carrier tracking loop. Even so, an offset will arise due to the doppler rate encountered in the orbit. The worst value of this rate is 225 rad/sec, leading to a steady-state phase error of

$$\theta = \sin^{-1} \frac{\dot{D}}{W_n^2} = \sin^{-1} \frac{225}{(18)^2} = \sin^{-1} (0.69) = 44 \text{ degrees} \qquad (51)$$

where $\dot{D}$ = doppler rate and W_N = natural loop frequency.

Lock may not be sufficiently sustained in the high-rate part of the orbit to permit command reception, because of the 8.5 db degeneration. However, in the low-rate sections of the orbit, the effect of the integrator will be felt, lowering the threshold and permitting commands to be received with reasonably high probability.

3. The PN synchronization loop.

    a. Evaluation of average PN code acquisition time. After the space-craft PN generator is in phase with the PN component of the received signal, the synchronizing loop can be treated as a normal loop except that pull-in must be fast; no slippage is allowable. As can be seen from the loop error function, if one-half cycle of slippage occurs from the lock point, the PN codes will no longer be in phase and lock will be impossible. The frequency to which the loop locks is always the same, Δf away from the VCO idling frequency. The offset is provided between the received frequency and the VCO idling frequency so that the spacecraft PN generator, which is driven by the VCO, will run at a different rate than the transmitter PN generator; and the two codes will slip past each other until they come into phase, at which time lock should occur. It is desirable to have the offset frequency, Δf, as large as possible so that the codes will come into phase quickly. The average acquisition time is the time required for the local PN code to slip half its length with respect to the received

PN code, since all starting phase discrepancies are equally probable. (The actual pull-in time once the PN codes get in phase will be a negligible part of the acquisition time.)

Richmond has stated that for no-slip pull-in

$$\Delta\omega \;<\; T_2 \left(\frac{G}{T_1}\right) \;.$$
(52)

As shown elsewhere the loop transfer function is

$$H(s) \;=\; \frac{1 + T_2\, s}{1 + T_2 s + \dfrac{T_1}{G}\, s_2^2} \;=\; \frac{1 + \left(\dfrac{3}{4\,B_L}\right) s}{1 + \left(\dfrac{3}{4\,B_L}\right) s + \left(\dfrac{9}{32\,B_L^2}\right) s^2}$$
(53)

where T_1 and T_2 are defined by the filter transfer function.

$$F(s) \;=\; \frac{1 + T_2\, s}{1 + T_1\, s} \qquad \text{and } 2B_L \text{ is the noise bandwidth. This gives}$$

$$T_2 \;=\; \frac{3}{4\,B_L} \qquad \text{and} \qquad \frac{T_1}{G} \;=\; \frac{9}{32\,B_L^2}$$
(54)

so equation (52) can be rewritten as

$$\Delta f \;\le\; \left(\frac{1}{2\pi}\right)\left(\frac{3}{4\,B_L}\right)\left(\frac{32\,B_L^2}{9}\right) \;=\; \left(\frac{4\,B_L}{3\pi}\right) \;=\; 0.425\,B_L \;.$$
(55)

Figure 39 shows a plot of average acquisition time versus noise bandwidth. It was obtained from the following considerations. The frequency of the local clock is $f_L = f_r + \Delta f$ where f_r is the frequency of the received clock. The period, P_L, of the local PN code in terms of P_r, the period of the received PN code is

$$P_L \;=\; P_r \left(\frac{f_r}{f_L}\right) \;.$$

The number of times the local PN code must cycle to gain one bit with respect to the received code is

$$N \;=\; \frac{P_r/n_i}{P_r - P_L} \;=\; \frac{1}{n_i}\,\frac{f_L}{\Delta f}$$
(56)

where n_i is the number of PN bits per cycle.
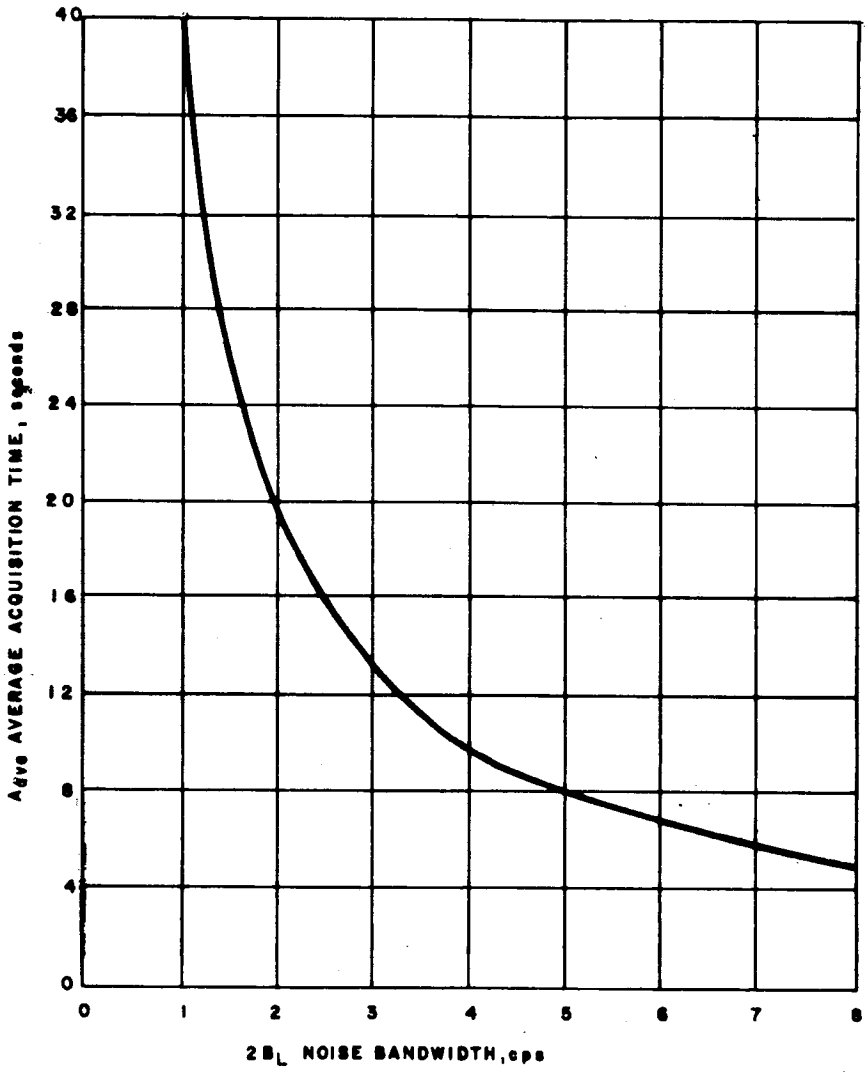
Figure 39 AVERAGE ACQUISITION TIME

The average acquisition time is

$$A_{ave} = \frac{n_1}{2} NP_L = \frac{1}{2} \frac{P_r f_r}{\Delta f} \quad . \tag{57}$$

If Δf is taken as $0.4\, B_L$ the average acquisition time becomes

$$A_{ave} = \frac{5 P_r f_r}{4 B_L} \quad . \tag{58}$$

$P_r = 0.75$ sec and $f_r = 20\text{-}2/3$ cps will be shown to be suitable values. Therefore,

$$A_{ave} = \frac{5}{4} \frac{(3/4)\,(20\text{-}2/3)}{B_L} = \frac{19.375}{B_L} \quad . \tag{59}$$

$B_L = 0.5$ will be used. Hence, $A_{ave} = 38.75$ seconds which is longer than the 30 seconds required to receive a twenty information bit command word.

From equation (53)

$$T_2 = \frac{3}{2} \text{ seconds, } T_1 = \frac{9}{8} G \text{ seconds} \quad . \tag{60}$$

The loop gain can be found from the allowable steady-state phase error. For a one degree phase error,

$$G = \frac{\Delta \omega}{\Phi} = \frac{2\pi(0.2)}{2\pi(1/360)} = 72 \tag{61}$$

which sets

$$T_1 = 81 \text{ seconds} \quad . \tag{62}$$

b. **Threshold.** It was given that the probability of losing lock in the synchronizing loop during a command could not exceed 10^{-3}.

$$\text{Hence } (1 - P_L)^{30 \times 2 B_L} = 0.999$$

where the length of the command frame is 30 seconds. For $2B_L = 1$ cps

$$(1 - P_L)^{30} = 0.999$$

whence

$$P_L = \frac{0.001}{30}$$

$$= 3.3 \times 10^{-5} \quad .$$

Using the same technique as that in the design of the carrier loop, we find the RMS angle is 22. 2 degrees. This requires an increase in threshold by

$$= \left(\frac{55}{22.2} \right)^2 = 6.1 \quad .$$

i. e. , by 7. 85 db.

Thus, the synchronizing threshold (with the additional degradation of 3 db due to PN correlation) is 5 + 7. 25 + 3 = <u>15.85 db.</u>

4. <u>Command data threshold.</u> Using parity for every information bit, a bit error probability of 2. 6 x 10^{-3} is required.

Due to the noisiness of the synchronizing loop, the differentially coherent curve is used.

Threshold = 7. 22 + 1. 5 = 8. 72 db

Data Rate = 2/ 3 information bit/ sec.

a. <u>Selection of required command error detection technique.</u> It is shown that for the required probability of losing lock in the synchronizing loop and for the lowest value of probability of receiving without error, a command word consistent with the required minimum word acceptance probability, that the command decoder needs an error detection capability. Three error detection techniques were considered: (1) a simple parity check on the information bits, (2) a parity check bit for each information bit, and (3) a combination of the first two. Number (1) was inadequate, number (2) was satisfactory, and number (3) was appreciably better than required.

Let

P_1 be the probability of a data bit error.

P_B be the probability of an information bit error.

Q_w be the probability of a word being received correctly.

Let

P_w be the probability of a word being received incorrectly.

Q_B be the probability of no error in an information bit.

Q_A be the joint probability of not losing synchronization and not detecting an error.

P_o be the probability of losing synchronizing lock during a command word.

It is required that the probability of not losing lock in the synchronizing loop during a command word be 0.999. It is also required that Q_A shall be 0.9. Finally, the word error rate for a system using an error detection scheme shall be the same as for a system without such a scheme in which the bit error rate is 10^{-5}.

For a non-error correcting system with 20 bits per word we have a word error rate

$$P_w = 1 - Q_w$$

$$= 1 - (1 - P_B)^{20}$$

$$= 1 - (1 - 10^{-5})^{20}$$

$$\approx 20 \times 10^{-5} \quad .$$

1) <u>Simple parity check on total number of information bits</u>. In this case 21 information bits are received.

$$Q_w = (1 - P_1)^{21} \quad .$$

Also

$$Q_A = (1 - P_o)(Q_w + P_w) = 0.9 \quad .$$

Approximately

$$(1 - P_o)(Q_w) = 0.9 \quad .$$

Hence,

$$Q_w = \frac{0.9}{0.999} = 0.9009009$$

whence

$$P_1 = 4.95 \times 10^{-3} \quad .$$

For this format

$$P_w \cong 1/2 \ (k) \ (k + 1) \ P_1^2 \ (1 - P_1)^{k-1}$$

where

$$k = 20$$

$$P_w = 1/2 \ (20) \ (21) \ P_1^2 \ (1 - P_1)^{19}$$

$$= 4.68 \times 10^{-3} \quad .$$

This word error probability is too high.

2) **Parity check for each information bit.** In this case, 40 data bits are received. A parity check bit is sent with each information bit. That is, a 0 is sent as 10 and a 1 as 01. This means that an information bit will be incorrectly interpreted if and only if both the information bit and its parity check bit are incorrectly detected. Such a scheme always will detect an odd number of errors and it will detect most combinations of an even number of errors. Then the probability of an error in an information bit is $P_b = P_1^2$. The probability of a k bit word being received correctly is $Q_w = Q_b^k = [(1 - P_1)^2]^k$ $\cong (1 - 2k \ P_1)$, while the probability of receiving it incorrectly is $P_w = [P_1^2 + (1 - P_1)^2]^k - (1 - P_1)^{2k}$

whence,

$$P_w \cong k P_1^2 \ [1 - (2k - 2) \ P_1]$$

$$Q_w = (1 - P_1)^{40} = 0.90090$$

$$P_1 = 2.6 \times 10^{-3}$$

$$P_w = 20 \ P_1^2 \ [1 - 38 P_1]$$

$$= 1.22 \times 10^{-4} \quad .$$

This is very close to the required value.

3) **Combination of the first two methods.** The value of P_w can be reduced even more at low cost by transmitting a parity check bit for all the information bits. (This bit would be transferred as an information bit and therefore would have its own parity check bit). This code then would detect odd numbers of errors in the reconstructed information bits. The result of combining these two error-detecting schemes is a triple error-detecting code that also will detect any other errors.

In this case,

$$P_b = P_1^2 \; , \; Q_w = Q_b^{\,k+1} = [(1 - P_1)^2]^{\,k+1}$$

or

$$Q_w \quad 1 - 2 \; (k + 1) \; P_1$$

$$P_w = \binom{k+1}{2} (P_1^2)^2 \; [(1 - P_1)^2]^{(k-1)} + \binom{k+1}{4} (P_1^2)^4 \; [(1 - P_1)^2]^{(k-3)}$$

$$+ \binom{k+1}{6} (P_1^2)^6 \; [(1 - P_1)^2]^{(k-5)} + \ldots$$

$$= 1/2 \, (k) \, (k + 1) \, P_1^4 \; [1 - (2k - 2) P_1] \; .$$

Notice that the probability of incorrectly receiving a command word has been greatly decreased by the addition of two more redundant bits.

$$Q_w = 1 - 2 \; (k + 1) \; P_1 = 0.9009009$$

$$= 1 - 42 \; P_1$$

$$P_1 = 2.5 \times 10^{-3}$$

$$P_w = 1/2 \, (20) \, (21) \, P_1^4 \; [1 - 38 \, P_1]$$

$$= 7.46 \times 10^{-9}$$

which is considerably less than the required value of 20×10^{-5}.

b. **Coding Voyager communications.** The ranges over which the Voyager communications will work are large. Naturally, the question of coding command or information data arises. And if this feature were shown to be

necessary, the selection of a method of coding poses a problem. The require-ments for the command link are examined first. One of the primary functions of the command link would be to rectify failures that could occur in many of the equipments on the lander. In the case of the Martian lander, which has and requires a self-righting capability, a hemi-omni antenna will be used.

At the greatest ranges (of the order of 360-million kilometers), it can be shown that the power required for carrier lock exceeds that required for data and synchronization by some 8 to 10 db. This fact, coupled with the desire to maintain a high degree of reliability and simplicity in the command receiver, indicates that any complex coding of the command data is not merited.

A very similar argument applies to the transmission of low-rate engineer-ing status data through the lander's low-gain antenna directly to the DSIF. In addition, the slow rate of change of these data and the fact that communication times exceeding four hours are possible, suggest that alternative mehtods of data reduction at the DSIF would be possible.

Coding could be applied with advantage to the high-gain lander data link with only slight additional complexity. The extra equipment required at the DSIF is not considered to be a problem.

1) <u>Coding methods</u>. Coding methods can be divided into two broad cate-gories depending on whether coherent detection is an integral part of the de-coding process: (1) incoherent error detecting and correcting codes are de-coded subsequent to coherent detection of individual bits, and (2) coherent biorthogonal codes are decoded coherently by maximum likelihood detectors. The coherent codes are really extensions of the ordinary PCM-PSK transmis-sions, having a more complex envelope.

As an example of the latter, the digilock coding system consists of an alphabet of 32 different pulse trains. Each group of 5 information bits, taken together, determines which of the 32 biorthogonal wave forms will be trans-mitted. The selected pulse train modulates the phase of the transmitter. At the receiver, the incoming IF waveform is passed through 32 matched filters, each matched to one of the permissible transmitted waveforms. It is hypo-thesized that the signal which was transmitted is the one matched to the filter having the greatest output. This decision results in the emission of a particular 5-bit pulse train from the receiver, corresponding to the original group of 5 information bits in the transmitter.

The incoherent codes are efficient as long as the SNR does not fall below the design value. If it does, the probability of more errors occurring per word than the code was designed to handle becomes large and the error rate rapidly increases. The coherent coding methods do not show the same kind of improve-ment threshold.

The digilock coding system requires only a small investment in extra equipment and power at the transmitter. The receiving equipment is relatively complex. It appears well suited to the task of transmitting data from vehicle to DSIF where the heavier decoding equipment is located in Earth. When the data rate is high and almost all the power in the transmitted signal resides in the data, and when the received bit-error rate is in the order of 10^{-3}, use of a 5-bit digilock system will reduce the transmitted power requirement by 3 db or increase the system margin by the same amount. (See refs. 12 and 13).

According to the results of this study, error-correcting codes with equal improvement possibilities have not been instrumented for space vehicles.

In the case of transmission from vehicle to Earth via the omnidirectional antenna, where most of the transmitted power resides in the carrier and relatively little are the data, improvement due to coding is hardly worth the effort; because it improves only the SNR in the data channel, whereas improvement is really needed in the carrier channel.

5. The ranging subsystem. Basically, the ranging system can be decribed as follows. A pseudonoise waveform 10^9 bits long is transmitted from Earth to the spacecraft at a rate of 10^6 bit/sec. A code generator in the spacecraft is synchronized with the received code, thereby permitting a clean reproduction of the received signal to be retransmitted by the spacecraft. By means of phase lock techniques, a second code generator on the ground is locked to the received code. The two ground-based code generators then are compared in phase to determine total transit time or range. The code acquisition both in the spacecraft and on the ground is accomplished in a manner very similar to the acquisition of the PN code in the command demodulator and detector. The acquisition procedure is complicated by the need to acquire rapidly and to keep the equipment in the spacecraft as simple as possible. Reference (14) claims a range measure to a resolution of 1.25 meters by considering the phase shift in the carrier as well as in the codes.

Figure 39A shows a block diagram for the ranging channel subsystem.

The wideband ranging signal is taken from the transponder at the output of the first IF amplifier, passed through an isolation amplifier, and run into a mixer. To accommodate this signal, a bandwidth of 3.5 mc was picked for the first transponder IF amplifier. The signal can be written as

$$IF = A \sin \{ w_I t + m [\cos w_c t] RC(t) \} \tag{63}$$

where m is the modulation index, $RC(t)$ is the binary ranging code and $\cos w_c t$ is a shorthand notation for the square wave clock. The other input to the mixer comes from the phase switch which can be thought of as a balanced modulator, and can be written as

$$Ref = B \ RC(t + r) \cos w_I t . \tag{64}$$

The mixer output is the product of equations (63) and (64).

$$P = \frac{AB}{2} \, RC\,(t + r) \, \sin m \; RC\,(t) \left[\cos w_c t\right] . \tag{65}$$

Since $\sin(-x) = -\sin x$ equation (65) can be rewritten as

$$P = \left\{ \frac{AB}{2} \, RC\,(t + r) \, RC\,(t) \, \sin m \right\} \left[\cos w_c t\right] . \tag{66}$$

Clearly if $r = 0$, $P = \left[\dfrac{AB}{2} \, \sin m \right] \left[\cos w_c t\right]$.

The possible values of $RC\,(t + r)\,RC\,(t)$ are shown below in (a). The probability of these values are shown in (b) below.

		$RC\,(t + r)$				$RC\,(t + r)$	
		1	−1			1/2	1/2
$RC\,(t)$	1	1	−1	$RC\,(t)$	1/2	1/4	1/4
	−1	−1	1		1/2	1/4	1/4

Value Chart	Probability Chart
(a)	(b)

Evaluation of $RC\,(t)\,RC\,(t + r)$ Product

Therefore the expected value of the coefficient of $\cos w_c t$ in equation (66) is,

$$\frac{AB \, \sin m}{2} \left[(1) \, \frac{1}{2} + (-1) \, \frac{1}{2} \right] = 0$$

for the case where r is not zero.

The phase-lock loop, which has a noise bandwidth of one cycle, acquires the clock, $\cos w_c t$, whenever the locally generated ranging code is in phase with the received ranging code. As in the command synchronizing channel, the code generator is driven by the loop VCO. The correlation detector indicates lock. The receiver-code combiner, code-component generator, and transmitter-code combiner are rather complex, due to the requirement of a short acquisition time for the very long ranging code.

After acquisition, the ranging system operation can be described as follows. There are three ranging code generators, two on the ground and one in the spacecraft. The signal from the transmitter coder (XC) is received by the spacecraft where the carrier is regenerated by the spacecraft coder (SC). The carrier is then modulated by the (SC) signal and retransmitted. On the ground the received signal is again regenerated by the receiver coder (RC). The phase difference between the outputs of (XC) and (RC) is a measure of the transit time to and from the spacecraft. If the ranging code is transmitted at 10^6 bits/sec a phase difference of one bit between the outputs of (XC) and (RC) corresponds to a range of 150 meters.

Reference (14) states that relative displacement can be measured to within one-half a digit period. This corresponds to a range resolution of 75 meters. It also states that a vernier, based on the RF phase displacement, will permit a range resolution of 1.25 meters.

In their experimental program, JPL has used a ranging code containing 10^9 bits and requiring 10^3 seconds to transmit. This extreme length and the very narrow noise bandwidth in the ranging channel's clock loop would lead to a fantastically long acquisition time if the scheme used in acquiring the synchronous code in the command receiver were used here. To avoid this, the ranging code is constructed from a set of shorter codes which are acquired sequentially. This implies a need for operating in several different modes, each characterized by a different code, during acquisition. A further requirement on the ranging system is that the (SC) and the associated logic circuitry dictated by the multimode operation be as simple as possible. To accommodate this requirement, the (RC) was given a great deal of flexibility.

In the JPL system, the (SC) operates in only three modes (ref. 15, page 76). In mode I, the transmitter code combiner output consists of the clock alone. In mode II, it consists of an acquirable code (reference 16, page 36) which is a function of all ranging code components, and in mode III, the code combiner output is the ranging code itself. While the (SC) is in mode II, the (RC) passes through eight different modes, one for each of the component codes, one for the clock, and one for their combination. The amount of correlation between the (SC) acquirable code and the (RC) signal determines the proper time for (RC) mode switching.

6.   The command system

a.   General characteristics. Commands will generally be received by a separate command system using a doubly redundant, crossed bi-cone, omnidirectional antenna system. The receiver for this system is similar to the receiver used in the transponder discussed in the previous subsection. The telecommunications design control chart for this system is shown in table 7. At a command bit rate of 2/3 bit/sec, a worst case carrier performance margin of -1.28 db can be expected at the worst case range of 3.6×10^8 km. The details of command demodulation and detection are now discussed.

TABLE 7

COMMAND TELECOMMUNICATIONS DESIGN CONTROL CHART

PROJECT: VOYAGER
CHANNEL: MARS ORBITER, COMMAND LINK
MODE: S-BAND OMNI-ANTENNA

No.	Parameter	Nominal Value	Tolerance (decibels)	Worst Value
1.	Total transmitter power	+80.0 dbm	±0.1	+79.9 dbm
2.	Transmitting circuit loss	-0.6 db	±0.2	-0.8 db
3.	Transmitting antenna gain	+51.0	±0.5	+50.5 db
4.	Transmitting antenna pointing loss	---		---
5.	Space loss = 32.46 +20 log F +20 log R F 2120 mc, R 3.6×10^8 km	-270.18 db	---	-270.18 db
6.	Polarization loss	-1.5 db	±1.5	-3.0 db
7.	Receiving antenna gain	+3.0 db	+0.0 -1.0	+2.0 db
8.	Receiving antenna pointing loss	-1.5 db	±1.5	-3.0 db
9.	Receiving circuit loss	-0.1 db	maximum	-0.1 db
10.	Net circuit loss	-219.88 db	+3.7 -4.7	-244.58 db
11.	Total received power	-139.88 dbm	+3.8 -4.8	-144.68 dbm
12.	Receiver noise spectral density (N/B) T system _____ NF _4db_	-169.8 dbm	±1.0	-168.8 dbm
Carrier Performance				
13.	Carrier modulation loss	-2.0 db	---	-2.0 db
14.	Received carrier power	-141.88 dbm	+3.8 -4.8	-146.68 dbm
15.	Carrier APC noise ($2B_{LO}$ = 10 cps)	+10.0 db	in 12	+10.0 db
	Carrier track (1-way)			
16.	Threshold SNR in $2B_{LO}$			
17.	Threshold carrier power			
18.	Performance margin			

TABLE 7 (Concl'd)

No.	Parameter	Nominal Value	Tolerance (decibels)	Worst Value
	Carrier - Track (2-way)			
19.	Threshold SNR in $2B_{LO}$			
20.	Threshold carrier power			
21.	Performance margin			
	Carrier - command			
22.	Threshold SNR in $2B_{LO}$	+12.4 db	±1.0	+ 13.4 db
23.	Threshold carrier power	-147.4 dbm	±2.0	- 145.4 dbm
24.	Performance margin	+ 5.72 db	+5.8 -6.8	- 1.28 db
	Subcarrier Performance			
	Command Channel			
25.	Bit rate (1/t) 2/3 bps	-1.76 db	---	- 1.76 db
26.	Required ST/N/B Pe = 2.6×10^{-3}	+7.22 db	+1.5 -0.0	+ 8.72 db
27.	Threshold subcarrier power	-160.82 dbm	+1.5 -1.0	- 159.32 dbm
28.	Modulation loss	-3.0 db	---	- 3.0 db
29.	Received data subcarrier power	-142.88 dbm	+3.8 -4.8	-147.68 dbm
30.	Performance margin	+17.94 db	+4.8 -6.3	+ 11.64 db
	Synchronization channel			
31.	Sync APC noise BW ($2B_{LO}$ = 1 cps)	+0.0 db	±0.2	+ 0.2 db
32.	Threshold SNR in $2B_{LO}$	+14.85 db	±1.0	+ 15.85 db
33.	Threshold subcarrier power	-154.95 dbm	±2.2	- 152.75 dbm
34.	Modulation loss	-3.0 db	---	-3.0 db
35.	Received Sync subcarrier power	-142.88 dbm	+3.8 -4.8	- 147.68 dbm
36.	Performance margin	+12.07 db	+6.0 -7.0	+ 5.07 db

b. Command demodulation and detection

1) General system characteristics. A block diagram of the command demodulator and detector (CDD) is shown in figure 40. The signal removed from the transponder phase-detector output can be represented as the product of D, the command data, PN a pseudo-noise code and $(2 f_s)$ the clock, multiplied by two in frequency. All three of these are binary waveforms taking on only the values plus one or minus one. A PN generator driven by the loop VCO is included in the CDD. If it is assumed that the locally generated PN signal is in phase with the PN component of the incoming signal, then their product will be plus one and the PN factors throughout can be disregarded. The input signal is run through parallel channels, one of which is shifted in frequency by f_s. The two channels are then filtered leaving D times the fundamental of the f_s. (The period of D is much longer than that of f_s.) Multiplication of these paralleled signals cancels D, since $D^2 = 1$, and leaves only f_s which is acquired by the phase lock loop. The PN generator has associated with it a word detector which produces a synchronization pulse, once each cycle of the PN code. This code period is also the bit period of D.

The synchronization pulse is used in the command bit detector to discharge the integrate-and-dump filter and for sampling. The quadrature detector produces an output whenever the synchronous phase-lock loop loses lock. This output is used to prevent the acceptance of a command word. If the locally generated PN code is not in phase with the received PN code, the loop input will be noise-like, preventing lock. In this case, the VCO will generate a frequency slightly higher than twice the clock frequency. This will cause the PN generator to speed up until its output is in phase with the received PN code. The CDD, therefore, has three outputs which are fed to the command decoder: the sequence of command bits, the synchronization pulse and the out-of-lock signals. The primary difference between this subsystem and that used in the Mariner is that here one input signal contains both the synchronous and data information. This is discussed in more detail in a later subsection.

The transmission rate for the information bits is 2/3 bits/sec. The noise bandwidth in the synchronizing loop was set at 1.0 cps, which leads to an acquisition time in the synchronizing a loop of 38.8 seconds, which is longer by 8.8 seconds than the transmission time for a 20-bit command word.

The detection scheme illustrated in figure 40 is that proposed in ref. (14). It has the advantage that less power is required than for the arrangement used for Mariner R. A comparative analysis of the synchronization properties of the two systems is now performed.

c. Comparative analysis of the synchronizing loop lock characteristics for Mariner and Voyager. The objective of this section is to show that the locking characteristics for the loop proposed in ref. (14) is identical to that previously used for Mariner R.
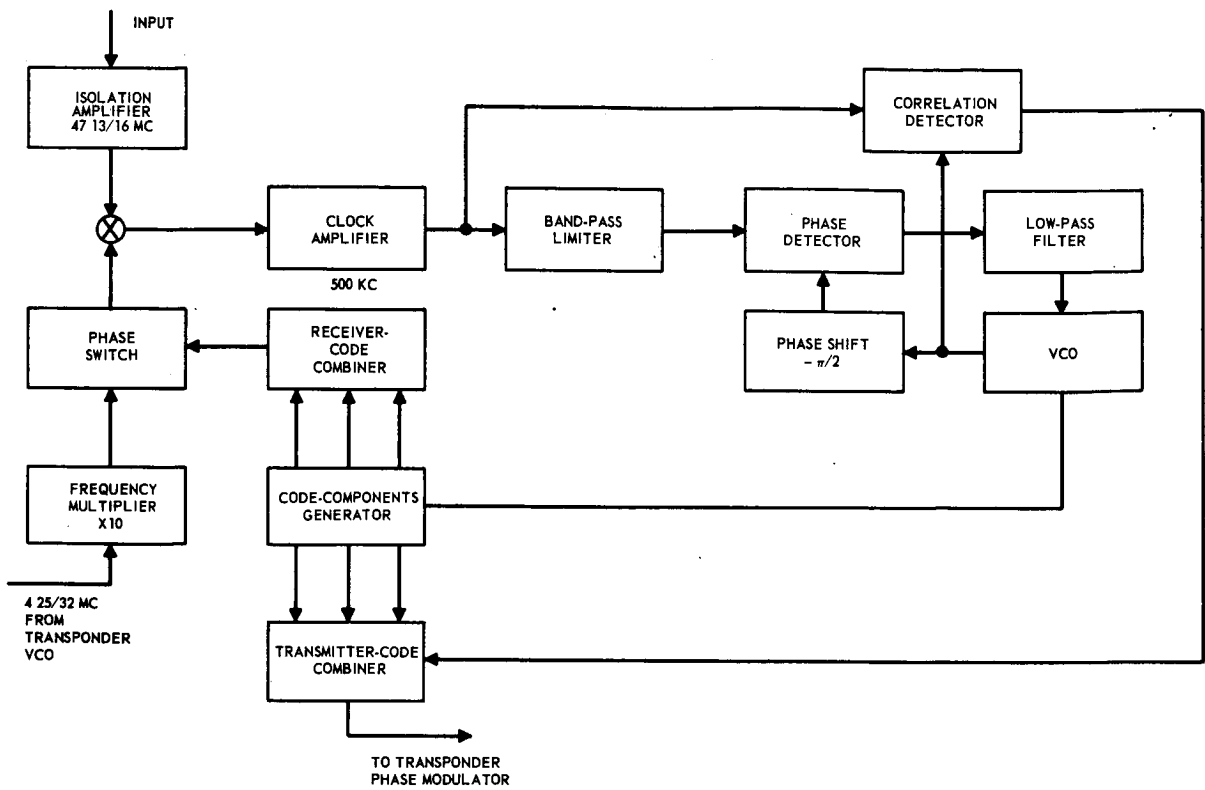
Figure 39a RANGING CHANNEL
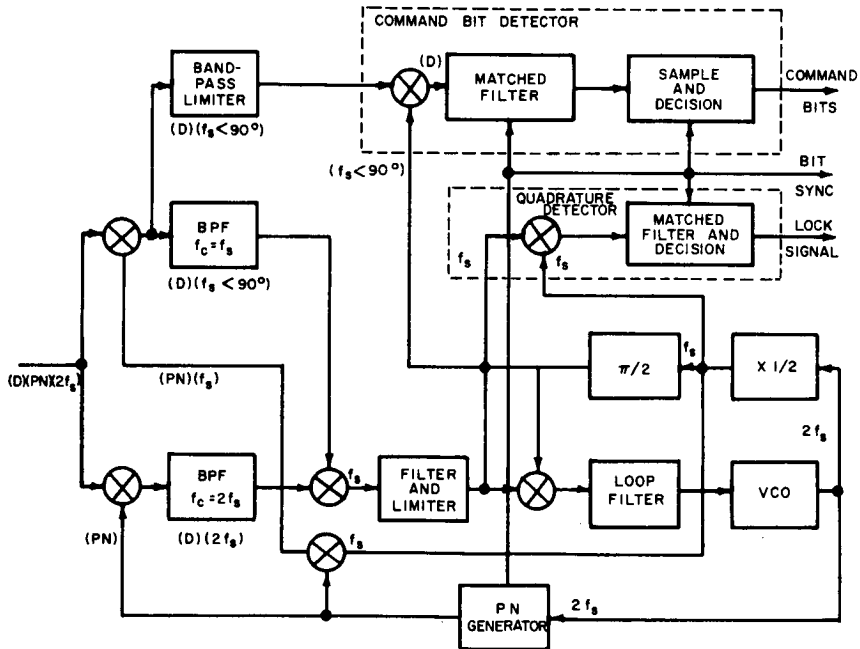
Figure 40 COMMAND DEMODULATOR AND DETECTOR

-120-

Synchronization pulses are provided in the spacecraft by the circuit of figure 41. The code generator has associated with it a word detector which produces one synchronization pulse for each code cycle. When the code generator in the spacecraft is running in synchronism with the code generator in the transmitter, the synchronization pulses will occur at the end of each command bit. The code generator is driven into synchronism with the transmitter code generator by the VCO which follows the transmitted clock signal. The double-loop configuration of figure 41 was used in the Mariner because it is very difficult to build a wideband multiplier with a dc output when the input S/N is low. The operation of the double loop now will be considered in detail.

If the loop is not in lock there will be a time difference, τ, between the incoming code and the locally generated code. The output of the first mixer will then be

$$\text{code } (t) \text{ clock } (t) \text{ code } (t + \tau) \quad .$$

This signal is mixed with a locally generated clock (t) which has been shifted a quarter of its period, P. The error signal driving the VCO is the integral of this second product. (The integration is due to the filter.)

$$E(\tau) = \int_{\text{period } = P_1} \text{code } (t) \text{ clock } (t) \text{ code } (t + \tau) \text{ clock } \left(t + \frac{P}{4} + \tau\right) dt \quad . \tag{67}$$

The period, P_1, is a multiple of the period of the code, clock product. (This integration period is necessary to get the error function which JPL derived and experimentally verified.) The integral of equation (67) can be approximately factored as

$$E(\tau\lambda) = \left[\int_{P_1} \text{code } (t) \text{ code } (t + \tau) dt \right] \cdot \left[\int_{P_1} \text{clock } (t) \text{ clock } \left(t + \frac{P}{4} + \tau\right) dt \right] \quad . \tag{68}$$

The two factors of equation (68) can be recognized as the correlation functions of the code and the clock, respectively. The correlation of a square-wave clock with itself shifted $P/4$ is shown in figure 42.
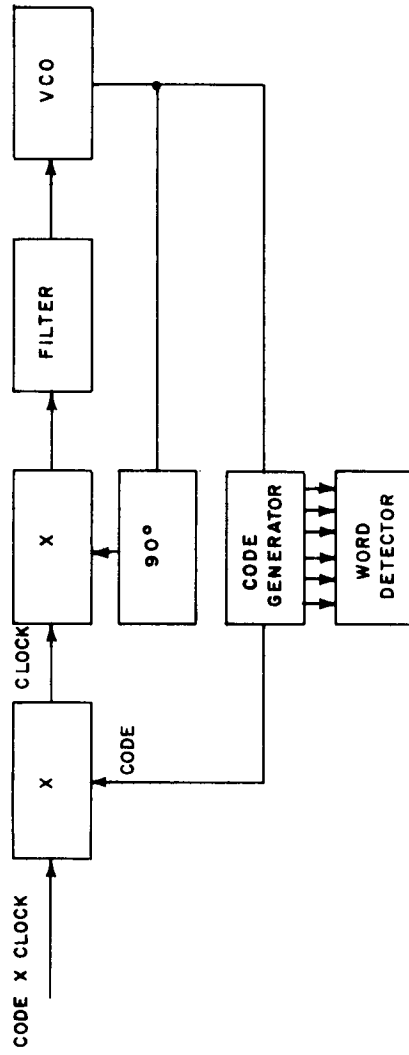
Figure 41 MARINER R LOOK

63-9685

-122-

As an example the code will be taken to be an m-sequence of length 7. The code and its correlation function are shown in figure 43.

If the clock period equals two code bit periods the composite error function will be as shown in figure 44. (P_1 = 14 code bit periods.)

When E (r) is approximated by the product of the two correlation functions $b = \dfrac{P_1 (P_1 + 1)}{2} = 105$ while $a = P_1 = 14$. When E(r) is evaluated exactly from

equation (67) the shape of E(r) is the same as for the approximation. However, b = 12 and $a = 4$.

For the approximate correlation function, $b/a = \dfrac{P_1 + 1}{2}$ which gets large for

P_1 , so that the low level ripple becomes less significant. Therefore, in the practical (long code) case the correlation function can be approximated by figure 45.

The vertical axis of figure 45 can be thought of as the VCO frequency axis since this coordinate is proportional to the VCO control voltage. The frequency f_o is the VCO offset. Consider the effect of operating at certain r. For $r = r_1$, if the LO (the code generator) starts to gain (decreasing r) the VCO will speed up decreasing r even more. If initially the LO started to fall behind (increasing r) the VCO would slow down causing a greater increase in r. Therefore, r_1 is an unstable point. For $r = r_2$, if the LO starts to gain it will continue undisturbed. If it starts to fall behind, the VCO will speed up forcing r back toward r_2 . For $r = r_3$, if the LO gains, the VCO will speed up causing it to gain more. If the LO is falling behind, it will continue undisturbed. For $r = r_4$, if the LO starts to gain, the VCO slows down while if the LO starts to fall behind the VCO speeds up so r_4 is a stable lock point.

For $r_5 = r$, if the LO starts to gain, it will continue undisturbed while if it starts to fall behind, the VCO will slow down causing it to fall farther behind. For $r = r_6$, if the LO starts to gain the VCO will slow down forcing r back to r_6 . If the LO had started to fall behind it would have been undisturbed. It can now be seen that r_4 is a stable point, r_2 is quasi-stable for the case where the VCO offset frequency is less than the lock frequency while r_6 is a quasi-stable point for the case where the VCO offset frequency is greater then the lock frequency.

The existence of the quasi-stable points is a serious problem since JPL has shown experimentally that the loop will often lock at these points. It can be seen from figure 45 that if the waveform between r_3 and r_5 was repeated every P_o sec, the number of stable points would be doubled and the quasi-stable points would be eliminated. As it is, the alternate waveforms are inverted. Considering this waveform (from r_3 to r_5 in figure 45) in more detail it is seen to be the product of the two waveform segments shown in figures 46 (a) and (b).

$$\int_{P_I} CLOCK\ (t)\ \ CLOCK\ (t + \frac{P}{4} + \tau\ )\ dt$$
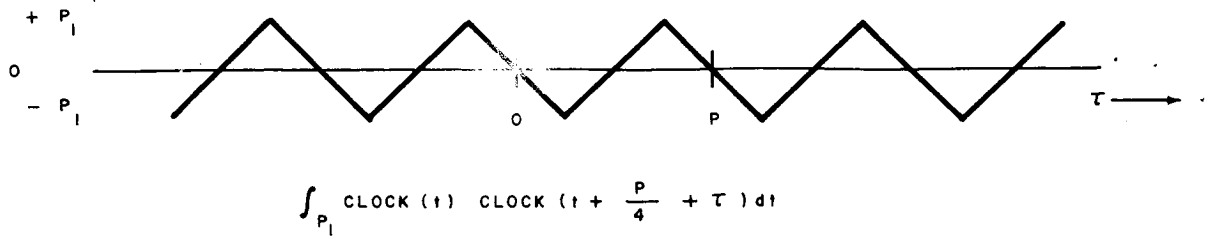
CLOCK (t)

63 - 9686

Figure 42 CORRELATION OF A SQUARE WAVE CLOCK

CODE (t)

$$\int_{P_I} CODE\ (t)\ \ CODE\ (t + \tau)\ dt$$
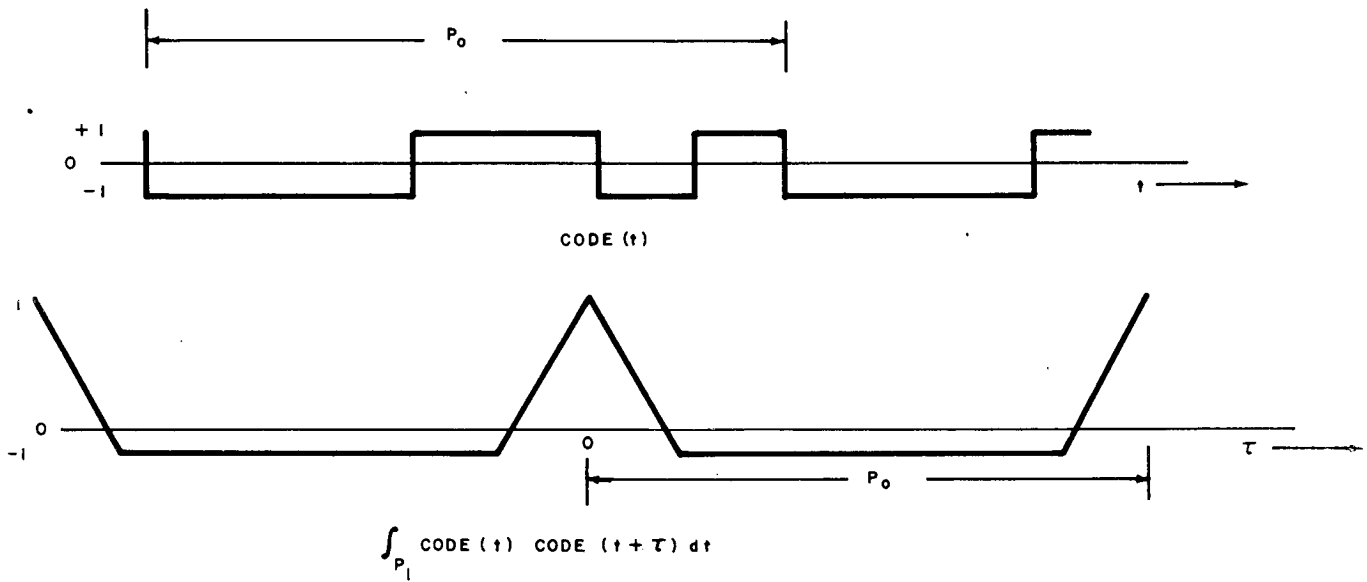
Figure 43 CORRELATION FUNCTION OF A CODE

P/2

E (τ)
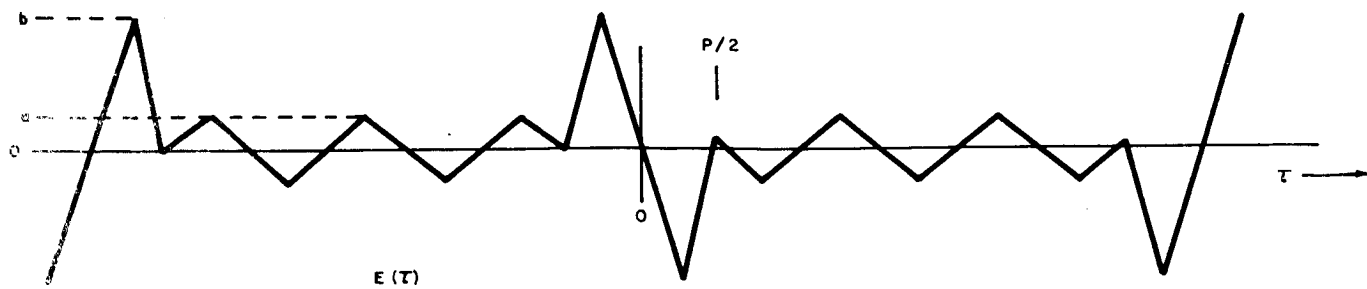
63 - 9687

Figure 44 COMPOSITE ERROR FUNCTION

-124-

The ratio of code bit period to the clock period is an important parameter and it seems that the selected ratio (two code bit periods equal to one clock period) was a good one since an increase in the clock frequency by a factor of two would require the multiplication of waveforms (a) and (c) in figure 46. This would introduce a quasi-stable point in the immediate vicinity of the stable lock point. If the clock frequency had been decreased, the composite correlation functions would be the product of waveforms like (a) and (d) in figure 46.

Since the peaks of the two factors are widely separated, the slope ($\Delta f/r$) is less than it need be. (Notice how the factorization of equation (1) facilitates the analysis of this waveform.) Having the clock period equal to two code bit periods means that a code period will not be an integral number of clock periods since the PN code has an odd number of bits. It is this fact that causes the segment of triangular waveform of figure 45 to alternate in sign. Recalling that the waveform of figure 45 is the product of the waveforms of figures 42 and 43 and noting that the clock has no parameters that can be varied it appears that what is needed is a code with an autocorrelation like that of figure 47.

JPL found that the term-by-term product of an m-sequence with the clock gives such a code. If the m-sequence, a pseudo-noise code, is represented by the letters PN and the clock is represented by f_s , the modified code can be written as PN* = PN × f_s .

Equation (67) can now be written as

$$E(r) = \int_{P_1} PN^*(t) \times f_s(t) \times PN^*(t+r) \times f_s < 90 \text{ percent } (t+r) \, dt. \quad (69)$$

Consideration of the factored form of equation (69) has indicated that E(r) will look like figure 48.

This is verified by the following calculation.

When A* B is the convolution of A and B, (PN × f_s)* (PN × f_s <90 degrees) gives

$\ldots$, 0, +12, 0, +4, 0, −4, 0, +4, 0, − 4, 0, +4, 0, + 12,

0, − 12, 0, −4, 0, + 4, 0, −4, 0, + 4, 0, − 4, 0, − 12,

0, +12, 0, +4, $\ldots$

where

(PN × f_s) is ++ - - + + + + - - - - - - - - - + + - - - - + + + + + +

and

(PN × f_s < 90 degrees) is - + + - - + - + + - + - + - + - - + + - - + + - + - - + - + - + •

-125-
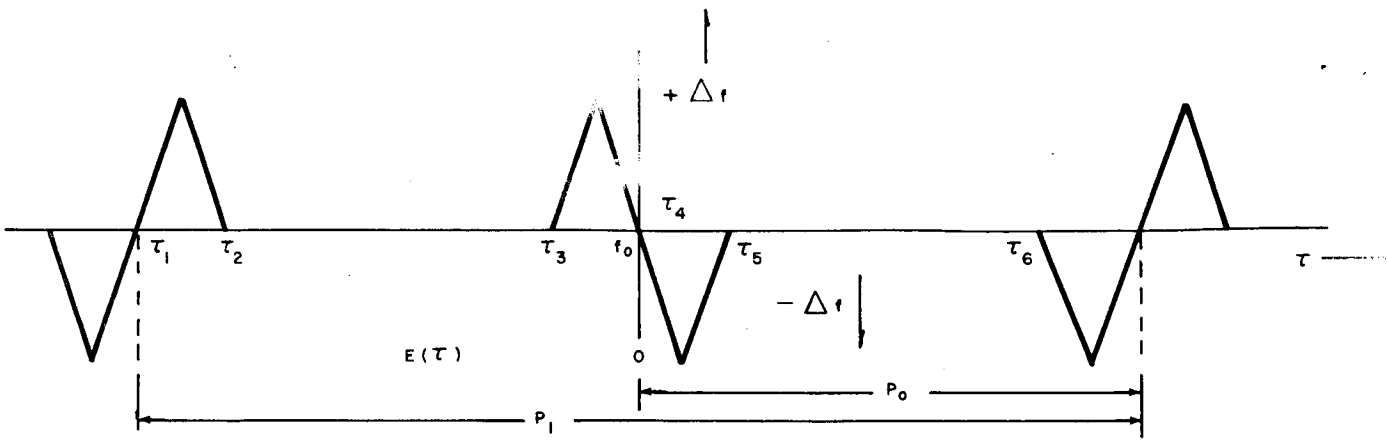
63-9688

Figure 45 APPROXIMATE CORRELATION FUNCTION

CODE CORRELATION
FUNCTION

CLOCK CORRELATION FUNCTIONS
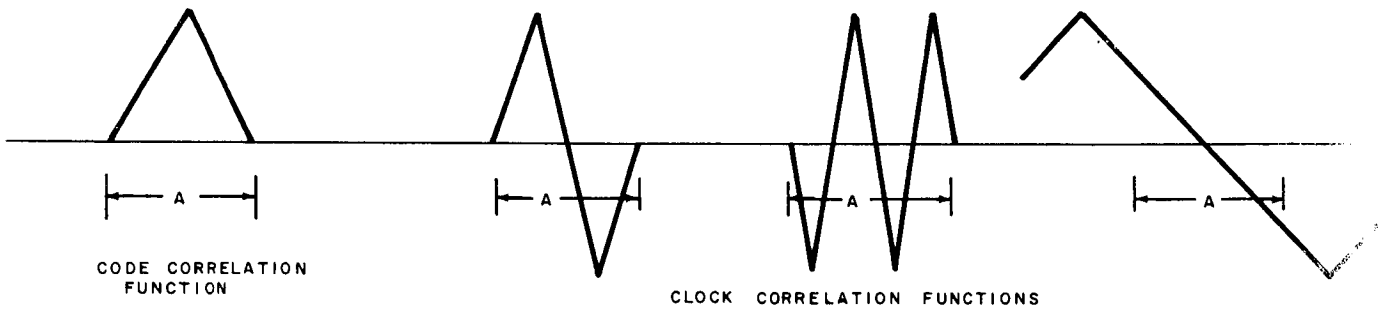
63-9689

Figure 46 CORRELATION FUNCTIONS
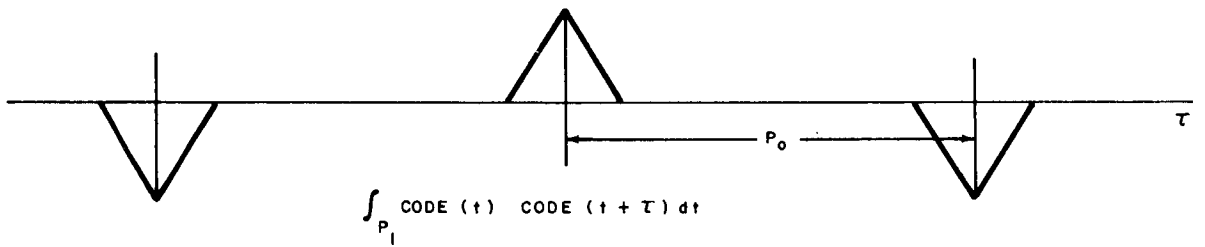
$\int_{P_1}$ CODE (t) CODE (t + τ) dt

Figure 47 $\int_{P_1}$ CODE (t) CODE (t + τ) dt

E (τ)
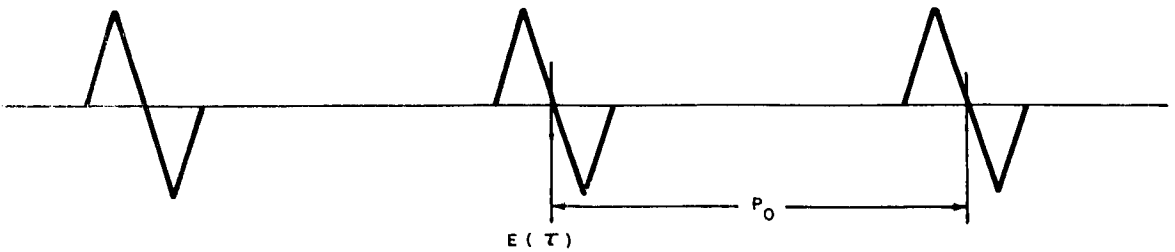
63-9690

Figure 48 ERROR FUNCTION E(τ)

-126-

These were found from

PN: - - - - - - + + + + - - + +

f_s : - - + + - - + + - - + + - - + +

f_s L 90 degrees: + - - + + - - + + - - + + - - +

and

(PN* × f_s)* (PN* × f_s < 90 degrees) gives

. . . . 0, + 16, 0, 0, 0, 0, 0, 0, 0, 0, 0, 0, 0, − 16 ,

0, + 16, 0, 0, . . .

where   PN* = PN × f_s .

This VCO control voltage, which has a stable lock point every PN code period and no quasi-stable lock points, is the one used by JPL in the Mariner spacecraft. Figure 49 shows the implementation used by JPL. Although the ninety degree phase shift is now associated with the received wave, equation (69) still applies, the factors are just rearranged.

2) <u>Analysis of proposed Voyager loop.</u> For the Voyager, it is proposed that D(t) modulate the synchronizing code. This scheme shown in figure 50 requires less power but does introduce complications in the synchronizing loop since D(t) must be removed from the incoming signal before the loop can lock.

Operation of the loop depends on the filters A and B. To determine the amplitude of the output of filter A, the multiplier output will be multiplied by f_s, the filter's center frequency, and then integrated.

$$R_1 (\tau) = \int [D (t) PN^* (t) f_s (t + P/4) PN^* (t + \tau)] f_s (t + P/4) dt \qquad (70)$$

where   PN*   is the synchronizing code

f_s is the square wave clock

P   is the clock period .
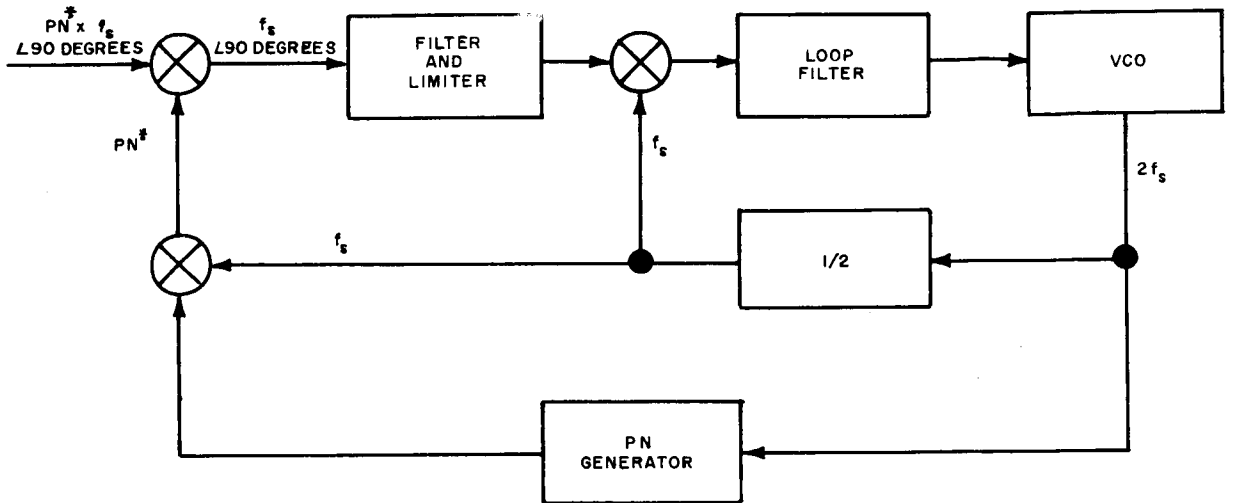
63-9691

Figure 49 MARINER PHASE LOCK LOOP
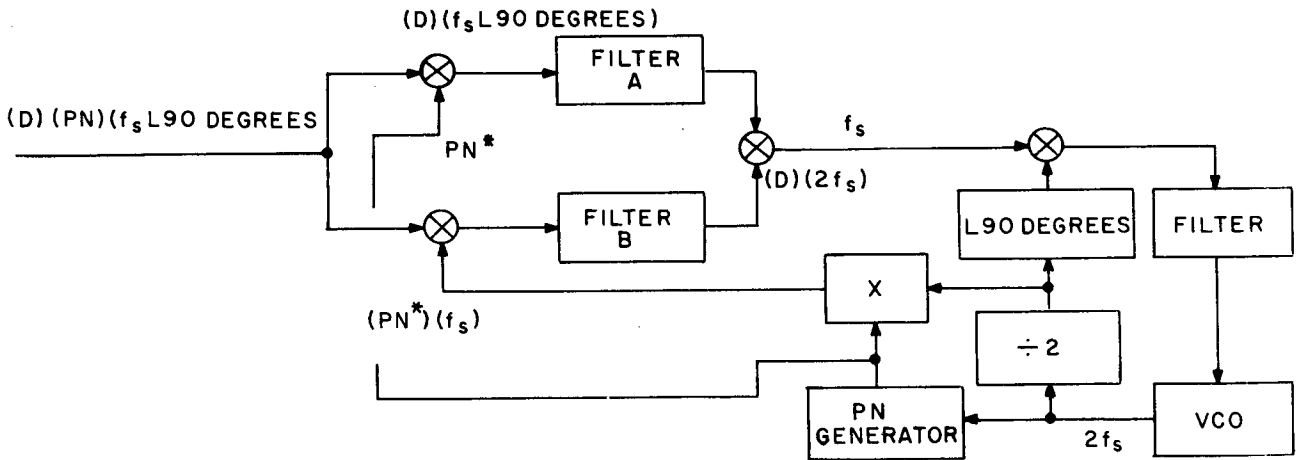
63-9692

Figure 50 PROPOSED VOYAGER LOOP

(P equals twice the bit period of the PN* code)

Since D(t) is a low frequency modulation it can be taken outside the integral leaving,

$$R_1(r) \cong D \int PN^*(t) \, PN^*(t + r),$$ (71)

which is just the correlation function of the synchronizing code. It is sketched in figure 51.

A similar analysis of the output of filter B which has its center frequency at $2 f_s$ gives

$$R_2(r) = \int [D(t) \, PN^*(t) \, f_s(t + P/4) \, PN^*(t + r) \, f_s(t + r)] \, 2 f_s(t) \, dt$$ (72)

where

$$2 f_s(t) = f_s(t) \, f_s(t + P/4)$$ (73)

$$R_2(r) \cong D \int PN^*(t) \, PN^*(t + r) \, f_s(t) \, f_s(t + r) \, dt$$ (74)

which is just the auto-correlation of PN.

$$R_2(r) \cong D \int PN(t) \, PN(t + r) \, dt$$ (75)

since $PN^* = (PN) \, (f_s)$. This function is shown in figure 52.

The two filter outputs are mixed producing

$$[R_1(r) \, f_s(t + P/4)] \, [R_2(r) \, 2 f_s(t)] = R_1' \, R_2' \, f_s(t)$$ (76)

-129-
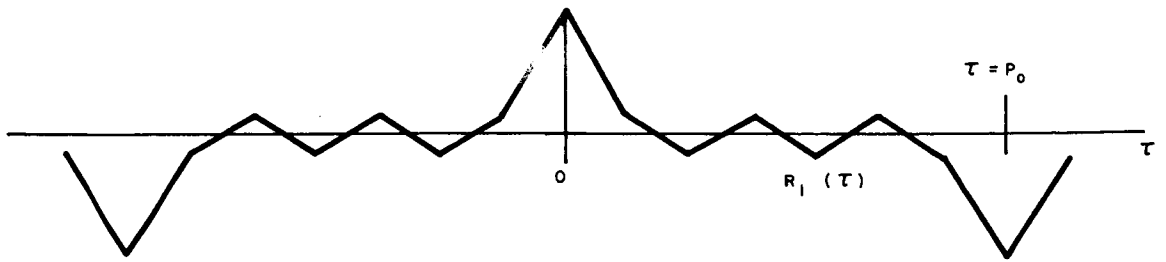
63-9693

Figure 51 CORRELATION FUNCTION OF SYNC CODE
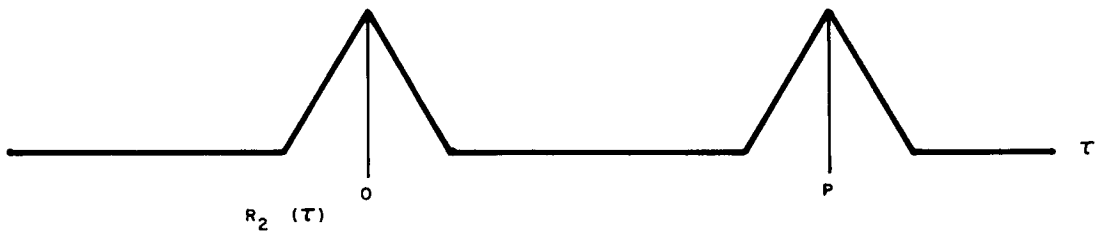
Figure 52 AUTO CORRELATION OF PN
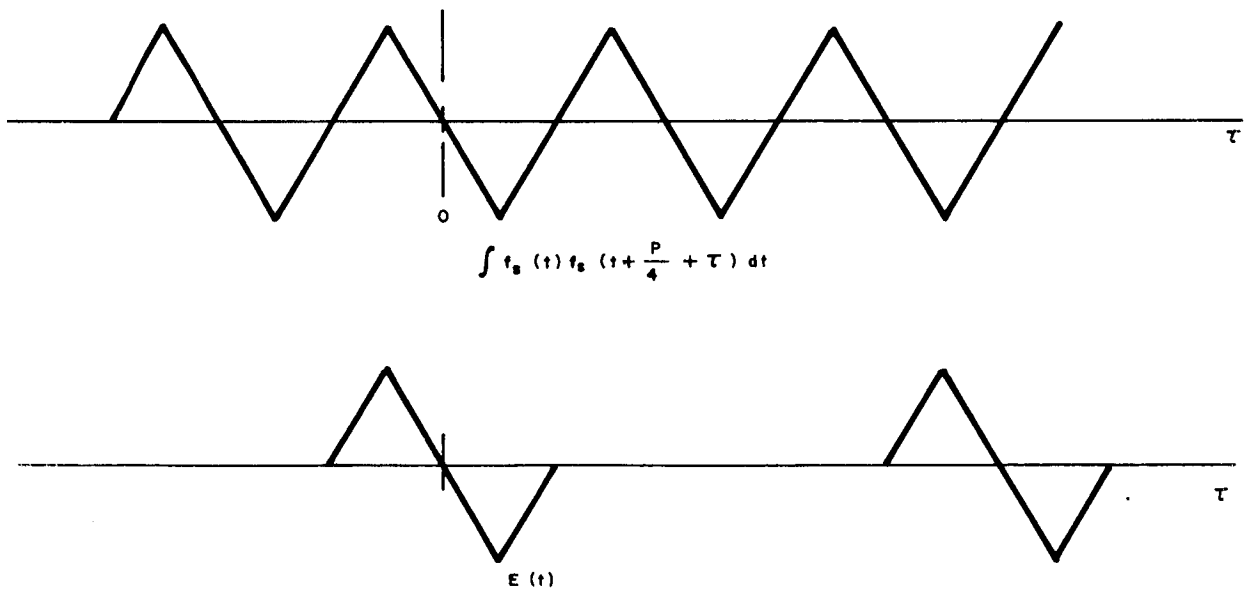
63-9694

Figure 53   25 a) $\int f_S(t) f_S (t + \frac{P}{4} + \tau) dt$ 25 b) $E(\tau)$

where $R(r) = D(t) R'$. Notice that the D's drop out. This signal then enters the loop where it is mixed with $f_s(t + P/4 + r)$. The error function or VCO control voltage is the integral of this product.

$$E(r) = \int R_1'(r) R_2'(r) f_s(t) f_s(t + P/4 + r) dt \qquad (77)$$

$$= R_1 R_2 \int f_s(t) f_s(t + P/4 + r) dt . \qquad (78)$$

The integral is sketched in figure 53a, and $E(r)$ is shown in figure 53b.

Therefore, the error functions of the two systems shown in figures 49 and 50 have the same form.

d. <u>Command decoder</u>. The last component to be discussed is the command decoder. Command words are assumed to be made up of 20 information bits. Each of these information bits is transmitted as a pair of bits which will be called data bits for purposes of differentiation. The decoder has two bit reconstructors which convert the received data bits to information bits. Two bit reconstructors are necessary since it is not known initially which pairing of the data bits should be made. The decoder programer prevents the use of a command word either if an error is detected in reconstructing the information bits, or if the synchronizing loop loses lock. The reconstructed command word moves into a shift register which is just long enough to store the command address (7 bits for the orbiter and 6 bits for the lander). This shift register is connected to an address recognition matrix which, when the shift register is filled, opens a gate to route the remainder of the command word. Since the only transmitted pairs are (1, -1) and (-1, 1), the system has an error detection capability. The primary purpose of sending an information bit as two short bits is to reduce the acquisition time of synchronizing phase-lock drop by a factor of 2. The lander command decoder should weigh one pound, occupy 11 cubic inches and take 5.5 watts. The orbiter requires twice as much power; however, weight and volume are only about 20 percent greater.

The period of an information bit has been set at 1.5 seconds. Each information bit will be sent as a pair of data bits each of which has a period of 0.75 seconds. Only the pairs (1, -1) and (-1, 1) will be used to represent information bits. The PN generator will go through a complete cycle in 0.75 seconds. If n_1 is the number of PN bits per cycle, the clock frequency, f_s , will be $n_1/1.5$ cps with $2 \times$ PN bits per clock cycle. For convenience in building the narrow band filters in the paralleled branches at the CDD input, n_1 should probably be greater than 15. The code length n_1 must satisfy the relation $n_1 = 2^n - 1$ where n is some integer. As has been shown, the average acquisition time in

the synchronizing loop is directly proportional to the clock frequency and hence to n_1. For these reasons n_1 will be picked to be 31 making $f_s = 20\text{-}2/3$ cps. The primary advantage in sending each information bit as a pair of bits is that it halves the period of the PN cycle and, therefore, the synchronizing loop acquisition time. There is also a small power savings due to the error detection inherent in this scheme. The spacecraft decoder is shown in figure 54.

It is the function of the bit reconstructor to interpret the pair (1, -1) as a -1, the pair (-1, 1) as a + 1 and the pairs (1, 1) and (-1, -1) as errors. Notice of a detected error would then be sent to the programer which clears the shift register, SR, associated with the matrix and gates off its input until the command word is begun again. Notice that the bit reconstructor must know which pair of data bits corresponds to a given information bit. This information could be provided in more than one way. First, the command word could be preceded by a short code word which would, upon recognition, activate the decoder and provide the bit reconstructor with its needed information. A possible prefix, suggested by JPL is (-1, -1, -1, 1, 1, 1,). When no command is being sent, the decoder continually receives plus ones. The above prefix never could be misinterpreted as a set of data bits but use of this word would effectively lengthen the command word by 3 bits and decrease its probability of acceptance. Second, two bit reconstructors could be used in such a way that they would examine different pairings of the data bits. In this case an error would not be indicated until both bit reconstructors had found an error. If no command word was permitted to begin with 2 plus ones or 2 minus ones (as information bits), one of the bit reconstructors would find an error within 3 data bits and it could stop reconstructing bits, thereby reducing memory requirements.

It seems that the mechanization of the second method would be simpler than that of the first and, as mentioned before, it requires two less information bits in the command word. For these reasons the second method is suggested, in which case the work synchronization recognition block in figure 54 would be identical to the bit reconstructor and error detector.

e. Spectrum of the received command. A noise-like pulse train is transmitted from the Earth to the spacecraft which, upon being decoded, provides synchronization. pulses and a coherent reference for the command detector. This pulse train is a modified maximal-length shift-register sequence, or m-sequence. M-sequences are often referred to as pseudo-noise and will therefore be represented by the letters PN. The PN is modified by multiplication with a square wave which has a period equal to the period of one PN bit. The effect of this is to replace each plus one in the PN by the pair (-1, + 1) and each minus one by the pair (+ 1, -1). Also, the period of the product is twice that of the PN since the PN contains an odd number of bits (2^{n-1}). Perhaps it should be emphasized that the synchronous waveform is periodic.
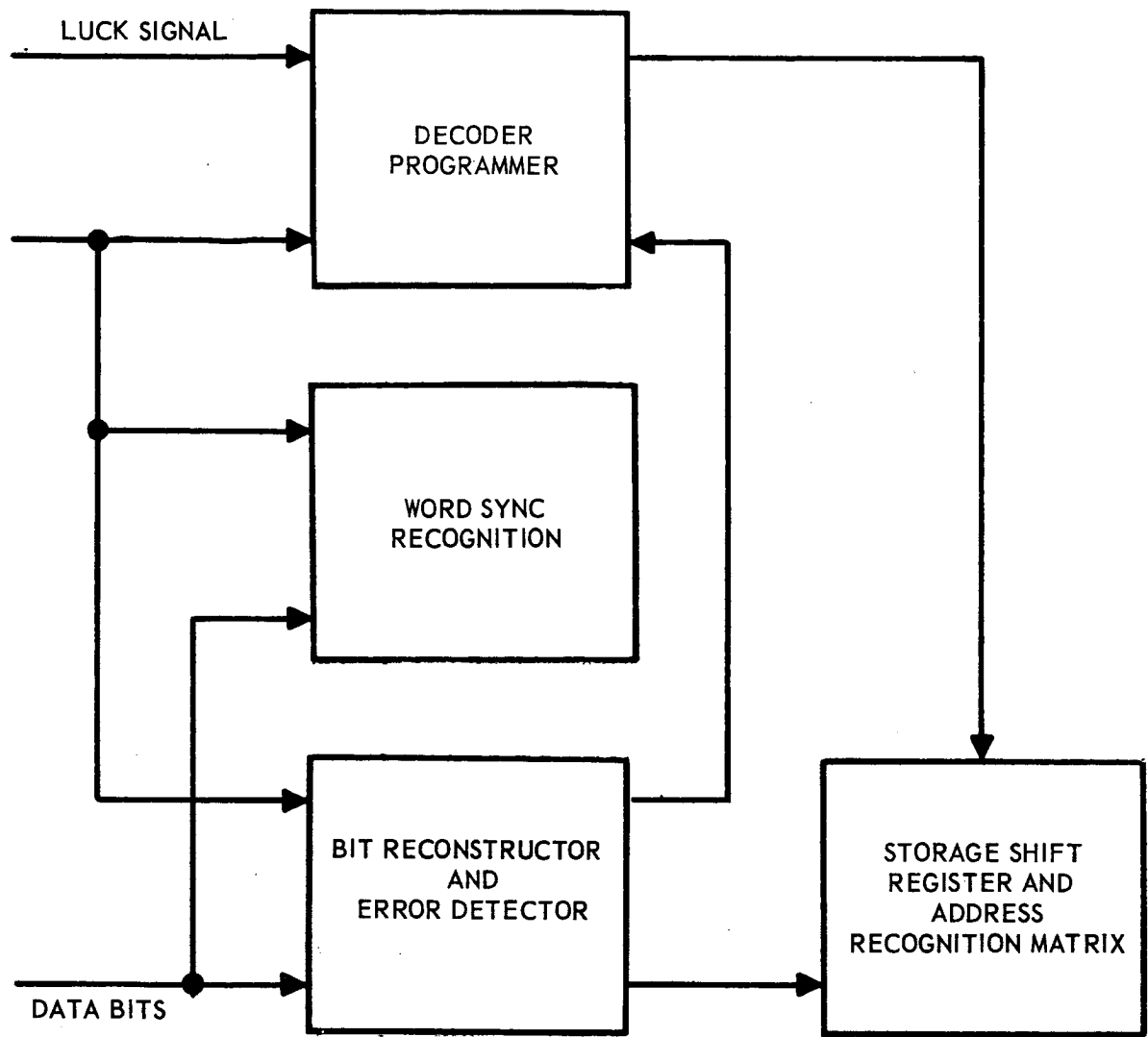
63-9695

Figure 54 COMMAND DECODER
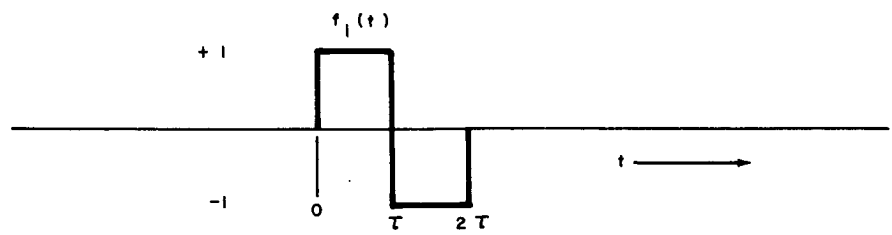
63-9653

Figure 55 RECT. FUNCTION

-133-

Consider the waveform shown in figure 55. The rect function has been defined as

$$\text{rect } t = \begin{cases} 1, & \text{for } |t| < \dfrac{1}{2} \\[2ex] 0, & \text{for } |t| > \dfrac{1}{2} \end{cases}$$

(79)

$$f_1(t) = \text{rect}\left(\frac{t - \tau/2}{\tau}\right) \ \text{rect}\left(\frac{t - 3\tau/2}{\tau}\right) .$$

The voltage spectrum of $f_1(t)$ is given by

$$F_1(w) = (\tau \text{ sinc } f\tau) \ [e^{-\pi i f \tau} - e^{-\pi i f 3\tau}]$$

(80)

where

$$\text{sinc } f\tau = \frac{\sin \pi f \tau}{\pi f \tau} .$$

Equation (80) can also be written as

$$F_1(w) = 2/\pi f \ \sin^2 \pi f\tau) \ e^{-2\pi i f\tau + i \pi/2} .$$

(81)

The synchronizing waveform consists of a train of pulse pairs like those of figure 55 with polarity determined by PN so it can be written as

$$f(t) = \sum_{k=1}^{2^n-1} a_k \left\{ \text{rect}\left[\frac{t - (4k-3)\tau/2}{\tau}\right] - \text{rect}\left[\frac{t - (4k-1)\tau/2}{\tau}\right] \right\}$$

where $\displaystyle\sum_{k=1}^{2^n-1} a_k$ is the PN waveform and a_k is either plus one or minus one.

By analogy with equations (80) and (81) the voltage spectrum of $f(t)$ can be written as

$$F(w) = (2/\pi f) \ (\sin^2 \pi \ f\tau) \sum_{k=1}^{2^n-1} e^{-\pi i f (4k-2)\tau + i \tau/2} .$$

(83)

The envelope of the power spectrum is now proportional to,

$$G(f) = \frac{\sin^4 \pi f \tau}{(\pi f \tau)^2} \quad . \tag{84}$$

The synchronizing waveform $f(t)$ which is defined in equation (82) phase modulates the carrier w_0 with a modulation index, m, giving as the transmitted signal,

$$s(t) = \sin [w_0 t + m f(t)] \quad \text{or} \tag{85}$$

$$s(t) = \sin w_0 t \cos mf + \cos w_0 t \sin mf \quad .$$

Notice that $f(t)$ takes on only two values, $+1$ and -1. Therefore, $\cos mf = \cos m$ while $\sin mf = f \sin m$.

$$s(t) = (\cos m) \sin w_0 t + f (\sin m) \cos w_0 t . \tag{86}$$

When $m = \frac{\pi}{2}$ the first term which is the carrier is suppressed and

$$s(t) = f(t) \cos w_0 t \quad . \tag{87}$$

The transponder loop locks onto the carrier and suppresses it at the output of the loop phase detector as a plot of $\left| \frac{(s)}{\theta_i(s)} \right| = \left| 1 - H(s) \right|$ shows. (See figure 100 on page 128 of ref.17) Therefore, the portion of the spectrum that is taken from the transponder phase detector output is just the second term of equation (86) shifted down in frequency by w_0

$$s(t) = f(t) (\sin m) \sim f(t) . \tag{88}$$

This signal is then processed by the command detector.

In the Voyager, the command word will modulate the function $f(t)$. The command word is made up of a sequence of plus ones and minus ones which change polarity only once during each period of $f(t)$. This does not alter the previous results except that $f(t)$ should be replaced by $D(t) f(t)$ in equations (85), (86), and (88) where $D(t)$ is the command word.

f. S-band power amplifiers

1) General discussion. The requirements for telecommunications of the   Voyager mission include higher power than has been previously required for space missions and extreme reliability and long operating life. When operating at increased transmitter powers, the transmitter electrical efficiency becomes a dominant consideration due to its influence on the size and weight of the primary spacecraft electrical system.

An amplitron power amplifier was selected for the S-band transmitters. This device has an overall efficiency of 50 percent including filament power.

Two cascaded amplitrons will be operated from an individual, conservatively designed power supply. The two halves of the amplifier essentially will be identical, consisting of an amplitron and its power supply. Due to the unique feedthrough feature of the amplitron, when either of the amplitrons is not operated, the power output from the amplifier will be one-half (3 db down) the maximum output power.

Three levels of power output are required, namely, 35, 70, and 120 watts. The 70-watt level is required by the lander, the other two by the orbiter. The basic configuration for all amplifiers is indicated in figure 56. The two cascaded amplitrons will be operated from an individual, conservatively designed power supply. The two halves of the amplifier essentially will be identical, consisting of an amplitron and its power supply. By exercising separate control over the two halves of the amplifier, the power output can be stepped in three increments either automatically or by remote control through DSIF command, as a function of the communications range. The three levels of transmitter power available would be the high-power levels previously mentioned which differ by 3 db, and the driver power level attenuated by the insertion loss of the amplifier (approximately 1.3 db), or about 1.5 watts.

Since each amplifier contains two amplitrons and two power supplies, it is useful to extend the redundancy consideration inherent in the design by considering the possibility of cross-connecting power supply 1 and tube 2, and tube 1 and power supply 2. This extends the redundancy inherent in the amplifier by allowing for the possibility of operation (with only a 3-db reduction in power) after a single failure of both an amplitron and a power supply. The switching requirement for this feature is illustrated in figure 57. In the worst case it is necessary to switch at 2.5 kv in an argon atmosphere.

In addition to the availability of the switch, the decision would have to be made whether to control the state of the switch internally within the amplifier through a logic network which would monitor power output and voltages internal to the power supplies, or whether to command the state of the switch externally to the amplifier, such as through remote command.

However, the reliability improvement with the feature of cross-connecting is illustrated in the two equations below: equation (89) represents the situation without cross-connecting; equation (90) represents the situation with the switch present. In both equations R_a is the reliability of the amplitron and R_p is the reliability of the power supply. R_s is the reliability of the switch where reliability is equal to 1, the probability of failure.
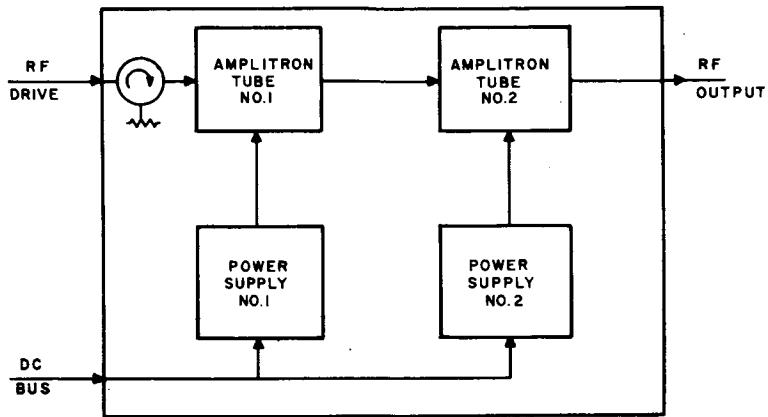
Figure 56 BASIC AMPLITRON AMPLIFIER BLOCK DIAGRAM
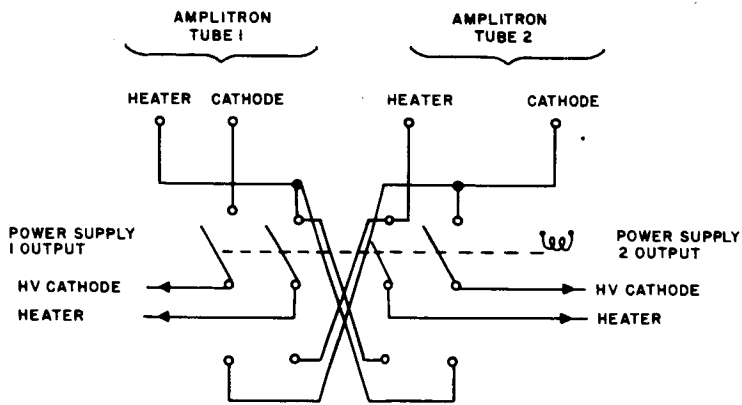
63-9697

Figure 57 BASIC AMPLITRON SWITCHING REQUIREMENTS

$$R = 1 - (1 - R_a R_p)^2 \qquad\qquad (89)$$

$$R = [1 - (1 - R_a)^2][1 - (1 - R_p)^2] R_s . \qquad\qquad (90)$$

Preliminary analysis, based on conservative parts reliability estimates, indicated that the amplifier, less amplitrons, will have a MTBF of 30,000 hours.

Amplitron MTBF is estimated at 33,000 hours. With proper design, the switching mechanism to be used could approach 100-percent reliability, although detailed analysis during the program will be made to substantiate this assumption. Based upon these MTBF's and a 150-day mission, the reliability of the configuration shown in figure 56 is, by equation (89), equal to 0.958. For the configuration of figure 57 the reliability is by, equation (90), increased to 0.9766. These values, though based upon conservative estimates for electronics and amplitron MTBF, already approach the desired reliability requirement of 0.995. With effective reliability and part application controls, and moderate part improvement programs, there is confidence that this goal of 0.995 will be met.

While the requirements indicate four different amplifier designs, namely, 35, 70, and 120 watts for both the Mars and Venus orbiters and Mars lander environments, only three designs will be developed and all designs will be essentially qualified for both environments. The requirements imposed by both environments will not severely influence the individual designs.

2) Detailed discussion

a) 35-watt amplitron amplifier. The 35-watt power amplifier will use the QKS 1051 amplitron which is expected to be fully qualified in advance of the amplifier development. The basic power supply for the amplitron has already been developed by Raytheon under a company-sponsored program.

The block diagram of the amplifier is indicated in figure 58. No circulator is required between the two amplitron stages for isolation because the second amplitron stage provides only 3 db of gain. The typical voltage versus current characteristics of the amplitron and the power supply are plotted in figure 59. In the presence of an RF drive signal, a sharp gauss line appears in the amplitron characteristics at a voltage corresponding to the frequency of the drive signal. As shown in the figure, presence of the gauss line allows considerably more current to be drawn accompanied by increased RF-power output or amplification of the drive signal. The amount of current drawn and the power

-138-

```
2 W RF          40 W
DRIVE           LOAD

QKS 1051        QKS 1051        35 W
AMPLITRON       AMPLITRON       OUTPUT

        H   C           H   C
    HIGH VOLTAGE
    SWITCH (IF USED
    FOR REDUNDANCY)

    H       HV          H       HV

AMPLITRON           AMPLITRON
POWER SUPPLY        POWER SUPPLY
(SEE FIGURE         (SEE FIGURE
    )                   )

        DC                  DC

DC                  DC CONTROL
INPUT
```
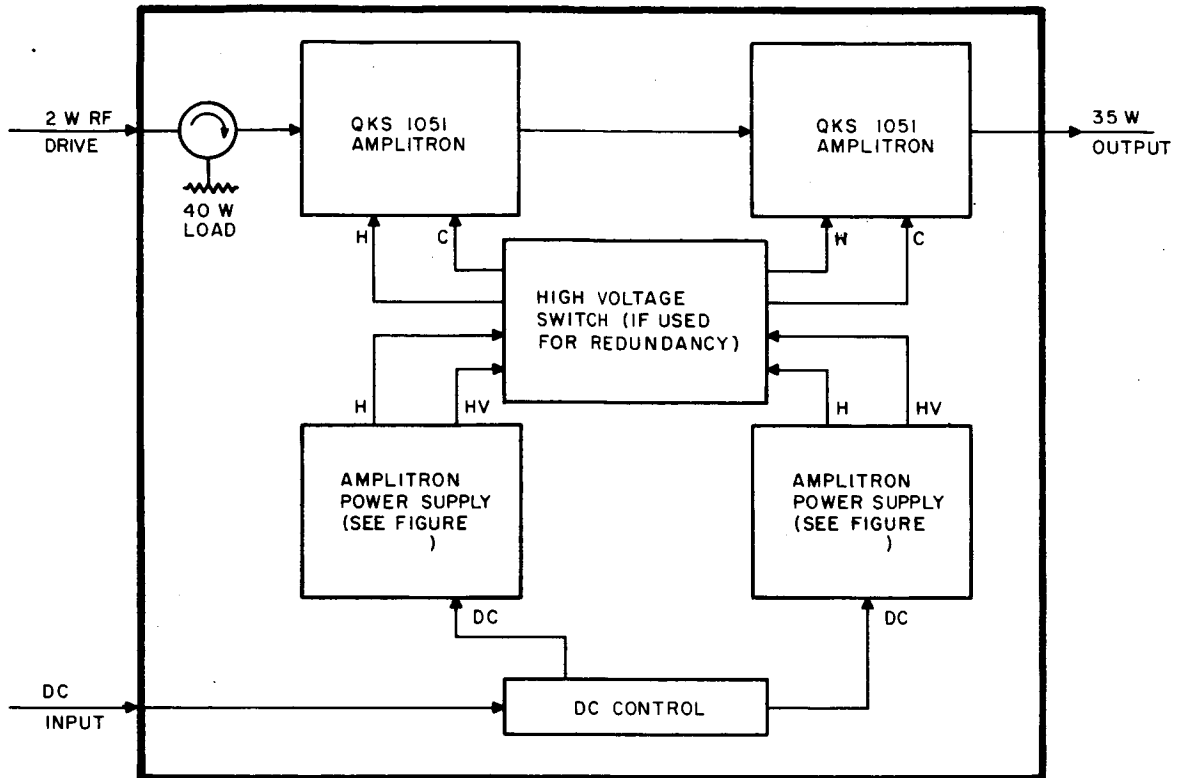
WEIGHT = 10 pounds
VOLUME = 180 in^3
EFFICIENCY = 40-50 percent
POWER OUTPUT = 1.5/18/35 W

63-9698

Figure 58 DETAILS OF 35-WATT AMPLITRON AMPLIFIER
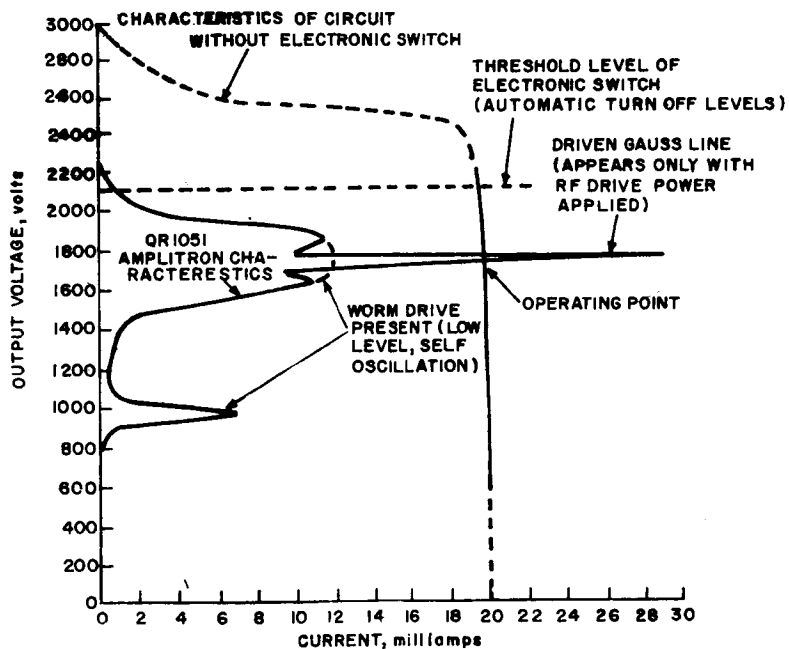
63-9699

Figure 59 QKS 1051 POWER SUPPLY CHARACTERISTICS

-139-

output are determined by the power supply characteristic and its intersection with the tube characteristic. Current regulation is therefore employed to stabilize the operating current, and therefore the power output.

The amplitron power supply is an all solid-state dc-to-dc converter. The basic power supply design has been evolved which has an electrical efficiency of 80 percent. Considerable electrical testing has been performed to ensure that this design approach is compatible with the amplitron. The characteristics of the power supply with anode current set at 20 milliamps is shown in figure 59. This basic design has been used in a system of similar requirements and has passed environmental qualification test program.

A block diagram of the present amplitron power-supply design is shown in figure 60. The power supply operates from a nominal 10-kc square wave and regulation is achieved by a switching technique which pulse width modulates the basic 10-kc signal. Power amplification and conversion to the appropriate impedance level is achieved in the push-pull switched transistor amplifiers. Regulation is performed at the input to these amplifiers at low power level by a magnetic amplifier. In addition to line and load regulation of 1 percent, this technique has features of extremely high efficiency, and in addition the transistors are used in the switched mode resulting in a low power dissipation and high reliability.

The current ripple is less than 0.1 percent. The phase modulation caused by this ripple is less than 1 degree peak at a 20-kc rate. These characteristics appear satisfactory for the Voyager system.

In addition to the current regulation, the power-supply design incorporates several features developed especially for the amplitron. These include programed heater warmup at increased power, and an automatic feature to ensure proper mode acquisition.

When the dc power is applied to the power supply, the heater circuit is energized and operated at a 7.8-watt level for 40 seconds. During this period the anode supply is not energized. After the warmup interval, heater power is reduced to a nominal 3.5 watts and the anode supply is energized. The anode output voltage increases until the amplitron and power-supply characteristics intersect. If this does not occur, for example, because of the absence of an rf-drive signal, the voltage will continue to rise above the voltage range corresponding to the frequency of operation. The high-voltage condition is used to control an electronic switch, which turns off the entire power supply. (This is indicated as 2100 volts in figure 59. Recycling can be obtained by automatic programing (by interrupting in input dc line).

A hermetically sealed reed relay manufactured by Computer Company, Inc., meets the nominal requirements for cross-connecting of amplitrons and power supplies mentioned above. The relay is rated for 5 kv at 50 watts, is
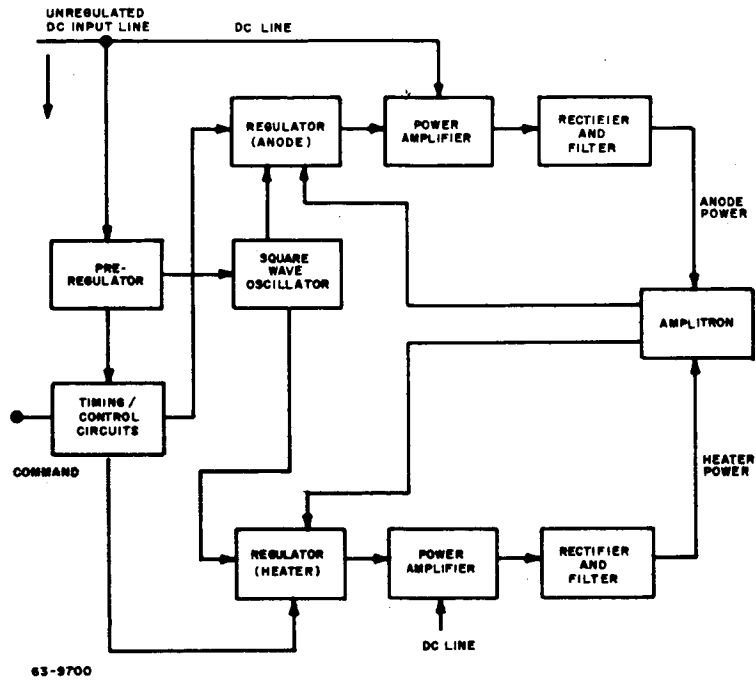
Figure 60 AMPLITRON POWER SUPPLY BLOCK DIAGRAM
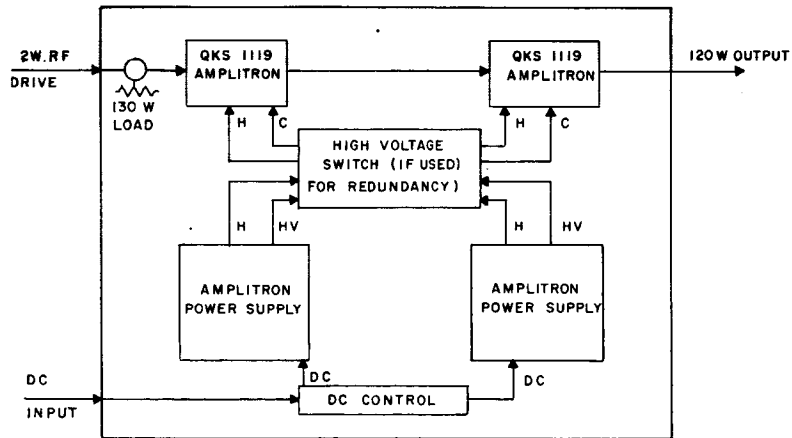
WEIGHT	16 LB	
VOLUME	275 IN^3	
EFFICIENCY	50 %	
POWER OUTPUT	1.5/60/120 W	

Figure 61 DETAILS OF 120-WATT AMPLITRON AMPLIFIER

-141-

2. 34 in.[3] in volume and is operated electrically by a solenoid. The switching required here would be a one-shot operation, needed only for the case of a failure of both an amplitron and a power supply which were not connected in the original state of the switch.

The power supply to be developed for use in the 35-watt Voyager amplitron amplifier will be basically similar in design to the power supply described above. The design task will draw on the considerable experience already gained with this type of power supply and especially with the critical magnetic component designs. The task will be to refine the present design for ultimate efficiency and performance while minimizing the number of electrical parts for highest reliability and ease of manufacture.

b) 120-watt amplitron amplifier. The 120-watt amplitron amplifier for Voyager will use similar techniques to those described above, and its block diagram is shown in figure 61. The amplitron tube to be employed is the QKS 1119 having a nominal power output rating of 70 watts. Each amplitron stage will be operated at an approximately 60-watt power-output level. Here again the circulator and loads are available. All redundancy and reliability features in the 35-watt amplifier will be present in the 120-watt amplifier design.

The power supply to be developed essentially will have the same block diagram as that for the 35-watt amplifier. The anode circuit will require approximately 100 watts of dc power which is within present capabilities of silicon high-frequency transistors. At the initiation of the development, if it proves that a qualified transistor of the required ratings is not available, the power-output capability can be extended by paralleling power amplifiers having a high-voltage output connected in series. It is expected that magnetic-amplifier timing and control, preregulator, and oscillator circuits can be developed for common use in the 35-watt and 120-watt amplifier. This fact is another inherent advantage in the amplitron-amplifier power supply which has been designed by Raytheon.

An adequate switch for performing the high-voltage switching function needed for cross-connecting as described above is not available due to the higher current level required. However, requirements are within the state of the art; any switch could be qualified if it were felt desirable from an operational or systems point of view to include this feature.

3) Development plan for amplitron amplifiers. While 35-, 70-, and 120-watt amplifiers are needed for operation in both the lander and orbiter environments, it is planned to develop but a single design for each amplifier. An initial task will be to develop an environmental model incorporating the most severe conditions of both lander and orbiter environments. This environmental model will be used in early engineering development testing.

While the electrical requirements of the two power supplies required are very different, the design approach which has been established allows for common components within the power supply. It is therefore planned to develop both amplifiers within a single engineering group.

Initial design activity will be directed toward ensuring that the assumption that preregulator oscillator, timing and control, and magnetic-amplifier circuits can be used in a common design for both power supplies. When this is assured, design activity will concentrate on developing the circuits for early engineering environmental testing. This early testing will reveal design margins and give confidence in the basic procedures. One of the design goals will be to achieve a design of minimum parts. It is primarily in the aforementioned circuits that the majority of parts are found. The early testing of these circuits will permit extensive concentration on their simplification.

It will be the goal of the development plan to test as early as possible the complete amplifier design for the environmental model established. This test will assure timely completion of the final amplifier qualification test program.

Throughout development, extensive use will be made of Raytheon's experience with this type of power supply design. Production facilities of the Raytheon Waltham operation currently engaged in manufacture of such a power supply will be used for the manufacturing program. These personnel will become involved in the design and test procedures early in the program to assure the timely release to production.

3.4 Detailed Description of In-Orbit Communication Link

The data monitored in this phase is primarily mapping data acquired through a television camera system. There is additional scientific and engineering status information acquired through a sampled data system similar to, but less complex than, the system used in the lander. As discussed in the lander section, the orbiter must also be capable of receiving data from the lander, for subsequent retransmission to Earth.

Since the orbiter will be placed in an elliptical orbit an altimeter will be used to set the focusing of the mapping optics system. The data from the image orthicon television camera will be stored in a tape recorder in a manner similar to the operation of the lander vidicon sampled data system. Since the amount of data handled by the orbiter mapping is much greater than in the lander, dynamic braking will be used in the orbiter tape recorder to minimize tape wastage. The input bit rate to the recorder, from a 5-bit gray scale analog to digital converter, is approximately 160,000 bits per second. The orbiter recorder will record at a speed approximately three times faster than the lander recorder. However, the playout speed is also about three times faster, keeping the ratio of record to playback speeds about the same as in the lander recorder.

The mapping data acquired during a single pass of the orbiter will be stored in one of two tape recorders used in mapping. When the orbiter begins the next pass, as indicated by the altimeter, the mapping data will be recorded in the second recorder. The first recorder will begin playing out its stored data through the directive link used in this phase, namely, the 8-foot parabola and 120-watt S-band transmitter. The communication link parameters associated with this phase are listed in table 8. At a transmitted bit rate of 4590 bits per second, a worst case data performance margin of +2.19 db can be expected at a worst case range of 3.6×10^8 km.

The 8-foot parabolic antenna selected for this system is not the optimum antenna required to minimize the in-orbit link system weight. The optimum antenna diameter is 13 feet as determined in the following section. The 8-foot antenna was selected to minimize solar pressures. The transponder, ranging, transmitter and command functions associated with this link were discussed in the in-transit section. Most of the design figures for this link were taken directly from the analysis performed for the in-transit case. However, a second antenna optimization was carried out for the load profile which will occur in orbit. Although this yielded value of 13 feet the weight penalty incurred through using an 8-foot dish is slight.

1. <u>Optimum antenna diameter.</u> Those weights which are a function of antenna diameter are

TABLE 8

IN-ORBIT TELECOMMUNICATIONS DESIGN CONTROL CHART

PROJECT: VOYAGER
CHANNEL: MARS ORBITER TO DSIF
MODE: 8-FOOT PARABOLA

No.	Parameter	Nominal Value	Tolerance (decibels)	Worst Value
1.	Total transmitter power 120 w	+50.79 dbm	+0.0 -0.79	+ 50.0 dbm
2.	Transmitting circuit loss with diplexer	+1.0 db	+0.0 -0.5	-1.5 db
3.	Transmitting antenna gain	+32.7 db	+0.91	+ 31.79 db
4.	Transmitting antenna pointing loss	-0.3 db	+0.3 -0.2	- 0.5 db
5.	Space loss = $32.46 + 20 \log F + 20 \log R$ F 2300 mc, R 3.6×10^8 km	-270.83 db	---	- 270.83 db
6.	Polarization loss	-0.0 db	+0.0 -0.08	- 0.08 db
7.	Receiving antenna gain	+61.0 db	+0.0 -0.5	+ 60.5 db
8.	Receiving antenna pointing loss	---	---	---
9.	Receiving circuit loss	-0.1 db	maximum	- 0.1 db
10.	Net circuit loss	-178.53 db	+1.21 -2.19	- 180.72 db
11.	Total received power	-127.74 dbm	+1.21 -2.98	- 130.72 dbm
12.	Receiver noise spectral density (N/B) T system 50°K NF	-181.43 dbm	±0.7	- 180.73 dbm
	Carrier Performance			
13.	Carrier modulation loss			
14.	Received carrier power		negligible	
15.	Carrier APC noise BW ($2B_{LO}$)			
	Carrier track (1-way)			
16.	Threshold SNR in $2B_{LO}$			
17.	Threshold carrier power			
18.	Performance margin			

TABLE 8 (Concl'd)

No.	Parameter	Nominal Value	Tolerance (decibels)	Worst Value
	Carrier - track (2-way)			
19.	Threshold SNR in $2B_{LO}$			
20.	Threshold carrier power			
21.	Performance margin			
	Carrier - telemetry			
22.	Threshold SNR in $2B_{LO}$			
23.	Threshold carrier power			
24.	Performance margin	Corresponds to Subcarrier SNR Degradation of 1.5 db	+ 3 db	
Subcarrier Performance				
	Data channel			
25.	Bit rate (1/t) 4600 bits/sec	+36.62 db	---	+ 36.62 db
26.	Required ST/N/B Pe = 5×10^{-4}	(8.7+1.5) db	±1.0	+ 11.2 db
27.	Threshold subcarrier power	-134.61 dbm	±1.7	- 132.91 dbm
28.	Modulation loss	---	---	---
29.	Received data subcarrier power	-127.74 dbm	+1.21 -2.98	- 130.72 dbm
30.	Performance margin	+6.87 db	+2.91 -4.68	+ 2.19 db
	Synchronization channel			
31.	Sync APC noise BW $(2B_{LO}$			
32.	Threshold SNR in $2B_{LO}$			
33.	Threshold subcarrier power	← ——— negligible ——— →		
34.	Modulation loss			
35.	Received Sync subcarrier power			
36.	Performance margin			

1) Weight of storage battery

2) Weight of the solar cell array

3) Weight of the antenna.

The reference orbit, 1700 x 10,000 km, has a period of 7.33 hours with an Earth umbra of approximately 1.42 hours. Periapsis mapping would take place for approximately 1.56 hours. The power loadings for the various phases of the orbit are tabulated below.

a. Constant power loading

Command transponder	20 w
Command decoder	11 w
G&C Complex	162 w
Altimeter	80 w
Scientific instruments	28 w
1 recorder	6 w
Total	307 w

b. Mapping requirements

Recorder (1)	6 w
Cameras	44 w
Multiplexing equipment	3 w
Total	53 w

c. Transmission requirements

Transmitter (eff = 0.5)	$2 P_T$ w
Drivers	20 w
Recorder (1)	6 w
Total	$2P_T + 26$ w

During an orbit, a duty cycle pattern, as shown in figure 62, results. Initially it is assumed that there is negligible sun umbra.

$380 + 2P_T$

$327 + 2P_T$

307

$327 + 2P_T$

T_1 T_2 T_3 T_4

|← 1.56 HOURS →|← 2.18 HOURS →|← 1.42 HOURS →|← 2.18 HOURS →|

MAPPING   EARTH UMBRA

|← 7.33 HOURS →|
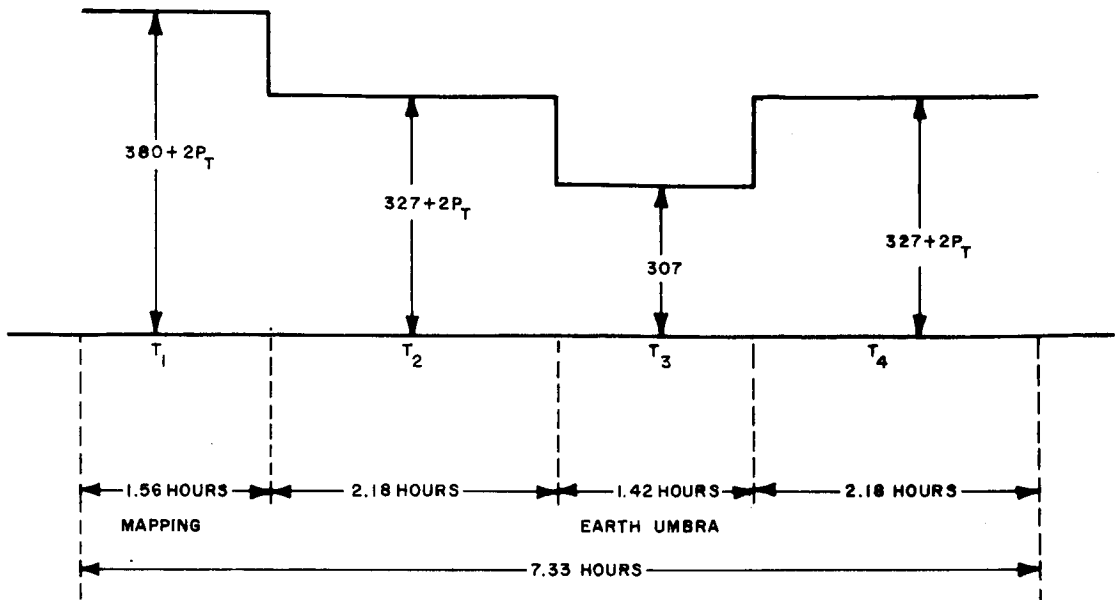
63-9702   Figure 62 IN-ORBIT LOAD PROFILE

Let amplitron efficiency = 0.50

     Let P_S = solar cell raw output power

       $2P_T$ = transmitter input power

     Let 0.85 = power converter efficiency (typical)

For $0.85\, P_S > 327 + 2P_T$, i.e., $P_S > 385 + 2.35\, P_T$

$$\text{Battery WH} = \left[\frac{380 + 2P_T}{0.85}\right] - P_S \quad 1.56$$

$$= (443 + 2.35\, P_T - P_S)\ 1.56$$

$$= 691 + 3.66\, P_T - 1.56\, P_S$$

For a battery discharge rate $= \dfrac{10}{1.56} = 6.41$: Capacity factor = 0.708

$$\text{Battery Weight} = \frac{WH}{6.4 \times 0.708} = \frac{WH}{4.52} \tag{91}$$

$$= \frac{691 + 3.66\,P_T - 1.56\,P_S}{4.52}$$

$$= 153 + 0.81 P_T - 0.35 P_S \tag{92}$$

Also, with a battery recharge efficiency of 0.8,

$$0.85\left(P_S - \frac{327 + 2P_T}{0.85}\right)\,2.18 \times 2 + 0.85\left(P_S - \frac{307}{0.85}\right)1.42$$

$$= \frac{691 + 3.66\,P_T - 1.56\,P_S}{0.8}$$

$$0.85\,P_S - 1680 - 8.72\,P_T + 0.85\,P_S - 436$$

$$= 863 + 4.58\,P_T - 1.95\,P_S$$

Thus:

$$3.65\,P_S = 2979 + 13.30\,P_T$$

$$P_S = 3.64\,P_T + 819 \tag{93}$$

$$P_T = 0.27 P_S - 224 \tag{94}$$

Weight of solar cells at 4 w/ft^2 and 1.2 lb/ft^2

$$= 0.3\,P_S \text{ lb.} \tag{95}$$

Weight of antenna $= 3.7\,D$ \hfill (96)

Total Variable Weight

$$= 153.0 + 0.81\,P_T - 0.35\,P_S + 0.3\,P_S + 3.7D$$

$$= 153.0 + 0.81\,P_T - 0.05\,(3.64\,P_T + 819) + 3.7D$$

$$= 153 - 41 + (0.81 - 0.182)\,P_T + 3.7D$$

$$= 0.628\,P_T + 112 + 3.7D \tag{97}$$

from general control chart shown in optimization of lander direct link,

$$P_T = \frac{BR^2}{1.19 \times 10^5 \times D^{1.875}} \tag{98}$$

Total variable wt

$$= \frac{0.628\ BR^2}{1.19 \times 10^5 \times D^{1.875}} + 112 + 3.7D$$

For min. wt., we have

$$\frac{1.875 \times 0.628 \times BR^2}{1.19 \times 10^5 \times D_{opt}^{2.875}} \pm 3.7$$

whence $D_{opt}^{2.875} = 2.68\ BR^2 \times 10^{-6}$ $\tag{99}$

Minimum weight obtained from D_{opt} is

$$= \frac{0.628\ BR^2\ D_{opt}}{1.19 \times 10^5 \times 2.68 \times BR^2 \times 10^{-6}} + 112 + 3.7\ D_{opt}$$

$$= 1.975\ D_{opt} + 112 + 3.7\ D_{opt}$$

$$= 5.67\ D_{opt} + 112 \tag{100}$$

The weight penalty incurred in using a nonoptimum diameter D is:

$$= \frac{0.628\ BR^2}{1.19 \times 10^5 \times D^{1.875}} + 112 + 3.7D - 5.675\ D_{opt} - 112$$

$$= \frac{0.628\ D_{opt}^{2.875}\ D}{1.19 \times 10^5 \times 2.68 \times 10^{-6} \times D^{2.875}} + 3.7D - 5.675D \left(\frac{D_{opt}}{D}\right)$$

$$= 1.975 \left(\frac{D_{opt}}{D}\right)^{2.875} + 3.7D - 5.674D \left(\frac{D_{opt}}{D}\right)$$

$$= D \left[1.975 \left(\frac{D_{opt}}{D}\right)^{2.875} (D) - 5.675 \left(\frac{D_{opt}}{D}\right) + 3.7 \right]$$

for 4590 BPS

and 360×10^8 KM

$$D_{opt}^{2.875} = 2.68 \times 4590 \times (360)^2 \times 10^{-6}$$

$$D_{opt}^{2.875} = 1600$$

$$D_{opt} = 13 \text{ ft}$$

Whence weight penalty for an 8-foot dish

$$= 8 \left[1.975 \left(\frac{13}{8}\right)^{2.875} - 5.675 \left(\frac{13}{8}\right) + 3.7 \right]$$

$$= 35.36 \text{ lbs.}$$

2. <u>Reception of lander data.</u> To provide for receiving data from the lander, a linear pulsed chirp receiver is included on board the orbiter. This receiving system will not interfere with the normal mapping function since the received lander data will be stored in a separate tape recorder. The details of chirp modulation were discussed in the lander section. The details of the integrated S-band altimeter/orbiter-lander command system and the chirp receiver will now be discussed.

a. <u>Orbiter altimeter with command capability.</u>

1) <u>General discussion.</u> In this conceptual design for an S-band integrated orbiter altimeter/orbiter-to-lander command system, reliability, minimum weight, size, and power consumption have been emphasized. Solid-state and microminiaturization techniques will be employed where feasible.

The proposed noncoherent pulse system serves as a combination altimeter/command link. A magnetron transmitter operates at 2.19 gc with a peak output power of 200 kw. The transmitted waveform is a coded 5-bit word with five 1-microsecond pulses spaced 2 microseconds apart. The waveform for the altimeter mode employs 5 "ones" or 5 pulses for the altitude measurement from 10,000 to 1500 km. When used as an interrogation command from 1800 to 1500 km to the lander receiver, the waveform consists of less than 5 pulses with the middle pulse shorted out in the modulator. A solid-state modulator generates the five 20-kv, 20-amperes 1-microsecond pulses. The modulation is triggered by a 33 cycle/sec synchronizer.

Selection of the operating frequency in the specified 2 to 2.3 gc will necessitate a component development program for the magnetron and the TR tube with associated test equipment. The development programs will not be major ones since tubes can be scaled and modified to perform in the desired range. Another area of component development will be the solid-state modulator to provide the coded waveform for both altitude and interrogation functions with minimum weight and power requirements.

Detection of any of the multiple pulses will provide a 1 percent range measurement, thus increasing the altimeter system reliability.

Duplexing is performed with a branch duplexer using a TR gas tube mounted on aluminum waveguide. Coaxial cable is used from the magnetron but a transition to waveguide is needed for obtaining the necessary 60 db of receiver isolation. No ATR is required. Insertion loss of the duplexer is 0.3 db each way and cable loss is an additional 0.2 db each way.

The output from the duplexer is fed to the altimeter receiver. A preselector could be included or a time sharing program could be applied to either blank the altimeter receiver or signal the computer to disregard altitude measurements during communication intervals.

Local oscillator for the system is a solid-state chain with a 30-mc crystal oscillator and four stages of multiplication providing 1 milliwatt minimum at 2.16 gc. Signals are heterodyned in a crystal mixer using a silicon diode. A 30-mc, 4-stage subminiaturized IF amplifier provides 100+db gain with 2 stages of AGC for 60-db dynamic range. The bandwidth of the IF is 3 mc and the noise figure is less than 4 db.

The output of the IF amplifier is fed to a crystal detector and 1 stage of video amplification. The video output is used to stop an eight-stage binary counter and also to stop a range transmission gate.

Range measurement is made by counting the number of pulses fed to the master computer. Each pulse fed to the computer is equal to 7.1 km. The train of pulses is generated by a 21.5-kc crystal oscillator which feeds both the eight-stage counter and the transmission gate. Pulses enter the counter and the gate simultaneously upon receipt of the altimeter synchronizer pulse. The eight-stage counter is employed with additional logic circuitry to indicate to the altimeter that the range is less than 1818 km and that the lander can be interrogated if it is so desired. Presence of the interrogation command voltage and the altimeter command will actuate the pulse cancellation circuitry.

Basic system operation is shown in figure 63 with pertinent system parameters tabulated in table 9.

TABLE 9

ORBITER ALTIMETER DESIGN PARAMETERS

1.	Average Power Output	33 watts
2.	Peak Pulse Power Output	200 kw
3.	Frequency	2.19 gc
4.	RF Power Source	Magnetron
5.	Range	1500 km (min.) 10,000 km (max.)
6.	Power Consumption	71 watts
7.	Modulation Waveform	5 coded pulses
8.	Range Accuracy	1 percent
9.	Weight	16.6 pounds
10.	Volume	199.0 in.^{3}
11.	Surface Reflectivity (0°)	0.1

2) Detailed system description

a) <u>Orbiter altimeter/lander command.</u> The orbiter altimeter/ lander command is an S-Band pulse system performing a dual service as (1) a command transmitter to the lander for interrogation, and (2) an altimeter functioning from 10,000 to 1500 km for camera focusing. Interrogation of the lander will range from 1800 to 1500 km. Altitude readout to assist in mapping will be available in a digital pulse train. The number of pulses will be directly proportional to range at 7.1 km/bit. Figure 64 describes the transmitted waveforms. Sensitivity calculations for the orbiter altimeter are shown in table 10.

TABLE 10

ORBITER ALTIMETER SENSITIVITY CALCULATIONS

$$P_t = \frac{(4\pi H)^2 \, KTB \, (NF) \, (S/N) \, L}{G_t \, \lambda^2 \, \sigma^\circ \, n} \qquad = 200 \text{ kw.}$$

where P_t = peak power

H = altitude (10,000 km)

K = Boltzmann's constant 1.38 (10^{-23}) joules/degree Kelvin

T = temperature 300°K

B = receiver bandwidth (3 mc)

NF = system noise figure, 10.3 db

S/N = signal-to-noise ratio (14.9 db)

L = System losses 5 db
    Transmission loss = 0.4 db
    duplexer   0.6 db
    Integration losses   1.0 db
                         2.0 db

G = antenna gain 17 db

λ = wavelength 1.3 (10^{-4}) km

σ = reflectivity 0.1

n = pulses per burst waveform 5

Pfd = false alarm probability 10^{-10}

Pd = probability of detection 0.90

    b) Transmitter. A fixed frequency S-Band magnetron serves as the transmitter operating at 2.19 gc. A magnetron is not currently available in the desired frequency band but will be scaled from current 3-gc magnetrons. An AFC loop will not be required since inherent stability and cavity design will satisfy system stability and bandwith requirements. The magnetron with integral magnet will weigh 3.5 pounds and will occupy a volume of 73.2 in.³ Transmitter/modulator design parameters are listed in table 11.
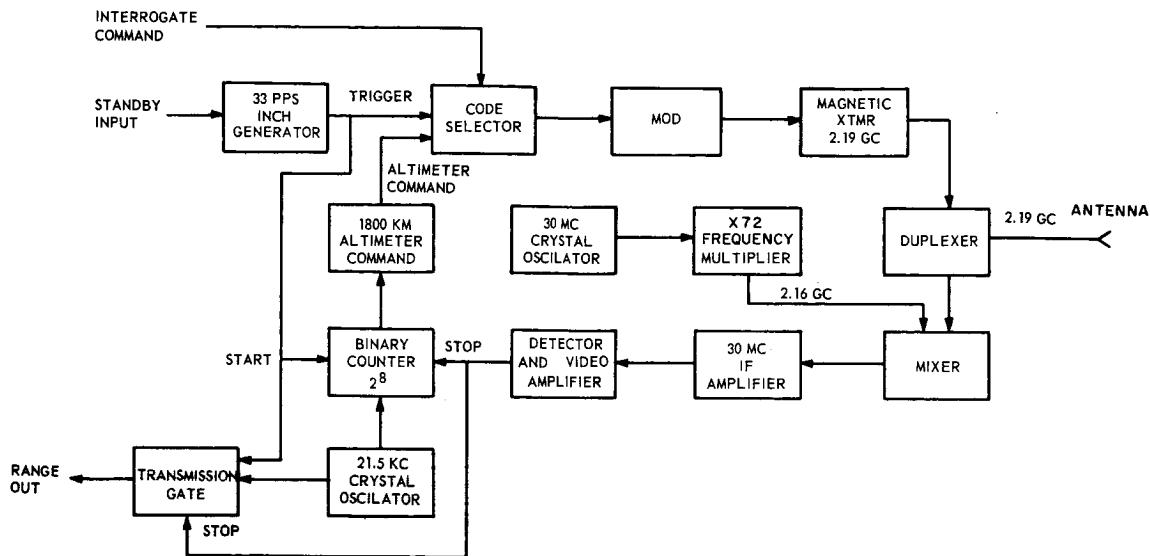
63-9703

Figure 63 ORBITER ALTIMETER/LANDER COMMAND
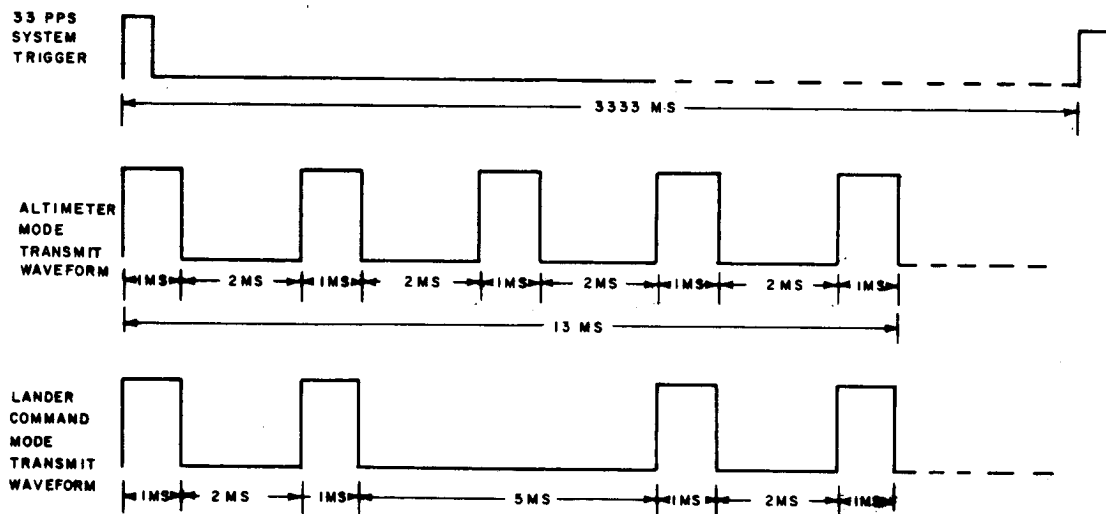
Figure 64 ORBITER ALTIMETER/LANDER WAVE FORMS

-155-

TABLE 11

DESIGN PARAMETERS FOR
TRANSMITTER/MODULATOR FOR ORBITER ALTIMETER

Frequency transmit	2.19 gc
Peak Power Output	200 kw (min.)
Pulse Width	1 Microsecond
Waveform--5-1 microsecond, pulses spaced	Altimeter mode
2 μ sec apart	
4-1 microsecond, pulses	Command mode
PRF	33 pps.
Magnetron Weight	3.5 pounds
Magnetron Volume	73.2 cubic inches
Frequency Drift (60 kc/°C)	300 kc (max)
Modulator/Transmitter Efficiency	50 percent
Peak Pulse Voltage	20 kilovolts
Peak Pulse Current	20 amperes
Filament Power (at 6.3 volts)	9 watts
Magnetron MTBF(Constant failure rate and	5000 hours
90 percent confidence)	
Modulator Weight	9 pounds
Modulator Volume	76 cubic inches
Modulator Component Count	105 parts
Modulator MTBF	10,000 hours
Modulator Power Input	66 watts

      c)   <u>Modulator/encoder.</u> An all solid-state modulator will drive the magnetron. Input waveform to the magnetron will be controlled by the encoder/synchronizer unit. A 5-bit message consisting of two "ones," a "zero," and two "ones" will be used to interrogate the lander. Altitude measurements will use a 13 microsecond word of five 1 microsecond pulses with 2 microseconds between pulses. Interrogation will use a 13 microsecond word with two 1 microsecond pulses spaced 5 microseconds from a second group of two 1 microsecond pulses. Spacing between the pulses is 2 microseconds. Delaying the pulses after the IF can be used to provide post-detection integration and additional reliability and accuracy, but is not planned since reliability is provided by multiple pulses and adequate S/N allowances. The four-pulse-coded waveform will only be transmitted to the lander when the encoder is commanded to interrogate and the altitude is compatible. Satisfying the two requirements will result in modulation of the transmitter with the preset code. A solid-state pulse generator will provide inhibit pulses to the modulator to prevent transmission of undesired pulses. The inhibit pulse will only occur when the altitude and interrogate commands are present. Figure 65 is a simplified schematic of the modulator.
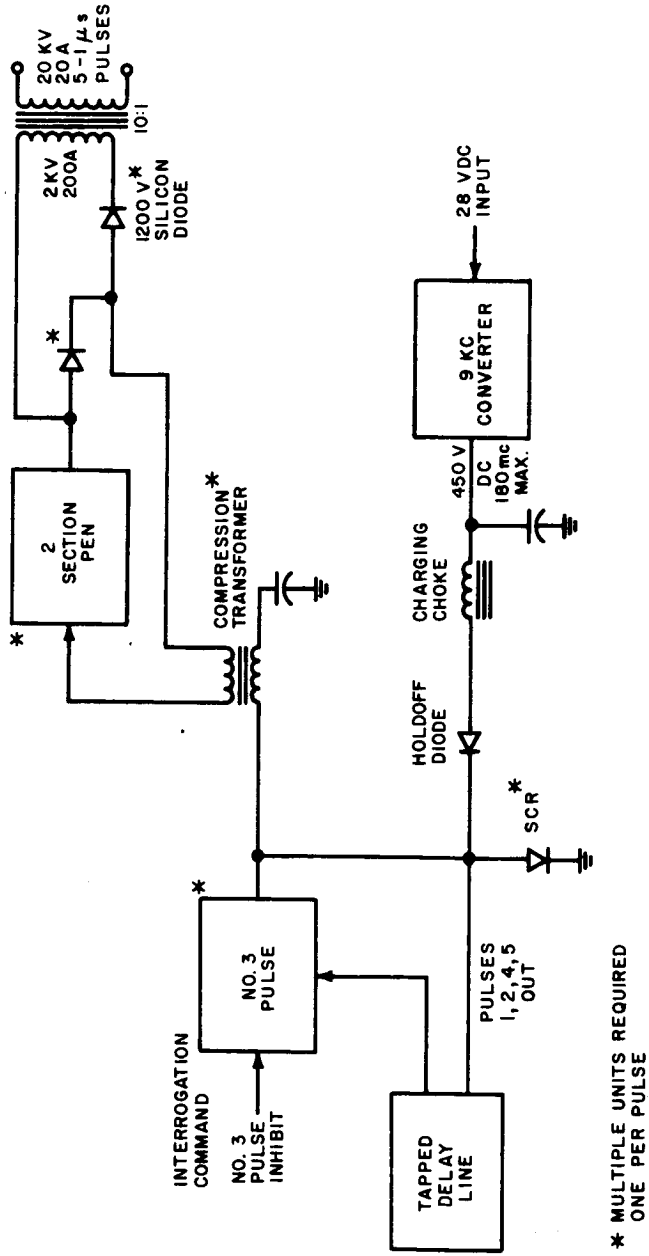
Figure 65   ORBITER ALTIMETER/LANDER COMMAND MODULATOR

63-9705

-157-

d) <u>Local oscillator.</u> Close frequency control of the magnetron will permit the elimination of the AFC loop and allow a solid-state oscillator/ multiplier chain to be used in lieu of a klystron or planar triode local oscillator. Major frequency drift of the magnetron will be due to temperature variation. A rated drift of 60 kc/°C in a controlled temperature environment of 5°C will provide 300 kc maximum drift. The solid-state local oscillator weighs 12 ounces and provides a minimum of 1 milliwatt of output power. No crystal oven will be required with $5(10^{-5})$ crystal stability giving a frequency drift of approximately 100 kc. This configuration will provide the simplest and lightest package commensurate with system weight and power requirements. The multiplier chain consists of 2 triplers, 1 quadrupler, and 1 doubler multiplying the fundamental frequency 30 mc by a factor of 72.

e) <u>Mixer/IF amplifier.</u> A branch duplexer with a TR gas protector tube mounted on an aluminum waveguide will control the signal flow to and from the antenna. Insertion loss is 0.3 db one way. The TR tube will require a development program and test equipment development. The return signal will be heterodyned in a crystal mixer capable of operating in a 150°C environment with a 5.5 db conversion loss and a 10-erg burnout rating. The receiver overall noise figure is 10.3 db.

$$F_{db} = L_c + 10 \log (F_{if} + t-1)$$

$$F_{db} = \text{overall receiver noise figure}$$

$$L_c = \text{crystal conversion loss (5.5 db)}$$

$$F_{if} = \text{IF amplifier noise figure (2.5)}$$

$$t = \text{crystal noise/temperature ratio 1.5}$$

Center frequency of the IF is 30 mc and the bandwidth is 3 mc. The IF is a four-stage microminiaturized unit with a noise figure less than 4 db, 100 + db gain, and 60 db AGC. Total weight of the IF is 3 ounces. Output pulses from the IF feed a solid-state detector and video amplifier to generate a stop pulse for the range counter and facilitate range measurement.

f) <u>Range processor.</u> Range will be determined by counting a 21.5-kc crystal-controlled clock. An eight-stage binary counter will start with an input signal from the synchronizer and will stop upon receipt of the video pulse; 21.5 kc will provide an accuracy of 0.5 percent of range for the specified 1500-km minimum altitude. The NT cut crystal is stable to ± 0.0.2 percent from -40 to 70°C. Overall system accuracy will be 1 percent. Output from the range processor will be supplied in a 21.5-kc pulse train whose number is directly proportional to the range at a value of 7.1 km per pulse. The synchronizer pulse will occur at a 33 pulse-per-second repetition frequency. A trigger signal will be supplied from the range counter to permit the lander to

be interrogated at ranges between 1500 and 1800 km. The range computer plus minor logic circuitry could be used to turn off the modulator during the portion of the orbiter trajectory when altimeter measurements are not required. Transmit "cease" and "start" signals are provided by the central computer during non-measurement periods. Filaments of the magnetron will be kept on during the inoperative phase of the trajectory and oscillators will continue to function for reliability purposes. At a predetermined time the modulator will be actuated by the central computer. Figure 66 is a preliminary schematic of the range computer and control logic. This modulator will permit selection of any code of pulses. Table 12 is a summary of the size, weight, and power requirement.

  b. <u>Relay telemetry receiver.</u> A simplified block diagram of the receiver is shown in figure 67.

   1) <u>RF preamplifier.</u> The 300-mc RF preamplifier will consist of two cascade stages in cascade each having a bandwidth of 30 mc and power gain of 15 db. The resultant overall bandwidth and power gain will be approximately 20 mc and 30 db, respectively. With this large bandwidth, the amplifier will exhibit excellent phase linearity over a 1-mc band about the center frequency.

  A germanium transistor amplifier will be chosen for this application because it is the simplest method of obtaining an overall noise figure of 4 db at this frequency and over the expected environmental temperature range of the package.

  This preamplifier will have a power consumption of approximately 0.75 watt. The size and weight will be about 4.5 in.^{3} and 0.3 lb., respectively.

  The parts count is as follows:

    Transistors   4

    Resistors   16

    Capacitors   5

    Transformers   3.

   2) <u>300-mc Mixer.</u> A single ended coaxial mixer will be used to heterodyne to the IF frequency of 27.27 mc.

  The mixer noise figure of 7.0 db offers negligible contribution to the overall receiver noise figure because of the 30 db of gain supplied by the RF preamplifier.

  The mixer will consist of 1 mixer diode and 1 mixer holder, will consume no power, will have a volume of about 0.75 in.^{3}, and will have an approximate weight of 1 oz.
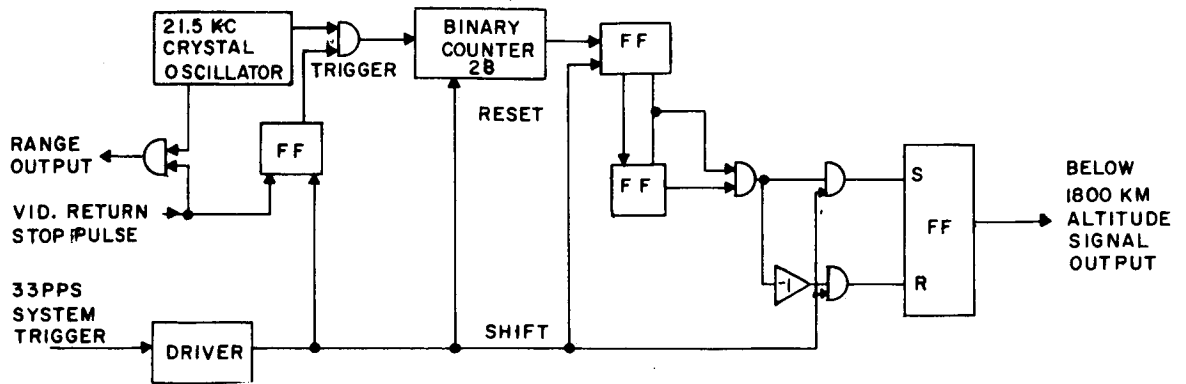
63-9706

Figure 66 MAXIMUM TEMPERATURE RISE OF POWER CONSUMING
EQUIPMENT BOXES
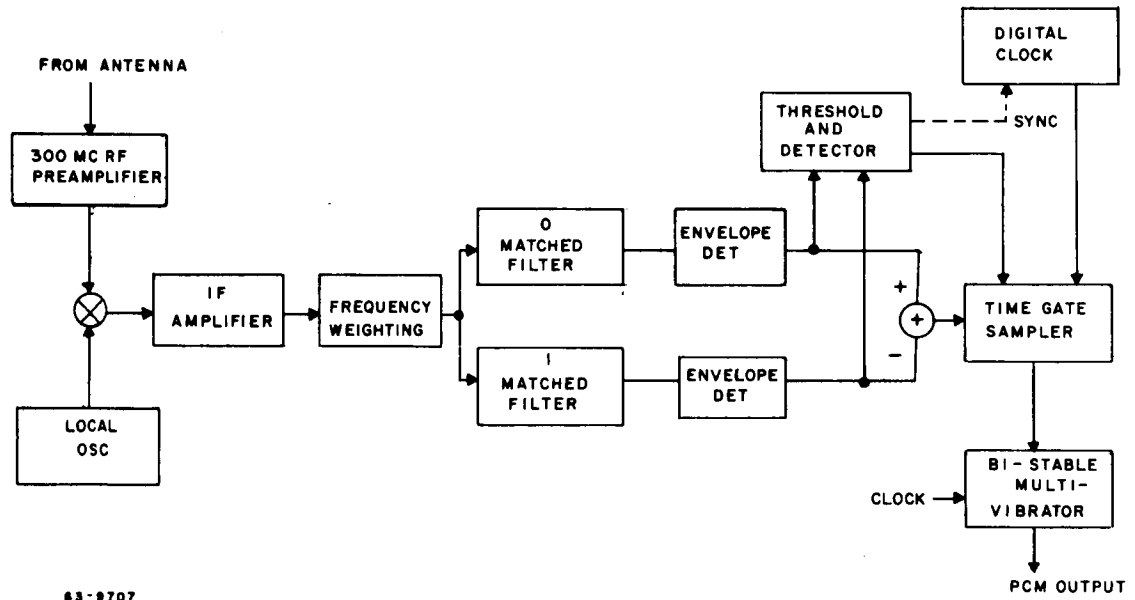
63-9707

Figure 67 ORBITER-BUS SURFACE CHARACTERISTICS

TABLE 12

ORBITER ALTIMETER/LANDER COMMAND LINK (S-BAND)

	Size (cubic inches)	Weight	Power
Encoder/synchronizer	7. 1	10 ounces	0. 70 watts (MTBF:500, 000 hours)
Solid-state mod	76	9. 0 pounds	66 watts (MTBF: 10, 000 hours)
Magnetron transmitter	72. 0	3. 5 pounds	(MTBF:5, 000 hours)
Duplexer	26 (2 x 4 x 2)	2 pounds	0. 10 watt
Range counter (8-stage counter)	4. 5	7. 5 ounces	1. 5 watts (MTBF:500, 000 hours)
Crystal L. O. (30 Mc) Frequency multiplexer	20. 0 (2 x 5 x 2)	12. 0 ounces	1. 0 watt (MTBF:10, 000 hours)
Detection and video amplifier 30 Mc IF amplifier (4 STG's) mixer	3. 3	5. 0 ounces ---	1. 5 watts
	198. 9	16. 6 pounds	70. 8 watts

3) <u>Local oscillator.</u> The local oscillator unit will provide local oscillator power for three separate mixers. A block diagram of this unit is given in figure 68. The unit consists of a 6.06-mc crystal-controlled transistor oscillator contained in an oven. The primary oscillator output is power-amplified and used to drive two transistorized multipliers via a buffer amplifier. A four-times multiplier stage provides local oscillator power at 24.24 mc to the processing mixer. A five-times multiplier provides local oscillator power at 30.3 mc through a buffer amplifier to another processing mixer and to a power amplifier. The output of the power amplifier drives two cascade varactor tripler stages whose output is the local oscillator for the receiver mixer. This last frequency is 272.7 mc.

The entire unit will consume approximately 5.7 watts; and the size and weight will be about 15 in.^{3} and 1.2 lb., respectively.

The parts will consist of:

17	Transistors
2	Varactors
1	Crystal
1	Oven
58	Resistors
72	Capacitors
22	Chokes
2	Potentiometers
4	Transformers.

4) <u>IF amplifier.</u> The 27.27-mc IF amplifier will consist of three staggered tuned cascade stages with an overall transitionally flat bandwidth of 4 mc. An AGC with a dynamic range of 10 db is employed. The overall power gain of the amplifier is 70 db.

The staggered tuned 4-mc bandwidth is chosen to provide good phase linearity and constant amplitude over a 1-mc band about the center frequency.

Because of the relaxed noise considerations at this lower frequency, silicon transistors could be used.

The IF amplifier will have a power consumption of about 2.1 watts, size and weight being approximately 4.0 in.^{3} and 0.15 lb., respectively.
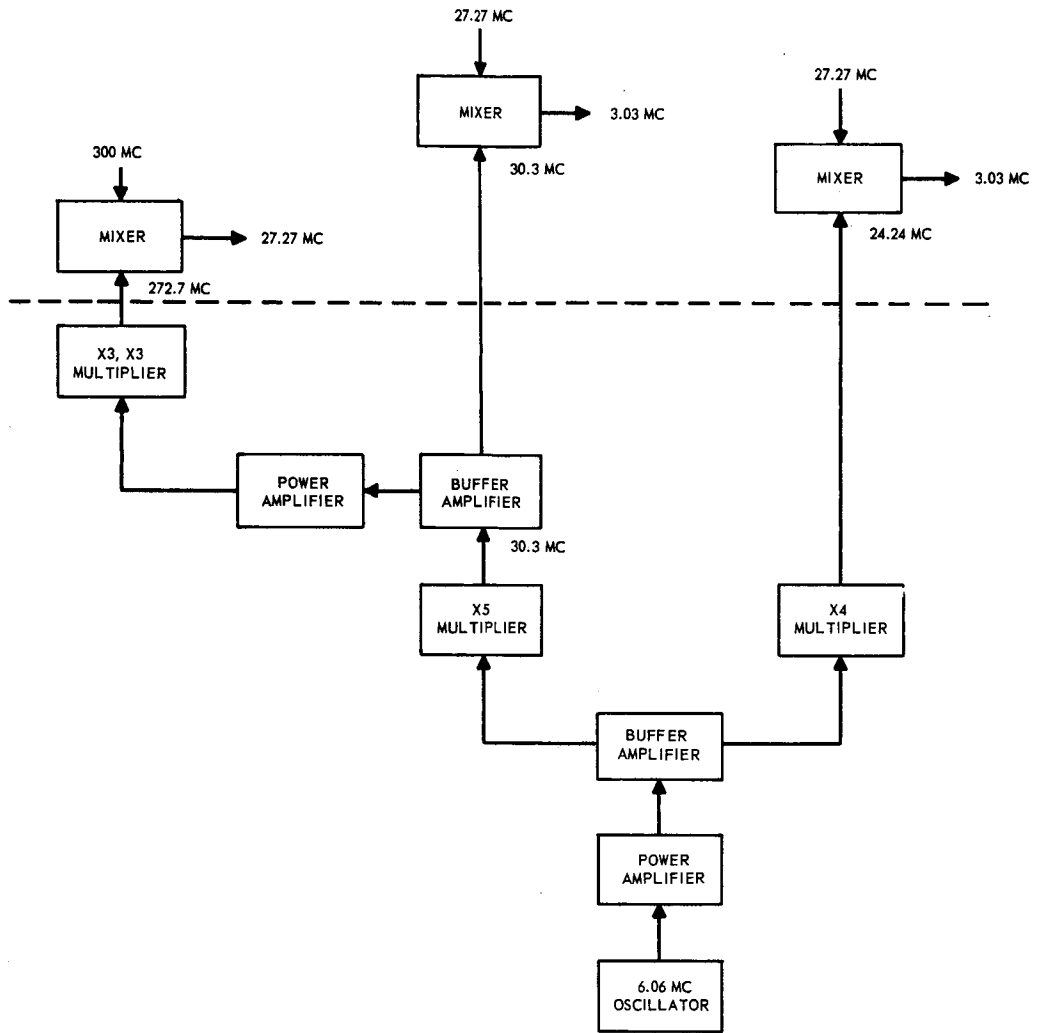
63-9708

Figure 68 LOCAL OSCILLATOR UNIT

The parts will consist of:

9	Transistors
40	Resistors
28	Capacitors
3	Transformers
3	Diodes
1	Choke.

5) <u>Receiver matched-filter decoder.</u> The matched-filter portion of the receiver is shown diagramatically in figure 69. As can be seen, this system is very similar to the transmitter encoder shown in figure 68. In fact, most all the components requiring detailed description are also employed in the transmitter and have been described in the transmitter section. The operation of this system is best described by following the signal flow through the block diagram.

The received signal, at a 300-mc center frequency is applied to the RF mixer, where it is heterodyned with a local-oscillator signal at 272.7 mc. This signal, as well as the other local-oscillator signals employed in the receiver, is derived from a frequency-synthesizer identical with that employed in the transmitter. The IF waveform, at a center frequency of 27.27 mc, is split between the "0" and the "1" decoding channels. In each channel it is mixed with a local oscillator which translates it to 3.03 mc. In the "1" channel, the L.O. is above the signal frequency. Since a "1", on transmission, is chirped downward, the output of this mixer will chirp upward for a received "1". The chirp filter, which is of the same type as that used in the transmitter, delays low frequencies more than the high frequencies. Since the low frequencies of the "1" signal occur first in the waveform, the filter will attempt to delay them into coincidence with the high frequencies which occur at the end of the waveform, thereby compressing the pulse. A "0" signal in this channel will be elongated by the dispersive action of the filter, giving rise to an output level far below that of the "1".

In the "0" channel, the local oscillator is below the signal frequency. The received "0" is chirped upward and it will still be chirped upward following the mixer. Since the chirp filter is identical to that used in the "1" channel, it will compress an upward-chirped signal and disperse one chirped downward. The "0" signal in this channel will, therefore, be compressed and the "1" dispersed.
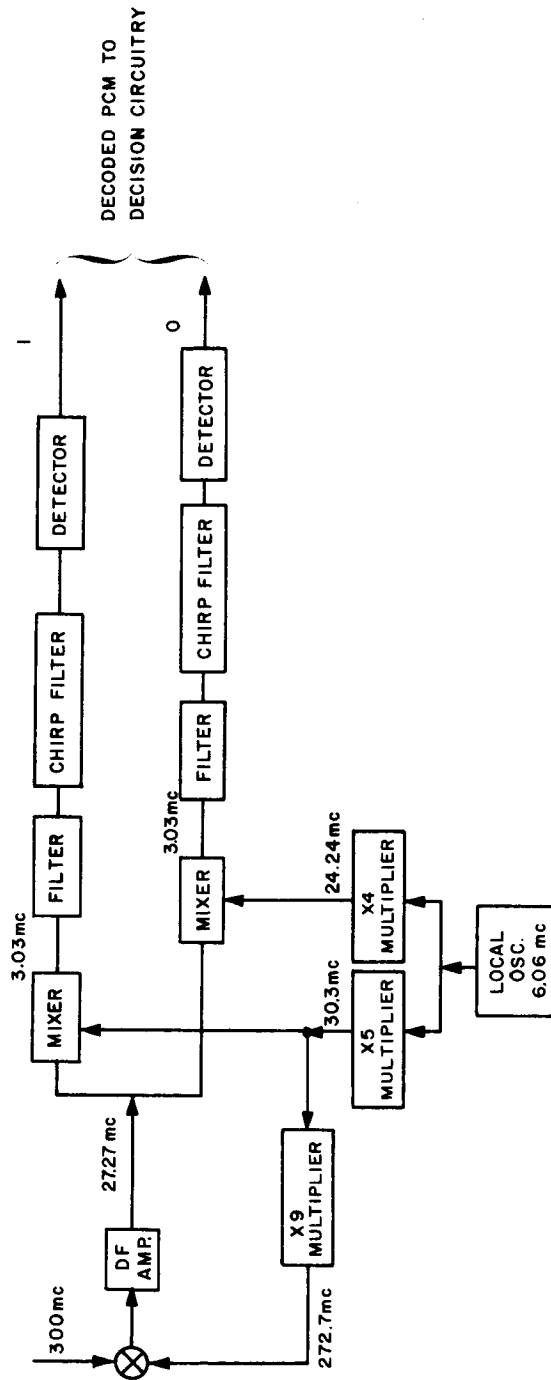
Figure 69 RECEIVER MATCHED FILTER DECODER BLOCK DIAGRAM

63-9709

-165-

Following the filters, diode detectors are employed to recover the envelopes of the waveforms. These envelopes are then presented to the decision circuits which will determine whether a "1" or a "0" is to be registered at the receiver output.

The Mars orbiter receiver circuitry is identical with that employed in the Mars lander transmitter encoder except for the elimination of many of the digital control components. The power, weight, and volume estimates used for the Mars lander transmitter encoder may be considered as conservative estimates for the Mars orbiter receiver decoder.

6) <u>Receiver decision circuits.</u> The decision circuits process the 1 microsecond compressed output pulses so as to produce a noise-free PCM stream in which multipath signals arriving greater than 1 microsecond after the direct signal have been eliminated. A basic block diagram of the decision circuits is shown in figure 70.

The first digits in the PCM transmission should be a stream of five zeroes followed by a one. The threshold and detector circuitry monitors the zero channel with a threshold set so that a signal-to-noise ratio of 16 db will produce an error probability of 5×10^{-4}. When this threshold is exceeded, the time gate sampler is energized which examines the output of the "0" channel 100 microseconds after the threshold is exceeded with a 1-microsecond sampling gate. If a message has begun, a zero will be present. If not, it is unlikely that noise will be present at the zero channel output exactly 100 microsecond after a false alarm. This check is repeated for the two identifying zeroes which follow the initial triggering zero. If these two zeroes are received, the decision system assumes that a message follows. If not, sampling is terminated. Five zeroes are used to guarantee that if the sampler should be triggered by noise immediately preceding an actual message, the sampler will reject the false alarm before all five zeroes have entered the receiver. Under the worst case, the system will begin sampling on the third zero and will still have two remaining zeroes to recognize message start.

The sixth digit in the starting stream, a "1", is used to indicate that the actual message is beginning and is necessary since sampling may begin in the middle of the 5-zero stream due to noise.

Once it has been accepted by the decision circuits that message transmission is in process, time gate sampling proceeds at a 10,000-pulse per second rate (the signalling rate) with time gates 1 microsecond wide (the compressed pulse width). Since the process has been triggered by the leading edge of the first pulse received, this process is in basic synchronism with the direct path signal and rejects signals later than the 1 microsecond width of the time gate. The sampling process is controlled by a 10^4 pps digital clock which is synchronized to start by the threshold and detector circuitry. Since timing errors will be present in the system, this clock is synchronized by the threshold and detector

circuit on the arrival of each new data bit. The allowable frequency control, however, is very small and equal to the anticipated timing drifts in the system. This is so as to prevent major resetting of the clock from spurious signals. Resetting is done in synchronism with time gating so that only those signals present when the time gate is open (1 microsecond) can correct clock error. Since this is accomplished for each bit, no major corrections are necessary and a low gain loop may be employed.

The output of the time gate sampler consists of 1-microsecond pulses of positive or negative polarity corresponding to zeroes and ones. These gated pulses are applied to a bistable multivibrator which is clocked by the sampling pulse and produces a noise-free 10 kilobit/sec PCM stream.

The digital logic portions of the decision circuits will utilize micrologic components to increase reliability and lower prime power requirements. The anticipated total power will be 1.1 watts, volume of 4.4 in.^{3}, and weight of 220 grams for the complete decision circuitry.

3. Science and engineering data. All additional science and engineering status measurements will be multiplexed and encoded in a manner similar to the system used in the lander. The monitored data will be stored in the tape recorder used to store the relayed lander data. Upon command from the DSIF, the normal mapping function of the orbiter will be interrupted and the science and engineering plus lander data will be transmitted to Earth. The recorded data will not be erased until commanded from the DSIF. Throughout the report, reference is made to the use of tape recorders as the bulk storage device. The reasons for choosing a tape recorder rather than a solid-state storage complex are now discussed.

63-9710
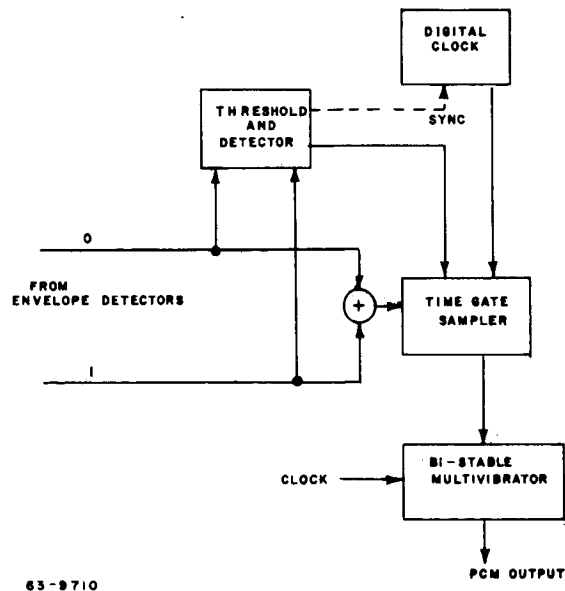
Figure 70 STRUCTURAL WEIGHT BREAKDOWN -- DOUBLE LANDER CONCEPT

-167-

3.5 Data Storage

1.   General requirements. As is discussed in various parts of the text of
this report, there are several instances where bulk storage of accumulated data
is required. This requirement occurs when (a) the data are acquired at too high
a rate for transmission, or (b) the data must be acquired at an inconvenient
time for transmission. In both cases, when the data are finally transmitted, it
must be in synchronism with an external clock. In many cases the data are not
acquired smoothly but rather are acquired in short, high-rate bursts. The stor-
age medium should be chosen to provide a maximum of smoothing of the data
before transmission. The storage devices must all be designed to have the re-
quired environmental, operational, and reliability characteristics for the par-
ticular system in which they will operate. Of particular interest are the require-
ments for sterilization of all components which will be landed on a planet surface
and for long reliable operating life. These requirements are the most severe
to be placed on the equipment.

2.   Specific requirements.

a.   Lander. A storage device is required on Mars lander vehicles
with an input bit rate capability of up to 40,000 bits/sec. The nominal input rate
is 12,500 3-bit words per second. These data consist of TV pictures and will
be acquired in bursts rather than continuously. The data must be played out for
transmission at a lower rate than it was acquired. The play-in to play-out rate
ratio may be required to be as high as 10:1 or as low as 1.2:1 depending on the
types of transmission used. This high rate storage system must have a total
capacity of approximately 10^8 bits to satisfy the mission requirements. A low
rate data storage system will also be required for the Mars lander vehicle.
This will be used to store the scientific and status data which is acquired at a
low rate and must be speeded up for playback. The input bit rate will be approxi-
mately 200 bits/second. This will consist of 5-bit words sampled at 40 words/
second. The data must be read out either 200 or 30 times faster depending on
the type of transmission utilized. The total capacity required will be approxi-
mately 10^8 bits. Still another storage system is required for a Venus lander
vehicle. In this case, the input and output bit rates will be about the same as
the Mars low rate system, but the capacity required will be about 1.5×10^6 bits.

All of the storage systems used in lander vehicles must be able to survive
and perform as specified after undergoing the standard sterilization procedure
for Voyager lander components. The reliability of the storage systems in terms
of the mission requirements must be as follows. After a transit shelf life of
300 days, followed by 150 days of which 50 days are actual working, the relia-
bility shall be 0.9966 with a confidence factor of 75 percent.

b.   Orbiter. The data storage systems on the Voyager orbiter vehicles
will be used for storage of mapping data and for intermediate storage of data

relayed from lander vehicles, as well as storage of scientific and status data taken by the orbiter itself.

The mapping data input rate can vary over a rather wide range, depending on the orbit used, the picture overlap, and the type of scanning. It seems that an absolute maximum input bit rate of about 200,000 bits/second will be a safe upper limit. These mapping data would be transmitted at approximately 4600 bits/second. The mapping data storage system capacity will have to be about 2.5×10^8 bits.

The data relayed from the lander will be at a rate of approximately 10,000 bits/sec. This data will also be retransmitted from the orbiter at 4500 bits/second. The capacity will be 1.5×10^8 bits/sec or equal to the capacity of both types of lander storage systems. This storage system will also be used to store the scientific data acquired by the orbiter.

The orbiter components will not have to be sterilized. The reliability requirements in terms of the mission requirements are as follows: for a total of 450 days of which 125 days are actual working, the reliability shall be 0.998 with a confidence factor of 75 percent.

    c.   Design tradeoffs. Two types of bulk storage systems have been considered for application to the Voyager programs. These are tape recorders, types of which have been used successfully on many satellite and space probe programs, and a new type of plated wire memory system which appears to be the most compact and rugged of the "solid" magnetic memory systems available. Although other types of memories could be considered for this application, these two have been chosen for comparison because they are felt to represent the most optimum techniques which do not involve greatly expanded technology.

In order to evaluate the relative merits of the two alternative techniques, it will be necessary to compare the size, weight, power consumption and reliability of systems using these techniques which are capable of performing the same data storage task.

    d.   Tape Recorders Description (Raymond Engineering Co.). The requirements listed above which are quite typical of all storage systems in deep space probes are for bulk storage and time expansion playback of stored data. The proposed recorder utilizing a single motor, a belt drive system with a true differential tensioning means, is about as simple a mechanical system as could be conceived. The use of a single motor results in the same accelerating torque in either mode of operation and eliminates the requirement for any clutching mechanisms.

The principles of operation of the proposed tape transport can be easily explained while observing figure 71. It shows the principal components of the
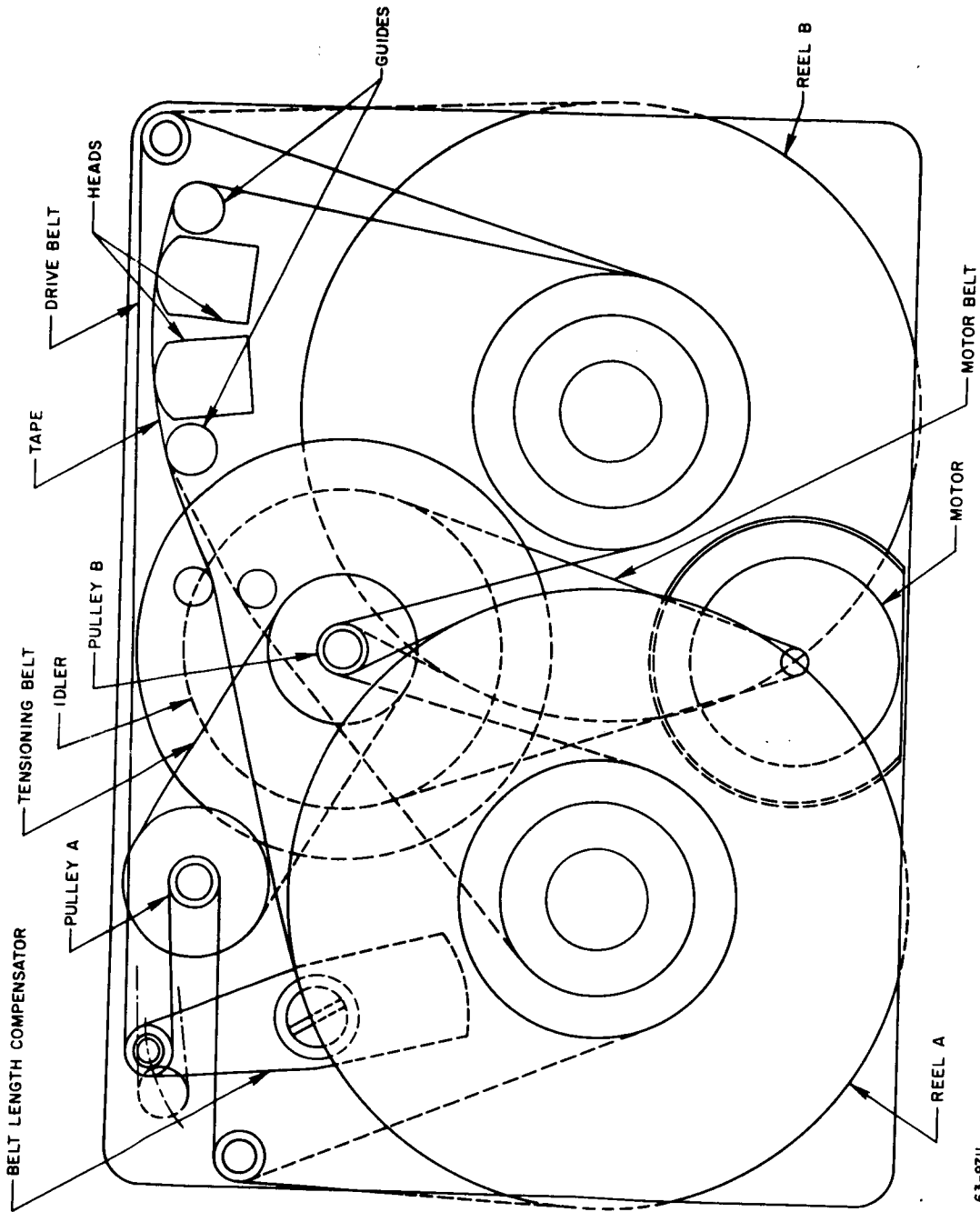
Figure 71 ISOELASTIC TAPE DRIVE

63-9711

GUIDES

REEL B

HEADS

DRIVE BELT

MOTOR BELT

TAPE

MOTOR

PULLEY B

IDLER

TENSIONING BELT

PULLEY A

BELT LENGTH COMPENSATOR

REEL A

-170-

system.   The recorder consists of two tape reels, a motor, idler pulleys, and a differential drive system consisting of pulleys A and B.   The diameters of pulleys A and B are adjusted so that the surface velocity of capstan B slightly exceeds that of capstan A.   The drive belt partially encircles both reels, two fixed idlers, and idler on the belt length compensator and pulleys A and B. The difference in speeds of pulleys A and B is such that when tape motion is from left to right on the drawing, the section of tape between pulley A and pulley B encompassing reel A is relaxed.   The section of tape between pulley A and pulley B surrounding reel B is under tension and is trying to go faster than the section of belt on the left of the drawing.   It can do this because it stretches slightly.   The linear tape velocity on the reel B tends toward a higher speed than does reel A and the tape itself is tensioned thusly.   For reverse operation, the thinking is reversed, and pulley B always rotates at a higher surface speed than pulley A.   As the tape travels from one reel to the other, the circumferential length of tape on both reels in contact with the belt varies. In order to compensate for this change, a belt length compensator is included. This consists of a pulley on a spring-loaded lever arm.   The amount of tape tension is governed by the spring force in the belt length compensator and the ratio in the speeds of pulleys A and B.   The tape tension resulting is high enough so that the tape will support itself, even through severe environments, without flanges on the reels.   Therefore, the incorporation of flangeless reels allows a further reduction in size of the tape recorder by overlapping the space occupied by the tape.   It is easily seen that the design is very simple and is readily adapted to the modular construction which is so necessary to the successful operation of spacecraft tape recorders.

Duplex-paired ball bearings are used exclusively in the construction of all the rotating components in our tape recorders.   This provides high radial and axial stiffness which results in a high resistance to vibration force.   Duplexing removes the need for any tailoring in the assembly of capstans, idlers, etc. Instead this job is done at the bearing manufacturers plant under extremely rigid controls.   Incidentally, all ball bearings purchased by this company in the future will be fabricated to more rigid quality control procedures than are generally practiced in the fabrication of a standard line of ball bearings.   An elaborate quality assurance program has been worked out with two suppliers to date.

Because of the extremely high stiffness resulting from the duplexing, problems could result in operation over wide temperature ranges if close attention were not paid to the temperature coefficients of expansion of the materials which comprise the subassembly.   The materials from which all our rotating components are fabricated have almost identical temperature coefficients of expansion.   This results in a slight weight increase; however, the added reliability is definitely worth the weight penalty.

The combination of the mass of the rotating components and the compliance of the balls can result in a resonant condition usually at high frequencies.

-171-

Part of the proposed program would include an attempt to remove the resonant frequency above any forcing function frequency to which the tape recorder would be subjected in vibration. This may not be convenient in some of the more massive components, in which case a vibration isolation system may be necessary. Such vibration isolation systems have been incorporated on recorders for many flight programs and have been considered highly desirable and acceptable. The resonant condition which does exist when subjected to a slowly varying sinusoidal vibratory sweep is so violent that the ball bearings are almost always destroyed; hence considerable care is necessary in this regard.

A single hysteresis synchronous motor is proposed to power the transport. The motor design originates from Herbert C. Roters, consultant, in Kew Gardens, New York. Raymond Engineering Laboratory is presently engaged in a program to manufacture motors designed by Mr. Roters. The main advantages of the in-house fabrication of these motors are that the rigid quality control procedures already in practice in other areas will be applied to this very critical component, in a manner which we believe is satisfactory to the fabrication of reliable flight hardware.

In order to provide the required speed ratio between the record and playback modes without clutches and other mechanical linkages, it is proposed that the motor operate at two speeds. This will be accomplished by adjusting the motor drive voltage and frequency. There are a number of means by which this can be accomplished. A very practical one is to provide an accurate time base and a series of binary dividers.

It is proposed that a six-pole motor operating at 12,000 rpm be supplied with a two-phase power source at 600 cps. This same motor operating at 375 rpm would be driven at 18.75 cps. It is easily seen that there is a limitation in the single-motor approach to the maximum ratio which can be realized. At lower speeds, cogging results and very low frequency drive signals have to be handled. At higher speeds, bearing life and drag become problems and the voltages required to drive the motor can exceed the capabilities of present day transistors. It is estimated that the motor drive power at the high speed mode of operation will require an average of 4 watts from the DC supply and a peak power up to 15 watts. At the low speed, it is estimated that not more than 2 watts will be required.

In order to describe the signal electronics system, reference is made to figure 72, which is a signal flow diagram for a generalized version of the recorder under discussion. This recorder can be adapted to meet any of the requirements outlined in section 3.5.

Parallel input data are coupled into the N + 1 stage shift register in the upper left corner of the drawing. The shift register, after accumulating N data bits, transfers the signal to the heads. This is accomplished by dividing the bit synchronizing signal by N or by using a word rate clock. A signal is recorded directly on the tape by the action of the record heads.
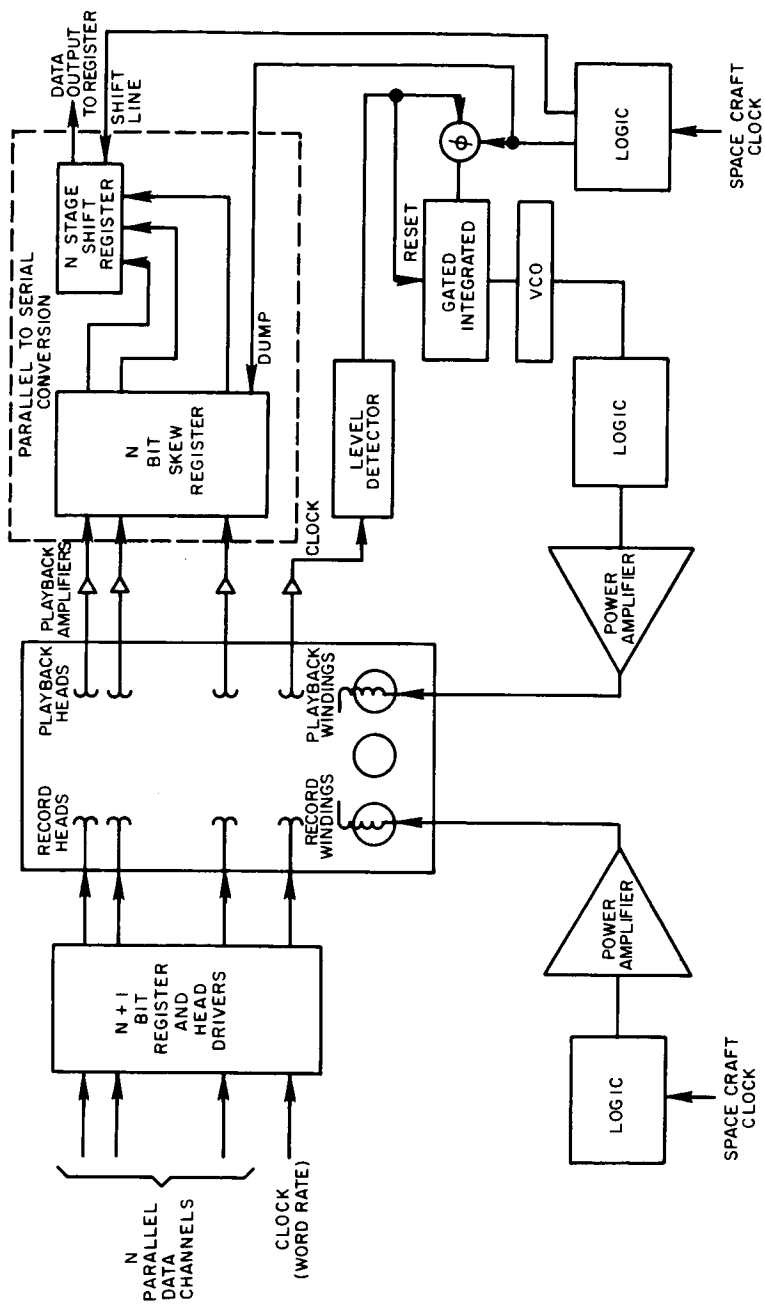
Figure 72   SIGNAL FLOW DIAGRAM OF VOYAGER TAPE RECORDER

63-9712

-173-

In the playback, parallel to serial conversion shown in the upper right hand corner of the diagram, the output from the playback head is amplified and stored in an N bit skew register. The outputs of the skew register are coupled into the set inputs of the N-stage shift register. The skew register is composed of N level detectors and N and invert gates. The output of the skew register is only presented to the N-stage shift register during the presence of a transfer pulse from the timing logic section which is shown further below on the drawing. The timing logic section provides the proper transfer and shift pulses from the reference clock signals. The shift register is so connected that the stored bits, in the presence of a bit synchronizing pulse, will read out the stored information serially to a one-stage clocking shift register. This shift register operates in synchronism with the N-stage shift register, but delayed part of a bit cell.

The output from the one-stage shift register is a replica of the input data, converted to NRZ serial form, and with a new time base (either expanded or compressed as desired).

This output is synchronous and without jitter, and allows the use of matched-filter detection techniques on the other end of the communications link. The output from the synchronizing channel is amplified, goes through a similar level detector, and into the phase comparator. A reference pulse from the timing logic section also couples into the phase comparator. The output of the phase comparator is coupled into the gated integrator which operates as a nonlinear filter. The output of the gated integrator controls the frequency of a voltage controlled oscillator which, after the required amplification and signal conditioning, drives the playback motor. The capability of multiple playback data rates is available, if desired. This phase-locked servo-loop is the means by which synchronous readout is accomplished.

3. <u>Magnetic plated wire memory (UNIVAC Div. of Sperry Rand Company)</u>. The UNIVAC Division of the Sperry Rand Corporation is developing a magnetic, thin-film, plated-wire memory element which appears at present to be the optimum type of "solid" memory system for this application.

a. <u>Basic operation of memory element</u>. The magnetic wire memory element is a 5-mil-diameter beryllium copper wire and has a 81 nickel-19 iron alloy electroplated surface of 10,000 A thickness. The magnetic surface is plated such that it has an anisotropy (easy) axis circumferentially around the wire and a hard axis along the length of the wire. Since the circumferential path is closed, the built-in anisotropy is enhanced by shape anisotropy.

Information is stored in the plating in the form of clockwise or counter-clockwise magnetization for 1 and 0 bits respectively. Figure 73 shows a plated wire in which the bits are stored under word lines, one of which is indicated. During the write operation, a word current is applied to the word line and a bit current to the plated wire itself. Coincidence of the two currents stores
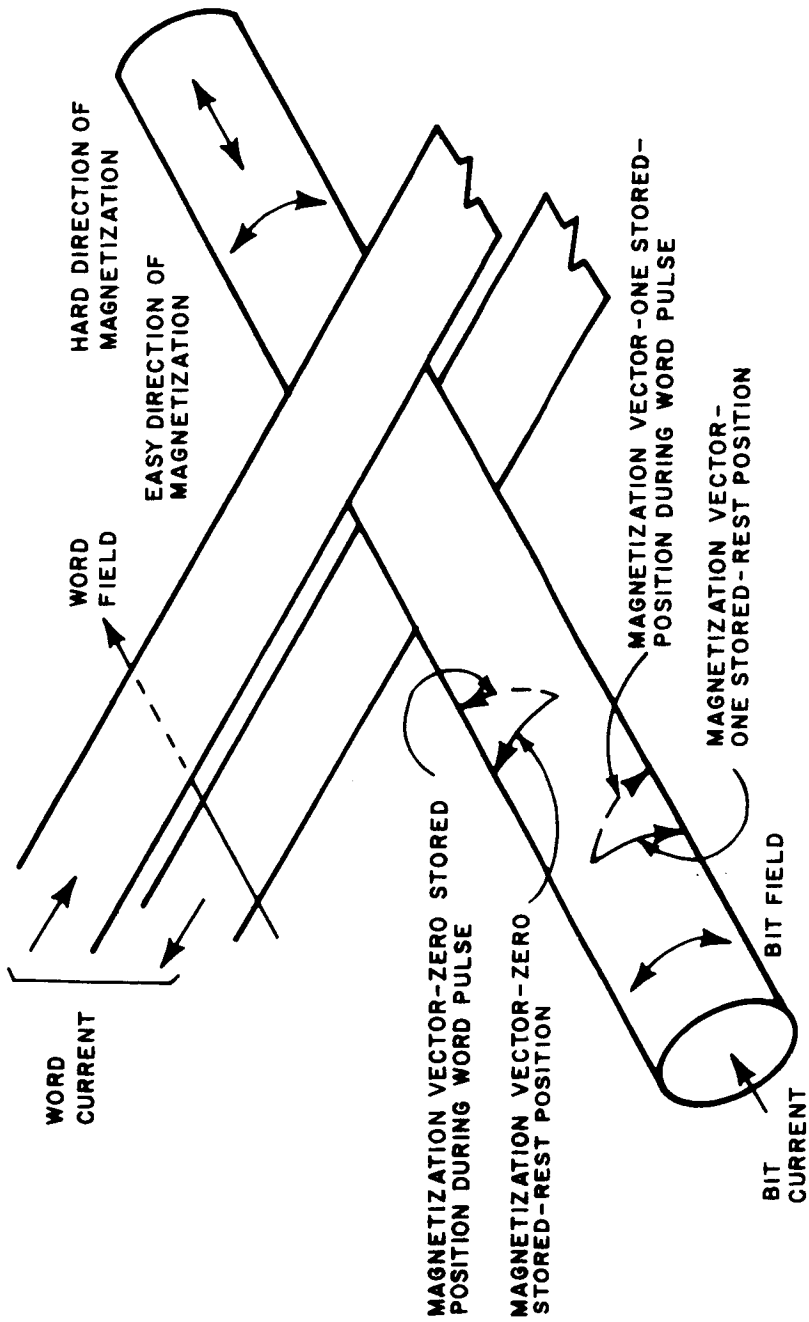
Figure 73 INFORMATION STORAGE ON PLATED WIRE

63-9713

-175-

a bit under the word line, the sense of the magnetization vector depending upon the polarity of the bit current. A multiplicity of 20-mil wide word lines wrap around each plated wire and are on 40 mil centers, leading to 25 bits per lineal inch of plated wire.

Readout is accomplished by applying a current pulse to only the work line which established a magnetic field along the hard axis. The circumferential magnetization vector stretches to an ellipse as indicated, tending to rotate towards the hard axis. This produces a decrease in clockwise flux linking the plated wire for a 1 (or decrease in counterclockwise flux for a 0), and a plated wire serves the triple purpose of write line, sense line, and structure vector rotates back to its original clockwise or counterclockwise sense, so the readout is a nondestructive operation. Details of the write and read operation are shown in figure 74. The word and bit pulses can be as short as 100 nanoseconds and are 800 and 25 milliamperes, respectively. Since the energy required to switch the magnetic material is very low (1/100 of that required to switch a typical 50-30 ferrite core) and because the frequency of operation is very low for space-craft operation (to match telemetry equipment), the overall power requirement for a memory unit is quite small.

Each word line encompasses many plated wires which are spaced at 30 wires per inch. Using this figure and the previously mentioned 25 bits per inch of plated wire, a surface packing density of 750 bits per square inch results. In practice, a grooved ground plane is used to contain the plated wires and the word lines are etched copper strips on a 1-mil epoxy fiberglass sheet. The ground plane serves as the current return for both the word and bit lines and acts as the principal mechanical support for the structure.

b. Circuit and system consideration. In order to discuss the electronic requirements of a plated wire memory system, it is helpful to assume the memory size and configuration. The size chosen for discussion is 8.4×10^6 bits.

It can be shown that if memory planes are built as square arrays a minimal number of drivers and amplifiers for that size memory results. For example, a 16-bit memory arranged in a 4 by 4 array requires $4 + 4 = 8$ drivers, while an 8 by 2 array needs 10 drivers. Also, as the total amount of storage increases and squareness is maintained, the number of circuits per bit decreases. An 8 by 8 array giving 64-bit capacity requires 16 drivers, contrasted with 8 required for the 16-bit array. Thus, if a memory unit of given capacity can be constructed as a single square array, the least number of circuits can be employed, yielding minimal power, volume, weight, and cost.

Practical limitations modify the above considerations. A memory plane cannot be made indefinitely large, with extremely long lines over which currents must be driven and signals sensed. The number of lines which can be switched into one circuit is limited. A word organized memory, which has a higher signal-to-noise ratio than an ordinary coincident-current memory, usually cannot be built as a square array.
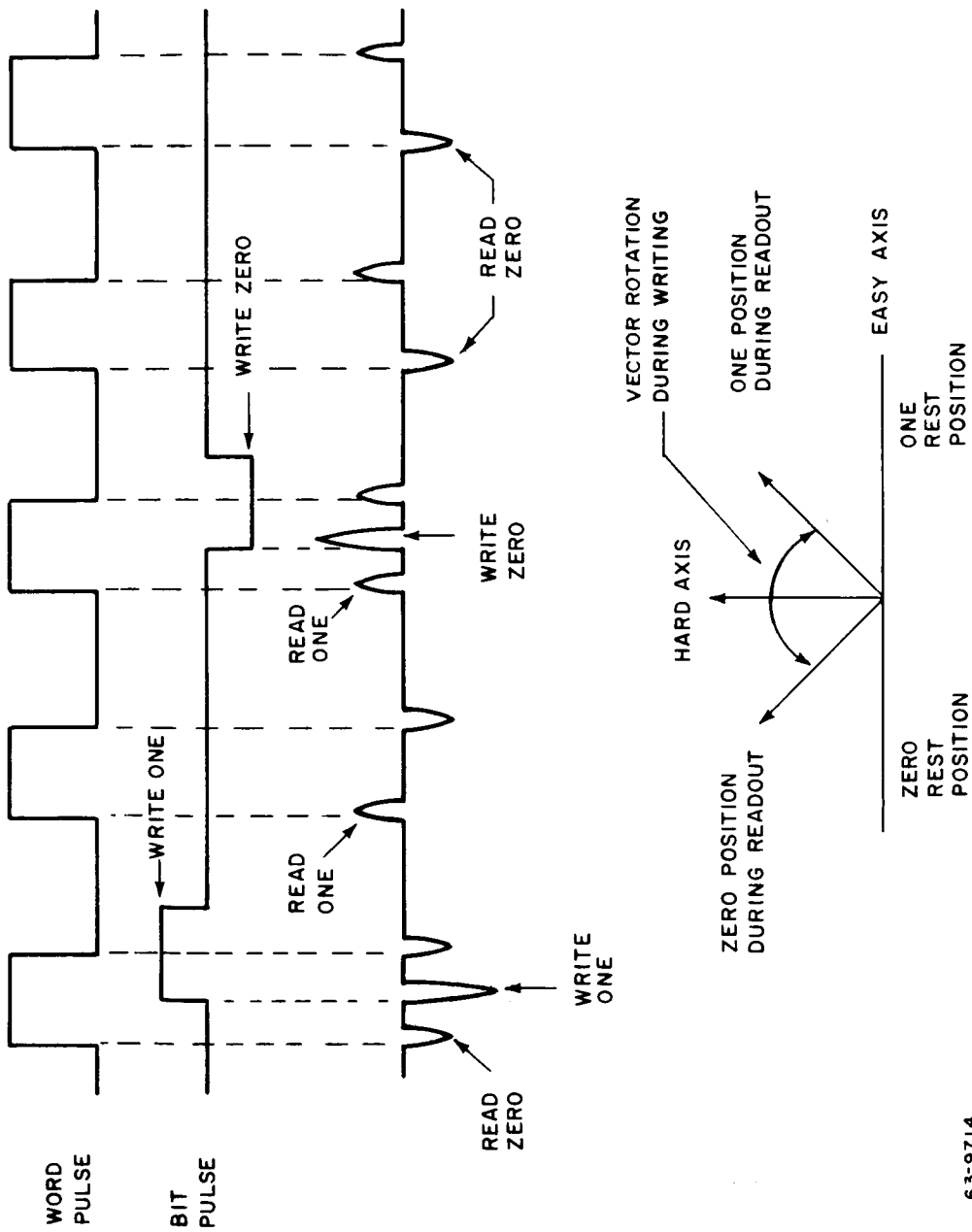
Figure 74 READ AND WRITE OPERATION

63-9714

-177-

As indicated earlier, after reading from the wire memory element, the magnetization vector returns to the same sense that it had before readout. This means that the element has a nondestructive readout property which can be used to combine the advantages of word-organization and squareness. One word line encompasses the plated wires associated with very many words. When the word line is pulsed, the large number of words are interrogated and the desired one is switched into the sense amplifiers, one such amplifier for each bit. However, the undesired words are not erased from the memory because of the nondestructive readout property.

According to present calculations, an 8.4×10^6 bit wire memory module can be built as a single electrical array (physically it is to be divided into a number of planes). The module is to be arranged such that there are 4096 word lines and 32 words of 64 bits each on every word line, implying that the array is 4096 by 2048. A practical consideration, the number of lines which can be switched into one sense amplifier, limits the size of the second dimension.

To construct the array, 17 grooved ground planes will be stacked. Plated wires will be mounted in the grooves on both sides of each ground plane (except for the two outermost planes; here the wires will be on the inboard side only). Word lines will thread between two ground planes each, serving two sets of mounted wires.

To drive the 4096 word lines, 64 switches and 64 current drivers will be used in a matrix fashion (figure 75). Sixty-four bit drivers will be switched into one of the 32 words associated with each of the word lines. Because of more critical nature of low level switching, 128 sense amplifiers will be used.

The drivers and switches are in turn to be operated by ring counters which will select the memory locations and will be sequentially stepped. A study has indicated that the ring counter approach uses few total components and less power than a binary counter-decoder arrangement. The sense-bit drive matrix will also be operated by a ring counter.

A 64-bit input-output register is to be used to break up incoming serial information into words and to restore the outgoing information into serial form. To accomplish this, a clock counted down modulo 64 is required.

These circuits and power supply converters (it is assumed that a single voltage, poorly regulated source will be available) will occupy between 400 and 500 in.^{3}. The total volume for the entire system will then be between 2000 and 2100 in.^{3}

While the memory is operating, the power demand will be a maximum of 205 milliwatts, assuming that the peak driver currents are drawn from capacitive storage. In a standby condition, the bit and word line drivers will not be operating, but sense amplifiers and logic circuits will still consume power, so the demand will fall off to about 190 milliwatts.
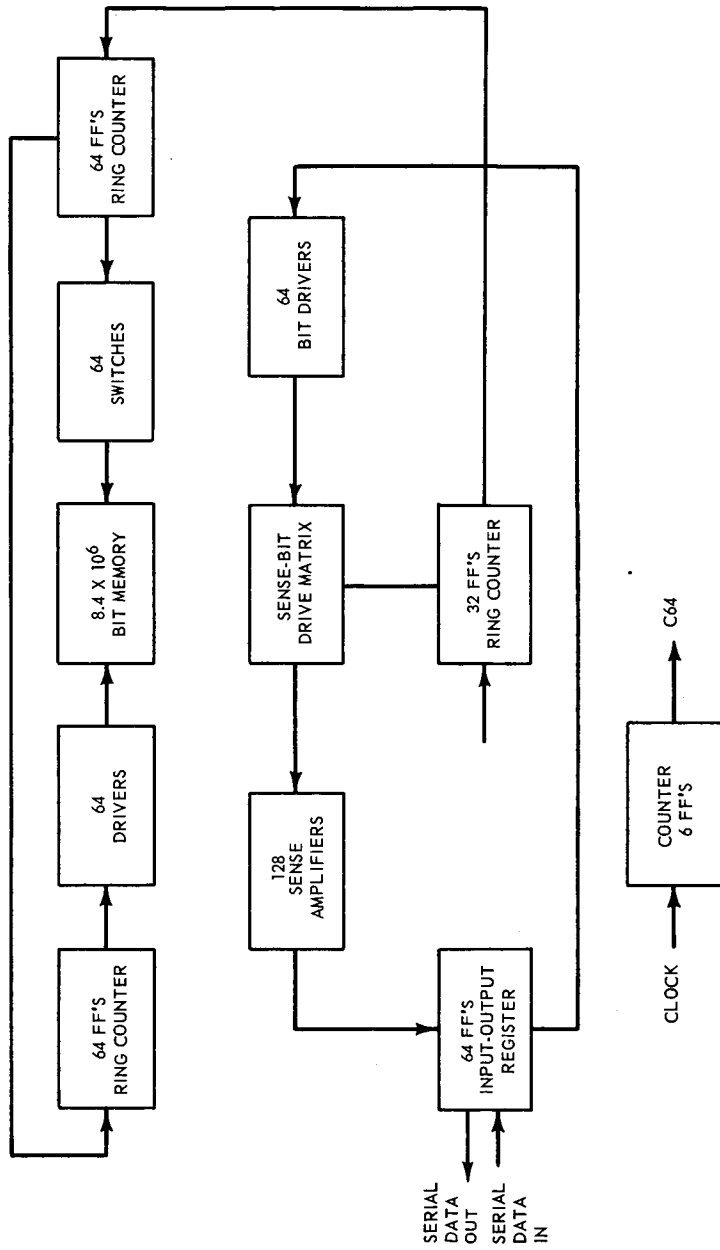
Figure 75 MEMORY UNIT BLOCK DIAGRAM

63-9715

-179-

4.   Comparison.   Both of the techniques discussed have been shown to be capable of being used to satisfy the bulk data storage requirements of Voyager. The choice of which technique will be used throughout the program must be made on the basis of the costs to the program in terms of size, weight understanding of all failure modes and their causes.   With such a program, reliability could be assured for either the compact matrix of fine wires required for a "solid" memory system or the belt driven transport required for the tape recorder.

In comparing the reliability of electronics in the two types of system it must be assumed that the circuitry will be similar in design and construction for both cases.   If this is the case, the relative reliability of the two systems will be grossly a function of the relative number of circuit elements in the two alternative systems.   In actually computing reliability, however, the fact that failure of one given element does not necessarily cause failure of the entire system must be taken account of and so the relation between the number of circuit elements and the reliability is not simple or even fixed.

In this case, the "solid" memory will contain a great many more circuit modules than the tape recording system; however, each circuit in the "solid" memory will directly affect proportionately less of the data.   About the only conclusion that can be reached is that a failure causing some error in the data is more likely to occur in the "solid" memory system, but if a failure does occur in the tape recorder, it would be more likely to debilitate the whole system.

a.   System size, weight, and power consumption.   The major difference between the two storage techniques discussed is in the size and weight required for a given storage capacity.   Figure 76 is a plot of data extrapolated from manufacturer's data.   It shows the large penalties which would be incurred by using the plated wire techniques for a high-capacity storage system.   This is particularly acute in the region of 10^8 bits which is typical of the Voyager requirements.   The volumes required in both cases are found to be approximately proportional to the weights.   A tape recorder with 10^8-bit capacity would occupy approximately 1200 in.^{3}, while a "solid" memory of similar capacity would occupy about 20,000 in.^{3}.   It can also be seen from figure 76 that for very low capacity systems (less than 10^6 bits) the two techniques begin to be competitive.   However, there does not seem to be any requirement for a low capacity storage unit in the present Voyager concept.   The power consumption required does not differ significantly between types of systems. Power consumption in both cases will be a function of input and output data rates rather than capacity and, in no practical case, will exceed about 12 watts.

b.   Conclusions and other considerations.   It is apparent that the weight penalty incurred by using a "solid" memory system could not be tolerated and that tape recorders must be considered the reference storage systems for Voyager.

Although tape recorders appear to be the only acceptable way of handling the Voyager bulk storage requirements, they are not without problems at this time. The major difficulty, aside from obtaining demonstrable reliability, is the requirement for sterilization of components to be landed on planet surfaces. There are critical materials used in the construction of the types of recorders being considered which would deteriorate under the heat of sterilization. Raymond Engineering Company, however, is at this time involved in a program aimed at locating and solving the design problems associated with the requirement for sterilization.
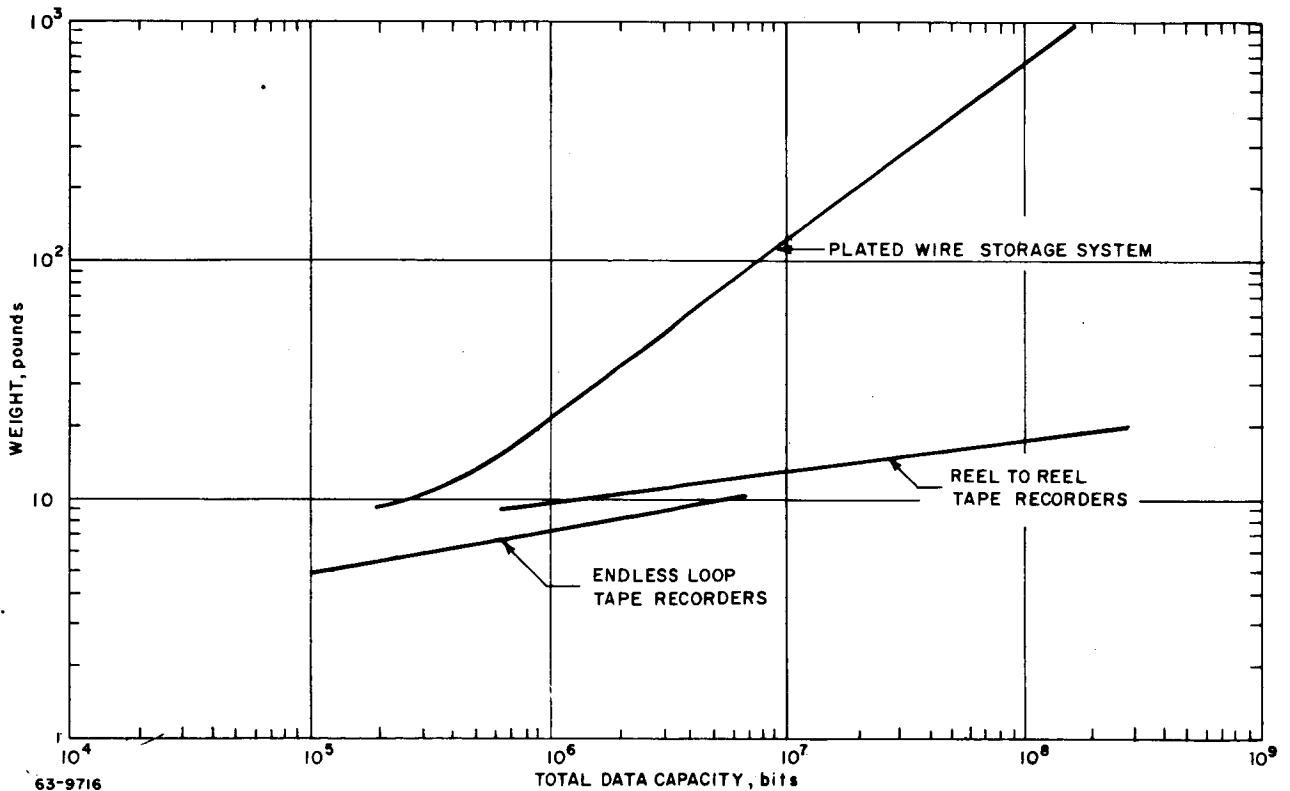
Figure 76 STORAGE SYSTEM WEIGHTS VERSUS TOTAL DATA CAPACITY

3.6 Antennas

Four antenna systems are used by the Mars orbiter: (a) a command antenna system, (b) an altimeter antenna system, (c) a VHF telemetry antenna system, and (d) the S-band directive antenna system. Discussion of each of these systems follows.

1. <u>Command antenna system.</u> Redundant omnidirectional S-band command antenna systems will be included on the orbiter-bus. These antenna systems will be truely redundant in that each system will operate independent of the other and each will provide electromagnetic coverage about the spherical region of space surrounding the spacecraft.

In the command frequency range, the dimensions of the spacecraft are many times the wavelength, and reflections by the spacecraft will result in major distortions of the primary pattern of most broad-beam radiation elements. The chosen radiating element design must, therefore, offer the means for minimizing the reflection effects due to the airframe and still provide a broad pattern.

The success of the mission may depend primarily on the command system. A system consisting of linearly polarized antennas feeding a common receiver will exhibit a polarization which varies from linear to elliptical to circular (either left- or right-hand sense) should the spacecraft assume a random motion. Since the Earth-bound command transmitting antenna is circularly polarized, signal fading with aspect angle to the spacecraft will be eliminated by using a polarization diversity receiving system consisting of two orthogonal, linearly polarized antennas, two receivers, and a summing network. Figure 77 shows a block diagram of the redundant system. With this system, either or both components of radiation from the ground transmitting antenna will be received regardless of the spacecraft orientation.

The recommended command receiver system allows omnidirectional coverage with two antennas since the antenna system can be considered as one composite antenna whose far field has both E_θ and E_ϕ components. Figure 78 shows the radiation patterns of orthogonal, 60-degree flare-angle, biconical dipoles for $ka = 1.5$, where $k = 2\pi/\lambda$ and a = half length of the dipole.[1] These patterns closely approximate those given by

$$E_\theta = E_m \sin \phi \text{ and } E_\phi = E_m \cos \phi$$

assuming equal field intensities at each antenna. Because each antenna feeds its own receiver, the relative pattern of the total electric field is

$$E_T = E_m \sqrt{\sin^2 \phi + \cos^2 \phi} = E_\theta + E_\phi = 1$$

which is a circle. The antenna system coverage, then, will be the solid of revolution enclosed by the patterns shown in figure 78, thereby forming an ellipsoid and ensuring omnidirectional coverage.

---

[1] Papas, C. H. and R. King: Radiation from Wide-angle Conical Antennas Fed by a Coaxial Line. Proc. IRE, vol. 39, p. 1269, November 1949.
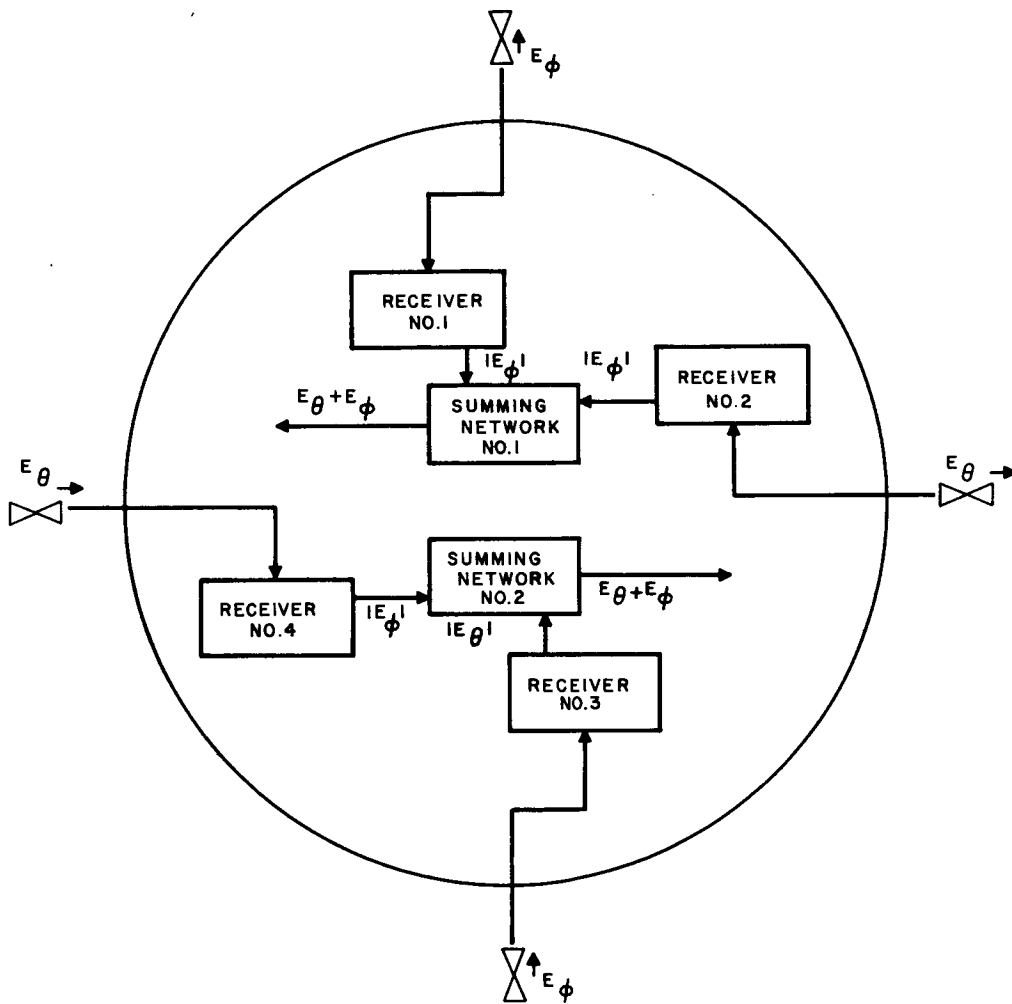
63-9717

Figure 77 COMMAND RECEIVER SYSTEMS
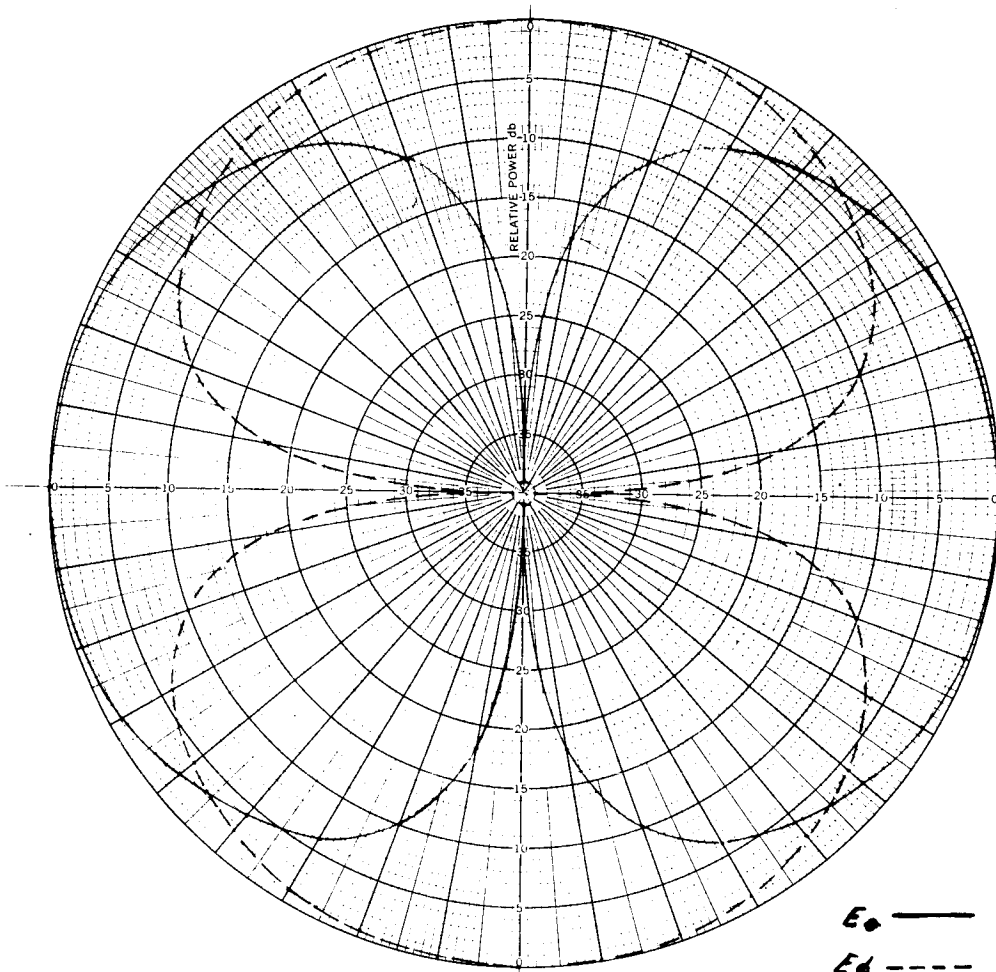
ANTENNA TYPE *Biconical*   LOCATION *Orbiter/Bus*   USE *Command Receiver*

TEST MODEL:	FREQUENCY: *2300* MCS
MODEL SCALE:	SCALE FREQUENCY: _____ MCS
CONDITIONS:	POLARIZATION:
CURVES PLOTTED IN:	$E\theta$:
VOLTAGE:	$E\phi$:
POWER:	PATTERN AREA:

$ka = 1.5$
where :
$k = 2\pi/\lambda$
$a = \frac{1}{2} k - \text{of}$
biconical dipole

ENGINEER   OPERATOR   FILE NO.   DATE

I.B.2.C-TWA-2

ANTLAB #42410

Figure 78 RADIATION PATTERNS OF INDIVIDUAL COMMAND ANTENNAS

The individual radiating elements for this antenna system will consist of biconical dipoles placed on the ends of short booms which will be deployed upon removal of the ascent shroud. Biconical antennas are recommended since the radiation patterns of these antennas can be shaped to reduce the constructive and destructive interference effects of the orbiter-bus airframe. Chokes on the support booms will further minimize pattern degradation by attenuating current flow on the support structure.

Static charges induced on the biconical antennas by solar winds will be shunted to ground potential by stub supports in the transmission lines.

The fundamental characteristics of the command antenna systems are tabulated in table 13 and apply to either a Mars or a Venus mission.

TABLE 13

COMMAND ANTENNA SYSTEM CHARACTERISTICS

Parameter	Characteristic
Operating Frequency	2300 mc
Operating Power	Nil
Polarization	Orthogonal Linear
Gain	0 db
Bandwidth	± 1%
VSWR	< 1.25:1
Weight	2 pounds per system

2. Altimeter antenna system. The 2190-mc altimeter performs two functions: (a) to continuously measure the altitude of the orbiter above the planet surface, and (b) to command the lander to play out its stored data to the orbiter. The two functions suggest different transmitter antenna beamwidth requirements: (a) a narrow beamwidth to obtain high gain for the altimeter function; and (b) an 84-degree beamwidth to illuminate the whole planet disk (from the periapsis altitude) for the command function. A transmitting antenna with an 84-degree beamwidth will serve both functions, if a high-gain antenna is provided for the altimeter at the receiving end of the system.

The transmitting antenna must be circularly polarized to enable it to send commands to a linearly polarized, randomly oriented command receiving antenna in the lander vehicle on the surface of the planet. The altimeter receiving antenna will be linearly polarized because of uncertainties regarding the handedness of the generally elliptical polarization of the energy reflected from the planet surface.

A transmitting helix and a receiving paraboloid with dipole feed are combined into a single, symmetrical unit by mounting the helix on the disk reflector of the dipole feed as illustrated in figure 79. The disk serves as a ground plane for the helix.

The coaxial feed lines for the helix and dipole are concentric. The center conductor for the dipole feedline in a hollow tube which also serves as the outer conductor of the coaxial feedline for the helix. The two feedlines are readily separated just behind the vertex of the parabola by means of a Tee connection in the outer coaxial line (dipole feedline). One arm of the coaxial Tee is terminated with a short circuited, quarter wavelength stub. The inner coaxial line (helix feedline) passes out through the short-circuited end of the Tee. The inner line carries the high peak power from the transmitter.

No critical breakdown problems are anticipated in the design of the feedlines. The feedlines will have a vacuum dielectric while operating in orbit. Insulating materials must be selected for very low outgassing characteristics for use in high RF fields in the high vacuum of space. The low average power (35 watts) and low feedline loss (less than 0.02 db) indicates that no problem in thermal dissipation should be encountered.

A balanced dipole feed is proposed for the altimeter receiving system in order to effect a greater isolation between helix and dipole. With suitable choking and feed through nulling, the isolation between transmitter and receiver can be in excess of 40 db to prevent receiver crystal burnout. With separate antennas for receiving and transmitting, duplexer losses have been eliminated from the system.

Table 14 summarizes the essential characteristics of the orbiter antenna system. The helix is designed for "in-phase" radiation from the individual turns, rather than for the conventional "increased directivity" phasing, in order to obtain the 84-degree beamwidth required. The "in-phase" condition also results in a higher illumination of the limbs of the planet disk in spite of lower on-axis gain. Side lobe and back lobe energy are reduced. A calculated radiation pattern for E_θ polarization is shown in figure 80.

Circularity of polarization is essential over the planet disk so that the linearly polarized, lander antenna will receive approximately the same signal amplitude for any orientation.

TABLE 14

ALTIMETER ANTENNA CHARACTERISTICS (WEIGHT 3 POUNDS)

	Transmitting	Receiving
Antenna type	Helix 1.7-inch diameter x 3.5 inches long	20-inch-diameter paraboloid
Frequency	2190 mc	2190 mc
Polarization	Circular	Linear
Beamwidth (3 db)	84 degrees	18 degrees
Gain (linear polarization)	5 db	19 db
Bandwidth	40 mc	40 mc
VSWR	1.20	1.20
Circularity (axial ratio)	1 db on axis 3 db at 1/2 power pts	--- ---
Power-handling capability	35 watts average 200 kw (peak)	--- ---
Isolation between transmitter and receiver	40 db	

*The gain of the circularly polarized helix is referenced to a linear isotropic source because the receiving antenna on the lander and the altimeter receiving disk employ linear polarization.
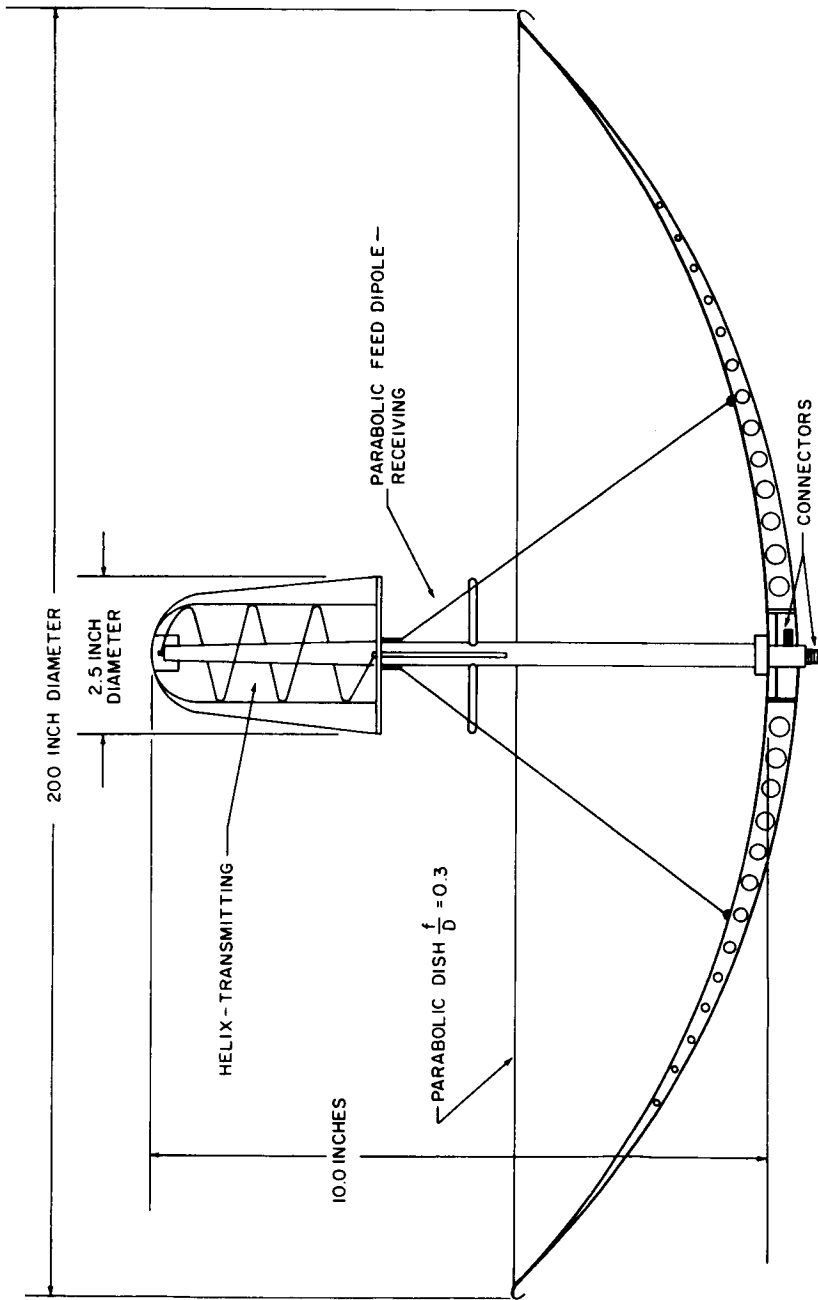
Figure 79 EXTERNAL CONFIGURATIONS OF ORBITER S-BAND
ALTIMETER ANTENNA SYSTEM

63-9719

-188-
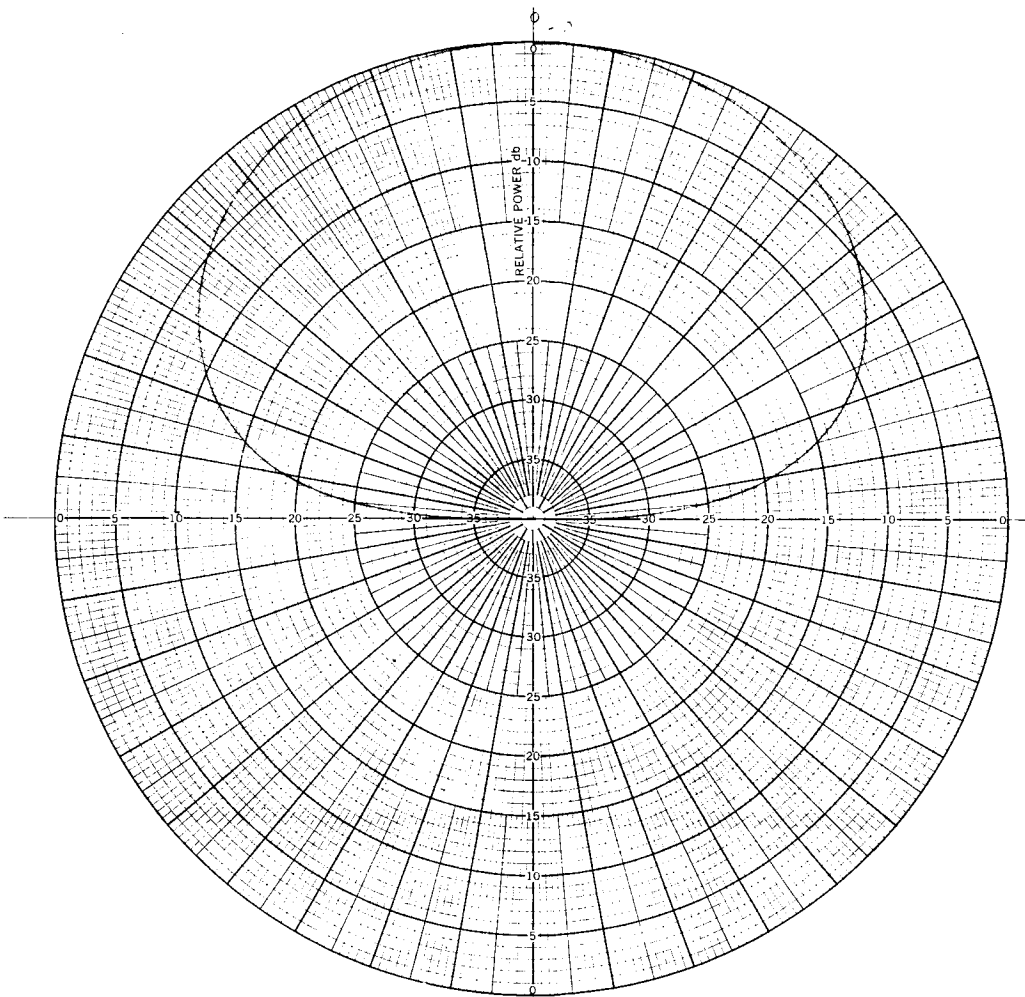
ANTENNA TYPE _HELIX_   LOCATION _____ USE _____

TEST MODEL: _____   FREQUENCY: _2190_____ MCS
MODEL SCALE: _____   SCALE FREQUENCY: _____ MCS
CONDITIONS: _____   POLARIZATION: _____
CURVES PLOTTED IN: _____   E θ : _____
VOLTAGE: _____   E φ : _____
POWER: _____   PATTERN AREA: _____

ENGINEER	OPERATOR	FILE NO.	DATE
			II. A. S. d - AKR-2

63-9720

ANTLAB #42410

Figure 80 S-BAND HELIX ANTENNA PATTERN

The beamwidth (18 dgreees) and the diameter (20 inches) of the receiving parabola are determined principally by the gain requirements and the space available on the gimballed platform already loaded with TV cameras, IR sensors, etc., which are required to be direct toward the center of the planet.

The RF circuits for the S-band transmitter and receiver should be mounted on the back of the paraboloid, or close by on the gimballed platform, so that coaxial rotary joints and feedline losses at 2190 mc can be eliminated. Slip-ring assemblies for DC power, control signals, and modulation/demodulation signals must be provided. These provisions can be made with greater reliability and less noise and signal loss than for S-band transmission lines.

3. <u>Relay antenna system.</u> A telemetry receiver antenna will be mounted on the orbiter to monitor both the VHF omnidirectional array on the lander and the VHF antenna that will be placed on the surface of the planet. Since these systems will be linearly polarized and since the latter will be randomly oriented with respect to the orbiting vehicle, a circularly polarized receiving antenna is required. Also, in order to illuminate the extremities of the planet with sufficient gain, a beamwidth of 84 degrees is required. A helix, radiating in the axial mode will be suitable. To obtain the beamwidth required, it will be designed for "in phase" radiation from individual turns, not the more normal "increased directivity" radiation mode.

In general, the helical beam antenna (a helix radiating in the axial mode) provides a well defined end-fire beam which is circularly polarized. Minor lobes are relatively small. Its mode of radiation is readily produced by a conductor formed as a helix of 12.5-degree pitch angle on a cylinder about one wavelength in circumference. The axial mode has the unique property that it may persist over a considerable frequency range with desirable pattern and impedance characteristics.

The axial or end-fire mode of radiation of the helix is most simply generated by connecting the inner conductor to the helical winding and mounting the outer conductor of the coaxial line to the ground plane.

A very simple approximation for the power gain of a helical beam antenna, with respect to an isotropic circularly polarized source can be expressed by the formula

$$\text{Gain} = 15 \, (C/\lambda)^2 \, n \, S/\lambda$$

or as a decibel ratio

$$= 11.8 + 10 \, \log_{10} C/\lambda^2 \, n \, S/\lambda \text{ db.}$$

It can then be referenced to a linear transmitter by subtracting 3 db for polarization loss. This formula neglects the effect of minor lobes and may be somewhat optimistic but usually not by more than 1 or 2 db. The gain can be precisely determined by comparing the antenna with a calibrated gain standard.

In designing the helix to radiate in the "in-phase field" radiation mode, the axial ratio will approach unity since this "in-phase field condition" is also the condition for circular polarization.

However, the axial ratio may be disturbed because the helix is mounted over the lens and telescoping equipment. Techniques such as trimming the tip of the helical winding, tapering the winding of the coil, moving the antenna on the lensing equipment will be employed to compensate for excessive pertubations in the axial ratio. An axial ratio of 1.0 db on axis is a reasonable objective.

A helix of three turns or more with a pitch angle of 12.5 degrees has a terminal impedance which is nearly a pure resistance. This can be estimated to within ± 20 percent accuracy by the expression,

$$R = 140\, C/\lambda.$$

In the case where $C = \lambda$, the terminal impedance will equal 140 ohms.

Since the antenna will be used in a receive application, a design objective of 1.5:1.00 is reasonable.

The antenna is capable of operating over a 1.75:1 band with no serious deterioration of its impedance or radiation pattern coverage. Table 15 lists the more important characteristics of the antenna.

A pictorial description of the antenna is shown in figures 81 and 82. Basically, it consists of 0.050-inch wire wound on three 0.500-inch supporting fiberglass rods. It will be mounted over the cylindrical tube protruding from the television camera, which is 16 inches long and 7.0 inches in diameter. The VHF transmitters and receivers will be mounted on the gimballed platform directly behind the antenna. Slip rings will be attached to the low frequency demodulated output of the receiver which will permit the gimballed arm to spin in a 360-degree arc.

120 DEGREE TYP

20 INCH DIAMETER

7 INCH DIAMETER

18 DEGREE TYP

0.25 PLASTIC RING STIFFENER 2 REQUIRED

13 INCH DIAMETER

26 INCHES

0.5 INCH FIBERGLAS ROD. 3 REQUIRED

0.06 COPPER

0.05 AL GROUND PLANE
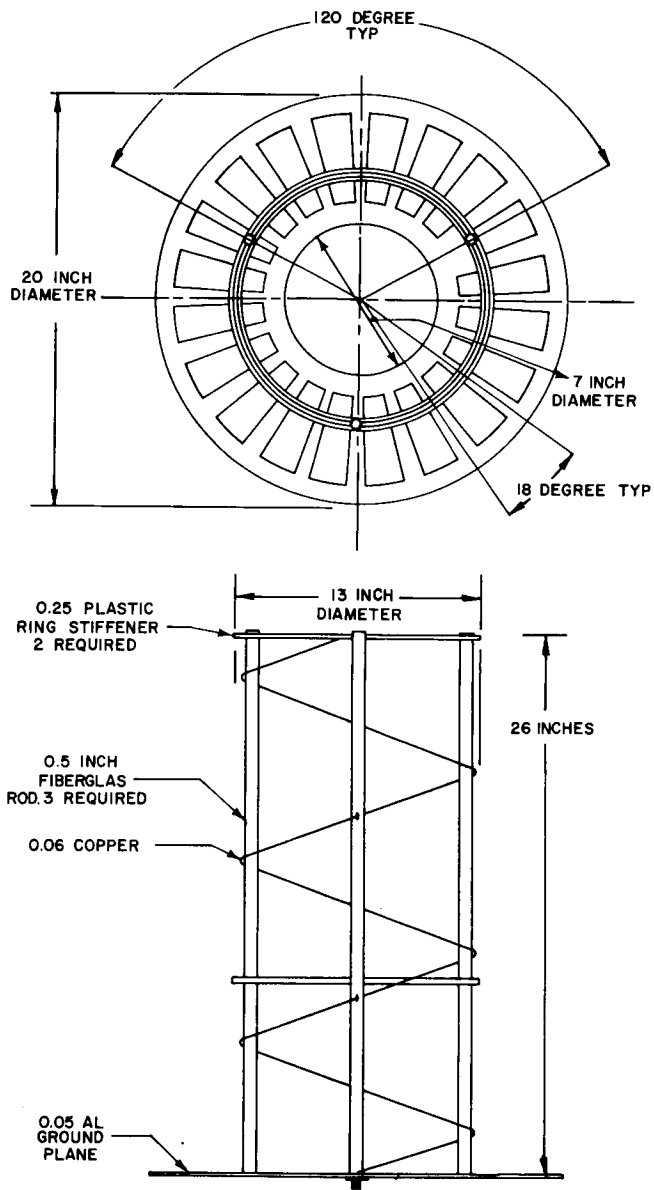
63-9721

Figure 81 VHF HELICAL ANTENNA

VHF HELICAL
ANTENNA

T V
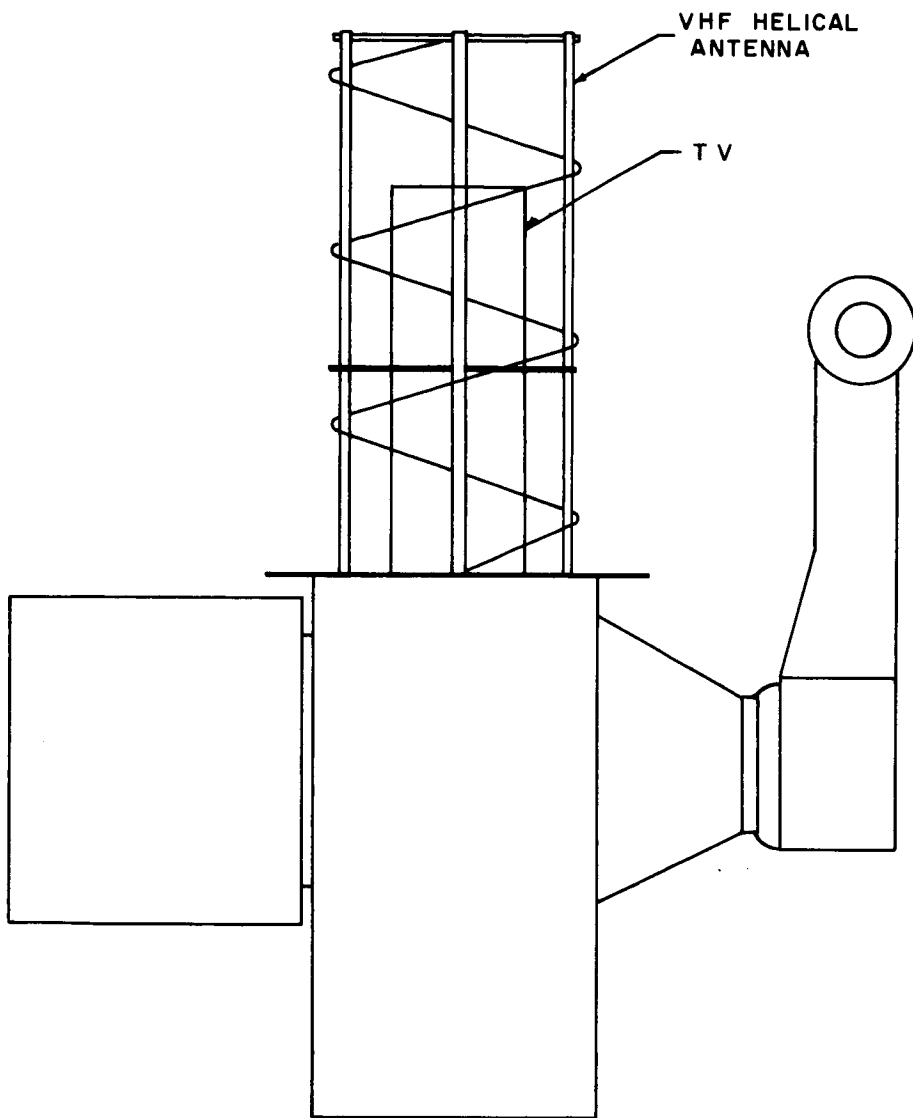
63-9722

Figure 82 VHF HELICAL PIVOT MOUNTED ANTENNA

TABLE 15

VHF CIRCULARLY POLARIZED HELICAL ANTENNA

Antenna Type	3 turn helix
Input VSWR	1.50:1.00 over the operating band
Gain of the Antenna	7.0 db referenced to a linear transmitting source
Polarization	Circular
Beamwidth	Approximately 84 degrees at the half-power points
Operating Mode	Receiving antenna
Weight	3 pounds
Axial Ratio	1 db on axis

4. **High-gain antenna system.** This section of the report presents the results of the orbiter-bus telemetry antenna design and development studies. The studies considered only radiating elements which exhibit high gain characteristics, since the antennas will service the two major communications systems on board the orbiter-bus portion of the spacecraft.

At UHF frequencies and above, where directive beams become practical, a choice is available between end-fire or broad-side arrays, a corner-reflector antenna, or a reflector using a curved surface for focusing incident energy. While the end-fire antenna exhibits an impedance bandwidth which is broad enough for this application, its gain limitation (only about 15 db) precludes its use here. Broad-side arrays can be used to produce high gains (greater than 30 db); however, they are limited by the number of elements required to approximate the reflector antenna. At least four array elements must be placed in each square wavelength of the aperture, so the feed system becomes prohibitively complex. The corner-reflector antenna has the same basic gain limitation as the end-fire array. The curved surface reflector antenna, on the other hand, has the basic advantage over the other elements considered in that high gains can be achieved with relative ease. Since reflectors utilizing the properties of a parabola have been found to be satisfactory in many different applications, including current space programs such as Ranger and Mariner II, the studies were directed toward examining antenna configurations which utilize parabolic reflectors.

A paraboloidal reflecting surface, which is formed by rotating the arc of a parabola about the line joining the vertex and the focal point, has been found to be the most useful high-gain reflector antenna. Typically, the reflector size is chosen to be as large as practical, and then the feed is designed for efficient illumination based on obtaining either maximum gain or a reduction in side lobes at the expense of a slight decrease in gain. Because of the large spacecraft to Earth communications distances involved with this program, it is desirable to maximize the antenna gain for a given reflector size. To satisfy this criterion, it has been found that the radiated energy from the primary feed should be distributed so that the field at the reflector edges is approximately 12 db below that of the center. This edge illumination value is general, however, and will change with the ratio of focal length to reflector aperture diameter (f/D ratio). For small f/D ratios, large space-attenuation factors are introduced in the edge illumination with corresponding reductions in maximum gains. As an example, with an f/D ratio of 0.25 the primary feed pattern will be down only 6 db for an edge illumination of 12 db;[1] therefore, the energy below the 6 db point is spilled over the reflector edge and is lost.

The physical constraints of the Voyager spacecraft limit the f/D ratio to 0.38; therefore, an optimum-gain figure of 55 percent of the gain from a uniformly illuminated aperture is reasonable. The orbital communications system will utilize an 8-foot-diameter parabola, while the in-transit system will use a 4-foot-diameter unit. The fundamental characteristics of the antennas are tabulated in table 16 and apply to either a Mars or a Venus mission.

Each parabolic antenna will utilize a vertex feed consisting of a rigid coaxial section extending through the vertex of the reflector and terminated at the focus by a radiating element which directs the radiation back onto the reflector. A balanced dipole-disk feed will be used as the primary illuminator since the resulting system is free from the squint phenomenon associated with an assymetric termination, thereby yielding a higher optimum-gain figure. Figure 83 shows the details of a typical dipole-disk feed;[2] however, to obtain maximum gain an empirical approach will be used to determine final feed dimensions and position.

The structural aspects of the orbiter-bus telemetry antennas was investigated by Ryan Aeronautical Company and the results of this work are given in detail in the appendix.

The design and fabrication techniques recommended are extensions of proven technology available today. This approach was chosen in order to ensure the timely availability of highly reliable hardware with a minimal expenditure of development effort.

---

[1] Kelleher, K. S.: Antenna Engineering Handbook. p 126, McGraw-Hill Book Company, Inc., 1st edition, 1961.

[2] Silver, S. Microwave Antenna Theory and Design. p 254, McGraw-Hill Book Company, Inc., N.Y., 1949.

TABLE 16

HIGH-GAIN ANTENNA CHARACTERISTICS

Parameter	8-Foot Parabola	4-Foot Parabola
Operating Frequency	2120 & 2300 mc	Same
Operating Power	120 watts	35 watts
Polarization	Linear	Same
Gain	32. 8 db	26. 8 db
Efficiency	$\geq$ 55%	Same
Half-Power Beam Width	3. 75 degree	7. 5 degree
Side Lobe Level	> -20 db	Same
VSWR for ± 1% Bandwidth*	1. 25:1	Same
f/D Ratio	0. 38	Same
Feed Type	Balanced Dipole-Disk Vertex Feed	Same

*Centered at each operating frequency.
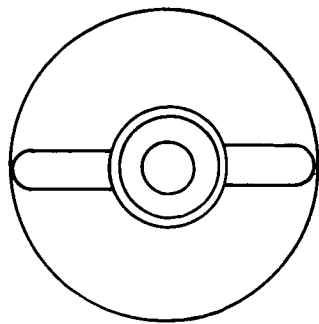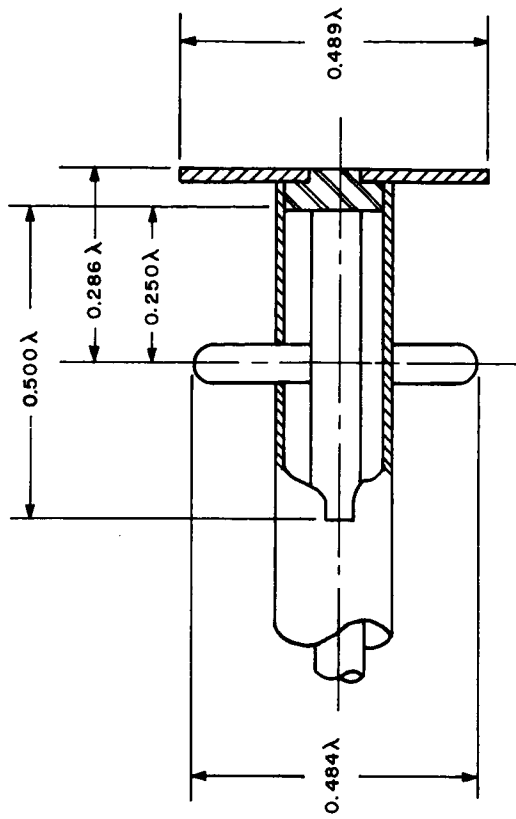
Figure 83 BALANCE DIPOLE DISC FEED

63-9723

-197-

PART II-VENUS ORBITER

3. 1 Communication System Requirements

The communication system requirements for the Venus Orbiter are similar
to those previously described for the Mars orbiter in that, in-transit, in-orbit,
and relay data from a lander will be transmitted to Earth along with range and
range rate information. This system will have the same command reception
capability as the Mars orbiter, but with an increased performance margin due
to the shorter range.

Since the surface of Venus is completely shrouded by clouds, mapping data
cannot be acquired by the TV camera system used in the Mars orbiter. In an
effort to obtain emission and reflection characteristics of the Venusian surface,
a radiometer and radar mapping system will be incorporated in the Venus
orbiter. The communication system used to monitor and store the acquired
mapping data will be similar to the system used in the Mars orbiter.

3. 2 General System Description

The orbiter communication system will transmit all data acquired by the
orbiter during its operational life through either of two highly directional
S-band communication links. The main communication link consists of a
steerable 8-foot parabola antenna and a 70-watt transmitter. This system is
used primarily to transmit the radar mapping data acquired during the orbital
phase. With a transmitted bit rate of approximately 3600 bits per second, a
worst case performance margin of +3. 93 db can be expected, at a worst case
range of 2. 6 x 10^8 km.

The secondary communication link consists of a steerable 4-foot parabola
antenna and a 35-watt transmitter. This system is used primarily to transmit
the guidance and control and engineering status data acquired in transit. At
a transmitted bit rate of 400 bits per second, a worst case performance margin
of +4. 96 db can be expected at a range of 2. 6 x 10^8 km.

These two links serve as redundant backups to each other. However, with
the 4-foot parabola, a reduced amount of mapping data will be transmitted.
Each of these links will contain coherent transponders to aid the DSIF in making
range measurements. They will also use command receivers to receive com-
mands from Earth. Commands will normally be received by a separate system
identical to the one in the Mars orbiter.

Data transmitted to the orbiter from either the capsule or lander will be
received by a system identical to the system used in the Mars orbiter; with
the exception that the integrated S-band radar altimeter/command system will

TABLE 17

SUBSYSTEM WEIGHTS, VOLUMES, AND POWER CONSUMPTIONS

Major Subsystem	Redundancy	Volume (cubic inches)	Weight (pounds)	Power Consumed (watts)
Eight-foot antenna (with drive)	0	--	29.6	--
Four-foot antenna (with drive)	0	--	14.8	--
Antenna driver amplifier	1	288	10.0	--
70-watt S-band power amplifier (with special power supply)	0	275	16.0	140
35-watt S-band power amplifier (with special power supply)	0	180	10	70
S-band transponder	Double redundant each parabola	1200	40	20
S-band command receiver	Double redundant each 2π steradians	800	28 .	56
Command decoder	1 (active	22	2	12
Multiplexer - encoder	1	300	18	3
Subcarrier modulator	1	80	4	3
VHF receiver	1	300	13	3
Venus VHF transmitter	1	140	8	10
S-band omni-antenna system	0	--	4	--
VHF helix antenna	0	--	2.5	--
Venus recorder No. 1	0	1150	16	6
Venus recorder No. 2	0	1150	16	6
Cabling and plumbing	-	--	20	--
		5885	251.9	329

TABLE 18

IN-TRANSIT TELECOMMUNICATIONS DESIGN CONTROL CHART

PROJECT: voyager
CHANNEL: Orbiter To DSIF
MODE: 4-foot parabola

	Parameter	Nominal Value	Tolerance (decibels)	Worst Value
1	Total transmitter power /35 watts	+45.44 dbm	+0.0 -0.5	+44.94 dbm
2	Transmitting circuit loss / with diplexer	-1.0 db	+0.0 -0.5	-1.5 db
3	Transmitting antenna gain /4-inch diameter	+26.65 db	± 0.46	+26.19 db
4	Transmitting antenna pointing loss	-0.2 db	± 0.2	-0.4 db
5	Space loss = 32.46+20 log F+20 log R F:2300 MC, R:2.6x10^8KM	-268.0 db	----	-268.0 db
6	Polarization loss	-0.0 db	+0.0 -0.08	-0.08 db
7	Receiving Antenna gain	+61.0 db	+0.0 -0.5	+60.5 db
8	Receiving Antenna pointing loss	---	---	---
9	Receiving circuit loss	-0.1 db	maximum	-0.1 db
10	Net circuit loss	-181.65 db	+0.66 -1.74	-183.39 db
11	Total received power	-136.21 dbm	+0.66 -2.24	-138.45 dbm
12	Receiver noise spectral density (N/B) T system 50°K	-181.43 dbm	± 0.7	-180.73 dbm
carrier performance				
13	Carrier modulation loss			
14	Received carrier power	◄——— negligible ———►		
15	Carrier APC noise BW (2B$_{LO}$)			
	Carrier track (1-way)			
16	Threshold SNR in 2B$_{LO}$			
17	Threshold carrier power			
18	Performance margin			

TABLE 18 (Concl'd)

No.	Parameter	Nominal Value	Tolerance (decibels)	Worst Value
	Carrier - track (2-way)			
19	Threshold SNR in $2B_{LO}$			
20	Threshold carrier power			
21	Performance margin			
	Carrier - Telemetry			
22	Threshold SNR in $2B_{LO}$			
23	Threshold carrier power			
24	Performance margin	Corresponds to subcarrier SNR degradation of 1.5 db	3 db	
Subcarrier Performance				
	Data channel			
25	Bit rate (1/t) 400 bits/sec	+26.02 db	- - - - -	+26.02 db
26	Required ST/N/B $P_e = 5 \times 10^4$	(8.8+1.5)db	±1.0	+11.3 db
27	Threshold subcarrier power	-145.11 dbm	±1.7	-143.41 dbm
28	Modulation loss	- - - - -	- - - - -	- - - - -
29	Received data subcarrier power	-136.21 dbm	+0.66 -2.24	-138.45 dbm
30	Performance margin	+8.90 db	+2.36 -3.94	+4.96 db
	SYNC channel			
31	SYNC APC noise BW ($2B_{LO}$)			
32	Threshold SNR in $2B_{LO}$			
33	Threshold subcarrier power			
34	Modulation loss			
35	Received SYNC subcarrier power	←	negligible	→
36	Performance margin			

TABLE 19

EARTH-TO-PLANET RANGES

Arrival Date Period	Worst Case Encounter Range		Worst Case Encounter + 30 Day Range		Worst Case Encounter + 150 Day Range	
	AU	KM	AU	KM	AU	KM
MARS						
14 Oct.-2 Dec. * (69)	1.38	207×10^6	1.58	237×10^6	2.37	356×10^6
28 Nov.-31 Dec. * (71)	1.19	179×10^6	1.47	220×10^6	2.40	360×10^6
4 Feb.* 27 Mar. (73)	1.97	296×10^6	1.73	260×10^6	0.88	132×10^6
VENUS						
7 Dec.-23 Dec.*(70)	0.47	70.5×10^6			1.49	224×10^6
18 Sept.-3 Oct.*(72)	0.97	145×10^6			1.68	252×10^6
7 Apr.*-20 Apr. (73)	1.73	260×10^6			1.19	179×10^6
11 Oct. - 31 Oct. *(75)	0.63	94.5×10^6			1.53	230×10^6

* Worst Launch Date

TABLE 20

IN-ORBIT TELECOMMUNICATIONS DESIGN CONTROL CHART

PROJECT: Voyager
CHANNEL: Orbiter to DSIF
MODE: 8-Foot Parabola

No.	Parameter	Nominal Value	Tolerance (decibels)	Worst Value
1	Total transmitter power / 70 watts	+48. 45dbm	+0. 0 -0. 5	+47. 95dbm
2	Transmitting circuit loss / with diplexer	-1. 0 db	+0. 0 -0. 5	-1. 5db
3	Transmitting antenna gain / 8-inch diameter	+32. 7db	±0. 91	+31. 79db
4	Transmitting antenna pointing loss	-0. 3db	+0. 3 -0. 2	-0. 5db
5	Space loss = 32. 46+20 log F+20 log R F:2300 MC, R:2. 6x10^8 KM	-268. 0db	--	-268. 0db
6	Polarization loss	-0. 0db	+0. 0 -0. 08	-0. 08db
7	Receiving antenna gain	+61. 0db	+0. 0 -0. 5	+60. 5db
8	Receiving antenna pointing loss	--	--	--
9	Receiving circuit loss	-0. 1db	maximum	-0. 1db
10	Net circuit loss	-175. 7db	+1. 21 -2. 19	-177. 89db
11	Total received power	-127. 25dbm	+1. 21 -2. 69	-129. 94dbm
12	Receiver noise spectral density (N/B) T System 50°K	-181. 43dbm	±0. 7	-180. 73dbm

TABLE 20 (Cont'd.)

No.	Parameter	Nominal Value	Tolerance (decibels)	Worst Value
	Carrier Performance -			
13	Carrier modulation loss			
14	Received carrier power	←	negligible	→
15	Carrier APC noise BS $(2B_{LO})$			
	Carrier track (1-way)			
16	Threshold SNR in $2B_{LO}$			
17	Threshold carrier power			
18	Performance margin			
	Carrier track (2-way)			
19	Threshold SNR in $2B_{LO}$			
20	Threshold carrier power			
21	Performance margin			
	Carrier - Telemetry			
22	Threshold SNR in $2B_{LO}$			
23	Threshold carrier power			
24	Performance margin	corresponds to subcarrier SNR degradation of 1.5db		3db
	Subcarrier Performance			
	Data channel			
25	Bit rate (1/t) 3600 bps	+35.5db	--	+35.56db
26	Required ST/N/B $p_e = 5 \times 10^{-4}$	$(8.8+1.5)$db	± 1.0	+11.3db

TABLE 20 (Concl'd)

No.	Parameter	Nominal Value	Tolerance (decibels)	Worst Value
27	Threshold subcarrier power	-135.57dbm	±1.7	-133.87dbm
28	Modulation loss	--	--	--
29	Received data subcarrier power	-127.25dbm	+1.71 -2.69	-129.94dbm
30	Performance margin	+8.32db	+2.91 -4.39	+3.93db
	SYNC channel			
31	SYNC APC noise BW ($2B_{LO}$)			
32	Threshold SNR in $2B_{LO}$			
33	Threshold subcarrier power			
34	Modulation loss			
35	Received SYNC subcarrier power	← Negligible →		
36	Performance margin			

Figure 83a COMMUNICATIONS SYST

63-9884

-206-

```
┌────────────────────┐          ┌────────────────────┐
│   COHERENT PSK     │◄─────────│      S-BAND        │
│  COMMAND RECEIVER  │          │   OMNI ANTENNA     │
└────────────────────┘          └────────────────────┘

┌────────────────────┐          ┌────────────────────┐
│      70 WATT       │─────────►│      8 FOOT        │
│      S-BAND        │          │ PARABOLIC ANTENNA  │
│    TRANSPONDER     │          │                    │
├────────────────────┤          │                    │
│      RANGING       │◄─────────│                    │
└────────────────────┘          └────────────────────┘

┌────────────────────┐          ┌────────────────────┐
│      35 WATT       │─────────►│      4 FOOT        │
│      S-BAND        │          │ PARABOLIC ANTENNA  │
│    TRANSPONDER     │          │                    │
├────────────────────┤          │                    │
│      RANGING       │◄─────────│                    │
└────────────────────┘          └────────────────────┘

┌────────────────────┐          ┌────────────────────┐
│       VHF          │◄─────────│       VHF          │
│   LINEAR CHIRP     │          │   HELIX ANTENNA    │
│     RECEIVER       │─────────►│                    │
└────────────────────┘          └────────────────────┘

┌────────────────────┐
│       VHF          │
│     COMMAND        │
│   TRANSMITTER      │
└────────────────────┘

┌────────────────────┐          ┌────────────────────┐
│      RADAR         │◄────────►│      8 FOOT        │
│     MAPPER         │          │ PARABOLIC ANTENNA  │
└────────────────────┘          └────────────────────┘

┌────────────────────┐
│    RADIOMETER      │
└────────────────────┘
```
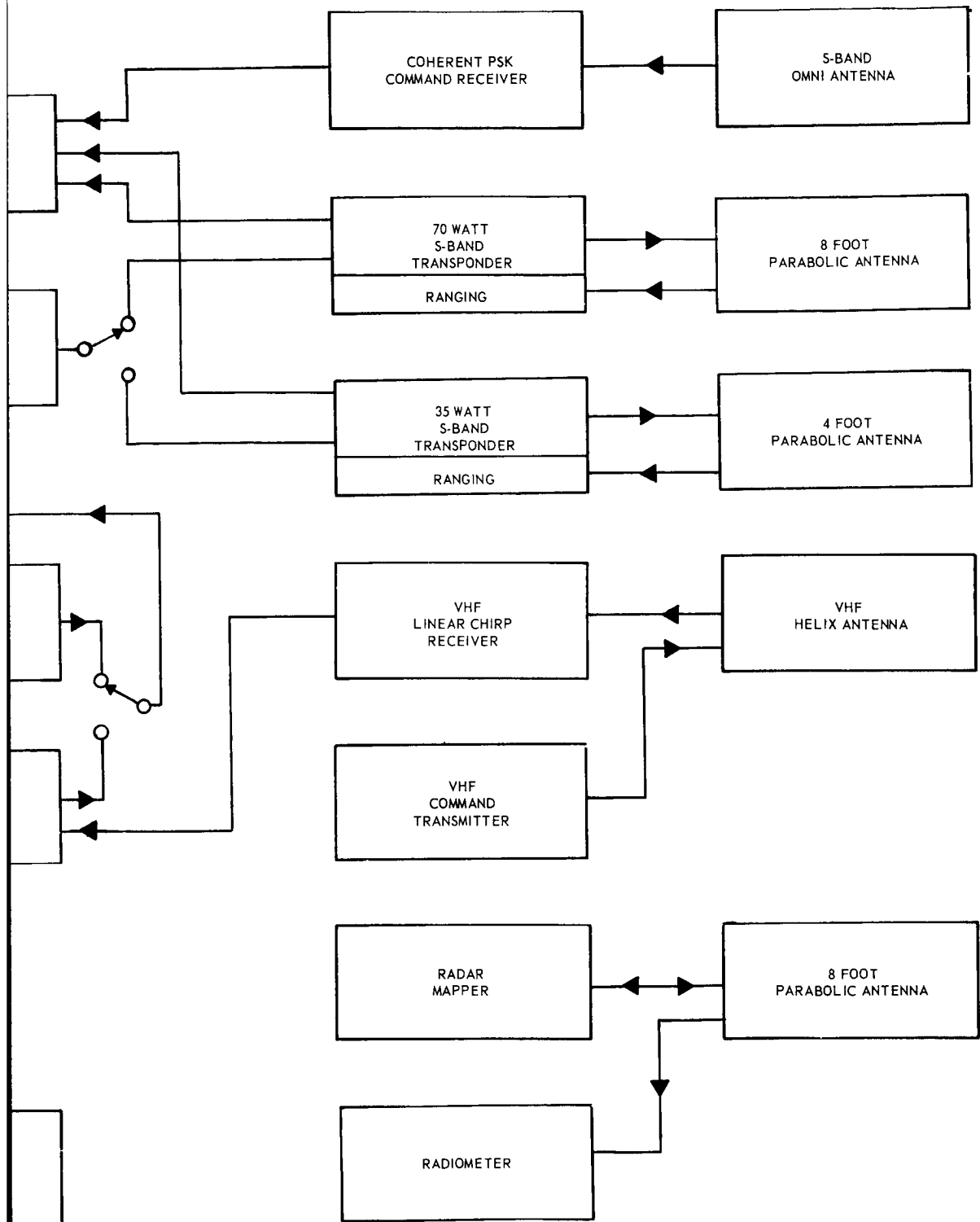
EM BLOCK DIAGRAM

not be used. Altitude information for the Venus orbiter is available from the radar mapping system. A separate command transmitter will be used to signal the lander to begin transmitting its stored data.

Since the total data acquired by either the capsule or lander is approximately two orders of magnitude less than that acquired by the Mars lander, a separate recorder for the lander data will not be used; the data will be stored in one of the two mapping recorders. The operation of the two mapping recorders will be identical to those used in the Mars orbiter.

The main source of power for the orbiter equipment will be a solar panel array as in the Mars orbiter. However, the panel area required for the Venus orbiter is approximately one third the area required for the Mars orbiter. While in orbit, the orbiter may pass through the Venus sun-umbra region. To provide power in this region, rechargeable storage batteries will be used.

To meet the reliability figure required of the orbiter, the communication will be 100 percent redundant. All redundancies in the communication system will be passive, except for the command systems, which obviously require active redundancy.

The total weights, volumes, and power consumptions of the orbiter communication system components are listed in table 17.

3.3 Detail System Description

A simplified block diagram of the orbiter communication system, which will meet all of the orbiter requirements is shown in figure 83A. Two direct-link communication systems were selected for the orbiter; one to be used in transit the other to be used in orbit.

1. <u>Detailed in-transit communication link description.</u> The communication link parameters associated with this phase are listed in table 18. The range indicated in this table is the maximum range that can be expected as determined for the launch opportunities listed in table 19. Except for the higher transmitted bit rate, the operation of this system is essentially identical to the operation of the Mars orbiter. The operational details of the transponder, ranging, command, transmitter, and antenna systems used during this phase are described in the Mars orbiter.

2. <u>Detailed in-orbit communication link description.</u> The data monitored in this phase is primarily mapping data acquired through a radar mapping system. In addition, scientific and engineering status information will be acquired and, also, data will be received from the lander.

a. <u>Mapping.</u> Mapping data will be monitored and stored in a method similar to the Mars orbiter. The communication link parameters associated with this phase are listed in table 20.

Since the resolution of the radar mapping equipment is less than that of the TV camera system used in the Mars orbiter, the total acquired mapping data will be less than that acquired by the Mars orbiter. For this reason, a transmitted bit rate of 3600 bits per second was selected for the Venus orbiter. At this bit rate, a worst case performance margin of +3.93 db can be expected using a 70-watt transmitter. The Mars orbiter required a 120-watt transmitter in the corresponding phase.

b. <u>Reception of lander data.</u> Reception of the capsule or heavy descent lander data during entry and descent into the Venusian atmosphere will be accomplished with a system identical to the one used in the Mars orbiter. These data will be stored in one of the two mapping recorders.

Reception of the heavy lander data acquired after landing will be accomplished with the same system. Since the total acquired data by either the capsule or the lander is approximately two orders of magnitude less than the Mars lander, a separate recorder to store the lander relayed data will not be used. The total time required to receive all heavy lander data is approximately 10 minutes. Since this is a small fraction of an orbiter period, the percentage of mapping data lost as a result of interrupting the mapping function to acquire the lander data is negligible.

3.4 Antennas

The command and high-gain antennas used in the Venus orbiter are identical to the ones used in the Mars orbiter. The command antenna used to interrogate the lander will be a VHF helix antenna similar to the S-band helix used in the integrated altimeter/command system in the Mars lander.

4. POWER SUPPLY

PART I -- MARS ORBITER

4.1 Power Source Selection

A number of space power systems could be suggested for the Mars orbiter, viz., solar cell array, RTG, solar collector with static or dynamic conversion, primary fuel cell, and nuclear reactor. With the exception of the first two, the remainder are not sufficiently advanced to consider. Little or no operational experience has been acquired, and little or no reliability information is available and it is acknowledged that the objective of Voyager is not to advance the state of the art in space power systems. Furthermore, the fuel cell and the nuclear reactor are simply too heavy for this application. The solar collector may be a reasonable power source for a later Venus orbiter.

The radio isotope thermoelectric generator (RTG) has been used a few times in space (Transit satellites) and several other generators are planned (Surveyor, Imp, Nimbus, OAO, OGO). An RTG offers several advantages, such as long life, insensitivity to vehicle orientation and incident solar flux, compactness, elimination of look angle problems and, at times, as in this case, weight savings (200 vs. 419 lbs. for solar array and batteries). The disadvantages associated with an RTG are: scarcity of suitable fuel, shielding requirement, handling problems, thermal control requirements, and less well-established reliability.

In the Mars orbiter case one objection is fundamental: inadequate supply of a suitable isotope. Approximately 800 watts are needed for the orbiter; assuming three complete RTG's will be required in early 1968 for the January, 1969, launch, 2.4 KW_e of isotope material must actually be supplied. This is much more than will be available in 1968 for either curium 244 or plutonium 238, even if allowances are made for a reasonable increase in conversion efficiency (from 5% to 7%) and for an increase in production capability (50%). In addition, it should be realized that the availability figures given in figure 84 represent maximum production capabilities and will not be met unless the demand exists. Lead time for production is 2 to 3 years. A complete discussion of isotope availability is presented in Section C of the lander design, volume V.

Other isotopes, with acceptable half lives (Cesium 137, Strontium 90) are similarly scarce for the 1969 launch and both of these would be handicapped by shielding requirements.

Apart from fuel selection problems, other considerations disfavor the RTG: 1) The cost of Curium-244 is estimated between $9,000. and $12,000. per electrical watt; this definitely places the RTG at a higher cost than a solar panel

ISOTOPE	$T^{1/2}$	DECAY	W_T/GRAM	W_T/CC	ENERGIES (Mev)		@$_{T-1/2}$ lbs/KWe	@T=1.5yr lbs/KWe	AVAIL. KWe			COST KWe	(1)LANDER WT/lbs RTG WEIGHT	(2) ORBITER RTG WT.	HEALTH ASPECTS
									'67	'68	'69				
Cesium 137	33.0yr		0.07	0.22	0.52 0.66	weak	632.0	326.0	0.85	1.8	1.8	2.7	145	551	Bad
Cerium 144	285.0d		2.3	13.8	0.3 2.98	weak	19.2	36.2	1.2	17.5	35.0	0.28	71	261	Very Bad
Curium 242	162.0d		120.0	1170.0	6.1	weak	0.368	1.91	2.8	2.8	2.8	7.1	63	244	Fair
Curium 244	18.5yr		2.3	22.4	5.8	weak	19.2	10.1	0.01	0.07	2.05	12.7	53	235*	Bad
Polonium 210	138.0d		140.0	1320.0	5.3	8	11.1	24.6	0.28	2.8	2.8	9.3	84	235	Very Bad
Plutonium 238	86.0yr		0.48	9.3	5.5	weak	92.0	47.0	0.53	0.7	0.79	22.5	76	272*	Very Bad
Promethium 147	2.6yr		18.0	1.0	0.2	weak	245.0	183.0	0.01	0.05	0.05	10.0	93	409	Good
Strontium 90	28.0yr		0.2	0.7	0.61 2.4	weak	221.0	114.0	1.6 0.01	2.5	2.5	2.0	100	339	Very Bad
Thulium 171	1.9yr		0.2	1.5	0.1	none	221.0	190.0	UNKNOWN				110	415	Excellent
Cobalt 60	5.3		16.6	1.87	0.3	1.33	2.68	1.63	UNKNOWN					235*	Very Bad

(1) 110 watt RTG, shield neglected.

(2) Shield Weight Neglected
Battery Weight Not Included

Figure 84 ISOTOPE AVAILABILITY CHART

63-8510

by a factor of about 512). The solar array configuration selected does not handicap the look angle of any instrument or antennas and no pressing need exists for a compact supply.

Consequently, since the vehicle configuration selected shall be essentially unchanged for Mars and Venus through at least the first two opportunities for each, serious consideration of the RTG at this higher power level is not anticipated before the 1973 opportunity.

4.2 Constraints and Configuration

The design of the solar array for the Mars orbiter is partially established by the fact that the average cell temperature at Mars perihelion will not be less than 35°C, while that at aphelion will not be less than 13°C. These conditions were established so that the waste heat rejected from the panel be sufficient to maintain reasonable vehicle temperatures. Were it not for this limitation, lower cell temperatures could be achieved which, from the point of view of the power source designer, are more desirable, since cell conversion efficiency increases with decreasing temperature at the rate of 0.5% per degree centigrade (28°C taken as 100%) as shown in figure 85.

The perihelion conditions prevail for the 1969 opportunity since the spacecraft will encounter the planet 7 days after Mars reaches perihelion, and the available power is ample to accommodate the load profile. For the 1971 and 1973 opportunity, however, the latter portion of the mission shall occur during the aphelion condition and, as will be shown in a later section, sufficient power may not be available from the solar array to permit continuous mapping on successive orbits for the presently available solar cell area.

Fixed solar panels have been selected by the spacecraft designers. This technique was chosen because it improves reliability (one of the most likely failure modes is failure to deploy) and simplifies the look angle problems which occur if both large antennas and large solar arrays were articulated. The present arrangement permits the 8-foot and 4-foot diameter communication antennas to be mounted on the array structure.

The concept for the Mars Orbiter solar cell array consists of two concentric discs which are fixed to the structure. The large disc has an outer diameter of 17.4 feet and inner diameter of 11.25 feet providing an overall area of 138 sq. feet. The small disc has an outer diameter of 9.28 feet and an inner diameter of 2.71 feet providing an overall area of 63 sq. feet. The total area of the combined structure is 201 sq. feet; however, the effective solar panel area is less than that number by 18 sq. feet. The reduction in panel areas is largely due to the packing factor for mounting flat 1 x 2-cm cells; a second order reduction is caused by mounting the four vernier rockets on the cell side
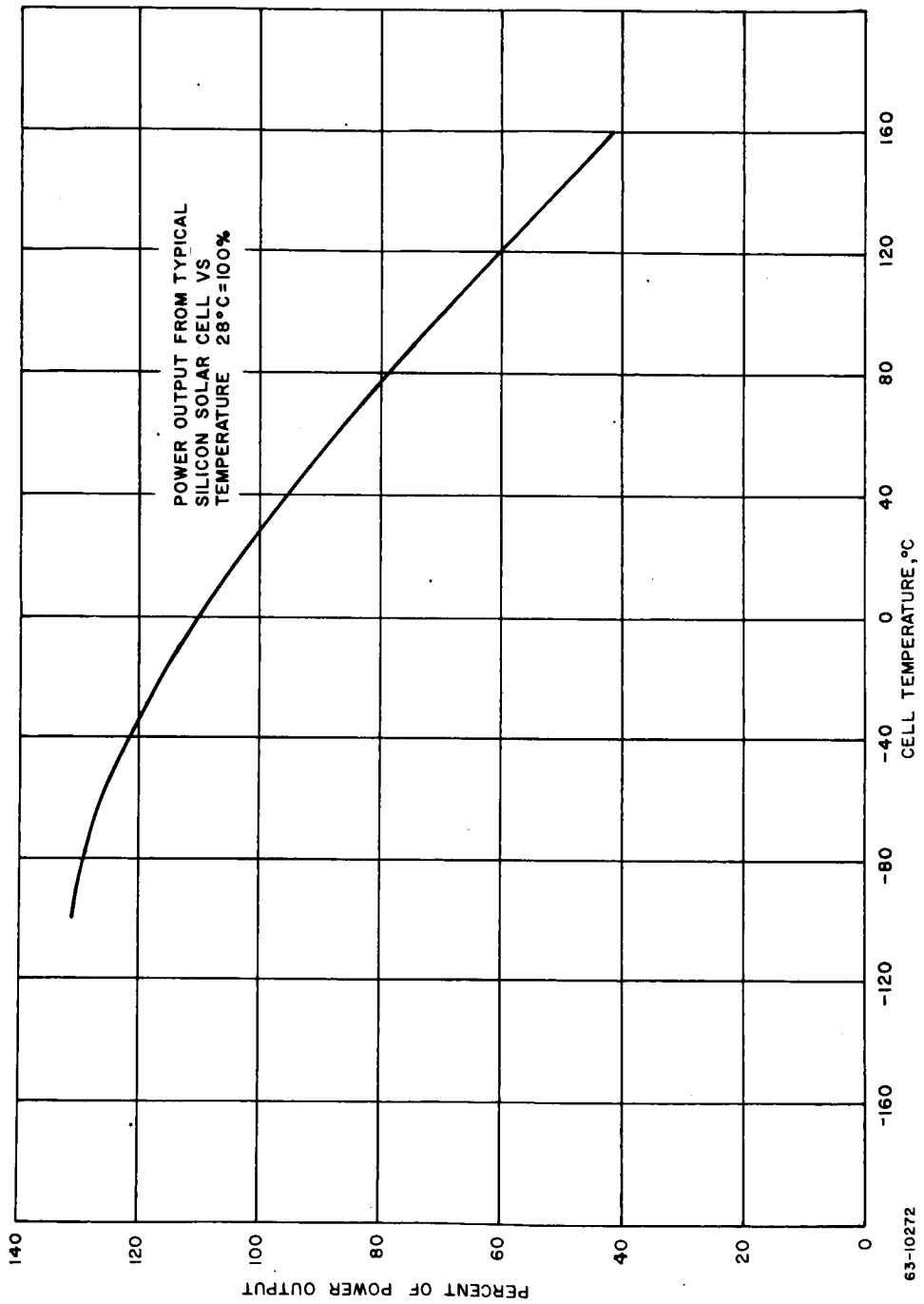
Figure 85 SOLAR CELL TEMPERATURE VERSUS EFFICIENCY

POWER OUTPUT FROM TYPICAL
SILICON SOLAR CELL VS
TEMPERATURE 28°C=100%

CELL TEMPERATURE,°C

PERCENT OF POWER OUTPUT

63-10272

-212-

of the large disc.

Structurally, both discs will be comprised of twelve radial segments. While the small disc is divided into twelve equal segments that differ only in provisions for mounting to the bus structure, the large disc has twelve segments, equal in size but different in supplemental structure, to provide windows for experiments, and provide mounting pads for attitude control jets, vernier rockets, sensors and other equipment. The segmented arrangement was chosen to facilitate fabrication, testing, shipment and replacement in the event of an inadvertent local failure.

4.3 Solar Cell Design

1. Solar cell cover. The design of the Voyager solar cells will be similar to that used on the other satellites and probes. The principal differences is the likely elimination of microsheet glass covers for the individual cells. The reasons for their tentative eliminations are given below; however, the results of the Mariner observations will bear very pertinently on the cell cover question and will serve as the most important influence on the final hardware decision.

The function of the covering, if used, would be to enhance the emissivity in the infrared as it is an effective means of reradiating heat into space and thereby reduce the cell operating temperature during exposure to direct sunlight. Elimination of the glass cover in the Mars case does not result in a high panel temperature because the alternative means of using a highly emissive rear surface is capable of maintaining as low a cell temperature as is tolerable. Of the two methods, the highly emissive back surface is far less expensive. In addition, this technique offers the advantage of lower weight (about 7 percent and a reduction of fabrication loss by 2 to 3 percent). Since the number of steps and components used in the fabrication and assembly process would be reduced, the resulting panel would be more reliable, less testing would be necessary, and there would be less breakage and fewer rejects. An important byproduct of the elimination of the cell cover is the elimination of the adhesive which is used between the glass and the bare cell. The adhesive is known to degrade under ultraviolet radiation.

a. Radiation effects. A second purpose of glass covers is to shield against energetic particle radiation of the type found in the Van Allen belts. No degradation in the performance of the solar cells is anticipated during the spacecraft's short duration transit through the Earth's radiation belts. As to whether radiation belts exist at Mars, no positive answer can be given. However, reasoning suggests there is, at worst, a very weak field. Mars is a smaller, lighter planet than earth and consequently could be expected to have a weaker field. More significant, however, is the existence of the two low

altitude moons, which would tend to sweep up any magnetically trapped charged particles. This fact is important because the density of a charged radiation belt is an equilibrium condition determined by the rate of particle capture (from galactic sources, solar flares etc.) and the rate of sweeping out. On this basis, the probability of the existence of a radiation belt at Mars dense enough to effect damage of a solar cell is low. In any case, N-on-P type silicon cells will be selected which are inherently more tolerant to radiation than are the P-on-N type.

b. <u>Micrometeorite effects.</u> It may be argued that the elimination of the cover glasses will expose the bare cell to direct damage by micrometeorite bombardment. A narrow range of particle energies probably exists which, on the high energy side, are unable to knockout a covered solar cell but which, on the low energy side will knockout a bare cell. The width of this spectrum, in effective hits per day, may be very narrow indeed. In any case, micro-meteorites travel in concentric circles about the sun. Since the solar panel is oriented normal to the sun, the path of the micrometeorites is parallel to the solar array. The panel areas thus exposed to the particle flux is vastly reduced and the entire panel may be protected from damage by providing particle inter-ception barrier along the edges of the structure. These observations should be similarly applicable to the asteroid belts.

2. <u>Solar cell interconnection.</u> Originally, solar cells to be used in space were connected electrically in series in modules of about five cells, and the solar panels were made up of the required number of such modules. The reasons for the series modules are as follows:

1. Early satellites, such as Vanguard, did not require parallel connections since a single solar cell provided the required current, and the required voltage could be obtained only by series connections.

2. The series connection permits use of the overlapping shingle whereby up to seven cells can be sweated together in series without wiring. The shingle also provided a higher packing factor since only the active areas of all cells (but one) were exposed.

The present trend, is to use modules of up to nine cells connected in parallel, because:

1) The most likely mode of solar cell failure is an open circuit. Failures due to solar cell short are rare by comparison. In this context, a parallel connection of solar cells is far more reliabile than a series connection.

2) Flat mounting of solar cells required by the parallel connection permits a stress relief type electrical connection to the upper terminal strip, which is not possible with shingled cells. Broken terminals are less likely.

In addition, flat mounting of solar cells as used in parallel connected modules avoid the 3-degree shingle angle, the shadowing of one solar cell by another in the shingle, and the weight of the excess adhesive fill under the mounted shingles and,

        3) There is no mechanical limit to the size or shape of a parallel module.

As to the maximum size of the parallel module, it is limited by the maximum usable area of sunlight provided by the solar simulator used in testing. Seven-cell modules are the present practical limit. The dimensions of a seven-cell module of 1 x 2 cm cells are nominally 2 x 7 cm. With the basic 5 or 7 cell parallel module, the required panel voltage and current are obtained by any suitable interconnection. To determine the required number of series modules, simply divide the output voltage (normally 36 volts) by the output voltage of a single average cell at the selected operating point. For cells with ten percent conversion efficiency operating at Mars aphelion with a surface temperature of about 13°C, a voltage of 0.350 volt will be obtained at maximum power (figure 86). Thus, for a 36 volts system, 103 parallel modules would be required.

The current output of a solar cell can be computed from the power and the voltage. Near Earth, a single 1cm x 2 cm solar cell in space sunlight will deliver a maximum power current of about 55 ma. At Mars this will drop to about 27 ma. (figure 87). Thus, a 7-cell module will produce about 0.189 ampere in space. It is a simple matter to connect the required number of series strings of modules in parallel to obtain the necessary output current. If failures due to wiring shorts and opens are avoided by careful design, the use of redundant connections or protective devices such as fuses and diodes are not necessary. A need for diodes does arise when, as in the present case, the panel is used to charge a storage battery. During the dark period, diodes between battery and panel (one diode for the whole panel or separate diodes for each series string) prevent the battery from discharging into the panel.

With the foregoing discussion in mind, it appears advisable to follow the common practice of isolating series strings from each other and from the battery by a single diode placed in each series string. Thus, for the seven-cell module example given above, the diode is rated at only 0.189 amperes and 36 volts, a modest requirement. Cross connecting the series strings at intermediate intervals would, by redundance, reduce losses if a particular series string should open up.
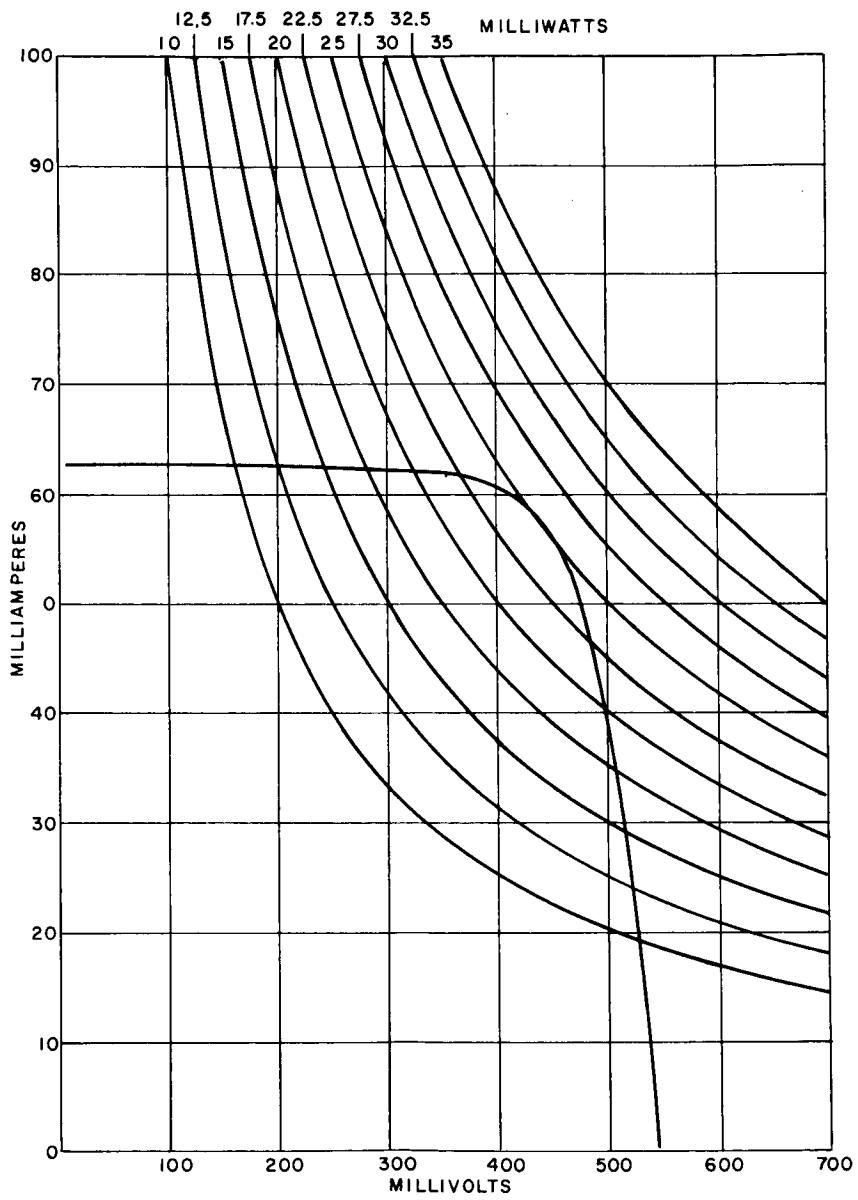
Figure 86 SOLAR CELL VOLTAGE-CURRENT CHARACTERISTIC
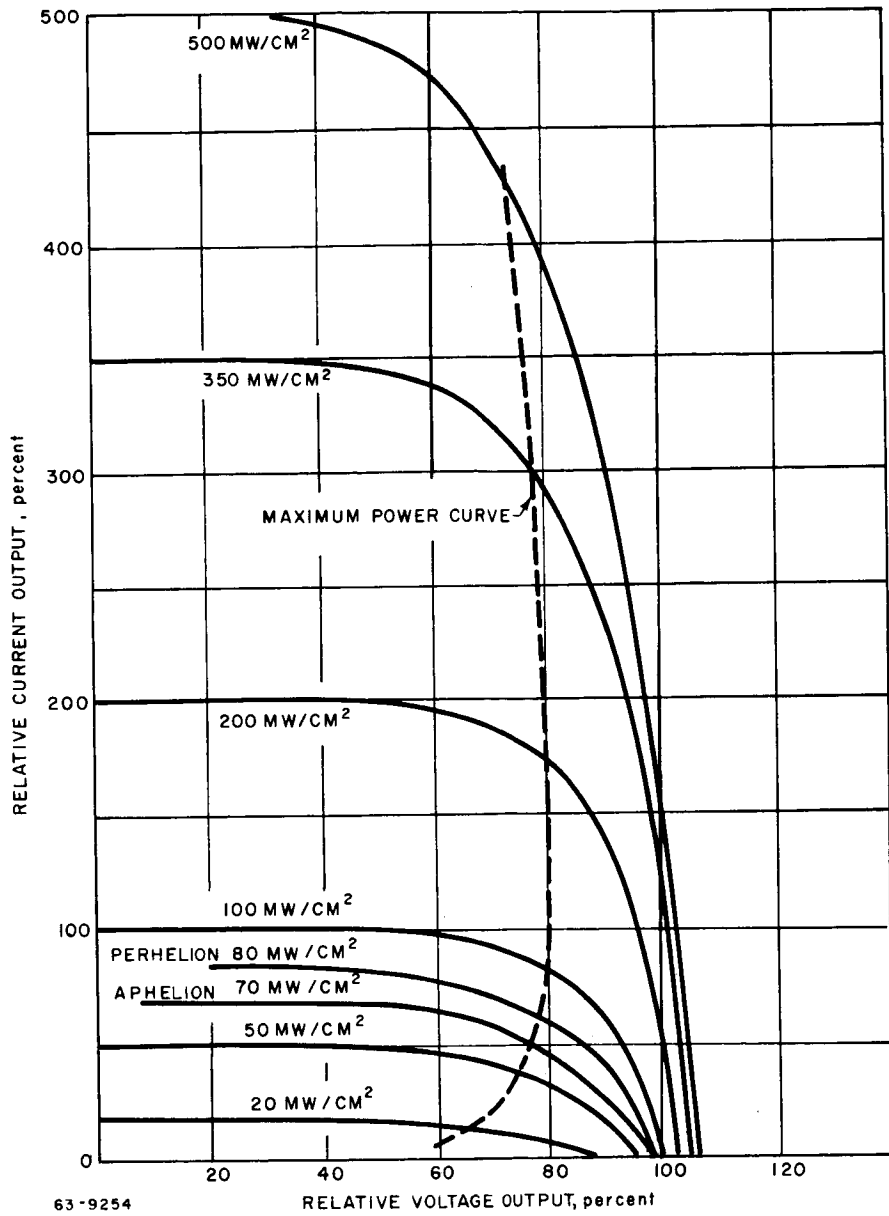
Figure 87 SOLAR CELL PERFORMANCE VERSUS INCIDENT ENERGY

63-9254

-217-

4.4 Available Power

Assuming flat mounted 1cm x 2cm cells with a packing density of 420 per square foot, the raw electrical power available per square foot of solar array is given by:

$$420\left(\frac{S}{R^2}\right) A \eta \ (1-.005 \ \Delta T) \ (1-\text{fabrication loss})$$

where

S is the solar constant at 1 A.U. outside the Earths atmosphere.
0.140 watts/cm^2

R is the Mars distance from the sun in A.U., 1.38 AU at perihelion and
1.68 at aphelion

A is the area of the 1 x 2 cm cell, less contact and grid area,
1.9 cm^2.

η is the efficiency of the solar cell at 28°C and air mass zero, 10%

ΔT is the excursion in cell temperature from 28°C, the cell temperature
is 13°C at aphelion and 32°C at perihelion

Fabrication loss includes assembly, mismatch, and transmission losses, approximately 8 percent for coverless cells.

Using the above relationship, it is found that the solar cell array will deliver a maximum power of 5.3 watts per square foot at Mars perihelion and 4.05 watts per square foot at aphelion. The variation in output power as a function of date for a solar panel at Mars is given in figure 88.

<u>Power Requirements.</u> The worse case power condition is defined by the aphelion condition at which 732 watts of raw electrical power is available. To maximize power utilization, the consumer list was prepared on the assumption that a nominal efficiency of .85 will be realized from the power conditioning equipment. Power conditioning, as used here, is defined to mean all auxiliary equipments between the primary power source and the load; it includes battery charges, converters, inverters and regulators. An 85 percent overall efficiency for the conditioning system in the Voyager Spacecraft is considerably higher than the 54 percent which was achieved by Mariner B. This increase in system efficiency can be achieved primarily because of the elimination of the transformer rectifier units shown in figure 89, which is a block diagram of the Mariner power system. The figure was reproduced from JPL technical report 32-424. As illustrated, the majority of the power is distributed on the
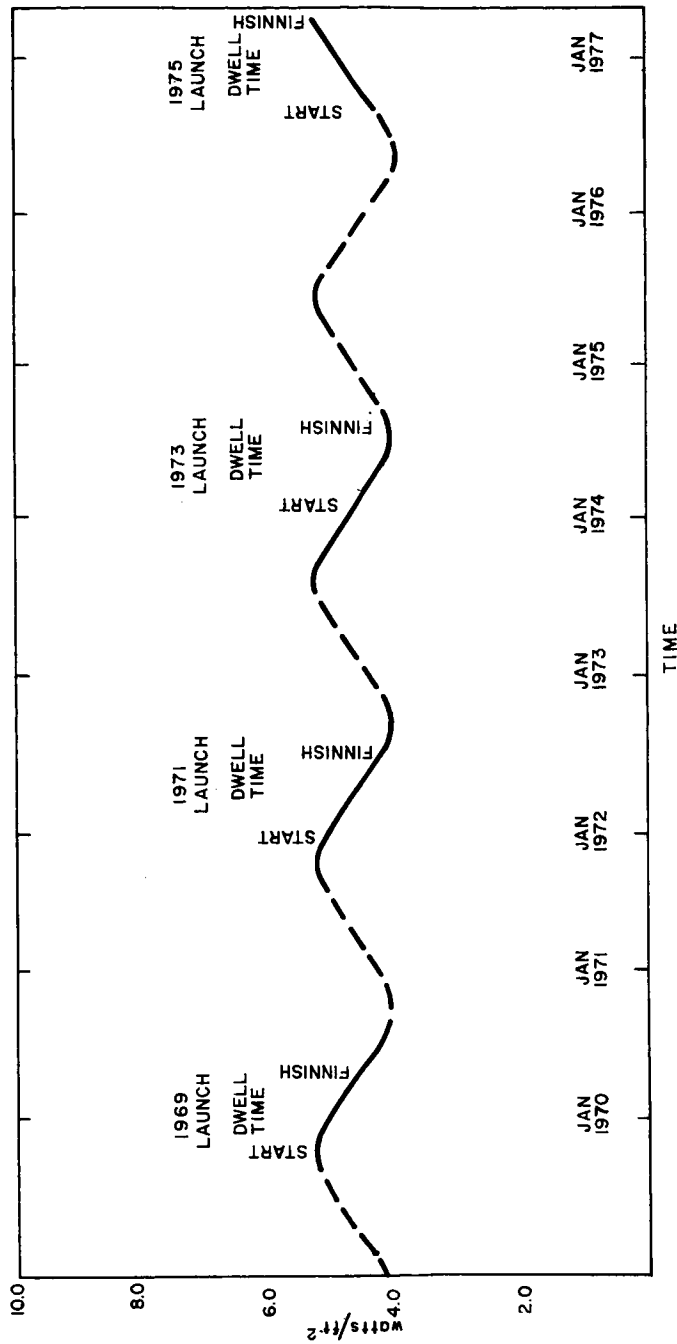
Figure 88 SOLAR PANEL VARIATION AT MARS

63-9251
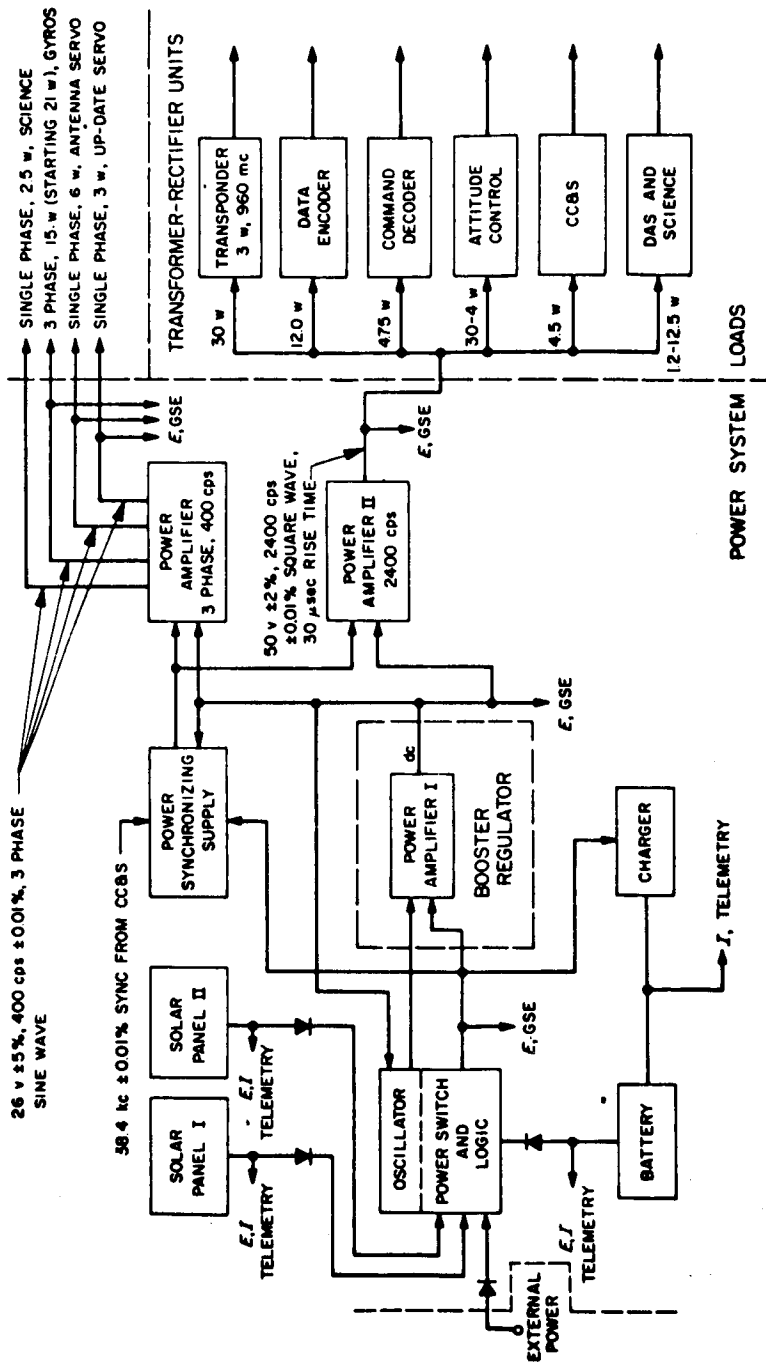
Figure 89 MARINER B POWER SYSTEM

-220-

63-10194

2400 cps ac bus to the users transformer-rectifier units. This technique, although well suited to situations in which the various load power requirements (voltage, frequency ripple, regulation) are in a state of flux, is necessarily inefficient since it must accommodate these variations. Other sources of power loss are the diode in series with the booster regulator and the 2400 cps inverter transistor.

A more efficient method of power utilization is the phase control voltage regulation converter which is used on some of the later satellites like OAO. A brief description of the system is included in a later section, however, it should be noted here that by handling all the power in one transformer, there is a weight and efficiency saving over the use of individual TR units. All outputs can be regulated to a ± 2 percent for load and line changes, with converter efficiency of 85 percent.

This method permits elimination of the separate regulator converter for the communications transponder. Table 21 gives the Mars orbiter-bus requirements.

Mapping from apoapsis was established as the worst case from the point of view of maximum power system weight. The corresponding profile for this situation is shown in figure 90. This loading condition will result independently of the Mars position in its orbit; however, the greatest penalty occurs at aphelion because insufficient energy is available during the sunlit portions to recharge the batteries. The result of this loss in energy is that some mapping information will be sacrificed on the succeeding orbit in order to permit recharge. Figure 91 indicates that the aphelion condition will not be encountered during the 150 day lifetime of any of the Voyager missions.

From table 21 it will be seen that the power requirements during the sunlit portion of the orbit are 619W. (Note that some items are used in active redundancy.) This level refers to the load power; it does not include the converter regulator efficiency which, when considered, establishes an input requirement of 728 watts which is just 5 watts less than the 732 watts available from the solar panel. This marginal situation takes place during the last two months of the 1971 mission and throughout nearly the entire 1973 mission. By these times, however, more efficient cells may be used or the load requirement may have diminished. For the 1.5 x 10 km near polar orbit selected, 1.56 hours of each period shall be in shadow. Since 307 watts are required during this period, it is obvious (in the case of the late 1971 and 1973 missions) that the batteries must be charged on the previous orbit during which the load has been sufficiently reduced to accommodate recharge. The weight of the nickel cadmium battery corresponding to this energy requirement is:
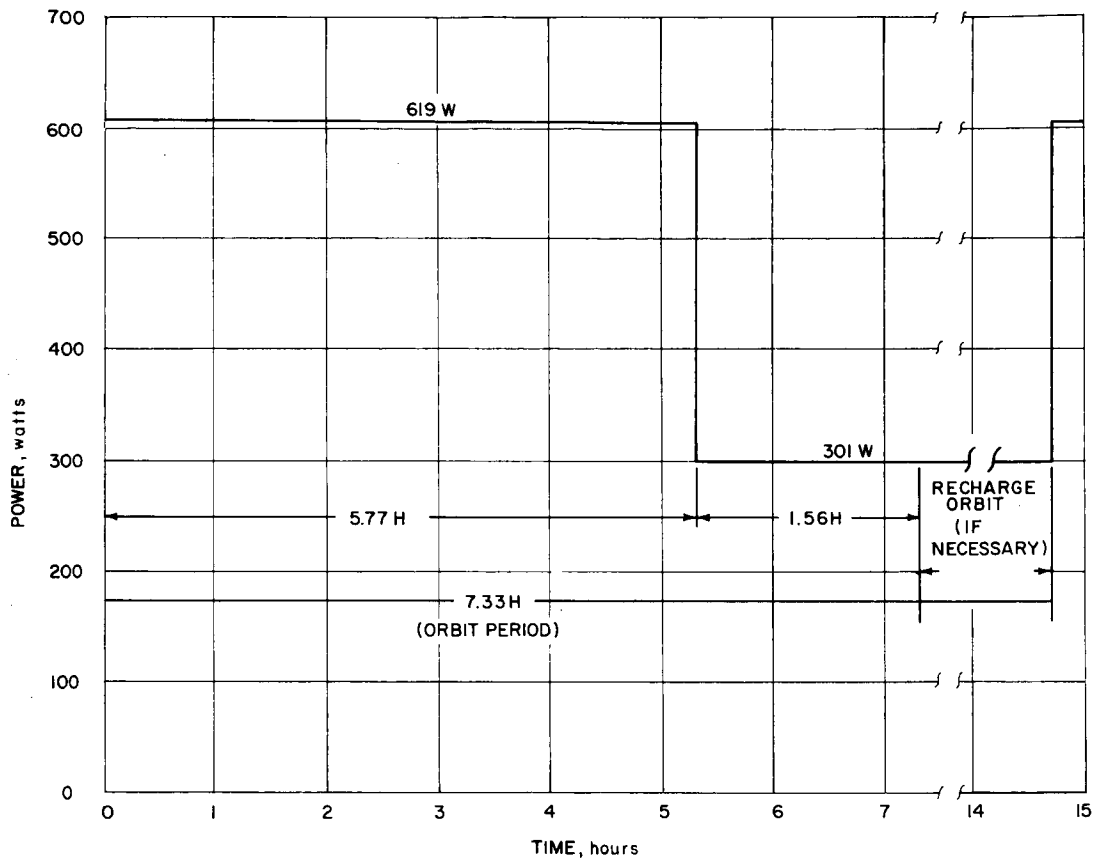
Figure 90 MARS ORBITER POWER PROFILE
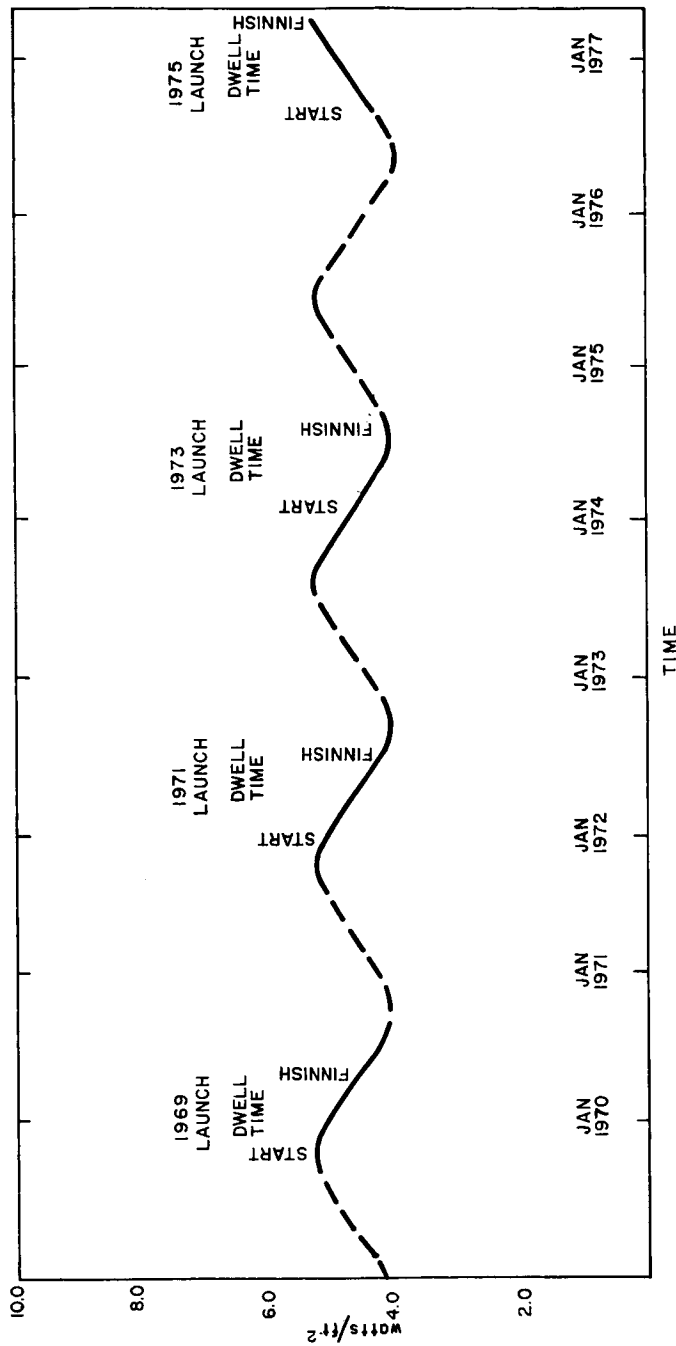
Figure 91 SOLAR PANEL VARIATION AT MARS

63-9251

-223-

TABLE 21

MARS ORBITER-BUS POWER REQUIREMENTS

	Power (watts)	Use
120-watt S-band power amplifier	240	Sun
Driver amplifier	20	Sun
35-watt S-band power amplifier	70	Transit
S-band transponder	20	Sun and Umbra
Command decoder	6	Sun and Umbra
Multiplexer encoder	3	Sun
Subcarrier modulator and PN generator	3	Sun and Umbra
VHF receiver	3	Sun
S-band altimeter	80	Sun and Umbra
Command generator	2	Sun
Digital computer unit		
Guidance		
Central programer and sequencer	162	Sun and Umbra
Attitude control		
Mapping recorder 1	6	Sun and Umbra
Mapping recorder 2	6	Sun and Umbra
Relay recorder	6	Sun
Power conditioning equipment	111	Sun and Umbra
TV cameras	21	Sun
Science	28	Sun and Umbra

$$\frac{(1.56 \text{ hr}) \dfrac{(307)}{0.85}}{\dfrac{(7 \text{ wh})}{\text{lb.}} (0.715)} = 112 \text{ lbs.}$$

A 50 percent depth of discharge is assumed. The .715 factor appears in order to compensate for a discharge time of less than the nominal 10 hour rate (figure 92).

4.5 Battery Selection

During the expected 150 day life of the mission, the battery will experience about 500 charge-discharge cycles. The storage battery most suited to this requirement is nickel-cadmium. Since silver-cadmium will easily tolerate this cycling and has a higher theoretical energy density, it would appear from a cursory examination that the silver cadmium is preferable, but in point of fact, (1) the energy density of the finished package is no greater, (2) the silver corrodes the separator, thereby materially reducing life; and, most significant from a reliability aspect, and (3) silver-cadmium battery cannot tolerate continuous overcharge beyond the second oxide level. Overcharge at this level will produce oxygen and hydrogen gas and, if the pressure exceeds the permissible limit, a catastrophic failure may occur. Therefore, venting is required with the consequent liberation of gas and corrosive vapor.

In the sealed nickel-cadmium battery, however, the gasing condition is prevented because an excess of negative over positive active material is present. Sealed cells are so manufactured that the positive electrode reaches the charged state first. The further passage of current causes the positive electrode to give off oxygen before the negative can reach the fully charged state. If proper access of the oxygen gas to the negative plate is provided, such as by use of a porous separator, a reaction between oxygen and metallic cadmium will occur to give cadmium oxide. Thus, the negative electrode will never reach full charge if the rate of oxygen recombination is sufficient to consume oxygen at the rate liberated. An equilibrium state is thereby reached which prevents the buildup of any approciable gas in the cell.

For reasons of reliability and power performance, nickel cadmium batteries have been selected for the reference design.
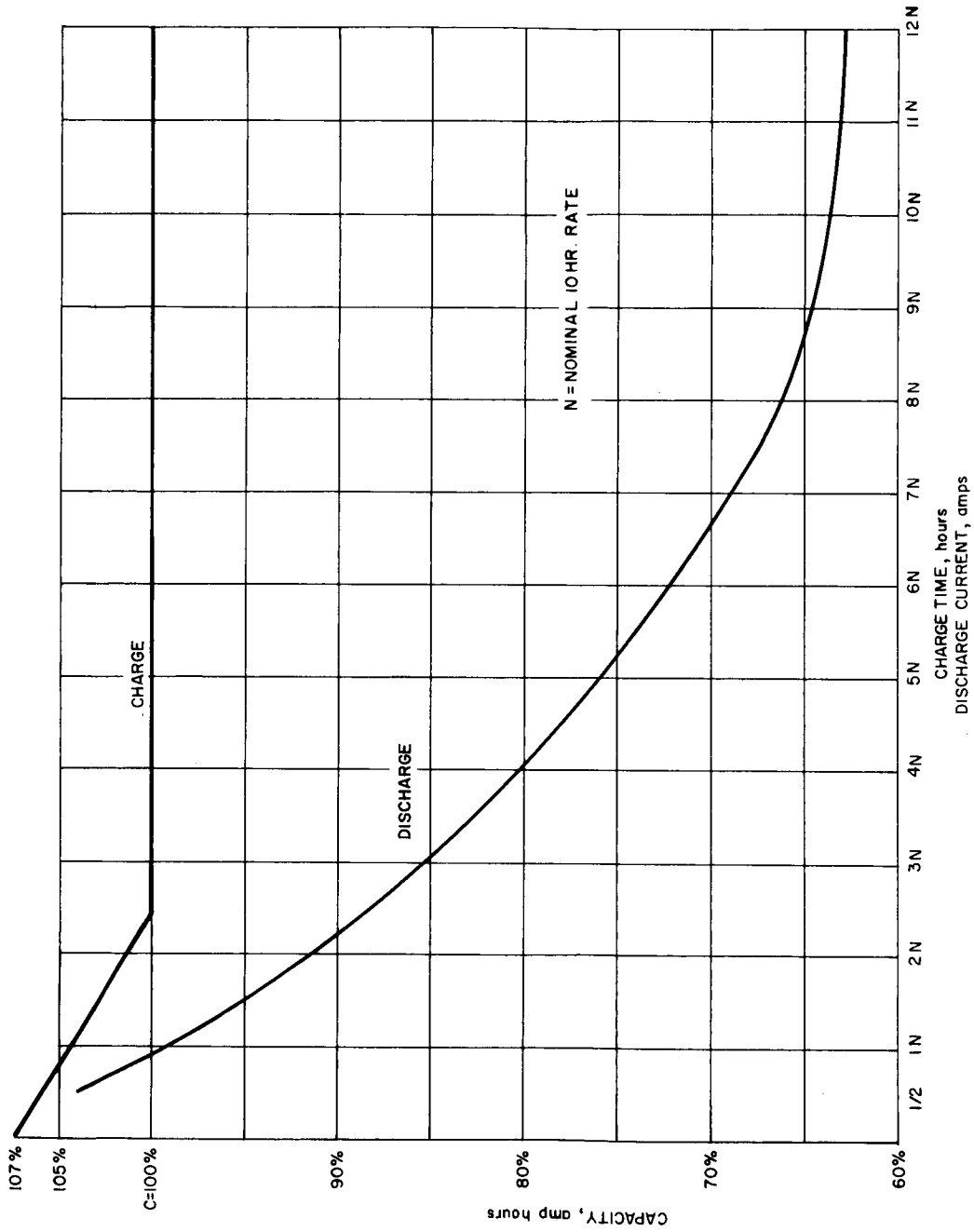
Figure 92 NICKEL-CADMIUM BATTERY CAPACITY VERSUS DISCHARGE TIME

63-8435

4.6 System Description

From the simplified power system block diagram shown in fig. 93, it will be seen that the main functional elements are the solar array, two identical sealed nickel-cadmium battery charge control, a converter regulator to develop the required output voltages, and the necessary control and selector circuitry for reliability through redundancy. The main battery provides power during orbit in the dark and during orbit in the sunlight if the peak system load exceeds the solar array capacity. For system loads below the solar array capacity, pulse width regulators 1 and 2 provide charge and trickle charge currents to the main and standby batteries. Since these regulators draw pulses of current, an averaging filter is used at the output of the solar array to smooth the current demand. A diode is placed at the output of the array to isolate it from the battery during orbit in the dark. Under all conditions, the converter regulator is directly connected to the solar array.

1. Charge control. Since the two batteries and charge control circuits are identical, only one will be described. When the orbiter comes out of the dark, the main battery will attempt to regain its stored energy as fast as possible. The pulse width regulator will be controlled by the current sense to limit the charge current, by the charge control to limit the charge voltage, and by the temperature sense to prevent thermal runaway. The charge current will be limited at the beginning of charge to prevent the battery from absorbing the total solar capacity to the detriment of the system load. The charge voltage will be limited at the middle and end of charge to prevent gassing of the electrolyte for increased internal resistance and generated heat.

The temperature sense reduces the charge voltage during and at the end of charge to minimize energy waste and build up of battery temperature. When the main battery has been fully charged, it will remain on trickle charge and be isolated from the main bus by a diode until the main bus voltage dips during peak loads or during the next dark period. Pulse width regulator Number 2 will provide a trickle charge to the standby battery throughout the sunlit period.

The charge control will maintain the two modes of charging as long as the input voltage of the converter regulator remains above a satisfactory limit. When the voltage decreases below a preset limit, the selector operates a relay which switches the standby battery on the main bus and reverses the charge control connections to the pulse width regulators. The selector may be actuated by a ground control command to select either battery and override an automatic change-over. Power for the selector is obtained from the solar array or the batteries through a diode logic, thus maintaining operation as long as main bus voltage is available.
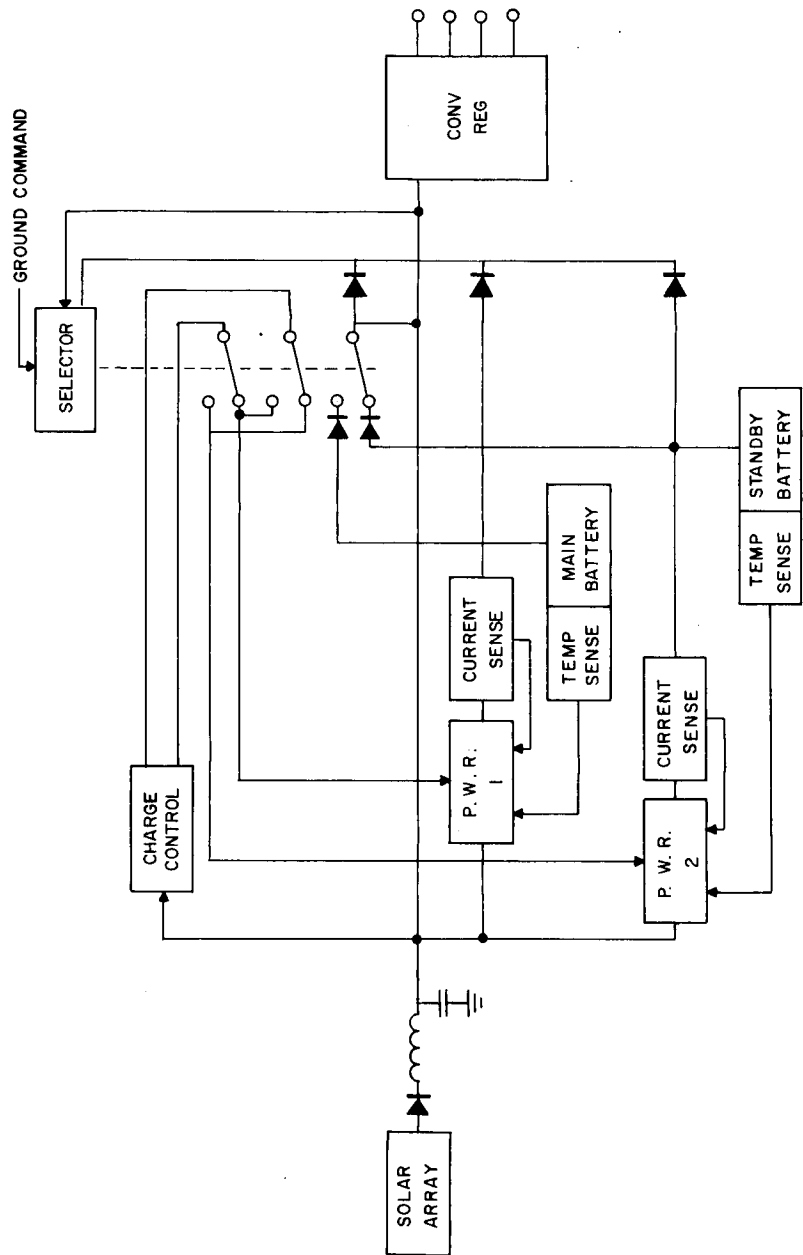
Figure 93 MARS ORBITER POWER SYSTEM BLOCK DIAGRAM

a. <u>Pulse width regulation.</u>   The pulse width technique of voltage re-
gulation involves somewhat more weight than do the less efficient means of volt-
age regulation.   Generally a light weight system is more desirable than a highly
efficient one when ample excess power is available.   However, in the present
case, where large amounts of power are involved and the mission is approach-
ing the power limited point, it is more desirable to pay the weight penalty and
achieve the attendant efficiency gain.   As was inferred, this method of voltage
regulation is not in widespread use and therefore a brief description of its
operation is warranted.

The pulse-width regulator is a switching type regulator offering efficiencies
of 90 to 95 percent.   Its operation is shown in fig. 94.   Six functional elements
are illustrated.   Regulation is accomplished in a manner similar to a servo
amplifier in that an error or difference voltage is used to control the output
and thereby minimize the error.   The voltage difference between a reference
and a sample of the regulated output is detected and amplified by the comparison
element.   The driver element senses the magnitude of the amplitude of the
error signal and varies the duty cycle of the switching transistor (on time to
off time) in a direction to correct any deviation from the preset voltage.   The
comparison element takes a true sample of the output voltage to compare with
the constant reference voltage.   A resistance divider across the regulated out-
put is used as the comparator.   Effects due to temperature are minimized by
the use of wirewound resistors with low temperature coefficients.

Silicon breakdown diodes are used as a voltage reference.   A series com-
bination of low voltage silicon diodes with extremely low temperature coeffic-
ient is utilized to provide a near constant voltage reference.

The gate winding of the magnetic amplifier is excited by a high-frequency
signal from the multivibrator.   High frequencies are used to increase the re-
sponse time of the system for faster correction of output voltage changes and to
reduce the size of the magnetic components.   The error signal is applied to the
control winding of the magnetic amplifer and varies the delay or firing angle
(time required to saturate the core of the magnetic amplifier), which in turn
varies the timing of the magnetic amplifier output to the switching transistor.
The magnetic amplifier circuit approach is highly reliable.

By varying the timing of pulses to the base of transistor, the transistor
can be switched on and off with a varying duty cycle.   This is illustrated in
fig. 95.   When the switch is on, the losses are a function of the transistor
saturation resistance which is extremely low.   During the transistor off period
no losses are sustained.   Efficiency is very high and power handling capability
is also very high.

A filter circuit follows the switching transistor to average the pulsed out-
put.   A typical sequence of events can be followed to demonstrate circuit per-
formance.   For example, if the output regulated voltage tends to rise, the

-229-
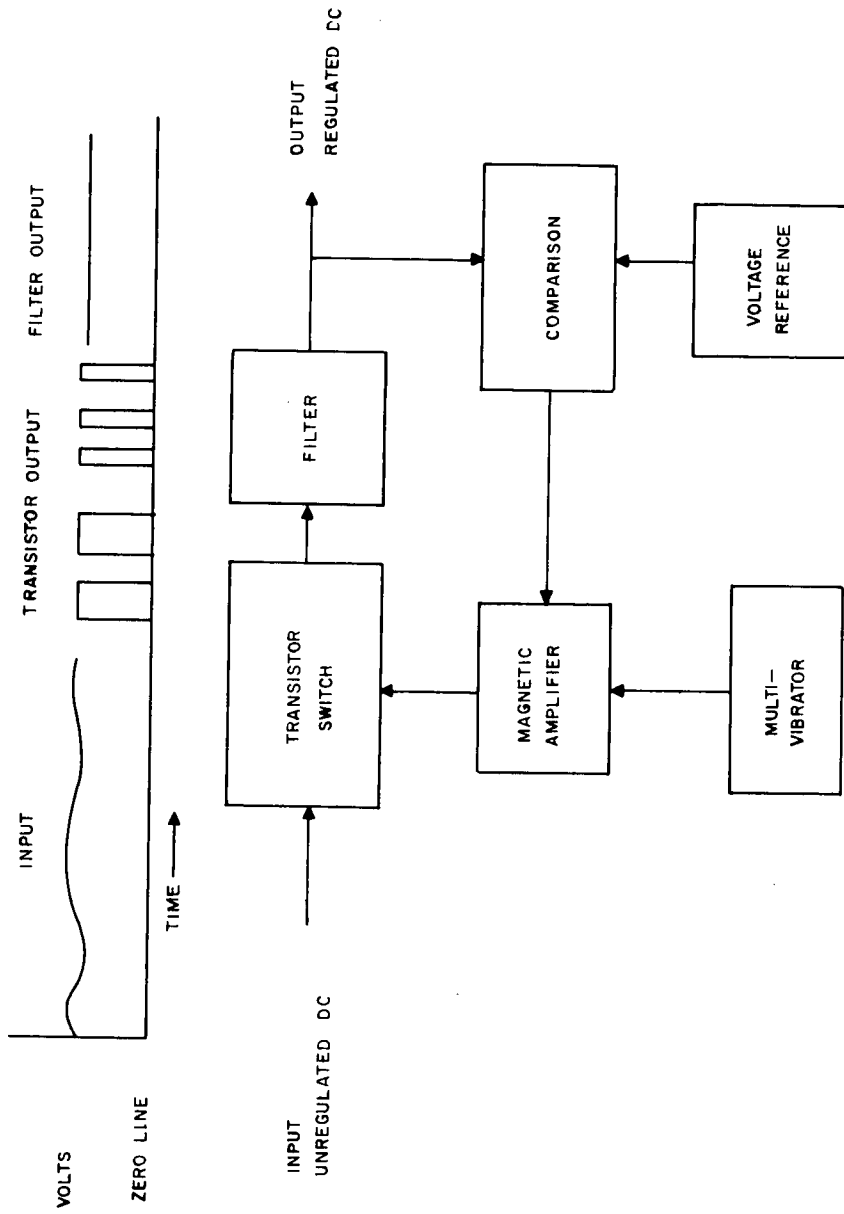
Figure 94 PULSE WIDTH REGULATOR BLOCK DIAGRAM

63-8434

-230-
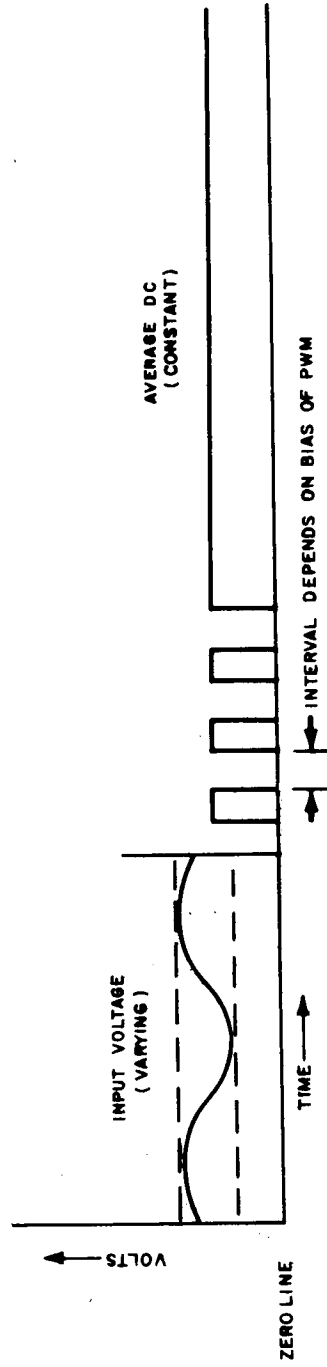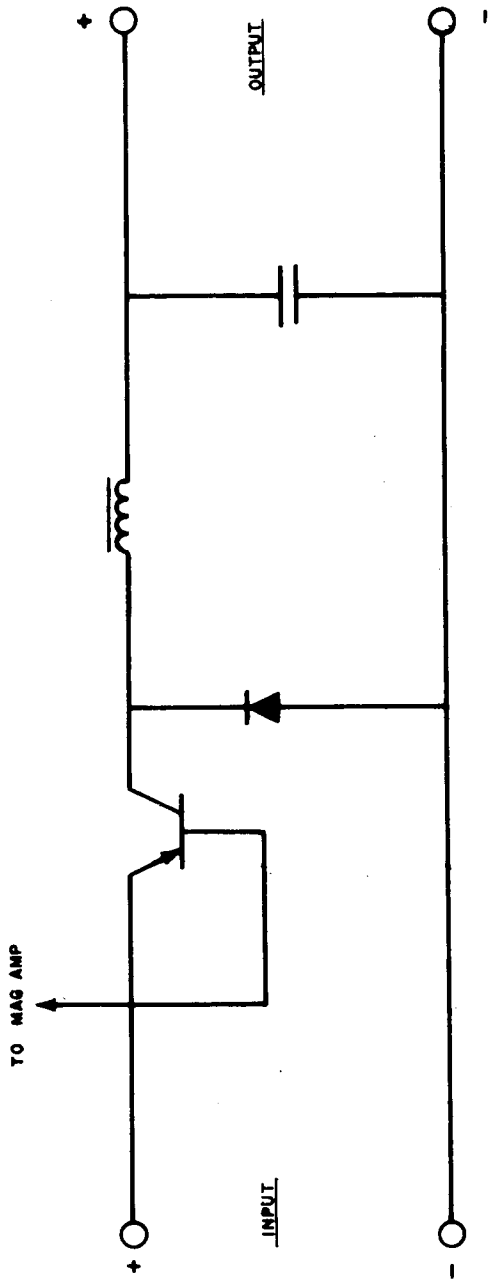
Figure 95 PULSE WIDTH REGULATOR SWITCHING SCHEME

63-8433

-231-

comparison element will sense this increase. This increase in output voltage will be compared to the stable reference voltage, and result in an error signal. The error signal is fed back to the control winding on the magnetic amplifier, which reduces the time duration of the gate winding pulse output. Base drive to the switching transistor is shorter in time duration, giving a shorter on time. The filtered output of pulses from the switching transistor will result in a lower average regulated and corrected output voltage.

Current protection can be easily accommodated by adding a current sense circuit in series with the output. A second comparison element will compare the sensed current, which is translated into a proportional voltage, with the reference voltage. This difference voltage or error signal is fed into a second control winding on the magnetic amplifier, which will control the time duration of the high frequency pulse output from the magnetic amplifier as previously described.

The pulse width or switching type regulator provides good regulation and temperature stability. Power dissipation is low and the regulator exhibits better reliability and high power capacity than conventional series type regulator circuits. Low losses eliminate the need for large heat sinks and the full current capability of the switching transistor can be utilized.

2. <u>Converter regulator</u>. The converter regulator is a phase control device which converts dc to dc with maximum efficiency. The input power drives a master oscillator and, through a variable phase shift network, a slave oscillator. The two oscillators generate square waves which are summed up to produce a quasi-square wave. The average value is inversely proportional to the phase delay. By sampling the average output voltage and comparing it to a fixed reference, an error signal is generated to control the phase delay. If the output tends to rise, the error signal increases and causes the phase delay to increase and cancel the rise. Since the output is a quasi-square wave in the primary of the output transformer, the secondary may contain as many windings as required output voltages in unlimited values. Each output is rectified and filtered for dc or ac.

a. <u>Phase control voltage regulation.</u> Phase control voltage regulation, a form of nondissipative pulse width regulation, is a highly efficient method used for regulating the outputs of dc-dc converters and dc-ac static inverters.

The basic elements of a typical phase control voltage regulator circuit include two static inverters (a master oscillator and a slave oscillator), a phase shift network (magnetic amplifier), a voltage sense circuit, and a voltage reference circuit. Short circuit protection may be added by adding a current sense circuit and a current reference circuit. Figure 96 is a block diagram of a basic phase control voltage regulator circuit with short circuit protection added.
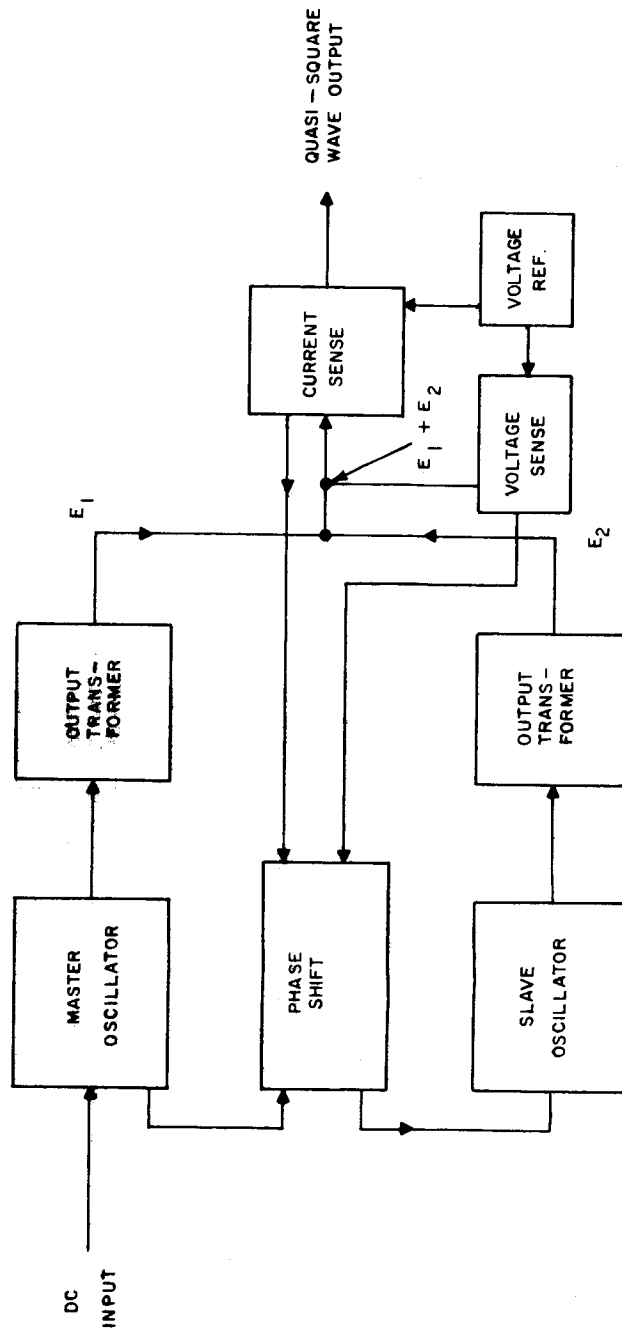
Figure 96 PHASE CONTROL REGULATOR BLOCK DIAGRAM

63-8430

-233-

The phase control method of voltage regulation operates on the principle of output regulation by control of the phase relationship between equal outputs of two static inverters. This is done by controlling the delay of a synchronizing signal from inverter 1 (master oscillator) to inverter 2 (slave oscillator). The delay, or firing angle of magnetic amplifier, is controlled by the time required to resaturate the magnetic amplifier and varies according to control winding current (figure 97). Control winding current is determined by variations in output voltage and varies accordingly.

For example, when the input voltage rises, the output voltage also rises. The increase in output voltage is sensed by the voltage sense circuit and compared with a stable zener reference circuit. The difference is then fed back to the voltage regulation control winding of the magnetic amplifier, which in turn causes an increase in control winding current. The increase in control winding current causes a corresponding increase in the magnetic amplifier firing angle and increases the delay of the sync signal from inverter 1 to inverter 2. The phase relationship between the outputs of inverter 1 and inverter 2 increases and causes a corresponding decrease in total output to correct for the rise in input voltage. Figure 98 illustrates the effect on total output by varying the phase relationship between the outputs of inverter 1 and inverter 2. Note that the output voltage is a quasi-square wave.

Short circuit protection, like voltage regulation, is accomplished by controlling the phase relationship between the outputs of inverter 1 and inverter 2. When a short appears across the output, the load current increases beyond a predetermined limit. This increase is sensed by a current sense transformer and induces a voltage in its secondary also beyond a predetermined limit. This voltage is compared with an established reference and the difference is fed back to a second control winding in the magnetic amplifier. The increase in control winding current caused by the difference voltage is such that it results in a maximum delay between the sync signal from inverter 1 to inverter 2. This maximum delay results in maximum phase shift between the outputs of inverter 1 and inverter 2 and the total output drops to zero (figure 98).

4.7 System Weight

As established in section 4.4, 112 pounds of nickel cadmium batteries are needed to accommodate the energy requirements of the spacecraft. To achieve the necessary power system reliability, a minimum of 55 percent redundancy shall be required which corresponds to 176 pounds of batteries. The 200 square foot solar panel weighs 243 pounds and the power conditioning equipment weight amounts to 42 pounds.

Therefore, the power system weights is
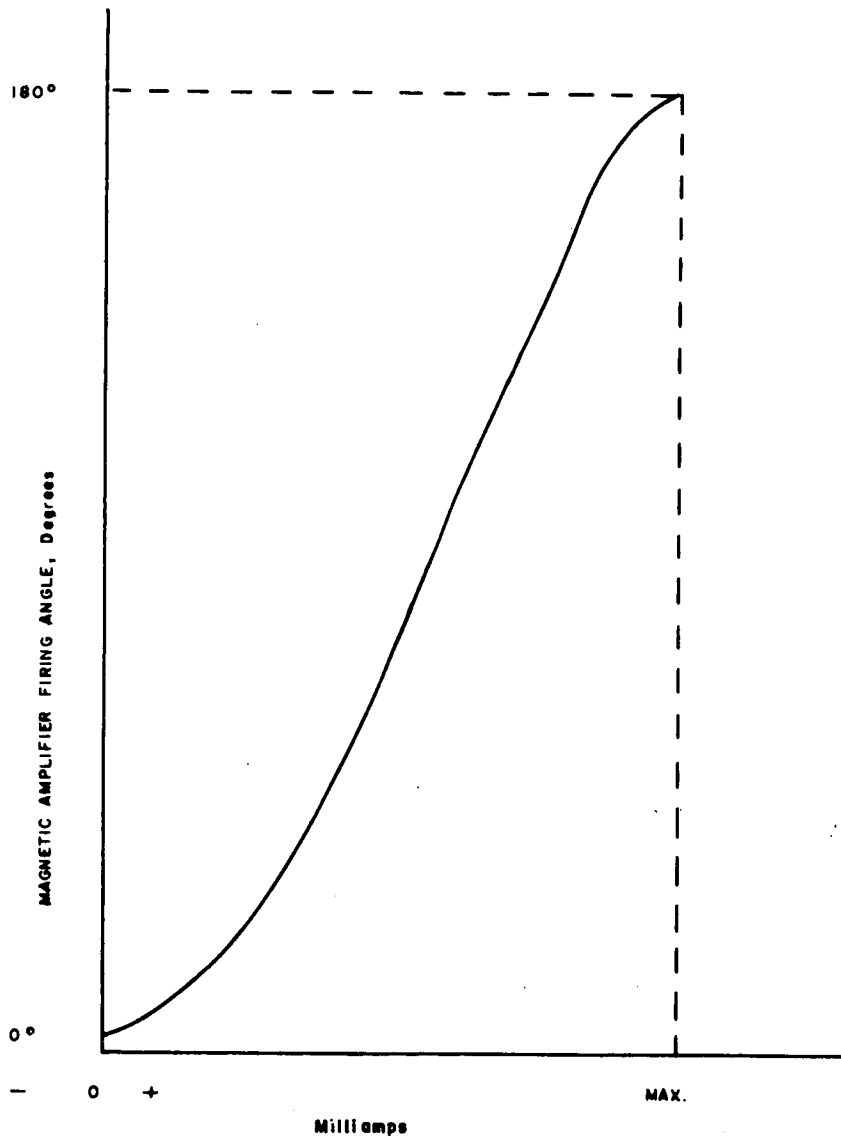
Figure 97 MAGNETIC AMPLIFIER CONTROL CHARACTERISTIC

63-8431

-235-

A. IN PHASE   B. 100° OUT OF PHASE   C. 180° OUT OF PHASE

MASTER
OSCILLATOR
OUTPUT

E_1

SLAVE
OSCILLATOR
OUTPUT

E_2

TOTAL
OUTPUT
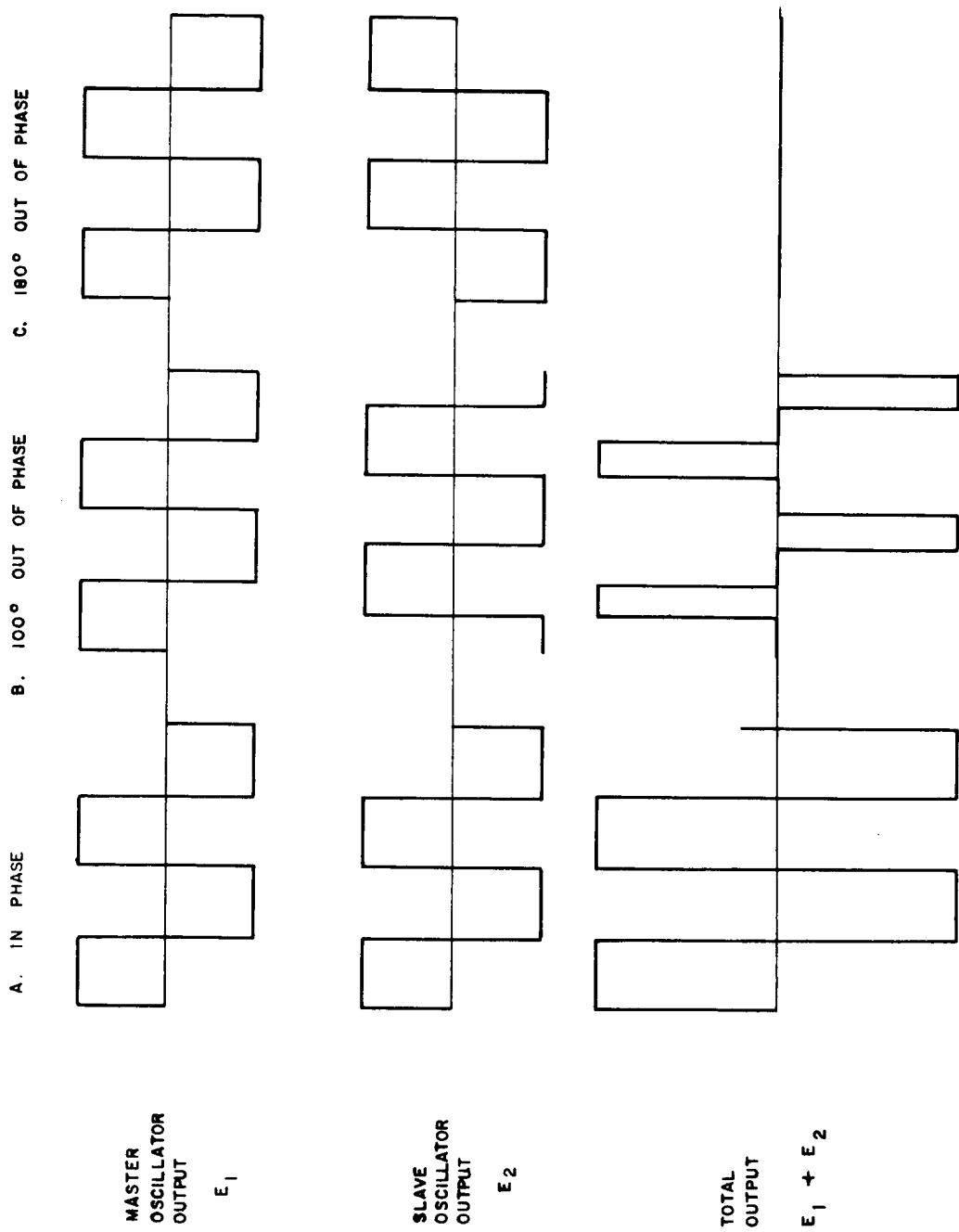
$E_1 + E_2$

Figure 98 PHASE CONTROL REGULATOR PHASE RELATIONSHIPS

63-8432

-236-

Batteries   176 pounds

Solar Panel   243 pounds

Power Conditioning   42 pounds
                         461 pounds

4.8 Power Supply Improvements

Certain advances in technology are to be anticipated and, while the concepts previously discussed are not based on incorporating anticipated improvements, it is pertinent to mention such possible improvements and to evaluate the possible gains. Avco would make use of the latest state of the art at the time the hardware design is undertaken, if at that time there is sufficient data to justify the incorporation. Among the improvements which can reasonably be expected are the following.

1. Lightweight solar cells. It seems reasonable to anticipate cells of lighter weight, and the cell plus installation and wiring weights will be on the order of 0.4 pound per square foot, as compared with 0.5 pound per square foot used for this study. For 200 square feet of solar panel area, this would amount to a saving of 20 pounds in cell weight. This reduction in weight would also be reflected in the panel structural weight; and for the configuration under study, it might be expected to reduce the panel substrate by 20 to 25 pounds. Considering cells plus structure, the total weight reduction could be in the range of 40 to 45 pounds.

2. Larger cells. Progress is being made in the manufacture of 2 x 2 cm cells and these larger cells represent certain cost advantages over the 1 x 2 cells considered in this study. Installation costs may be reduced in proportion to the number of cells used and in view of the many steps required to install cells, such as inspection, testing, grading, matching, soldering and bonding, the savings may be appreciable.

3. Concentrator type panel. The use of concentrators in combination with solar cells has been under study for some time. While the basic study presented in this report has been concerned with a nonconcentrating system, (because such a system does not require an advance in the state of the art), the use of concentrators may be expected in the near future and appears to offer a means of reducing overall solar panel costs. The schematic for two such concentrating systems is shown in figure 99.

5. Energy storage. Although nickel cadmium batteries were selected for the energy storage device, this gives by no means a light weight system. Nickel cadmium was selected almost wholly on the grounds that it has accummulated a

REFLECTED PORTION OF SUN'S ENERGY
(DIRECT RAYS NOT SHOWN)

REFLECTORS

CONCENTRATOR ARRAY

CELLS

SAWTOOTH ARRAY
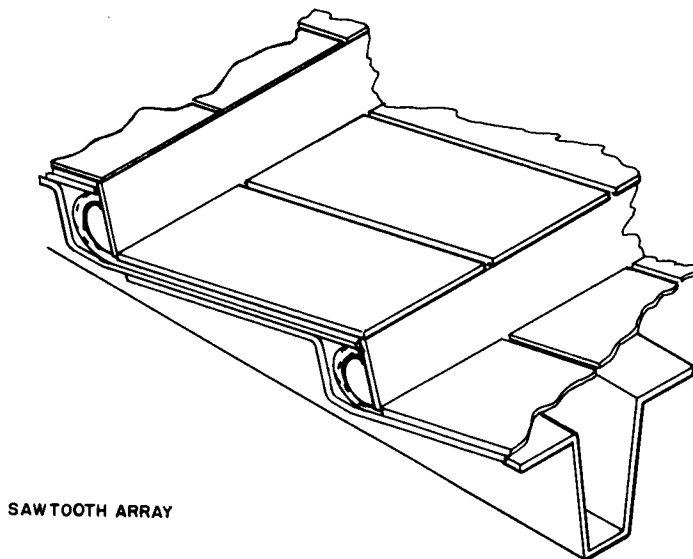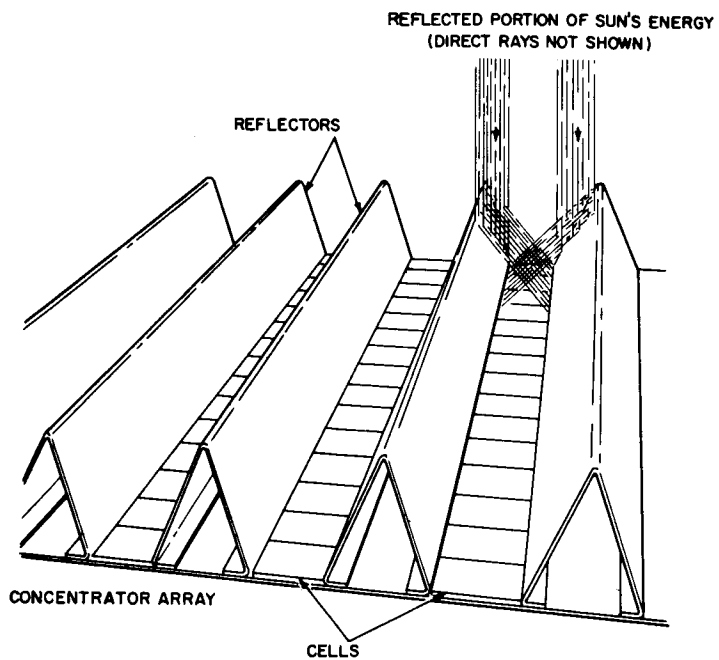
63-8438

Figure 99 CONCENTRATOR PANEL TYPES

-238-

great number of operating hours in the space environment.

Development of the higher energy density silver cadmium is proceeding at a rapid pace and the present limitations of the system, due largly to gassing and insufficient operating data, might be removed in the near future.

Regenerative hydrogen-oxygen fuel cells appear to offer the ultimate in light-weight energy storage but acceptable flight models are unlikely to be available before the second Mars shot. The weight advantage when available would amount to between 72 and 84 pounds. This is based on an anticipated usable energy density of 20 watt-hours per pound.

4.1 Power Source Selection

The power system for the Venus orbit-bus case shall be almost identical to that discussed for Mars. The following sections shall be confined to a discussion of significant differences. If all objections made against the RTG for the Mars case (Section 4.1) could be removed, a further objection becomes prominent when the RTG is considered for Venus, namely the RTG weighs somewhat more, 200 pounds versus 156 for the solar array - battery combination.

4.2 Constraints and configuration

The basic limitation to solar cell performance at Venus is the high cell temperature of 220°F. Since,as will be shown in the following paragraphs, 11.5 watts per square foot may be obtained, a solar panel area of approximately 70 square feet is needed. The configuration will be similar to the Mars orbiter with the exception that the smaller disc will be eliminated and the 138 square foot area available on the larger disc will not be fully utilized. The structure, however, will be present for mounting various equipment and it represents a capability for mounting additional solar cells if required. Flat mounted cells will be used and the array configuration is of the conventional flat type.

1. <u>Cell design.</u> Every effort shall be made to reduce cell temperature. Microsheet glass covers therefore are definitely required N on P, 1 x 2 cm silicon cells will be selected although N on P is no longer a great advantage because measurements indicate the lack of radiation belts about Venus.

4.3 Emissivity considerations

At thermal equilibrium, the ideal solar cell would be designed so as to absorb energy at (0.4 u - 1.1 u) and emit energy at all others. The emissivity of the front surface of a solar cell may be enhanced greatly by means of a coating which is transparent in the active region of the spectral response of the cell and opaque with a high emittance in the infra-red. A number of techniques are available for accomplishing this, such as thin film of silicon monoxide, various types of glass covers and organic coatings. None of these methods offer 100 percent transmittance and therefore all reduce cell efficiency. Hence, some tradeoff must be made between emissivity and power output. The results of this trade off can be seen in table 22 which provides a comparison of the relative performance of each of the several coverings. The last covering in the table , 6 mil glass covering together with a .415 u blue filter, a 1.15 u red filter and a reflection band filter result in the highest percent power gain (11.2 percent) over the bare uncovered cell.

TABLE 22

COMPARISON OF RELATIVE EFFECTIVENESS
OF CELL COVERINGS

Cell & Modifications	α	ϵ	α/ϵ	T°C	%Power of Power at 28°C	%Power Gain from bare cell
Ideal Cell	0.70	1.00	0.70	28	100	-
Bare Cell	0.935	0.368	2.54	85	77	-
Cell with 1.11 Sio Coating	0.874	0.642	1.36	63	86	4.3
Cell with 0.006" glass and A-R Coating	0.813	0.835	0.974	46	92	15.8
Cell with 0.006" glass, 415 m blue & A-R Coatings	0.81	0.835	0.97	46	92	8.5
Cell with 0.006" glass, 415 m blue, 1.15 red and A-R Coatings	0.70	0.835	0.84	35	96	11.2

The 0.415 uv interference film serves to prevent degradation due to ultraviolet damage of the epoxy adhesive used to cement the glass in place. The film has a sharp cutoff between 0.40 and 0.45 u with an optimum near 0.415 for blue shifted cells. With 6 mil glass and the A-R coatings (anti-reflective) this filter will produce an increase in efficiency of 8.5 percent over that of the bare cell but a reduction in efficiency of 7.3 percent over that obtained with the glass and A-R coatings. However, this loss must be tolerated in order to improve the long term reliability. The 1.15 u red filter rejects about 50 percent of all solar energy at wavelengths longer than 1.15 u thus maintaining lower temperature by reflecting a great portion of the non-useful part of the spectrum.

It is this combination of a 6 mil glass, A-R coatings, UV and I.R. film filters which will be used on the solar cells for the Venus orbiter.

Available Power. - At .732 A.U. both increasing temperature and increasing solar radiation play important roles in the performance of a solar cell. The incident energy varies inversely as the square of the distance from the sun and is :

$$\frac{1400}{R^2} \quad \text{watts per square meter}$$

where R is the distance to the sun in astronomical units.

The absolute temperature of a solar panel will vary inversely as the square root of the distance from the sun, i.e.,

$$T = \frac{T_1}{\sqrt{R}}$$

where T is the temperature of the panel at R astronomical units and T_1 is the temperature at one astronomical unit. The value of T_1 is not to be taken as that for an Earth satellite panel; in the latter case the temperature is somewhat higher due to Earth radiation and albedo and depends on orbit parameters.

The power output of a solar panel as a function of temperature can be approximated by the linear relation.

$$P = P_{28} \{1 - [0.005 (T - 301)]\} .$$

where P_{28} is the power output at 28°C, and T is the absolute temperature in degrees Kelvin. The above relation certainly is not valid above 228°C (501°K) since then the power output would be negative but is usable up to about 150°C.

When the foregoing relations are combined, an expression is obtained for the power output of a solar panel as a function of distance from the sun as follows:

$$P = \frac{P_1}{R^2} \left[2.515 - \frac{0.005\, T_1}{\sqrt{R}} \right] \text{ watts}$$

where

P_1 is the power output of the panel at one A. U

T_1 is the panel temperature in degrees Kelvin at one A. U.

R is the distance to the sun in A. U.

At one A. U. from the sun (but away from the Earth), a well designed solar panel will produce about 9 watts per square foot at a temperature of 34 to 40°C. Using the latter value in the above equation,

$$P = \frac{9}{R^2} \left[2.515 - \frac{1.565}{\sqrt{R}} \right] \text{ watts per square foot}$$

At the distance of Venus from the sun, 0.723 A. U., the expected power output is 11.7 watts per square foot with a panel temperature of about 94°C. In the vicinity of Venus, due to albedo and heat radiation, the power output would be less because of the slightly higher temperature, calculated to be almost 110°C. Consequently the corrected power output per square foot shall be 11.5 watts/ft². This method corroborates the result obtained if the relationship in section 4.4 of the Mars orbiter is used.

4. 4 System Description

The load profile shown in figure 100 was prepared from the list of power consuming equipment shown in table 23 and from knowledge of their operating periods during orbit.
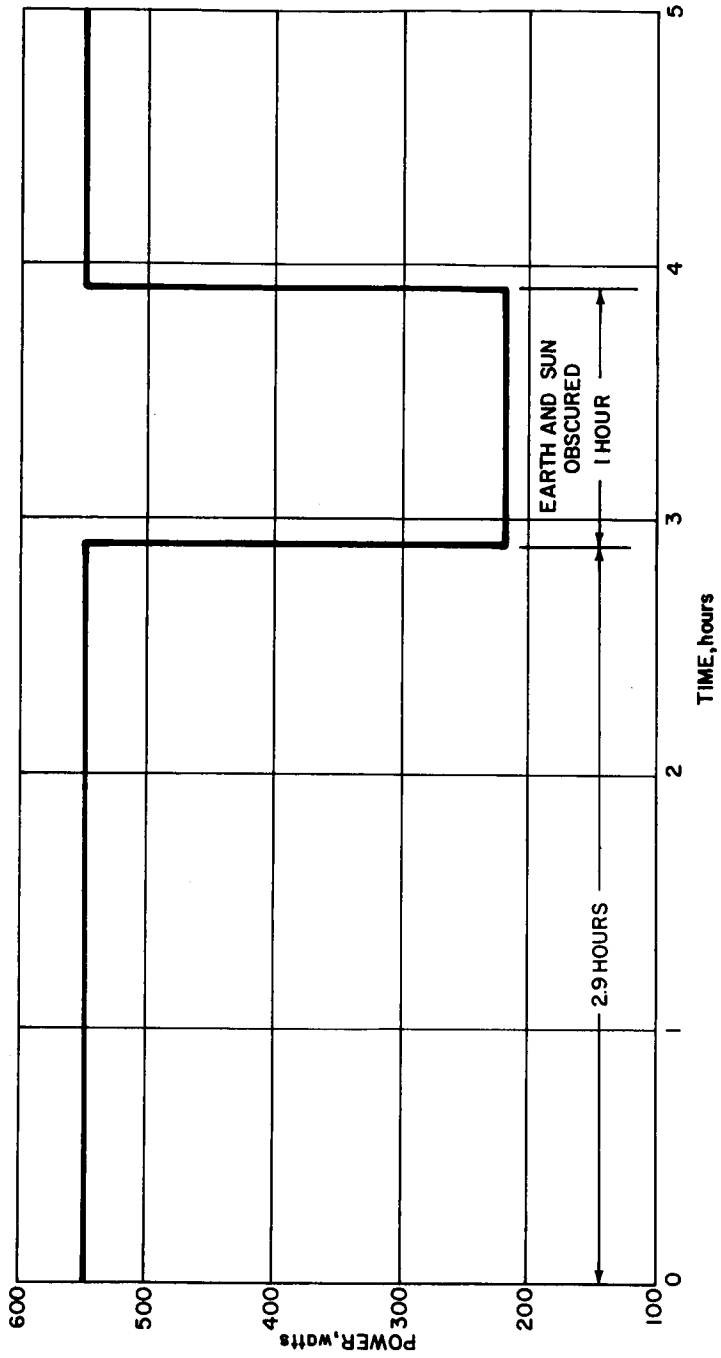
Figure 100 LOAD PROFILE FOR VENUS ORBITER

-244-

TABLE 23

VENUS ORBITER/BUS POWER REQUIREMENTS

Major Subsystem	Power (W) Consumed	Use
70W S-Band P.A. (with special P.S.)	140	Sun
35W S-Band P.A. (with special P.S.)	70	Transit
S-Band Transponder	20	S
S-Band Command Receiver	14	S&Umbra
Command Decoder	6	S&U
Multiplexer-Encoder	3	S
Subcarrier Modulator P.N. Generators	3	S&U
VHF Receiver	3	S
VHF Transmitter	10	S
Guidance & Control	162	S&U
Venus Radar Antenna System	150	S
Venus Recorder No. 1	6	S
Venus Recorder No. 2	6	S&U
Science	28	S&u

The spacecraft shall be in sun shadow for 1 hour, during which 220 watts must be provided by the battery. For the same reason as discussed in the Mars case, nickel cadmium was selected as the energy storage material.

The battery size needed to provide this requirement is :

a.   Load Watt Hours $= \dfrac{220}{.85} = 260$ wh

where .85 is the convertor regulator efficiency

b. Battery Weight $= \dfrac{260 \text{ wh}}{\left(\dfrac{14 \text{ wh}}{\text{lb}}\right)(.5)(.635)} = 58.5 \text{ lbs.}$

where .5 is the depth of discharge

.635 is the capacity factor

The solar panel size needed to supply the load during sunlight and to accomodate battery recharge is:

$(.85 \text{ P}_s - 551)\, 2.5 = \dfrac{260 \text{ wh}}{.8}$

where .8 is the battery storage efficiency

.85 is the converter regulator efficiency

551 is the load requirement in watts

2.5 hours is the time that the solar panels are charging the batteries

$\text{P}_s = \dfrac{662}{.85} = 780 \text{ watts}$

$\text{Area} = \dfrac{700 \text{ watts}}{11.5 \text{ watts/ft}^2} = 68 \text{ ft}^2$

$\text{Panel Weight} = (68 \text{ ft}^2)\, 1.2 \left(\dfrac{\text{lbs}}{\text{ft}^2}\right) = 81.5 \text{ lbs.}$

Power system weight. Total power system weight is established by providing a 50% redundancy for the batteries.

Batteries	88 lbs (includes 50% redundancy)
Solar Panel	81 lbs
Power Conditioning	25 lbs
	194 lbs.

5. GUIDANCE

5.1 Introduction

Studies performed on those aspects of the Voyager mission which would affect the guidance system characteristics required for the orbiter-bus vehicle are reported in this section. The limited duration of the studies permitted selection of feasible, though not necessarily optimal system configurations. The on board guidance system selected will perform the terminal guidance functions only. The assumptions have been made that the boost guidance will be handled by a system in the booster and that midcourse guidance will be handled by DSIF in the manner of the Mariner missions. The only exception to this ground rule is that the digital computer of the guidance system will be used occasionally during some control modes and for sequencing when no guidance operations are going on. The functions performed by the guidance systems can best be described in terms of the following mission phases.

1. <u>Sun-Canopus acquisition and vehicle orientation</u>. Following completion of earth launch and injection into a heliocentric transfer orbit for Mars, the Voyager vehicle will be separated from the booster. At this time the SCS is required to orient the vehicle from a random position to a Sun-Canopus reference frame. A signal will activate the guidance computer which will command pitch and yaw maneuver via the gyros till the SCS Sun sensors have acquired the Sun. The computer will then command roll maneuvers until Canopus is acquired. The SCS then holds this attitude and the guidance computer is turned off during the cruise period.

2. <u>Midcourse trajectory correction</u>. Start of the midcourse correction to the vehicle orbit will be by a command signal from the DSIF. The computer will then command a sequence of events. First, the gyro and accelerometer heaters will be turned on. After stabilization of the inertial components has been effected, the gyros will be put into a pulse rebalance mode. Then the SCS maintains attitude control of the vehicle while the computer accumulates gyro pulse outputs to determine the gyro drift rates. At completion of drift trim, the gyros will be put into the control mode and the attitude control of the vehicle transferred to them. The computer will command gyro torque rates which will both minimize drift and orient the vehicle to the proper attitude for thrusting. At a time predetermined by DSIF, the computer will command thrust on and will monitor the accumulating ΔV from the accelerometer aligned along the thrust axis. When the DSIF prescribed ΔV has been acquired, the computer will send a thrust cutoff signal. At this point the computer will signal the SCS to reacquire the Sun and Canopus. At completion, the computer will turn off and the SCS will hold the cruise mode attitude. This procedure will be repeated for all midcourse trajectory corrections.

3. **Orientation for lander separation.** The functions required here are similar to those during midcourse correction. The sequence of events will be: activation, gyro drift trim, orientation for lander separation, attitude hold for the separation perturbation, and reorientation to the Sun Canopus reference attitude.

4. **Orbiter slowdown.** The sequence of events for this operation will be: orientation for the slowdown attitude prescribed by DSIF, command, monitor and terminate the thrust required for the slowdown maneuver, and reorient for Sun and Canopus acquisition.

5. **Approach navigation and trajectory correction.** During approach navigation, the vehicle will remain oriented with respect to the Sun and Canopus. The auxiliary star tracker and planet tracker are turned on and pointed to acquire the desired star and Mars. Using two star-planet angles and the planet range, the computer will update the approach trajectory information. In addition the spacecraft will telemeter the optical readings to Earth to supplement DSIF data for ground-based computations of the trajectory. If an orbit correction is required the procedure described under the midcourse correction phase will be initiated. After completion, the cruise attitude will be resumed until orientation for orbit injection.

6. **Injection into orbit about Mars.** The sequence of orbit injection guidance begins with reorientation of the vehicle for retro-thrusting. This will be a programmed maneuver; at a predetermined time, the computer will command thrust-on and send the SCS, the pitch and yaw attitudes to be effected during the thrust period. At completion of the maneuver, the SCS will return the vehicle to the Sun-Canopus reference attitude and the computer will start the in-orbit navigation phase.

7. **In-orbit navigation about Mars.** The in-orbit navigation operations are similar to those for the approach navigation. The auxiliary star tracker and horizon scanner are turned on and pointed for acquisition by computer command. Two star-to-planet angles are then measured during a couple of orbits to permit updating the navigation information. If an orbit correction is required it will be made as the approach and/or midcourse corrections. The vehicle is then turned back to the SCS for Sun-Canopus orientation during cruise till another navigation operation and orbit modification is required.

5.2 Guidance System

1. **System requirements.** The Voyager mission to Mars or Venus can be considered as having three major guidance phases: (1) escape from Earth; (2) heliocentric transfer; and (3) terminal maneuvers in the vicinity of the destination planet. Guidance during the first two phases will probably be similar to

that of Mariner II (i.e., DSIF). Maneuvers, however, in the vicinity of the planet may impose accuracy and response requirements upon DSIF which can not be satisfied. It remains then to evaluate the functions and performance required of the guidance system during the terminal part of the flight and to determine the additional instrumentation necessary or desirable to perform these functions. To determine these requirements, the terminal guidance phases required to achieve the objectives of the Voyager mission must be considered. For a typical mission to Mars, the spacecraft will consist of a lander which impacts Mars and an Orbiter which enteres a bound orbit about Mars. A possible sequence of guidance phases and guidance functions associated with the orbiter-bus spacecraft will be:

a.	Approach Navigation	Measurements and computations to determine the state of the orbiter-bus relative to Mars at a range of approximately 1,000,000 to 2,000,000 kilometers from the planet
b.	Approach Steering	Computations to determine the direction and magnitude of the velocity correction which would put the lander, after separation, on its impact trajectory to Mars. Computations of the direction and magnitude of the velocity required to slow down the orbiter.
c.	Approach Maneuver	After orientation of the orbiter to its thrusting attitude for the slowdown maneuver, the sensing of the correction velocity increment to command cutoff is required.
d.	Terminal Navigation	Measurements and calculations to update knowledge of the state of the orbiter.
e.	Terminal Steering Computations	Computations to modify the trajectory of orbiter if it is not headed toward the desired periapsis condition.
f.	Terminal Maneuver	Sensing of the correction velocity increment after orientation of orbiter to desired thrusting attitude.
g.	Orbit Injection Navigation	Orbiter state determination prior to orbit injection maneuver.

h.	Orbit Injection Steering	Computations to provide the proper thrust vector program for orbit injection.
i.	Orbit Injection Maneuver	Thrust vector commands, and execution of cutoff when proper injection velocity is reached.
j.	In-Orbit Navigation	Measurements and computations to determine planetary orbit of orbiter vehicle.
k.	In-Orbit Steering Calculations	Computation of velocity increment required to modify orbit if it is not within satisfactory bounds.
l.	In-Orbit Maneuver	Orientation to thrusting attitude and sensing of the velocity increment for in-orbit maneuver.

The guidance equipment required for these operations can have two extremely different configurations. The satisfactory performance of DSIF for Mariner II and the predicted tracking accuracies of DSIF make it desirable to consider a system as close as possible to DSIF for one extreme. The possibility of DSIF limitations coupled with the desirability of onboard measurements for primary, supplementary, or backup navigation, make it necessary to consider an essentially self-contained optical-inertial guidance system as the other extreme. The following sections describe and discuss the analysis performed and systems selected to satisfy the aforementioned requirements.

2. System performance and analysis.

a. Approach guidance. The initial approach guidance maneuver will be made at a distance between 500,000 and 2,000,000 kilometers from Mars. At these ranges, the predicted DSIF navigation accuracy is probably better than can be obtained using optical instruments. It is assumed, therefore, that the DSIF will be used for navigation and steering operations for the first approach guidance maneuver.

This maneuver consists of: (1) separating the lander from the orbiter-bus; (2) altering the lander trajectory to impact Mars; and (3) slowing down the orbiter to achieve the desired time of arrival separation with the lander, and arrive at a periapsis of 1700 km. The lander maneuver will be so precalculated and programmed that no guidance equipment will be required. When the proper range from Mars is reached, DSIF will send a command to the orbiter-bus to orient to the proper attitude for lander thrusting. The lander will then be separated from the orbiter-bus and spun up for stabilization. The orbiter slowdown maneuver will occur subsequent to lander separation. The proper vehicle attitude for retrothrust, and the magnitude of the ΔV to be obtained (a conventional

approach trajectory correction can also be included in this maneuver) will be
sent to the computer by DSIF. Since thrust direction will be essentially along
the flight path of the vehicle, it was anticipated that the errors in its application
might seriously affect the accuracy near periapsis passage of orbiter which in
turn seriously affect the injection accuracy and fuel requirements of the Mars
orbit injection maneuver. Consequently, an error analysis was performed to
determine the effect of the retrothrust maneuver errors and effect of the inac-
curacies in initial position and velocity as determined by the DSIF.

The description of the analysis is given in appendix B. The result of this
analysis indicates that the effect of the DSIF approach navigation inaccuracy
of 150 kilometers (1σ) in position was the dominant factor and the presumed
errors introduced by the retrothrust maneuver were negligible. (This factor
was one of several which influenced the selection of the "Orbiter slow-down"
technique for the attainment of the desired spatial-time-relationship between
lander and orbiter.)

b. Terminal guidance. Subsequent to the slowdown maneuver, ter-
minal guidance is "initiated" and continues to orbit injection. The range which
this guidance function covers will be from 500,000 km to approximately 10,000
km from the planet. Appendix C presents an analysis of the capability of DSIF
(doppler configuration) for providing the terminal guidance trajectory determi-
nation necessary for orbit injection. Detailed analysis was necessarily restric-
ted to a 1969 Mars Type II trajectory. It was found that the employment of only
DSIF information for terminal navigation and a minimum equipment system
which controls thrust using 3 gyros and 1 accelerometer would permit attain-
ment of an orbit around the planet with a 1σ uncertainty in periapsis altitude of
about 400 km and 1σ uncertainty in semi-major axis of about 1,700 km. The
other orbital parameter errors were so small as to be unimportant. Use of
3 gyros and 3 accelerometer control improves these uncertainties to approxi-
mately 200 and 1000 km, respectively. This performance was considered mar-
ginal and augmentation with on board optical instruments was felt desirable.
Table I of appendix C tabulates the relative effectiveness of DSIF doppler,
planet diameter measurements, and planet-star angle measurements in per-
forming trajectory measurements. Qualitative evaluation of the improvement
in performance that can be achieved indicates that either a planet angular dia-
meter measurement of a planet-star angle measurement using a star well out of
of the ecliptic will enhance DSIF performance. In parallel with the DSIF analy-
sis of appendix C, an analysis of a completely self contained system for termin-
al guidance was undertaken; results are reported in appendix D. Sufficient
results were obtained to permit intelligent assessment of the potential perform-
ance, problem areas, and hardware requirements.

c. Orbit injection. A variational program more fully described in
appendix E was developed to analyze orbit injection. A range of thrust levels
(constant) from 1,000 to 8,000 pounds was investigated for spacecraft weights

at orbit injection in the region 3,000 to 6,000 pounds. The optimum thrust orientation histories to minimize fuel requirements were determined for various planetary approach conditions. Two particularly interesting results were obtained with this program. It was determined that the gravity loss associated with finite burn times is effectively nil;i.e.,the attainable orbital payload is essentially independent of thrust level for the conditions evaluated. It was also determined that the thrust orientation time history for optimum injection is a reasonably linear function of time. This latter fact suggested the possibility of programmed orbit injection as described in appendix F. As presently envisioned a pitch attitude time history program of the form:

$$\theta = \theta_o + kt$$

where

θ = inertial orientation

k = constant

t = time

would be stored on the spacecraft. Values of θ_o, k, and t would be computed on Earth and telemetered to the spacecraft or computed on the spacecraft. Upon command from DSIF the injection process would be initiated. Spacecraft operation from thrust initiation to thrust termination would be independent of DSIF. An error analysis of the technique (appendix F) indicates that its performance is excellent and that the major errors in the resultant planetary orbit stem not from the orbit injection process but from state uncertainties at initiation of orbit injection.

Consideration was also given to the possibility of incorporating the terminal guidance maneuvers into the orbit injection phase. The primary purpose for this would be the elimination of at least one, and possibly more, engine restarts. Intuitively this approach should enhance reliability at the expense of decreased payload or increased orbital altitude. It was determined that the cost is moderate; approximately one foot per second will offset a one kilometer initial periapsis error when injecting into a 1500 x 10,000 km orbit.

The major difference in guidance requirements between orbiter slow down and orbit injection will be the necessity for the spacecraft to store a simple equation, and to command and monitor a continually changing vehicle attitude during thrust. The necessary instrumentation is in all other respects identical to that of orbiter slow down. A more complicated technique to perform orbit injection is presented in appendix K however, the simplicity of this open loop scheme coupled with its performance suggest its use as the reference method.

TABLE 24

GUIDANCE SYSTEM COMPONENT CHARACTERISTICS

	Weight (pounds)	Volume (in.^{3})	Power (watts)
1. Auxiliary star tracker	9	450	10.8
2. Planet tracker	35	3700	50
3. Planet horizon-scanner	12	600 (est.)	9
4. Three GG177 accelerometers and electronics	6	180	10*
5. Digital computer, input/output and power supply	49	1620	110
	111	6550	

* Accelerometer heater power is a maximum of 60 watts for a period not exceeding 20 minutes. Nominally it is approximately 12 watts.

   a. Computer

   1) Logical organization. The Honeywell Subminiature Computer has been designed for advanced aerospace applications. It is compact, light-weight, and has a memory capacity of 8,192 twenty-four-bit data words, or a maximum of 12,288 sixteen-bit instructions. Its solid-state biax memory provides random access in neither of 4,096 twenty-four-bit word banks, and features non-destructive readout. The 8,192 memory words are divided into two categories: 1,024 twenty-four-bit words capable of being altered under program control, ("hot" data) or scratch pad, and 7,163 twenty-four-bit words capable of being altered only by AGE and external control ("cold" data). Prominent features of the computer are:

      a) High computational rate with a minimum component count and power requirement

      b) Ability to store 8,192 twenty-four-bit words

      c) Biax ferrite memory elements for repeated addressing without loss or destruction of the stored information

      d) Logic and memory circuitry reliable over a temperature range of -55°C to 125°C

      e) Basic programming in microseconds; multiply time 242 microseconds

d. <u>Orbit determination</u>. Subsequent to orbit injection it is necessary to determine the planetocentric orbit attained by the spacecraft. If injection performance has been nominal, the spacecraft orbit will be known to first order as suggested earlier. JPL analysis (refs. 21 and 22), indicates that the DSIF capability to perform precise orbit determination probably transcends that of a self-contained system both in terms of accuracy and reliability. Spacecraft orbital positional information to tenths of a kilometer within a day or two after orbit attainment is the reported performance of DSIF in the aforementioned references. Therefore, strong justification for a self-contained orbit determination capability does not seem to exist. In spite of this, an analysis of the performance of an onboard optical system was performed - (appendix G). Performance is approximately comparable to that of DSIF.

The technique presented should be considered a typical possibility and is not suggested as optimum. Other possibilities are under consideration but contractual time limitations do not permit their presentation.

e. <u>Summary</u>. From the results of these preliminary studies, a reference guidance system consisting of DSIF augmented with optical sightings seems the preferred scheme to ensure modest accuracy with high reliability. A complete self-contained optical-inertial system, however, is recommended. In early flights, its role, although subordinate to DSIF, would provide an element of system redundancy. As experience with automated systems of this nature accumulates, it is anticipated that performance will grow correspondingly permitting such systems to be applied with confidence in applications for which DSIF may not be suited or available.

3. <u>System description</u>. The guidance system consists of a computer, auxiliary star tracker, planet tracker, planet horizon scanner, and an accelerometer package. A tabulation of the weight, volume, and power requirements of the components is given in table 24. Figure 101 is a simplified block diagram showing the interface between the guidance system components and the interfaces with the Canopus tracker and the rest of the stability and control system.
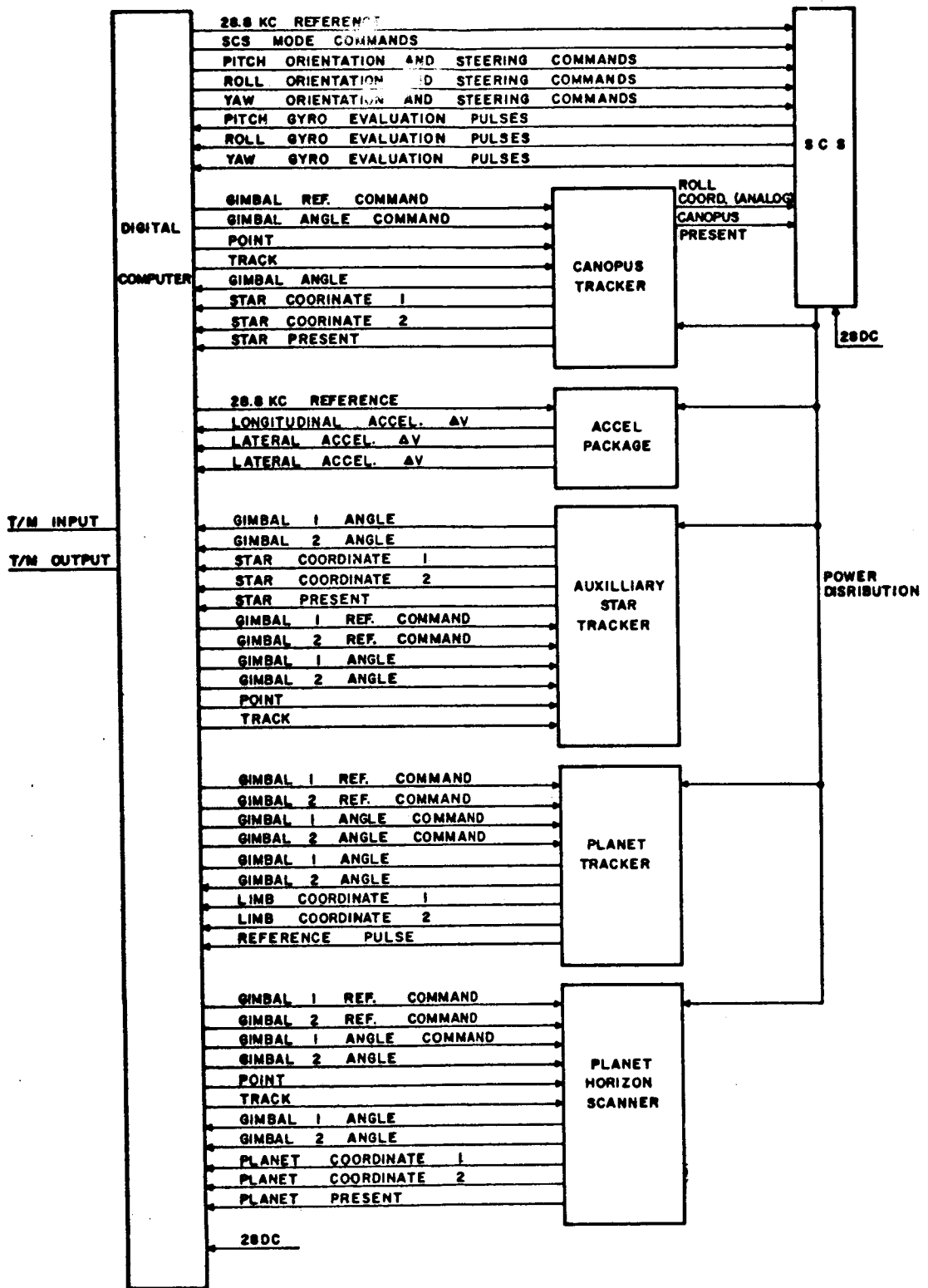
Figure 101 VOYAGER GUIDANCE SYSTEM BLOCK DIAGRAM

The computer is designed to produce a high computational rate with minimum power. This is done by incorporating several design features:

    a) A nondestructive readout magnetic core memory (biax core) is used for commands and data words

    b) Random access addressing is used for maximum programming efficiency

    c) Arithmetic operations are performed in a parallel-serial type system to obtain optimum efficiency

    d) Noise injected into the logic circuits is clamped to ground during nonclock time and is integrated during clock time. This feature greatly reduces the possibility of noise erroneously triggering the memory flip-flops

    e) A moderate clock rate (500 kc) lowers the power requirement for the logic circuitry

    f) All components operate at very low stress levels and all circuits have been engineered to ensure ample operating margins under combined "worst-case" conditions.

The computer uses a random address mode of operation with a nondestructive core memory. Arithmetic operations are performed six bits in parallel with four groups of six in serial. This combination produces a 24-bit binary word. Negative members are represented and stored in two's complement. In addition to its central memory, the computer contains two data registers (a 24-bit accumulator and a 6-bit multiplier-quotient register), memory selection registers, input-output buffer registers, an instruction register and a bit-time register.

    2) <u>Input and output processing.</u>

    a) <u>Main buffers.</u> The input-output buffers have addresses which cause the contents of the accumulator to be transferred to or from the buffers. Detection and transfer of address, and transfer of the accumulator to or from the buffers, occur in one instruction.

    b) <u>Telemetry.</u> If it is desired to transfer information out of the computer serially at a slow rate, such as to a telemetry unit, one bit at a time may be transferred to the telemetry flip-flop. This bit comes from the MSB of the accumulator and at the same time, the telemetry existence flip-flop is set. When the external device has accepted the information, it sends back a signal to reset the existence flip-flop, and the computer will send another bit to the telemetry flip-flop.

c) <u>Gyro torquing.</u> Three channels of gyro torquing are available. A gyro torque output instruction sets the gyro torque logic to the positive or negative state and selects the gyro to be torqued.

An addressable discrete indicates that the gyro torque logic is reset and another pulse can be commanded.

d) <u>Independent discrete output.</u> Thirty-one independent discrete outputs are provided. A discrete output is a signal having two logical levels, a zero and a one. It can be used to control any two state devices, such as a display light. The contents of the sign flip-flop is transferred to one of the 31 discrete flip-flops and the output of this flip-flop is the discrete ouput.

e) <u>Incremental outputs.</u> Twelve incremental stepping motor driven outputs are provided. When an incremental output is addressed, a 2-wire code determined by the states of bits 6 and 7 of the accumulator is provided to the designated decode logic. The decode logic provides a four-wire driver output to the stepping motor.

f) <u>Inputs.</u> The computer will accept the following inputs:

<u>Precounters.</u> There are four precounters in the computer; three of these are bidirectional and the other unidirectional. Each bidirectional counter has two input lines associated with it, one of which indicates a count in the positive direction, the other a count in the negative direction. These are used to partially accumulate the pulses received from the accelerometer electronics, which are proportional to changes in velocity. The total accumulation of these pulses is therefore proportional to total velocity. The incoming pulses must be a minimum of 4.3 microseconds, and a maximum of 8 microseconds wide. Also the positive and negative pulses cannot be present at the same time. The maximum repetition rate of these pulses is 120 kc. The unidirectional pulse has only one input associated with it and the incoming pulses must be a maximum of 4 microseconds and a minimum of 2.3 microseconds in width. The maximum rate of these pulses is 240 kc. All four of the precounters are six bits long.

3) <u>Packaging.</u> The computer is housed in a modular assembly of rugged construction to ensure reliable operation in stringent thermal and vibration environments. The design is simple to eliminate thermal interfaces, yet each major functional system is easily accessible and provisions are made for growth potential. See figure 102.

Connectors and cabling are given particular attention to prevent adverse connector movement and stress concentration at wiring terminations. The packaging techniques used in this design have been used successfully on numerous other contracts requiring similar environmental capability.
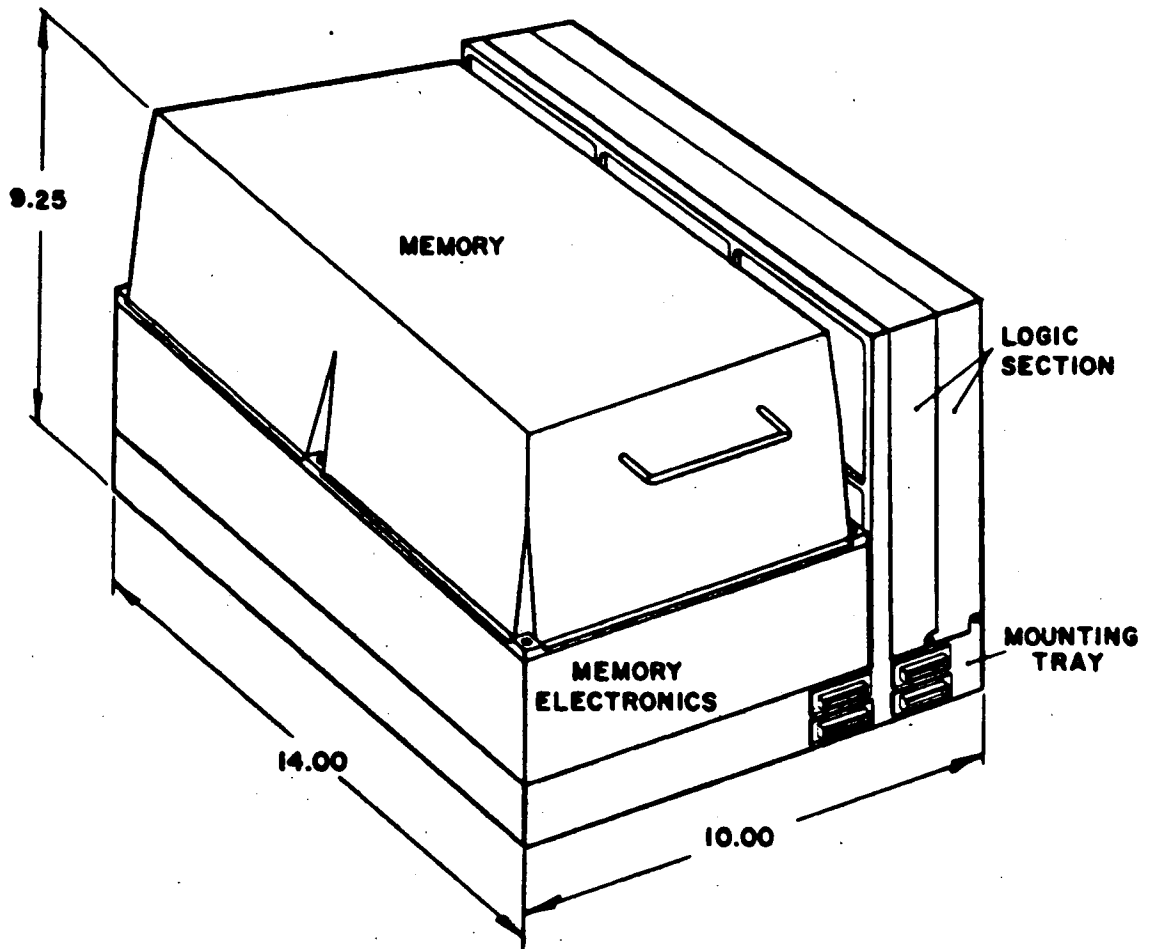
Figure 102 ORBITER COMPUTER

63-9619

The memory is designed as a completely removable assembly. The memory/memory electronics and logic section attach to the base tray. All housings are machined magnesium castings with a wall within them for component mounting.

a)   Memory - The memory housing contains the various core memory arrays. The main memory with its cold data is located in the upper section of the memory while the scratch pad, or hot data, is located in the lower housing. The scratch pad arrays are enclosed in an "oven" area and surrounded by insulation with heater wire laminated within the core boards to ensure immediate warm-up and to obtain even heat distribution throughout the scratch pad memory boards. The heater will be a "proportional" heater to eliminate affecting surrounding circuits.

Mounting of the ferrite biax elements throughout the memory is accomplished so that vibration and shock inputs are held to a minimum. All wires have welded terminations and multipin redundant contact strip connectors are used for interconnections. The memory is designed so that the scratch pad data section may be removed from the main memory allowing access to either section. While these sections are joined the unit is sealed against moisture and contamination.

b)   Memory electronics - This section contains the electrical components for the memory and supports the various connectors which mate with the memory.

c)   Logic section - Each logic board will hold two multilayer printed circuit boards back-to-back and each circuit board will have approximately 300 integrated circuits mounted on it. The integrated circuits will be mounted within modified TO-5 transistor cans. For additional strength the two multilayer circuit boards are separated by an "egg-crate" design of laminated epoxy. The multilayer boards and the epoxy egg-crate will have 0.006-inch of copper laminated to it for a positive thermal path. There will be two logic trays; each will hinge outward to allow access to their respective components. Each logic board will have within it connectors similar to those described for the logic in the standard unit.

b.   GG177 accelerometer. Hinged-pendulum miniature accelerometer GG177 is a damped-pendulum type; it combines high accuracy with compact size.

The design concept applies pulse rebalance to a flexure-supported pendulous mass. Displacement of the pendulous mass, resulting from sensed accelerations, induces a signal in the moving coil of a differential transformer-type pickoff. This signal is fed into a servo amplifier and is then returned as pulses (plus and minus) to the torque coils. This establishes torque balance in the presence of input accelerations so that an algebraic summation of the pulses becomes a linear measure of acceleration.

-259-

The hinged pivots are two flexure joints spaced apart, but contained within a common plane, so that the pivot axis is orthogonal with the sensitive axis of the accelerometer. This arrangement offers greater rigidity along the transverse axis of the accelerometer than could be accomplished with a single pivot and thereby reduces cross-coupling acceleration errors to a minimum. Accelerometer GG177 engineering development program has been completed and production units are presently being delivered on a high-volume basis. A cutaway view of accelerometer GG177 is shown in figure 103. The typical characteristics of the accelerometer are given in table 25.

     c.   <u>Accelerometer and electronics package</u>. The accelerometer electronics package will include all electronics required to rebalance three GG177 accelerometers and to provide incremental velocity pulses to the computer, along with precision timing for the orbiter system.

Construction of the unit will be compatible with its intended use and expected environment. All known successful weight saving techniques will be considered. Maximum use of miniaturization techniques, including the use of integrated circuitry, will be employed where practical. The weight of the accelerometer electronics orbiter package will not exceed six pounds and the solid state volume will not exceed 180 cubic inches.

A tentative inner package configuration of the unit is shown in figure 104.

TABLE 25

TYPICAL CHARACTERISTICS OF THE GG177
HINGED PENDULUM LINEAR ACCELEROMETER

PARAMETER	MAGNITUDE

<u>Accelerometer Characteristics</u>

Parameter	Magnitude
Pendulosity	2. 86 gm-cm
Hinge Axis Damping Coefficient	47,000 dyne-cm-sec
Pendulum Moment of Inertia, Hinge Axis	7. 06 gm-cm^2
Pendulum Characteristic Time	150×10^{-6} sec
Pendulum Freedom	0. 23 deg
Operating Temperature	170°F
Accelerometer Current Scale Factor	6. 0 ma/g

<u>Pickoff</u>

Parameter	Magnitude
Sensitivity	50 volts/rad

TABLE 25 (Concl'd)

PARAMETER	MAGNITUDE
Torquer	
Sensitivity	470 dyne-cm-sec
Maximum "g" Input	15 g
Characteristic Time	15×10^{-6} sec
Heater	
Voltage, RMS or dc	28 volts
Power	75 watts
Accuracy	
Bias Uncertainty	5×10^{-5} g
Scale Factor	0.005%
Null Shift	3 arc sec
Vibropendulosity	0.3×10^{-5} g/g^2

d.   Orbiter power supply.   The power supply used for the orbiter will use switching and pulse width regulator circuits developed by Honeywell.   This design has been used successfully on many programs, including DynaSoar.   The circuits and techniques developed are easily adapted to a wide range of power and voltage requirements.   The proposed power supplies yield what is considered the best combination of weight, volume and efficiency.

The orbiter power supply furnishes all the regulated voltages and power necessary to independently operate the computer.

All the dc voltages are provided from one pulse-width modulated regulator. The regulator is made up of a square-wave oscillator and a switching type power amplifier.   The output of the power amplifier is transformer coupled to the desired voltage level, rectified and filtered.   Supplementary secondary windings provide   ac voltages which are rectified and filtered to provide the necessary dc voltages.   A feedback and comparator circuit completes the regulator loop to maintain the required accuracy for variation in line, load and temperatures.

e.   Planet tracker.   A planet tracker is required by the guidance and navigation system to provide planet direction and range to the planet during approach navigation.   The most difficult requirement is achieving sufficient accuracy in range determination at the long ranges associated with approach.
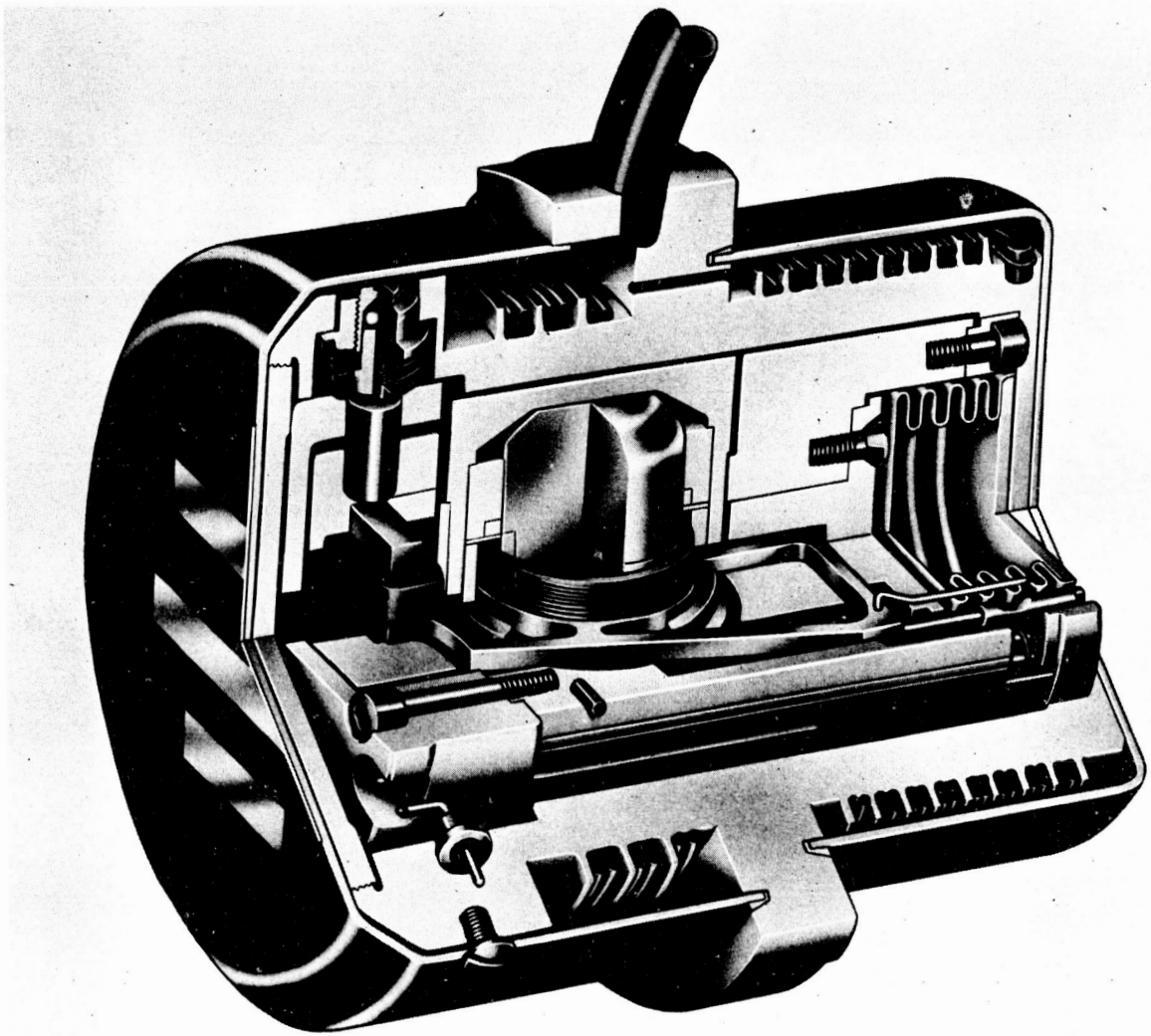
Figure 103   GG177 MINIATURE HINGED PENDULUM ACCELEROMETER
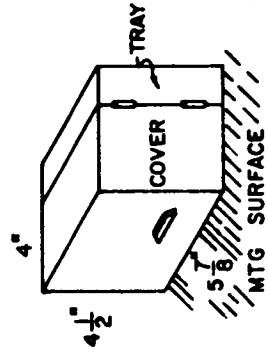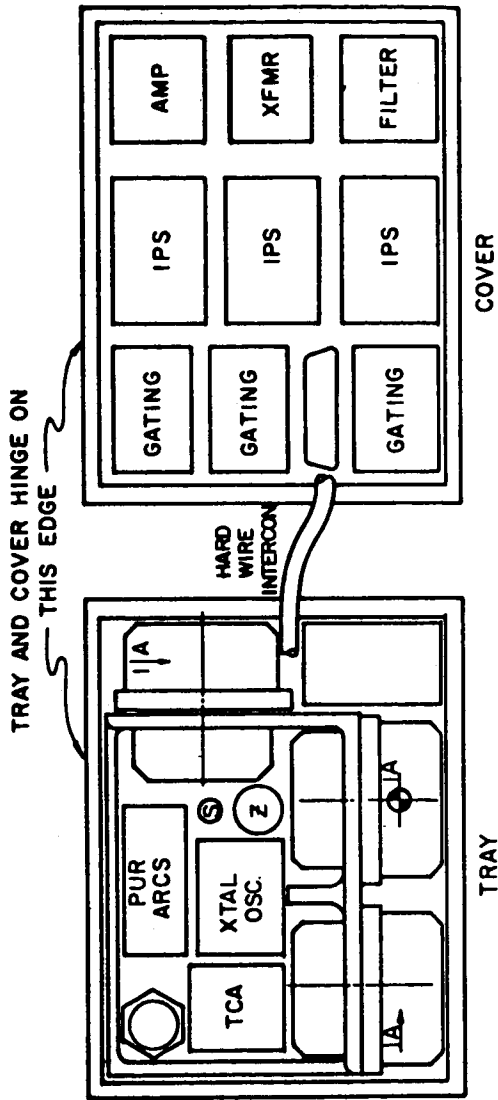
Figure 104 ACCELEROMETER ELECTRONICS

63-9621

Optical determination of range to the planet is accomplished by measuring the diameter of an image of the planet and computing the range, knowing optics focal length and actual planet diameter. Accuracy of measurement is limited by either resolution of the optical system or resolution of the detector utilized. Generally, optics resolution is or can be made better than any known detector resolution so that detector resolution is the limiting parameter. For a given focal length, f, ; detector resolution, a ; planet radius, R; uncertainty in planet radius, ΔR ; and desired range accuracy, $\Delta\rho$; the maximum range at which $\Delta\rho$ can be obtained is given by

$$\rho_{max} = \frac{f\Delta R}{a\sqrt{2}} \left[\left(1 + \frac{4R^2\Delta\rho^2 a^2}{f^2\Delta R^4}\right)^{1/2} - 1 \right]^{1/2} \tag{76}$$

Analysis of equation (76) indicates that ρ_{max} increases, as is desired, with increasing focal length, decreasing detector resolution, and decreasing uncertainty in planet radius. The items under control of the planet tracker designer are focal length, f , and detector resolution, a.

Mechanizations available fall into several categories:

1)   Utilizing a large area detector such as a photomultiplier with a scanning slit reticle at the optics focal point. Size determination would be made on the basis of pulse width.

2)   A mechanically scanned telescope, that is by means of rotating mirror or prism the field of view of a point detector (small area PbS), is moved through object space and the length of time taken to scan across the planet is a measure of the apparent diameter.

3)   A servo-driven gimbaled edge tracker in which the edge of the planet is tracked at three or more points around the horizon which yields sufficient data to determine apparent diameter.

4)   Electronic scanning by means of either a multielement detector mosaic or an image tube in which the planet image is electronically scanned to measure image size which is a measure of apparent diameter.

Since the required accuracy on measuring the apparent diameter is of the order of hundredths of a percent, the only mechanization suitable would be electronic scanning by image tubes.

Ruggedized image tubes have been tested to 2100 lines per inch resolution resulting in a resolution element size of 0.000475 inch per side.

Given a minimum achievable resolution element size the remaining parameter for a given $\Delta\rho$ is focal length, f. For a resolution element size of 0.000475, ρ_{max} is plotted as a function of the focal length, f, for various values of ΔR and $\Delta\rho$ in figure 105. Note that for ΔR = 10 km, a conservative value, the maximum distance for 1000 km range accuracy is 325,000 km while for ΔR = 0, maximum range approaches infinity with increasing focal length. For a value of ΔR = 3 km maximum range is 10^6 km but requiring a focal length of 300 inches, to say the least. Thus the maximum range which satisfies a $\Delta\rho$ of 1000 km is dependent on the acceptable value of ΔR and the optics focal length which determines weight and volume of the instrument.

Arbitrarily choosing, as a practical compromise, an 80-inch focal length which can be folded into a shorter tube length, a reasonable approximation to maximum range is 500,000 km. With 80-inch focal length the size of a resolution element is 3.4×10^{-4} degrees. Tube size is 1.08 inches by 1.44 inches, resulting in a maximum of 3000 resolution elements in the long dimension. Thus, total angular field of view is only about one degree, inadequate to cover any significantly lower altitudes. To increase the dynamic range either or both of two techniques can be employed; scan conversion by fiber optics and variable focal length optics.

In using fiber optics, the complete image plane is not scanned. One end of the fiber optics scan converter is positioned in the focal plane with fiber bundles placed only at specified image plane coordinates. The fibers then funnel down to the image tube photocathode, completely covering the sensitive surface. Then as the image tube continuously scans the fibers, it effectively is scanning only those image plane coordinates at which fibers were placed. The increase in field coverage available by this technique is limited by the useable field of the objective optics and/or packaging limitations.

As an example, if the fibers were arranged in "n" radial lines in the image plane, then each radius would contain $\dfrac{6.3 \times 10^6}{n}$ resolution elements. Each resolution element is 3.4×10^{-4} degrees. Thus, total coverage per radius would be $\dfrac{6.3 \times 3.4 \times 10^2}{n}$ degrees = $\dfrac{2 \times 10^3}{n}$ degrees. If there were 100 radii, each radius would then cover 20 degrees. With an 80-inch focal length, this would require an image plane diameter of 60 inches resulting in very large instrument size. Using 10^3 radii results in a required image plane diameter of only six inches, a much more practical size. However, in a 6-inch diameter image plane, the useful field would only be about ±2 degrees, which results in a greater dynamic range but still not sufficient.

If variable-focal-length optics were employed the dynamic range could be increased by another factor of ten within the limitation of practical image plane diameters. The total field coverage is inversely proportional to focal length so that by shortening the focal length as range to the planet decreases, total angular
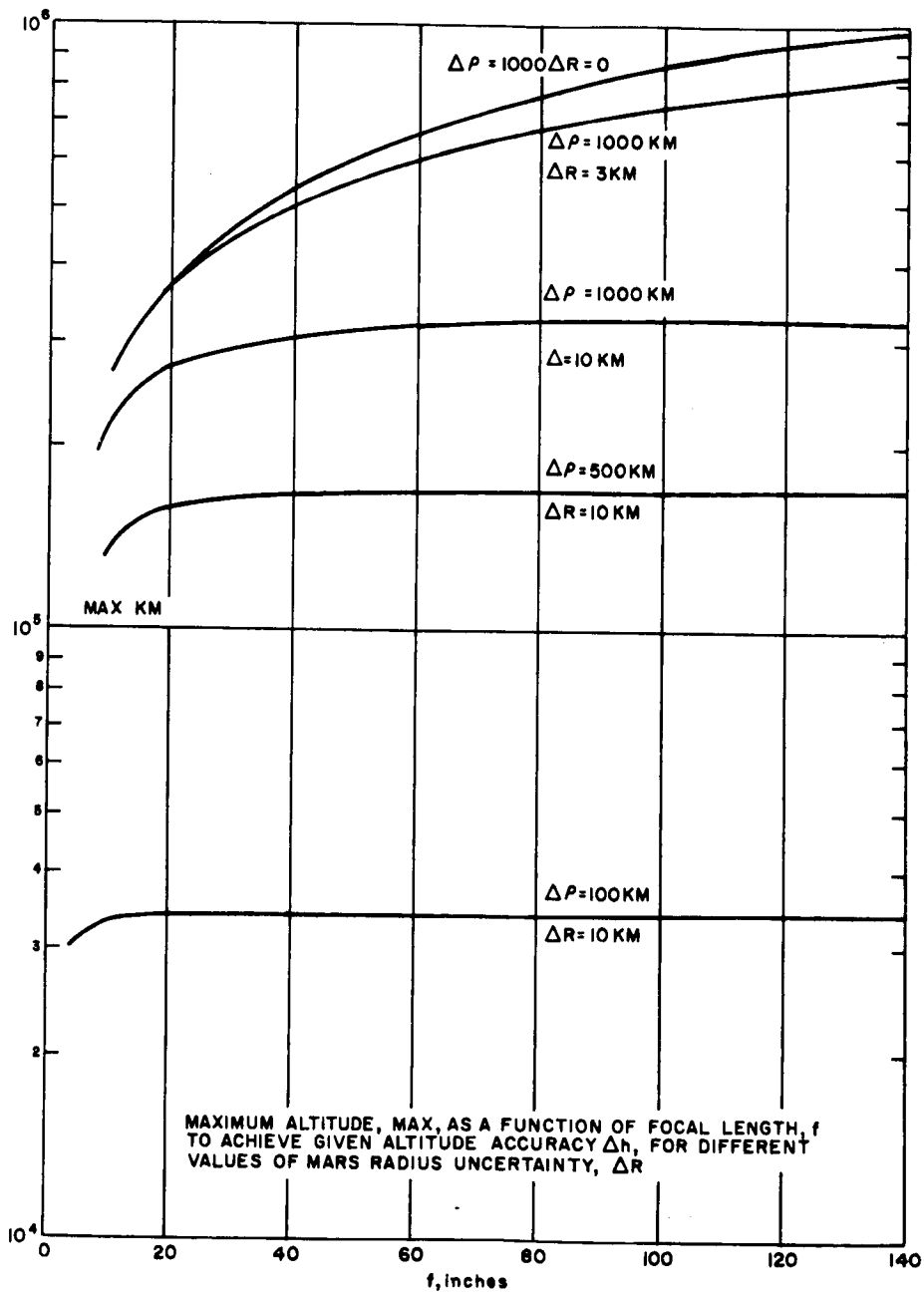
Figure 105 PLANET TRACKER PERFORMANCE

Graph labels:

$\Delta \rho = 1000 \Delta R = 0$

$\Delta \rho = 1000$ KM
$\Delta R = 3$ KM

$\Delta \rho = 1000$ KM
$\Delta = 10$ KM

$\Delta \rho = 500$ KM
$\Delta R = 10$ KM

MAX KM

$\Delta \rho = 100$ KM
$\Delta R = 10$ KM

MAXIMUM ALTITUDE, MAX, AS A FUNCTION OF FOCAL LENGTH, f
TO ACHIEVE GIVEN ALTITUDE ACCURACY Δh, FOR DIFFERENT
VALUES OF MARS RADIUS UNCERTAINTY, ΔR

f, inches

63-9622

coverage increases. Also, as focal length decreases, resolution element angular size increases, causing a worsening of range accuracy. However, since range accuracy is proportional to range squared and inversely proportional to focal length for a given resolution element linear dimension, and since focal length would vary linearly with range in a variable focal length system, range accuracy would improve with decreasing range. To minimize errors resulting from varying focal length, discrete steps would be used.

To simplify the scan electronics, two scan lines on the tube will be transformed into one radius. Thus each radius contains 6000 resolution elements and at the maximum focal length covers two degrees. The total number of radii is 1050, resulting in an angular separation between radii of 0.35 degree. To work at an altitude of 22,000 km, the useful field of view must be about ±10 degrees, so that the focal length must vary from 80 to 16 inches.

Zoomar, Inc. currently stocks a lens with focal length variation from 12 to 72 inches in a tube length of 25 inches and with remote control on focal length. Extending this design to a focal length of from 16 to 80 inches within a tube length of 25 inches should be possible. Allowing an additional four inches for the fiber optics assembly and 15-1/2 inches for the image orthicon tube, the minimum package length, exclusive of any electronics, would be 49-1/2 inches. However, the optical path could be folded.

Figure 106 presents the mechanical configuration showing subsystem part allocation. Optical axis pointing is achieved by a gimbaled mirror rather than gimbaling the complete tracker to reduce size, weight, and power.

Outputs of the planet tracker subsystem are binary numbers proportional to the polar coordinates, r, θ, of either the planet limb or terminator. The guidance computer will apply suitable equations to determine whether the set of points generated during a given frame describes a circle which would be the limb, or a noncircular conic section, which would be the terminator. In the process, the position of the center and the diameter of the image would be determined. The guidance computer will then generate gimbal drive signals to center the image in the orthicon field of view and signals to control the variable focal length optics. Once centered, more precise determination of planet diameter can be measured from which the required range accuracy will result.

    f.   Auxiliary star tracker (AST). The auxiliary star tracker is basically a gimbal-mounted image-dissector photomultiplier (PM) tube and associated electronics designed to track first magnitude stars and reject less bright stars. The instantaneous field of view is ±1.5 degrees in each of two orthogonal axes and the gimbaled field of view is ±40 degrees in one axis, by ±60 degrees in an orthogonal axis of rotation. See figures 107 and 108 for mechanical configuration. Accuracy is ±20 arc sec over the gimbal field of view and is obtained using high-resolution digital-gimbal loop and digital signal processing electronics on the PM tube output.
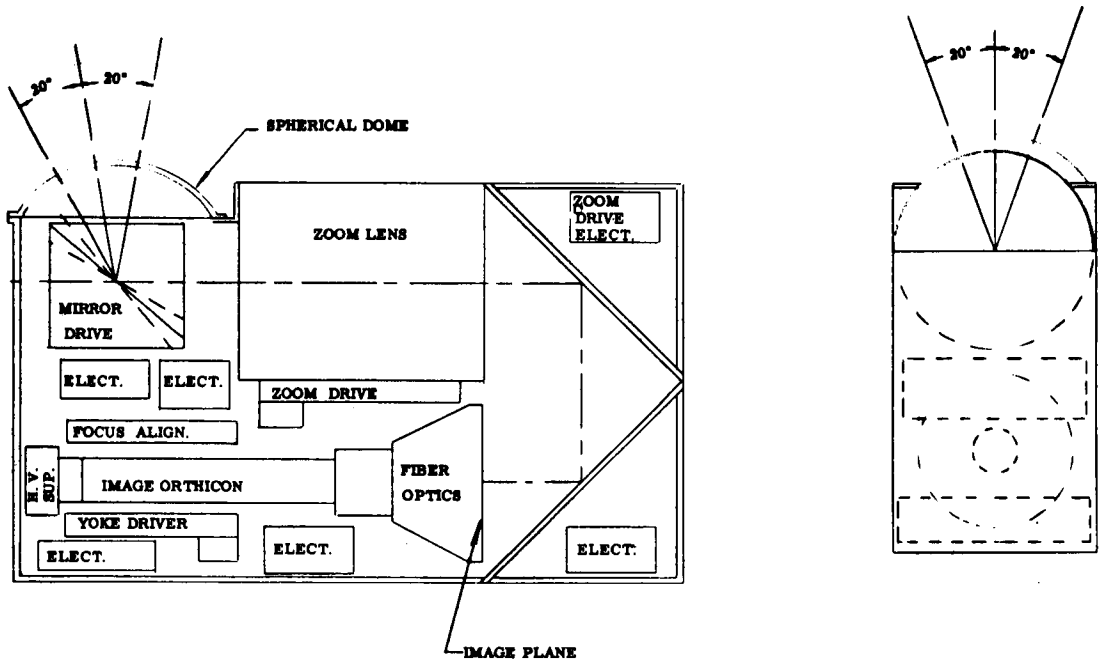
Figure 106 PLANET TRACKER MECHANICAL CONFIGURATION
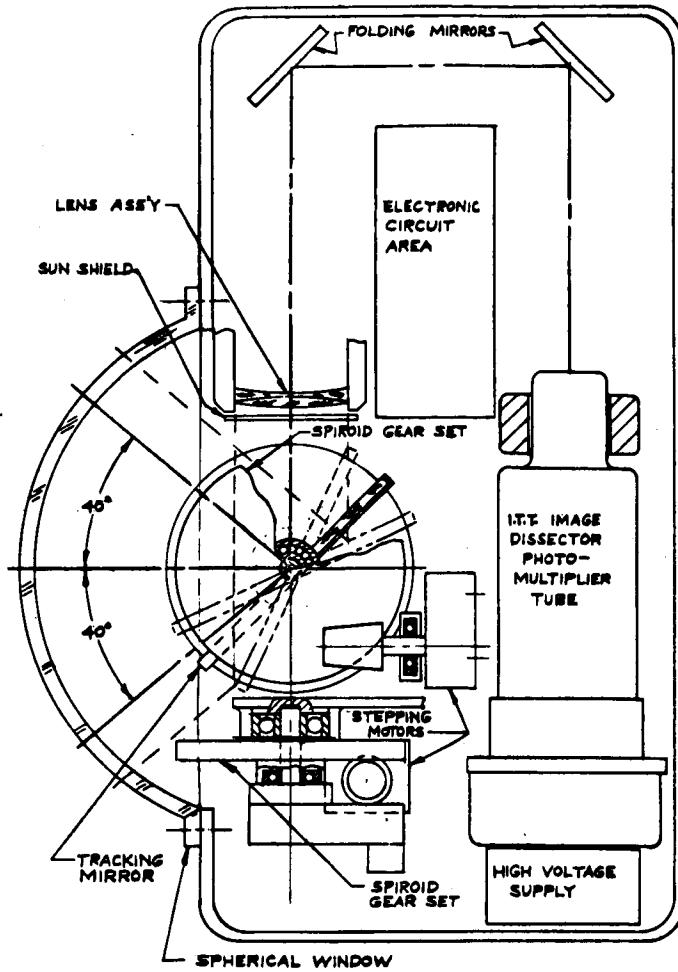
63-9623

Figure 108 AUXILIARY STAR TRACKER (SIDE VIEW)

63-9625

The detector utilized is an image-dissector PM which electronically scans the sensitive tube surface along two orthogonal scan paths crossing at the center of the sensitive area. If the star image is centered, the pulse train out of the PM tube will be symmetric, and all pulses will be of identical width. If the star is not centered, the pulse train will be asymmetric and pulses will be of unequal width. By splitting the PM pulses into azimuth and elevation (or X and Y) components sufficient information is available to determine the position of the star image.

To obtain the digital error signals the PM output pulses, after being split into azimuth and elevation components, are used together with scan reference signals to control an up-down binary counter. During the first half of the scan cycle, the counter counts up only while the PM output is above an established threshold. During the second half of the scan cycle the counter counts down only while the PM output is above the established threshold. The counter output at the end of a scan cycle is proportional to the difference in pulse width from the two halves of the scan cycle. If the star is centered, all pulse widths are the same and the up count equals the down count. If the star is decentered the difference in pulse widths, which is proportional to star position, will be in the counter and available to the digital control unit (DCU).

To reduce the amount of gimbal motion required during tracking, whenever the error signals exceed a certain preset level, the stepper motor is energized to reposition the gimbaled mirror.

The digital output required by the DCU prompted the used of a digital, rather than analog, gimbal loop. A completely digital mechanization does away with the need for any complicated analog-to-digital or digital-to-analog conversion; further benefits are also obtained. A pulsed gimbal readout can be used and is achieved by use of a coded wheel (Optisyn) claimed by the manufacturer, and others, to have an MTBF of 24 years. The digital mechanization can be used as a bang-bang servo system with the stepper motor being energized only periodically to make corrections, and then making the corrections by a fixed number of steps without the usual hunting in analog servo systems. And finally, the electronics available for use in digital mechanizations are more reliable than those available for analog mechanizations.

The gimbal readout system is a serial, rather than parallel, readout requiring knowledge of some reference or starting point from which to start counting. A special loop has been provided to enable the gimbal to acquire the reference position on command from the DCU. The loop is not shown in the block diagram but was included in reliability, weight, and power determination.

This tracker is a modification of the Canopus star tracker, using practically identical electronics and detector, with only slight differences in mechanical configuration. Consequently, considerable savings in cost would result from parallel development efforts.

g.   Planet horizon sensor.   Since the Jet Propulsion Lab (JPL) has funded a planet horizon sensor development program for a device capable of satisfying Voyager requirements, no design study on alternate design was performed.

Published information on the device indicates that the concept utilizes a multielement thermopile detector array in the focal plane of the objective optics with each detector being sequentially sampled to determine planet horizon position.   The resolution and null accuracy of the device is 0.5 degree within the expected orbit altitudes.   Altitude output is also available with accuracies ranging between 850 km and 50 km over the Mars orbit altitudes.

Previous concepts proposed by Honeywell to perform similar functions were based on similar detector arrays with the exception that the Honeywell concept utilized modulated flux density achieved by means of a solid state germanium modulator and the JPL-funded concept utilizes unchopped flux density.   Characteristics and capabilities of the two devices would be very similar except that development of the JPL-funded sensor will have been completed and paid for by the time of Voyager procurement.

4.   Reliability estimate.   The following is an analysis of the potential capability of the orbiter system to meet the requirement of 0.96 probability of success for the Voyager mission.   The design goal MTBF's of tables 27 through 30, and an arbitrary "on-off" switching cycle success probability of 0.9999, have been used.   Operational hours and number of switching cycles are assumed to be as shown in table 26.

TABLE 26

OPERATIONAL HOURS AND SWITCHING CYCLES

Black Box	Failure Rate (λ) in %/1000 Hours	Hours (t) in "on" State	λt x 10^5	Number of Starts
Accelerometer Block and Associated Electronics	6.4364	28	180.2192	5
Computer	19.69	93	1831.1700	35
Planet Tracker	9.880	24	237.120	1
Horizon Scanner	6.25	10	62.5000	1
Auxiliary Star Tracker	2.853	34	11.412	2

The formula used for probability of success for each black box is:

$$P = (P_o)(P_s)^n$$

where

P $=$ probability of success of a black box

P_o $=$ probability of no failures during the time it is in the "on" state, $e^{-\lambda_i t}$

P_s $=$ probability of success of one switching cycle

n $=$ number of switching cycles

The individual calculations are:

Accel: $\quad P_1 = (e^{-\lambda_1 t})(P_s)^n = [e^{-(0.00180)}][0.9999]^5 = 0.9977$

Computer: $\quad P_2 = (e^{-\lambda_2 t})(P_s)^n = [e^{-(0.01831)}][0.9999]^{35} = 0.9787$

Planet Tracker: $\quad P_3 = (e^{-\lambda_3 t})(P_s)^n = [e^{-(0.00237)}][0.9999] = 0.9975$

Horizon Scanner: $\quad P_4 = (e^{-\lambda_4 t})(P_s)^n = [e^{-(0.00063)}][0.999] = 0.9993$

Aux. Star Tracker: $P_5 = (e^{-\lambda_5 t})(P_s)^n = [e^{-(0.000114)}][0.9999]^2 = 0.9997$

The system probability of success is:

$$P_{system} = \pi P_i$$

$$= (0.9977)(0.9787)(0.9975)(0.9993)(0.9997)$$

$$= 0.9730$$

The above assumes a zero failure rate for components while in the "off" state. While such is clearly not the case, there are many unknown factors, such as the tendency of transistors to recover from radiation effects during their off state, which enter a reasonable estimate of a failure rate in the off state. Hence, as environmental effect studies are made after award of the contract, appropriate adjustments to the estimates will be made.

-273-

The advantages of using certified high-reliability parts are shown by tables 27 through 30.

TABLE 27

COMPUTER RELIABILITY GOAL ESTIMATES

Component	Number (N)	High Reliability Failure Rate in percent/1000 Hours (λ)	Nλ
Transistors	550	0.002	1.10
Diodes	1,050	0.001	1.05
Capacitors	300	0.001	0.30
Transformers	90	0.005	0.45
Resistors	2,000	0.002	4.00
Cores	194,300	10^{-6}	0.19
Integrated networks	2,100	0.006	12.60
			19.69

TABLE 28

AUXILIARY STAR TRACKER RELIABILITY GOAL ESTIMATES

Part	No. n	λ x 10^5	$n\lambda$ x 10^5	No. n	λ x 10^5	$n\lambda$ x 10^5
		Conventional			High Reliability	
Transistors						
Conventional	40	0.020	0.800	11	0.020	0.220
High reliability	-	-	-	29	0.002	0.058
Diodes						
Conventional	39	0.010	0.390	-	-	-
High reliability	-	-	-	39	0.001	0.039
Solid circuits	353	0.010	3.530	353	0.001	0.353
Resistors						
Conventional	146	0.020	2.920	-	-	-
High reliability	-	-	-	146	0.001	0.146
Capacitors						
Tantalum conventional	24	0.035	0.840	2	0.035	0.070
Tantalum high reliability	-	-	-	22	0.004	0.088
Paper conventional	28	0.005	0.140	-	-	-
Paper high reliability	-	-	-	28	0.001	0.028
Coils	6	0.030	0.180	6	0.030	0.180
ID tube	1	0.100	0.100	1	0.100	0.100
Motor	2	0.020	0.040	2	0.020	0.040
Shutter	1	0.100	0.100	1	0.100	0.100
Coded wheel readout	2	0.250	0.500	2	0.250	0.500
HVPS	1	0.930	0.930	1	0.930	0.930
			10.970			2.853

TABLE 29

PLANET TRACKER RELIABILITY GOAL ESTIMATES

	Conventional Design			High Reliability Design		
	No. n	λ x 10^5	λn x 10^5	No. n	λ x 10^5	λn x 10^5
Image orthicon	1	4.000	4.000	1	4.000	4.000
Transistors						
Conventional	35	0.020	0.700	12	0.020	0.240
High reliability	-	-	-	23	0.002	0.046
Diodes						
Conventional	20	0.010	0.200	-	-	-
High reliability	-	-	-	20	0.001	0.020
Resistors						
Conventional	130	0.020	2.600	-	-	-
High reliability	-	-	-	130	0.001	0.130
Capacitors						
Tantalum conventional	46	0.035	1.610	-	-	-
Tantalum high reliability	-	-	-	46	0.004	0.184
Paper or mica conventional	34	0.005	0.140	-	-	-
Paper or mica high reliability	-	-	-	34	0.001	0.034
Integrated circuits	96	0.010	0.960	96	0.001	0.096
Crystal	2	0.020	0.040	2	0.020	0.040
Coils	3	0.030	0.090	3	0.030	0.090
Transformers, high voltage	10	0.100	1.000	10	0.100	1.000
Power pack	2	0.930	1.860	2	0.930	1.860
Potentiometers	6	0.100	0.600	6	0.100	0.600
Coded wheel readout	2	0.250	0.500	2	0.250	0.500

TABLE 29 (Cont'd.)

	Conventional Design			High Reliability Design		
	λ No. n	λ x 10^5	λn x 10^5	No. n	λ x 10^5	λn x 10^5
Step motor	2	0.020	0.040	2	0.020	0.040
Zoomar lens	1	2.000	2.000 est	1	2.000	2.000
Totals			16.340			9.880

TABLE 30

PLANET HORIZON SENSOR
RELIABILITY GOAL ESTIMATE

MTBF: 16,000 hours

5.   Problem areas. There are problem areas in both the guidance equipment and guidance technique development areas. With respect to equipment:

a.   The planet-tracker scanner presently proposed is only a concept and the development time might be greater than the schedule for a 1969 Mars flight permits. This type of sensor has not been subjected to a great deal of development work to date and the concept suggested for this Voyager mission is a new and novel approach although it employs techniques and equipment that have been used in other optical instrument developments. This component or its equivalent should have a lead time preceding the assumed system contract go-ahead date.

b.   The reliability estimates are based on insufficient data. That is, the present reliability analysis considers only the operating time of the equipment, which is a small percentage of the mission time, and the effects of on-off switching. The extensive periods of nonoperating time in the space environment have not been considered because of lack of quantitative data. To ensure achievement of the desired reliability goals, parts and components will have to be built and tested in the proper environment to provide these data. This may require more lead time than presently anticipated.

With respect to the guidance techniques much can be done in the region of optimizing the navigation techniques for the terminal phases of the mission. The form of these techniques controls, in effect, the type of optical sensors required and has a considerable effect on the onboard computer design. These analyses can easily precede the assumed contract go-ahead date and should be supported with sufficient funding to permit significant effort.

6. STABILIZATION AND CONTROL

6.1 Introduction

This section describes the stabilization and control system (SCS) used to hold the vehicle at the desired attitude and to perform all orientation required for special maneuvers. A cold gas reaction control system is selected for its simplicity and proven high reliability. Configuration tradeoff studies show that the analog SCS is best in terms of reliability, weight, size, and power requirements. A Sun-Canopus reference frame was selected for the Sun-oriented vehicle. Gas-bearing gyros are used, because they have the greater life expectancy required for this mission.

The position control systems required to point the communication antennas at the Earth and the scientific payload at the planet are also described.

6.2 System Requirements

1. **Mission requirements.** The Voyager vehicle will operate for a maximum time of 300 days in a heliocentric orbit plus a maximum time of 180 days in a Martian orbit. The general tasks that the SCS will perform during this mission are as follows:

2. **Vehicle orientation.** Following completion of Earth launch and injection into a heliocentric orbit towards Mars, the Voyager vehicle will be separated from the Saturn booster. At this time, the SCS is required to orient the vehicle from a random position to a Sun-Canopus reference frame. The roll axis then points towards the Sun, and a preselected plane of the vehicle, containing the Canopus tracker and the vehicle roll axis, lies in the plane formed by the sun, Canopus, and the vehicle. This is the normal attitude-hold position for the vehicle during transit and Mars orbit cruise.

3. **Velocity correction.** During the cruise phase between Earth and Mars, it is possible to correct the vehicle's orbit by adding a velocity increment in a fixed direction. The SCS must then orient the vehicle to point the main engine in the proper direction, hold the vehicle in this orientation during the velocity correction, and reorient the vehicle to reacquire the Sun and Canopus references.

4. **Lander Separation.** Between one and four days from Mars, the lander will be separated from the orbiter. The SCS must then orient the vehicle to the correct position for pointing the lander thrusters, hold the orbiter at this position while the lander is separated and spun up, and reorient the orbiter to reacquire the Sun and Canopus references.

5.   Oribiter deceleration.   Following the separation of the lander, a velocity correction will be applied to decelerate the orbiter.   The SCS must orient the orbiter to the correct position, hold the vehicle during the velocity correction, and reorient the orbiter to reacquire the Sun and Canopus references.

6.   Orbiter retrograde firing.   Upon approaching Mars, the orbiter must be decelerated to permit it to orbit around Mars.   Prior to deceleration, the SCS will position the vehicle in response to orientation commands to obtain the desired initial thrust direction.   During the period of thrust   application, the SCS must direct the vehicle in accordance to DCU steering commands. Following thrust cutoff, the SCS must again reorient the vehicle to reacquire the Sun and Canopus references.

7.   Orbiting of Mars.   During the Mars orbit period, the SCS must maintain vehicle attitude with respect to the Sun and Canopus references when either the Sun or Canopus is occulted by Mars.

8.   Required SCS tasks.   The general tasks that the orbiter-bus SCS will be required to perform to accomplish these system requirements are outlined below:

    a.   Initial acquisition--after orbit injection and Saturn booster separation, and after any major disturbance, null initial body rates (up to 3 degrees/ sec.), acquire the Sun and Canopus references, and orient to a desired attitude.

    b.   Reference attitude hold--after acquisition is completed, maintain a desired attitude during interplanetary cruise and during Martian orbit (to within ± 0.5 degree), except for the discrete maneuvers described below.

    c.   Vehicle reorientations, as required, for the following purposes:

        1)   midcourse corrections

        2)   lander separation

        3)   orbiter slow-down thrust

        4)   navigation sighting (planet tracking, star tracking)

        5)   orbit injection (into Martian orbit)

        6)   orbit trim maneuvers

d. <u>Constant attitude during thrust periods, such as for</u>:

    1) midcourse corrections

    2) orbiter slow-down maneuver

    3) Martian orbit trim maneuver

e. <u>Response to steering rate commands</u> from the digital computer (in pitch and yaw) during the relatively long thrust period required for Martian orbit injection.

9. <u>Vehicle Reference Frame Selection.</u> The orbiter-bus (using solar power) will be designed so as to always keep one orientation with respect to the Sun, except while thrusting, separating the lander, or taking navigation sightings. The solar panels will be fixed to the spacecraft structure, and the orbiter-bus will be controlled with a body-mounted sun sensor so as to keep these panels normal to the sun line. Orientation about the sun line will be provided by a Canopus tracker which can be gimballed about one axis normal to the roll axis. This reference attitude will apply for both the interplanetary phase and the Martian orbit phase. Since the directions of Earth and Mars will be continuously changing, all antennas and other instrumentation which are not omnidirectional will be gimballed to point in the proper direction. The analysis of the antenna and payload position control systems is described in appendix H.

<center>6.3 Design Description</center>

1. <u>SCS performance</u>

a. <u>SCS modes and operation.</u> Examination of the tasks outlined in section 6.2 (System Requirements) indicates that there are a number of recurring operations which lead to the definition of specific system modes. Mode selection is made by the digital computer unit (DCU), except for the two occult modes. The twelve modes selected for the SCS are the following:

    1) Sun-acquire

    2) Canopus-search

    3) Canopus-acquire

    4) Transit cruise (gyros on)

    5) Cruise (gyros on)

<center>-281-</center>

6) Gyro evaluation

7) Gyro attitude hold (cold gas control)

8) Gyro attitude hold (thrusting)

9) Orientation command

10) Steering command

11) Sun-occulted

12) Canopus-occulted

The operation of each of these modes, along with its logic and switching (as defined in the diagram of figure 109)is discussed below.

b. <u>Sun-acquire mode</u>. The objective of the Sun-acquire mode is twofold: (1) to null the sun sensor inputs in pitch and yaw, thereby orienting the roll axis towards the Sun, and (2) to reduce angular rates about the roll axis to less than 0.01 degree/second. The Sun-acquire mode uses the 360-degree field of view coarse acquisition sun sensor as the attitude reference for the pitch and yaw axes. The pitch and yaw gyros are electronically caged and used as rate sensors for stability. The roll axis is not attitude referenced during this mode but uses the roll gyro as a rate sensor to reduce any angular rate about the roll axis to less than 0.01 degree/second. The cold gas reaction system is used to provide the control torques.

The normal occasion for using this mode is after initial separation from the booster or following any disturbance which would cause the spacecraft to move outside the ±0.25-degree linear field of view of the limit cycle sun sensor. In this mode, the SCS operates as follows: In the pitch and yaw axes, the sun sensor attitude output is summed with the gyro rate information and fed to the on-off level switch. The ratio of rate to attitude gain is 10:1. When the sum of the signals exceeds the ± 0.1 degree (or ± 0.01 degree/second) deadband of the switch, the proper jets are energized, driving the vehicle back towards a null on the sun sensor. The mode command logic commands the switchover from the coarse acquisition sun sensor to the limit cycle sun sensor the attitude reference when the sun is within the latter's field of view.

The roll axis operates in a like manner, except that no attitude signal is summed with the rate signal.

c. <u>Canopus-search mode</u>. With the roll axis oriented toward the sun by means of the limit cycle sun sensor, this mode locates the Canopus reference by establishing a roll rate of 0.1 degree/second and maintaining it until Canopus
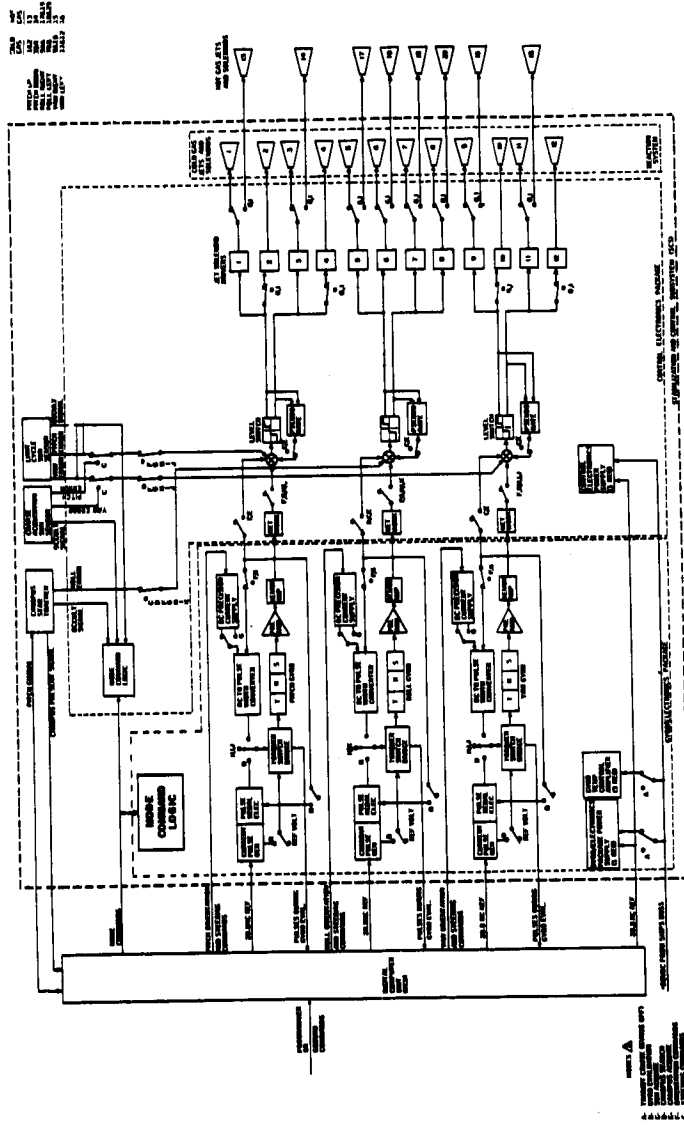
Figure 109 VOYAGER SCS FUNCTIONAL DIAGRAM

63-9294

enters the field of view of the star tracker. This roll rate is achieved by summing a bias signal with the roll rate signal. The on-off level switch energizes the jets until the sum of the roll rate gyro signal and the command bias signal drops below 0.01 degree/second. This results in a steady roll angular rate between 0.09 degree/second and 0.11 degree/second. While the vehicle is rolling, the Canopus tracker gimbal is commanded to slowly scan back and forth so that the Canopus tracker scans in helical patterns, as viewed from the spacecraft.

d. <u>Canopus-acquire mode.</u> The roll axis is oriented to the sun by means of the limit cycle sun sensor. Control in the roll axis differs from that used in either the Sun-acquire or Canopus-search mode. Immediately following the Canopus tracker's acquisition of Canopus, the DCU commands a switchover to the Canopus-acquire mode. The attitude signal from the Canopus tracker is summed with the rate sensor (roll gyro) output. (The roll rate search command is not used.) The error signal input from the Canopus tracker commands the roll jets so that their error is driven to a null, thereby orienting the preselected spacecraft plane with the sun-Canopus-spacecraft plane.

e. <u>Transit cruise mode (gyros off).</u> By far, the largest part of the heliocentric phase of the mission is spent in this mode. Its objective is to hold the spacecraft roll axis along the sun line and maintain a preselected vehicle plane (passing through the Canopus tracker and the vehicle roll axis) in the plane formed by the Sun, Canopus, and the spacecraft. To conserve fuel, the vehicle is held to limit cycle rates of 0.5×10^{-4} degree/second or less while operating in a dead-band amplitude of ± 0.1 degree. The gyros are denergized, and rate damping for stability is provided in all three axes by the use of pseudo-rate feedback around the reaction jet on-off level switching. The cold gas reaction jet system provides the necessary control torques. This mode also compensates for any steady-state disturbance torques about the pitch and yaw axes by means of periodic cold gas reaction torque. Such torques could arise from solar radiation pressure and/or meteorite impacts. The use of solar sails to reduce total impulse requirements was found to be undesirable. The cold gas possible savings are relatively small and the solar sails add some weight and complexity to the vehicle.

f. <u>Cruise mode (gyros on).</u> This is the primary mode during the Martian orbit and is nearly identical to the transit cruise mode except for one difference. The gyros are energized, electronically caged in the rate mode, and ready for use but are not utilized in the control loop. This allows their immediate use for attitude reference by simply uncaging and switching their output into the loop in the event of Sun or Canopus occultation. This mode is also used prior to any thrusting periods.

g. <u>Gyro evaluation mode.</u> This mode provides an accurate drift calibration of the gyros and is used prior to any maneuver using the gyros.

The SCS maintains the vehicle attitude with respect to the Sun and Canopus references identically as in the cruise mode. The difference between this mode and the cruise mode is in the caging of the gyros. They are caged by a precision pulse rebalance loop which provides angular information in the form of increments readily usable by the DCU. The SCS itself performs no calibration but provides the DCU with a measure of vehicle motion as sensed by the gyros. Since the vehicle is slaved to the Sun and Canopus, any net gyro motion will be indicative of gyro drift. The DCU stores this information and uses it to drift-compensate commands to the SCS during subsequent orientation maneuvers using the gyros.

h. <u>Gyro attitude hold (cold gas control) mode.</u> This mode provides an attitude hold capability at any arbitrary orientation and uses a single-degree-of-freedom integrating gyro for attitude reference in each vehicle axis. No maneuvering capability is provided. As shown in figure 109, these gyros are uncaged and their outputs are fed through a lead-lag network to provide control loop stability. The output from the network is in turn fed to the on-off level switch. From this point on, this mode operates as described in the cruise modes, maintaining limit-cycle amplitude of ± 0.1 degree. This mode is used during lander separation, navigation sightings, and during the nonthrusting periods when pointed for the ΔV corrections.

i. <u>Gyro attitude hold (thrusting) mode.</u> This mode is identical to the previous gyro attitude hold mode except that the control torques are provided by the hypergolic reaction jet system rather than by the cold gas jets for control. This mode is used during all velocity corrections with the exception of the Martian orbital ejection.

j. <u>Orientation command mode.</u> This mode is identical to the gyro attitude hold (cold gas) mode with the exception that DCU torquing commands to the gyros can be accepted as shown in figure 109. This mode is used for all orientations directed by the DCU during nonthrusting periods, such as for midcourse correction, lander separation, retrothrust, navigation sightings, and Martian orbit injection.

k. <u>Steering command mode.</u> This mode is identical to the gyro attitude hold (thrusting) mode with the exception that DCU torquing commands to the gyros can be accepted as shown in figure 109. This mode is used during retrograde thrusting for injection into Martian orbit.

l. <u>Sun-occulted mode.</u> This mode provides an attitude reference for the pitch and yaw axes when the sun is occulted. The pitch and yaw gyros are uncaged and replace the sun sensor as the attitude reference. Stability is achieved by using a lead-lag network on the gyro signals as in the gyro attitude hold modes described above. The roll axis continues to use the Canopus tracker as its reference and thus is identical with roll control in the cruise modes.

m. Canopus-occulted mode. This mode provides an alternate roll attitude reference while Canopus is occulated. This is done by uncaging the roll gyro and using it in place of the Canopus tracker as a roll reference. Stability is provided by the use of a lead-lag network on the gyro signal as in the gyro attitude hold modes. The pitch and yaw axes continue to use the sun sensor for their references and operate as described in the cruise modes.

n. Performance table. Table 32A describes the various phases of the Voyager Mars mission in terms of the variations in operating characteristics of the SCS. These charts serve to define the requirements to be met by the SCS, such as attitude errors, attitude changes, vehicle rates, etc. They also outline the SCS design in terms of how it will perform to meet these requirements (reference source, torque source, acceleration level, etc.).

1) Attitude hold and maneuvering accuracy performance. Table 32B summarizes the expected accuracies of the various elements comprising the stabilization and control subsystem. Taking the root sum square of these errors gives the following estimates of attitude accuracy: attitude hold only, ±0.15 degree; and orientation plus attitude hold, ±0.25 degree. The orientation accuracy number assumes a perfect computer signal from the DCU for torquing and less than one hour required for the maneuver.

TABLE 32B

SCS ATTITUDE HOLD AND MANEUVER ACCURACY

Item	Accuracy
Sun sensor or Canopus tracker	±0.01 degree
Limit cycle	±0.10 degree
SCS electronics	±0.05 degree
Switching and null ofset	±0.035 degree
Preamplifier null offset	Negligible
Demodulator null offset	±0.035 degree
Gyro drift	±0.10 degree
Uncompensated random drift	0.1 degree/hour
Spinmotor frequency reference error	0.01 per cent
Torquing	±0.18 degree
Gyro torquer linearity	0.05 per cent
Current source accuracy	0.10 per cent

TABLE 32A

VOYAGER SCS OPERATING CHARACTERISTICS

Mission Sequence	Pitch (3σ)	Yaw (3σ)	Roll (3σ)
Initial Acquisition			
A. Sun Acquire			
1. Initial attitude error	180 degrees	180 degrees	N.A.
2. Final attitude error	0.15 degree	0.15 degree	N.A.
3. Initial rate	1.7 deg/sec	1.7 deg/sec	1.7 deg/sec
4. Final rate	0	0	0.01 deg/sec
5. Time for completion	30 minutes	30 minutes	N.A.
6. Attitude reference	Coarse acquisition sun sensor	Coarse acquisition sun sensor	N.A.
7. Damping source	Gyro	Gyro	Gyro
8. Control moment source	Cold gas jets	Cold gas jets	Cold gas jets
9. Control moment accel.	0.005 deg/sec^2	0.005 deg/sec^2	0.01 deg/sec^2
B. Canopus Search and Acquire	N.A.	N.A.	
1. Initial attitude error	N.A.		180 degrees
2. Final attitude error	N.A.		0.15 degree
3. Search rate	N.A.		0.1 deg/sec
4. Attitude reference	Limit cycle sun sensor	Limit cycle sun sensor	Canopus
5. Rate source	Gyro	Gyro	Gyro
6. Time for completion	N.A.	N.A.	30 minutes
7. Control moment source	Cold gas jets	Cold gas jets	Cold gas jets
8. Control moment accel.	0.005 deg/sec^2	0.005 deg/sec^2	0.01 deg/sec^2
Transit Cruise			
1. Limit cycle amplitude	± 0.1 degree	± 0.1 degree	± 0.1 degree
2. Limit cycle rate	0.000025 deg/sec	0.000025 deg/sec	0.00005 deg/sec
3. Control moment source	Cold gas jets	Cold gas jets	Cold gas jets
4. Control moment accel.	0.005 deg/sec^2	0.005 deg/sec^2	0.01 deg/sec^2
5. Attitude reference	Limit cycle sun sensor	Limit cycle sun sensor	Canopus tracker
6. Damping source	Pseudo rate	Pseudo rate	Pseudo rate
Midcourse Correction			
A. Orientation Maneuver			
1. Accuracy	0.25 degree	0.25 degree	0.25 degree
2. Rate	0.1 deg/sec	0.1 deg/sec	N.A.
3. Time for completion	<30 minutes	<30 minutes	N.A.
4. Attitude reference	DCU command	DCU command	Gyro
5. Rate source	Gyro-network	Gyro-network	Gyro-network
6. Control moment source	Cold gas jets	Cold gas jets	Cold gas jets
7. Control moment accel.	0.005 deg/sec^2	0.005 deg/sec^2	0.01 deg/sec^2

Mission Sequence	Pitch (3 σ)	Yaw (3 σ)	Roll (3 σ)
Midcourse Correction (Concl'd)			
B. Orientation Hold			
1. Accuracy	0.25 degree	0.25 degree	0.25 degree
2. Limit cycle rate	0.000025 deg/sec	0.000025 deg/sec	0.00005 deg/sec
3. Limit cycle amplitude	± 0.1 degree	± 0.1 degree	± 0.1 degree
4. Time for completion	< 30 minutes	< 30 minutes	< 30 minutes
5. Attitude reference	Gyro	Gyro	Gyro
6. Rate source	Gyro - network	Gyro - network	Gyro - network
7. Control moment source	Cold gas jets	Cold gas jets	Cold gas jets
8. Control moment accel.	0.005 deg/sec^2	0.005 deg/sec^2	0.01 deg/sec^2
C. ΔV Firing			
1. Limit cycle amplitude	± 0.1 degree	± 0.1 degree	± 0.1 degree
2. Time for completion	< 30 seconds	< 30 seconds	< 30 seconds
3. Attitude reference	Gyro	Gyro	Gyro
4. Rate source	Gyro - network	Gyro - network	Gyro - network
5. Control moment source	Hot gas jets	Hot gas jets	Hot gas jets
D. Reorientation Maneuver			
1. Accuracy	0.15 degree	0.15 degree	0.5 degree
2. Rate	0.1 deg/sec	0.1 deg/sec	N.A.
3. Time for completion	< 30 minutes	< 30 minutes	N.A.
4. Attitude reference	Gyro/sun sensor	Gyro/sun sensor	Gyro
5. Rate source	Gyro - network	Gyro - network	Gyro - network
6. Control moment source	Cold gas jets	Cold gas jets	Cold gas jets
7. Control moment accel.	0.005 deg/sec^2	0.005 deg/sec^2	0.01 deg/sec^2
E. Canopus Acquire			
1. Initial attitude error	N.A.	N.A.	0.5 degree
2. Final attitude error	N.A.	N.A.	0.15 degree
3. Attitude reference	Limit cycle sun sensor	Limit cycle sun sensor	Canopus tracker
4. Rate source	Gyro	Gyro	Gyro
5. Time for completion	N.A.	N.A.	<30 minutes
6. Control moment source	Cold gas jets	Cold gas jets	Cold gas jets
7. Control moment accel.	0.005 deg/sec^2	0.005 deg/sec^2	0.01 deg/sec^2
Lander Separation			
A. Orientation Maneuver			
1. Accuracy	0.25 degree	0.25 degree	0.25 degree
2. Rate	0.1 deg/sec	0.1 deg/sec	N.A.
3. Time for completion	30 minutes	30 minutes	N.A.
4. Attitude reference	DCU command	DCU command	Gyro
5. Rate source	Gyro - network	Gyro - network	Gyro - network
6. Control moment source	Cold gas jets	Cold gas jets	Cold gas jets
7. Control moment accel.	0.005 deg/sec^2	0.005 deg/sec^2	0.01 deg/sec^2

Mission Sequence	Pitch (3σ)	Yaw (3σ)	Roll (3σ)
B. Orientation Hold			
1. Accuracy	0.25 degree	0.25 degree	0.25 degree
2. Limit cycle rate	0.000025 deg/sec	0.000025 deg/sec	0.00005 deg/sec
3. Time for completion	< 30 minutes	< 30 minutes	< 30 minutes
4. Attitude reference	Gyro	Gyro	Gyro
5. Rate source	Gyro - network	Gyro - network	Gyro - network
6. Control moment source	Cold gas jets	Cold gas jets	Cold gas jets
7. Control moment accel.	0.005 deg/sec^2	0.005 deg/sec^2	0.01 deg/sec^2
8. Limit cycle amplitude	± 0.1 degree	± 0.1 degree	± 0.1 degree
C. Reorientation Maneuver			
1. Accuracy	0.15 degree	0.15 degree	0.5 degree
2. Rate	1.0 deg/sec	1.0 deg/sec	N.A.
3. Time for completion	< 30 minutes	< 30 minutes	N.A.
4. Attitude reference	Gyro/sun sensor	Gyro/sun sensor	Gyro/sun sensor
5. Rate source	Gyro - network	Gyro - network	Gyro - network
6. Control moment source	Cold gas jets	Cold gas jets	Cold gas jets
7. Control moment accel.	0.02 deg/sec^2	0.02 deg/sec^2	0.01 deg/sec^2
D. Canopus Acquire			
1. Initial attitude error	N.A.	N.A.	0.5 degree
2. Final attitude error	N.A.	N.A.	0.15 degree
3. Attitude reference	Limit cycle sun sensor	Limit cycle sun sensor	Canopus tracker
4. Rate source	Gyro	Gyro	Gyro
5. Time for completion	N.A.	N.A.	30 minutes
6. Control moment source	Cold gas jets	Cold gas jets	Cold gas jets
7. Control moment accel.	0.02 deg/sec^2	0.02 deg/sec^2	0.01 deg/sec^2
Orbiter Retrofiring			
A. Orientation Maneuver			
1. Accuracy	0.25 degree	0.25 degree	0.25 degree
2. Rate	1.0 deg/sec	1.0 deg/sec	N.A.
3. Time for completion	< 30 minutes	< 30 minutes	N.A.
4. Attitude reference	Gyro	Gyro	Gyro
5. Rate source	Gyro-network	Gyro-network	Gyro-network
6. Control moment source	Cold gas jets	Cold gas jets	Cold gas jets
7. Control moment accel.	0.02 deg/sec^2	0.02 deg/sec^2	0.01 deg/sec^2
B. Orientation Hold			
1. Limit cycle amplitude	± 0.1 degree	± 0.1 degree	± 0.1 degree
2. Limit cycle rate	0.0001 deg/sec	0.0001 deg/sec	0.00005 deg/sec
3. Time for completion	< 30 minutes	< 30 minutes	< 30 minutes
4. Attitude reference	Gyro	Gyro	Gyro
5. Rate source	Gyro-network	Gyro-network	Gyro-network
6. Control moment source	Cold gas jets	Cold gas jets	Cold gas jets
7. Control moment accel.	0.02 deg/sec^2	0.02 deg/sec^2	0.01 deg/sec^2
8. Accuracy	0.25 degree	0.25 degree	0.25 degree

Mission Sequence	Pitch (3σ)	Yaw (3σ)	Roll (3σ)
Orbiter Retrofiring (Concl'd)			
C. ΔV firing			
1. Limit cycle amplitude	± 0.1 degree	± 0.1 degree	± 0.1 degree
2. Time for completion	< 30 seconds	< 30 seconds	< 30 seconds
3. Attitude reference	Gyro	Gyro	Gyro
4. Rate source	Gyro - network	Gyro - network	Gyro - network
5. Control moment source	Hot gas jets	Hot gas jets	Hot gas jets
D. Reorientation Maneuver			
1. Accuracy	0.15 degree	0.15 degree	0.5 degree
2. Rate	1.0 deg/sec	1.0 deg/sec	1.0 deg/sec
3. Time for completion	< 30 minutes	< 30 minutes	< 30 minutes
4. Attitude reference	Gyro/sun sensor	Gyro/sun sensor	Gyro
5. Rate source	Gyro - network	Gyro - network	Gyro - network
6. Control moment source	Cold gas jets	Cold gas jets	Cold gas jets
7. Control moment accel.	0.02 deg/sec^2	0.02 deg/sec^2	0.01 deg/sec^2
E. Canopus Acquire			
1. Initial attitude error	N.A.	N.A.	0.5 degree
2. Final attitude error	N.A.	N.A.	0.15 degree
3. Attitude reference	Limit cycle sun sensor	Limit cycle sun sensor	Canopus tracker
4. Rate source	Gyro	Gyro	Gyro
5. Time for completion	N.A.	N.A.	< 30 minutes
6. Control moment source	Cold gas jets	Cold gas jets	Cold gas jets
7. Control moment accel.	0.02 deg/sec^2	0.02 deg/sec^2	0.01 deg/sec^2
Navigation Sighting			
1. Limit cycle amplitude	± 0.1 degree	± 0.1 degree	± 0.1 degree
2. Limit cycle rate	0.0001 deg/sec	0.0001 deg/sec	0.00005 deg/sec
3. Time for completion	1 hour	1 hour	1 hour
4. Attitude reference	Gyro	Gyro	Gyro
5. Rate source	Gyro - network	Gyro - network	Gyro - network
6. Control moment source	Cold gas jets	Cold gas jets	Cold gas jets
7. Control moment accel.	0.02 deg/sec^2	0.02 deg/sec^2	0.01 deg/sec^2
8. Accuracy	0.25 degree	0.25 degree	0.25 degree
Orbiter Injection			
A. Orientation Maneuver			
1. Accuracy	0.25 degree	0.25 degree	0.25 degree
2. Rate	1.0 deg/sec	1.0 deg/sec	N.A.
3. Time for completion	< 30 minutes	< 30 minutes	N.A.
4. Attitude reference	Gyro	Gyro	Gyro
5. Rate source	Gyro - network	Gyro - network	Gyro - network
6. Control moment source	Cold gas jets	Cold gas jets	Cold gas jets
7. Control moment accel.	0.02 deg/sec^2	0.02 deg/sec^2	0.01 deg/sec^2

Mission Sequence	Pitch (3σ)	Yaw (3σ)	Roll (3σ)
B. Orientation Hold			
1. Limit cycle amplitude	± 0.1 degree	± 0.1 degree	± 0.1 degree
2. Limit cycle rate	0.00008 deg/sec	0.00001 deg/sec	0.00006 deg/sec
3. Time for completion	< 30 minutes	< 30 minutes	< 30 minutes
4. Attitude reference	Gyro	Gyro	Gyro
5. Rate source	Gyro - network	Gyro - network	Gyro - network
6. Control moment source	Cold gas jets	Cold gas jets	Cold gas jets
7. Control moment accel.	0.02 deg/sec^2	0.02 deg/sec^2	0.01 deg/sec^2
8. Accuracy	0.25 degree	0.25 degree	0.25 degree
C. ΔV Firing			
1. Limit cycle amplitude	± 0.1 degree	± 0.1 degree	± 0.1 degree
2. Limit cycle rate	0.03 deg/sec	0.03 deg/sec	0.01 deg/sec
3. Time for completion	< 12 minutes	< 12 minutes	< 12 minutes
4. DCU steering command	1 deg/sec	1 deg/sec	0
5. Rate source	Gyro - network	Gyro - network	Gyro - network
6. Control moment source	Hot gas jets	Hot gas jets	Hot gas jets
D. Reorientation Maneuver			
1. Accuracy	0.15 degree	0.15 degree	0.5 degree
2. Rate	1.0 deg/sec	1.0 deg/sec	1.0 deg/sec
3. Time for completion	< 30 minutes	< 30 minutes	< 30 minutes
4. Attitude reference	Gyro/sun sensor	Gyro/sun sensor	Gyro
5. Rate source	Gyro - network	Gyro - network	Gyro - network
6. Control moment source	Cold gas jets	Cold gas jets	Cold gas jets
7. Control moment accel.	0.03 deg/sec^2	0.03 deg/sec^2	0.02 deg/sec^2
E. Canopus Acquire			
1. Initial attitude error	N.A.	N.A.	0.5 degree
2. Final attitude error	N.A.	N.A.	0.15 degree
3. Attitude reference	Limit cycle sun sensor	Limit cycle sun sensor	Canopus tracker
4. Rate source	Gyro	Gyro	Gyro
5. Time for completion	N.A.	N.A.	< 30 minutes
6. Control moment source	Cold gas jets	Cold gas jets	Cold gas jets
7. Control moment accel.	0.03 deg/sec^2	0.03 deg/sec^2	0.02 deg/sec^2

TABLE 32A (Concl'd)

Mission Sequence	Pitch (3σ)	Yaw (3σ)	Roll (3σ)
Mars Orbit Cruise			
1. Limit cycle amplitude	± 0.1 deg/sec	± 0.1 deg/sec	± 0.1 deg/sec
2. Limit cycle rate	0.00015 deg/sec	0.00015 deg/sec	0.0001 deg/sec
3. Control moment source	Cold gas jets	Cold gas jets	Cold gas jets
4. Control moment accel.	0.03 deg/sec^2	0.03 deg/sec^2	0.02 deg/sec^2
5. Attitude reference	Limit cycle sun sensor	Limit cycle sun sensor	Canopus tracker
6. Damping source	Pseudo rate	Pseudo rate	Pseudo rate
Occultation			
1. Limit cycle amplitude	± 0.1 deg/sec	± 0.1 deg/sec	± 0.1 deg/sec
2. Limit cycle rate	0.00015 deg/sec	0.00015 deg/sec	0.0001 deg/sec
3. Control moment source	Cold gas jets	Cold gas jets	Cold gas jets
4. Control moment accel.	0.03 deg/sec^2	0.03 deg/sec^2	0.02 deg/sec^2
5. Attitude reference	Gyro	Gyro	Gyro
6. Damping source	Gyro - network	Gyro - network	Gyro - network

2. Components and block diagram

    a. __Major components.__ The functional diagram for the SCS designed to perform the tasks outlines described above is shown in figure 109. The major components used in the SCS and indicated on the diagrams are:

    b. __Sun and Canopus sensors.__ These sensors include the following:

    1) __Coarse acquisition sun sensor.__ This sensor is used for initial alignment of the spacecraft roll axis to the sun line, and therefore has an unlimited field of view. It initiates pitch and yaw commands to the vehicle so that the field of view of the limit cycle sun sensor can capture the sun line.

    2) __Limit cycle sun sensor.__ This sensor generates accurate pitch and yaw error signals for precision pointing of the vehicle X-axis along the sun line. High accuracy is obtained at the expense of a limited field of view.

    3) __Canopus star tracker.__ The star tracker generates roll error signals for accurate alignment of a preselected vehicle plane with the plane formed by the Sun, Canopus, and the spacecraft. This preselected plane passes through the vehicle roll axis and the Canopus star tracker.

    c. __Cold gas reaction system.__ Nitrogen gas jets are used for vehicle attitude control during all nonthrusting phases of the mission. Four jets in each axis provide a torque couple for pitch, yaw, and roll rotation in either direction. The system is comprised of 12 jets, two nitrogen storage tanks, a pressure regulator, pressure transducers, and other necessary plumbing.

    d. __Gyro/electronics package.__ The gyro/electronics package includes:

    1) __Three floated single-degree-of-freedom gyros.__ These gyros are rate sensors for damping and attitude sensors for attitude hold during spacecraft maneuvering and during Martian orbit when either the Sun or Canopus is occulted.

    2) __Power supply.__ This supply provides power to the gyros and their associated electronics.

    3) __Temperature control amplifiers.__ These circuits control gyro temperature within close limits to provide the necessary gyro accuracy.

    4) __Caging electronics.__ A precision current supply, a dc-to-pulse-width converter, and a torquer switch bridge allow caging of the gyros in a rate mode so that their output may be used for rate damping.

    5) __Evaluation electronics.__ A current pulse generator, pulse rebalance electronics, and a torquer switch bridge allow an accurate evaluation

of gyro drift during flight. To evaluate drift, the gyros are caged by these circuits while the spacecraft is attitude stabilized to the Sun and Canopus sensor inputs. Any gyro drift during this phase is apparent as torquing pulses and these are sent to the DCU where they are subsequently used to bias maneuvering commands. By this means gyro drift is effectively compensated and very accurate maneuvering can be accomplished even during extended missions.

e. Control electronics package

1) <u>Mode command logic.</u> This logic controls the switching necessary to provide the various SCS modes during the mission. The mode switching logic receives its commands from the DCU with the exception of the Sun and Canopus occultation signals which are generated by the Sun and Canopus sensors. Some of these mode command logic circuits is located in the gyro/electronics package.

2) <u>Jet solenoid drivers.</u> On-off commands to the cold gas jet solenoids and the hot gas jet solenoids are directed through these drivers by the on-off level switches and the mode command logic.

3) <u>On-off level switches.</u> These switches pass signals to the jet solenoid drivers when the switch inputs exceed a present deadband level.

4) <u>Pseudo-rate networks.</u> These networks around the on-off level switches provide system stability during Sun and Canopus attitude hold without the necessity for gyro rate information.

5) <u>Lead-lag networks.</u> These active networks on the inputs to the on-off level switches provide system stability during attitude hold with gyros, and during steering phases.

6) <u>Power supply.</u> This supply provides power to the control electronics, the Canopus star tracker and the sun sensors.

f. <u>Interface components.</u> The components shown in figure 109 which interface with the SCS are:

1) <u>Digital computer unit.</u> This component of the guidance and control system has an interface with the SCS to perform the following functions: selects the SCS modes by sending commands to the SCS mode command logic; determines the gyro drift rates prior to any orientation using the gyros; continuously computes and maintains a memory of the spacecraft attitude during all orientation phases, and commands the SCS with rate signals given in body axes; and supplies a precision 28.8-kc reference signal.

2) **Hot-gas reaction system.** This system provides three-axis attitude control during all thrusting phases of the mission. The signals to the hot gas reaction jet solenoids are provided by the SCS jet solenoid drivers when commanded by mode logic.

3) **Spacecraft power supply.** This supply provides raw 28-volt dc power to the SCS during flight. The spacecraft power is derived from solar panel arrays backed up by batteries.

g. **Component description.** The SCS consists of the following eleven basic components as installed in the spacecraft: reaction system; gyro/electronics package; control electronics package; Canopus star tracker; coarse acquisition sun sensor (five items); and limit cycle sun sensor (two items). For the purpose of describing the SCS components, the actual physical grouping is ignored. Instead the SCS is regrouped and described in terms of common equipment as follows: sensors; reaction system; and electronics.

h. **Sensors.** The sensors used in the Voyager SCS are described in the following paragraphs.

1) **Gyros.** The gyros for the SCS are the Honeywell GG159 gas bearing (MIG) gyro, which is the most highly refined floated gyro. A proven ceramic gas bearing motor is combined with a new frictionless hydrostatic fluid gimbal suspension. The gyro has spin motor rotation detection (SMRD).

2) **Sun sensors.** Two separate sun sensor units are used to provide sun acquisition without gimbals or complicated search maneuvers and to provide accurate sun reference attitude when the SCS is holding the vehicle roll axis parallel to the sun line. The sun sensor units are: (a) coarse acquisition sun sensor; and (b) limit cycle sun sensor.

a) **Coarse acquisition sun sensor.** The coarse acquisition sun sensor will give attitude indications of the Voyager spacecraft over a range of 360 degrees in pitch and yaw. The sensor is nearly identical to the acquisition Sun sensor to be used on the advanced orbiting solar observatory and will have been developed, qualified, and flown prior to its use in the Voyager program.

The pitch and yaw configurations are identical. The device consists of four silicon detectors in each axis, connected in a bridge network so that the bridge output is proportional to the sine of the angle between the controlled axis of the vehicle and the line-of-sight to the sun. This type of output signal results from the mounting geometry and the fact that individual cell current output into a low impedance load is proportional to illumination, or incident flux, in the sensitive spectral region of the detectors.

The detectors are mounted two to a head as shown in figure 110. Two heads are used in each axis and are mounted on the vehicle with their axis of symmetry aligned to the vehicle roll axis, one aligned to the + roll axis, the other to the -roll axis. Thus the detector normals make angles with the spacecraft roll axis of 45 degrees, 135 degrees, 225 degrees, and 315 degrees. Two null points exist; one at 0 degree and one at 180 degrees. The SCS cannot acquire the 180-degree null point, since at any attitude between 0 degree and 180 degrees, the output signal is positive and causes a vehicle rotation toward zero null and not towards 180 degrees null. The vehicle will similarly rotate towards zero null for attitudes between zero and -180 degrees. Thus the 180-degree null point is an unstable position and will not be of concern.

In addition to the output logic as discussed above, the outputs of all detectors in both axes are summed to provide an indication of Sun occultation. Regardless of vehicle attitude, the summation of detector outputs will remain above a certain level in bright sunlight. The only condition causing the signal summation to drop below this level is a decrease in solar illumination indicating occultation or impending occultation.

High reliability and low size, weight, and power consumption are achieved through the use of photovoltaic detectors operating as current sources which require no bias voltage, and integrated circuits, notably Texas Instrument solid circuits which perform the same function as a multicomponent circuit (e. g., amplifier) with the same weight, power, size, and reliability as a single transistor.

The volume occupied by the complete subsystem consisting of four sensor heads and one electronics package will not exceed four cubic inches. Weight will be only seven ounces, power drain only 0.35 watt. The MTBF is 240,000 hours based on high-reliability parts.

The null accuracy of the device will be about 1 degree, the inaccuracy resulting almost solely from the differences in drift characteristics between detectors.

b) Limit cycle sun sensor. The basic element of the limit cycle sun sensor is a critical angle prism. The prism is of isosceles geometry with the isosceles angles cut approximately at the critical internal reflectance angle of the glass material for the wavelength of maximum detector sensitivity. When the Sun's rays enter the prism normal to the front surface, they pass through the prism and strike the lateral faces at the critical angle, causing virtually all the incident radiation to be totally internally reflected.

A null signal is obtained when the silicon detector senses the Sun's rays through the scanning aperture in a vibrating reed. If the Sun's rays are shifted either to the right or the left, the angle of incidence to the further face

MOUNTING BLOCK

KOVAR BASE PLATE

DETECTOR

ELECTRICAL CONNECTIONS

VEHICLE ROLL AXIS

VEHICLE SKIN

DETECTOR

SUN

MOUNTING BLOCK

KOVAR BASE PLATE
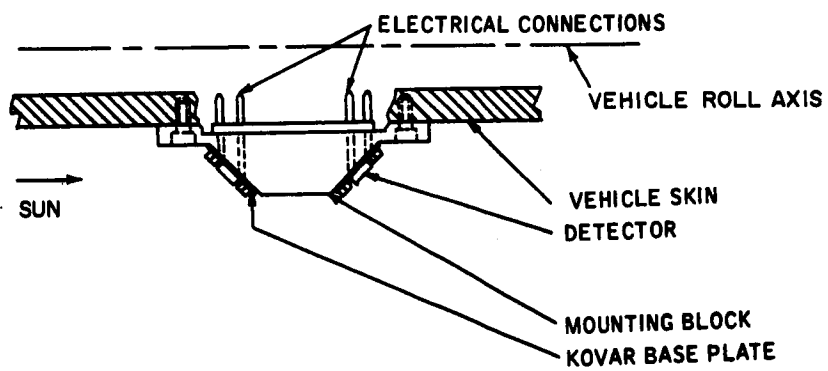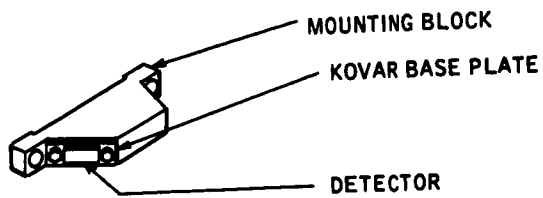
63-9295

Figure 110 COARSE ACQUISITION SUN SENSOR -- MECHANICAL CONFIGURATION

increases. Thus, a significant portion of the radiation is refracted through the prism and transmitted through the scanning aperture to the detector as an off-null signal. The radiation to the other face strikes at a reduced angle of incidence, which ensures a reflection. Since the transition from total internal reflection to refraction is abrupt, the sensor output is very sensitive to the angular position of the Sun with respect to the null position. The slope of the output near null is very steep, providing excellent null accuracy and linearity for small angular deviations. The truncated apex of the prism is opaque to eliminate direct rays from the Sun to the photo-sensor. The physical configuration of each of the single axis units is illustrated by the layout shown in figure 111. While most of the processing circuits will be located external to the tracker assembly, space is available in the sun sensor packaging for those portions of the circuits functionally required at this location.

Experimental data (figure 112) shows that the proposed sun sensor is capable of excellent tracking accuracy, has good linearity about the null-axis, and provides a wide acquisition field of view.

Device specifications are

Weight:	1.5 lbs.
Volume:	13 cubic inches in two packages
Power:	0.5 watt at +15 volts dc
MTBF:	133,000 hours
Accuracy:	better than 0.01 degrees
Instantaneous field:	± 0.25 degrees
Total field	greater than ± 5 degrees

i. <u>Canopus star tracker</u>. The Canopus star tracker performs two functions: provides the SCS with vehicle roll reference and provides the DCU with Canopus position for navigation. Consequently both digital and analog signals are required. This is achieved without complicated A/D or D/A conversion by feeding the components of the scan-generated error signal into both digital and analog signal processing electronics, and utilizing a digital gimbal loop. Thus analog error signals proportional to roll error are fed to the SCS and binary outputs sufficient to determine the position of Canopus with respect to a vehicle-fixed reference are fed to the DCU.

TYPICAL PRISM

↑
SUN

PRISM

PIVOT ADJUSTING SCREW
EACH SIDE OF CLIP

OUTER COVER

|←— 1.0 —→|

0.90

ELASTOMERIC VEE BLOCK
ONE EACH END OF PRISM

PRISM

CLAMPING SCREWS (2)

ANGLE HOLDING CLIP (2)

PIVOT PIN EACH END
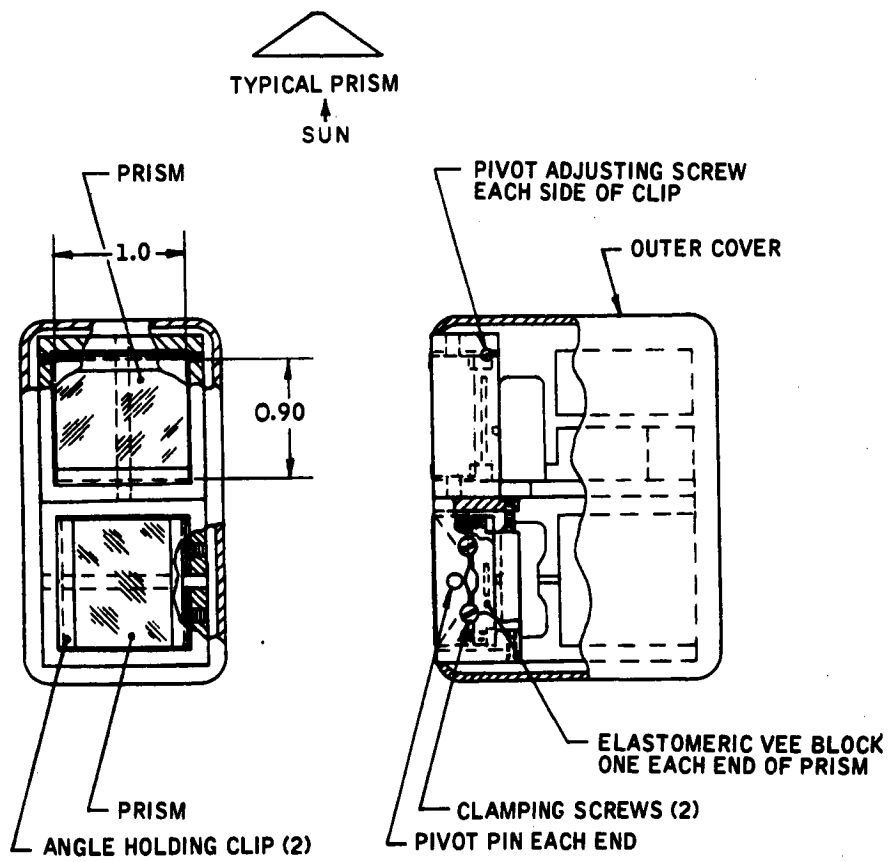
63-9296

Figure 111 LIMIT CYCLE SUN SENSOR MECHANICAL CONFIGURATION
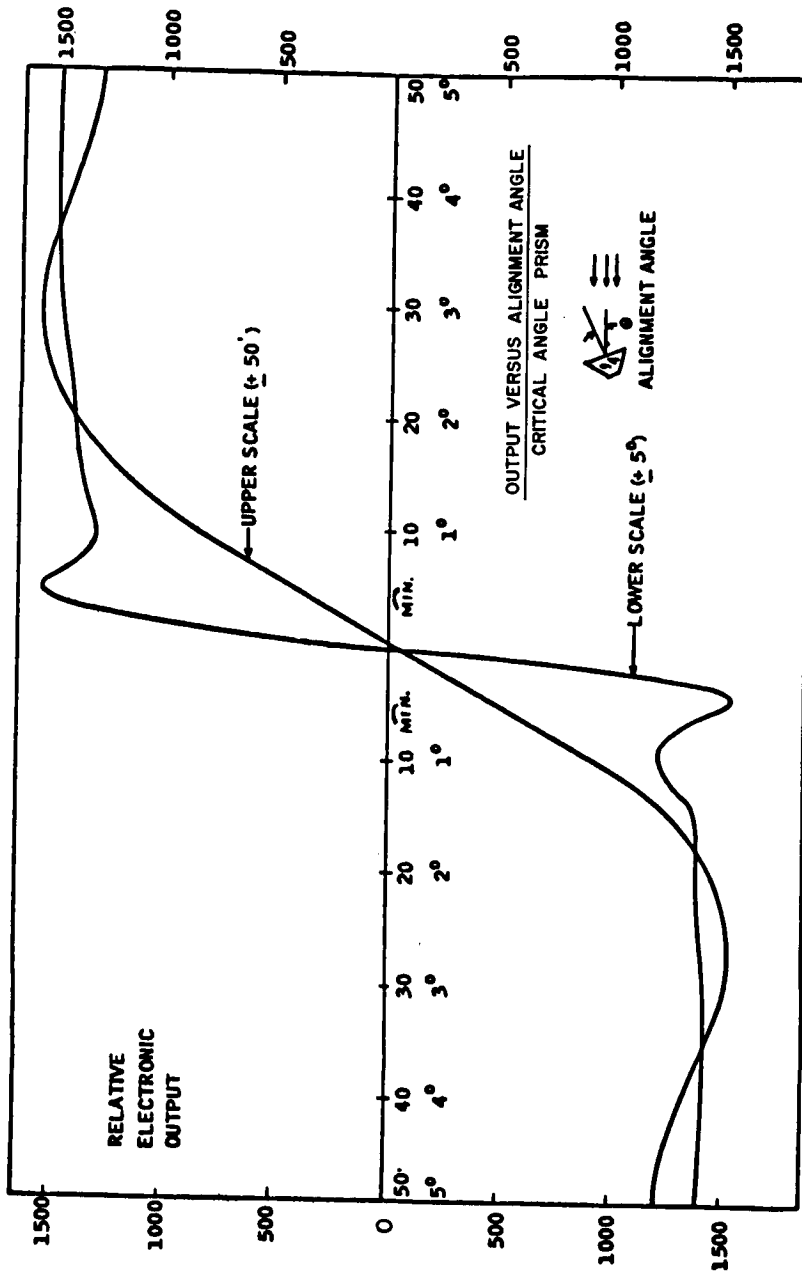
Figure 112 LIMIT CYCLE SUN SENSOR -- OUTPUT VERSUS ANGLE

63-9297

-300-

The star tracker's detector is an image dissector photomultiplier (PM) tube which electronically scans its sensitive surface along two orthogonal scan paths. The scan paths cross at the center of the sensitive area. If the star image is centered, the pulse train from the PM tube will be symmetric and all pulses will be of identical width. If the star is not centered, the pulse train will be asymmetric, and pulses will be of unequal width. By splitting the PM tube output pulses into azimuth and elevation (X and Y) components, a sufficient amount of information is available to determine the star image position. To obtain an analog signal, the roll error is synchronously demodulated at the scanning frequency. If the error is zero the signal will be a second harmonic and is filtered out. For a nonzero error, the filtered signal amplitude is proportional to error magnitude, and the phase gives roll error direction. To obtain digital error signals, the PM tube output pulses (after being split into azimuth and elevation components) are used together with scan reference signals to control an up-down binary counter. During the first half of the scan cycle, the counter counts up only while the PM tube output is above an established threshold. The counter output at the end of a scan cycle is proportional to the difference in pulse width for the two halves of the scan cycle. If the star is centered, all pulse widths are the same and the up count equals the down count. If the star is not centered, the difference in pulse widths, which is proportional to star position, will be in the counter and available to the DCU. To accommodate the apparent motion of Canopus during heliocentric orbit (Canopus is not a pole star), the stepper motor is energized to reposition the gimbal mirror whenever the error in the pitch axis exceeds a certain preset level; e.g., twice the limit cycle magnitude.

The gimbal readout consists of a coded wheel rigidly attached to the mirror gimbal shaft, a light source with collimating optics, and a photodetector with associated pulse amplifier electronics.

This method is preferred over using a prepackaged gimbal readout to realize a savings in mechanical moving parts since prepackaged readouts have additional bearings and shafts which are not necessary in this application.

The gimbal readout system is a "serial" rather than "parallel" readout which requires knowledge of some reference or starting point from which to start counting. A special loop has been provided to enable the gimbal to acquire the reference position on command from the DCU.

The mechanical configuration of the tracker is shown in figures 113 and 114.

FOLDING MIRRORS

ELECTRONIC
CIRCUIT
AREA

LENS ASS'Y

SUN SHIELD

I.T.T. IMAGE
DISSECTOR
PHOTO-
MULTIPLIER
TUBE

40°

40°

SPIROID GEAR SET

STEPPING MOTOR

HIGH VOLTAGE
SUPPLY

TRACKING MIRROR

CYLINDRICAL WINDOW
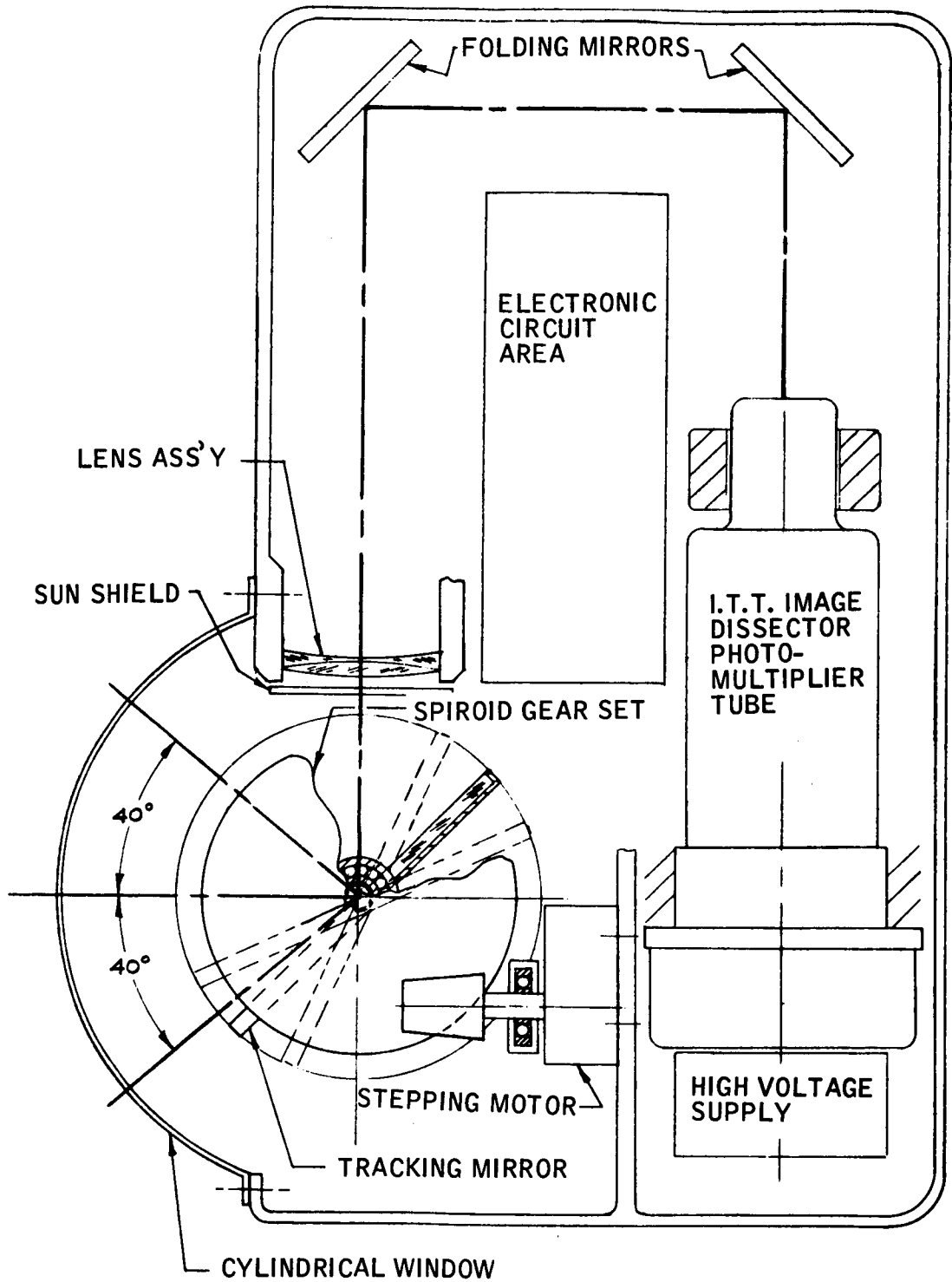
Figure 113 CANOPUS STAR TRACKER -- SIDE VIEW

LIGHT
SOURCE

CODED DISK

ELECTRONICS-PHOTO COUNTER

GIMBAL AXIS

ELECTRO-OPTICAL READOUT
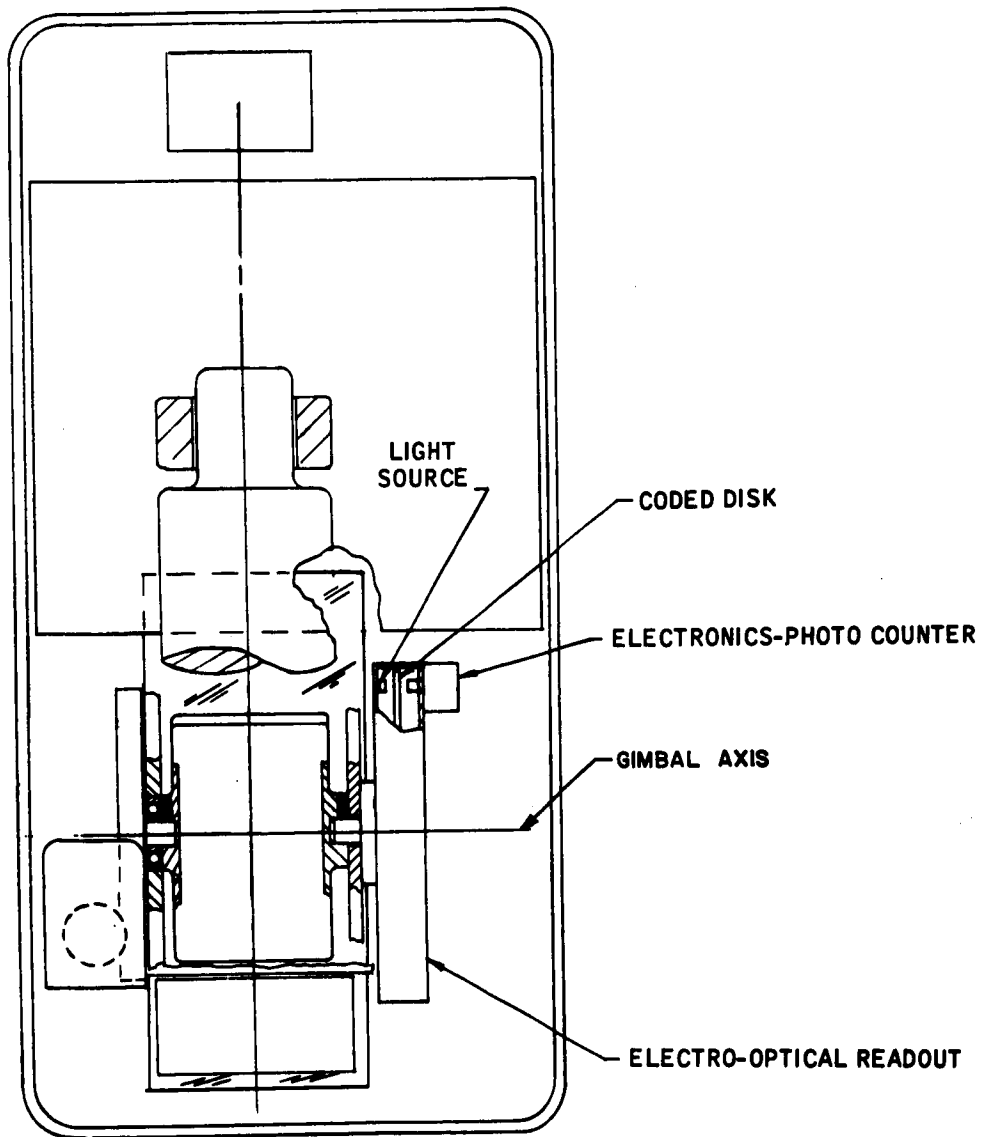
Figure 114 CANOPUS STAR TRACKER -- TOP VIEW

The Canopus star tracker characteristics and capabilities are:

Weight:	seven pounds
Volume:	350 cubic inches, one package
Power:	7.2 watt
MTBF:	64,500 hours (includes gimbal duty cycle)
Accuracy:	20 arc-seconds
Instantaneous field:	±1.5 degrees each axis
Total field:	±1.5 degrees roll
	±18 degrees pitch

j.   Reaction system.   The reaction system proposed at the present time for Voyager is a nitrogen cold gas system as shown in figure 115. The reasons for selecting this system and detailed weight and volume breakdowns are given in the tradeoff study section of this document. General characteristics of the system are given below.

Total system weight	53 pounds
Total system volume	2795 cubic inches
Jet thrust	0.03 lb/jet (twelve jets used)
I_{sp}	60 seconds
Storage pressure	3000 psi
Tank size	13.7 inches OD (two tanks used)
Tank weight	11.6 pounds each
Tank volume	1360 cubic inches each
Nitrogen volume	2580 cubic inches total
Tank material	titanium
Jet valve power required	approximately 100 ma at 28 volts
Tubing	3/16 inch OD stainless
Reliability	0.9997 (based on 11,160 hours operation)

The reaction system component failure rates are shown in the reliability analysis section.
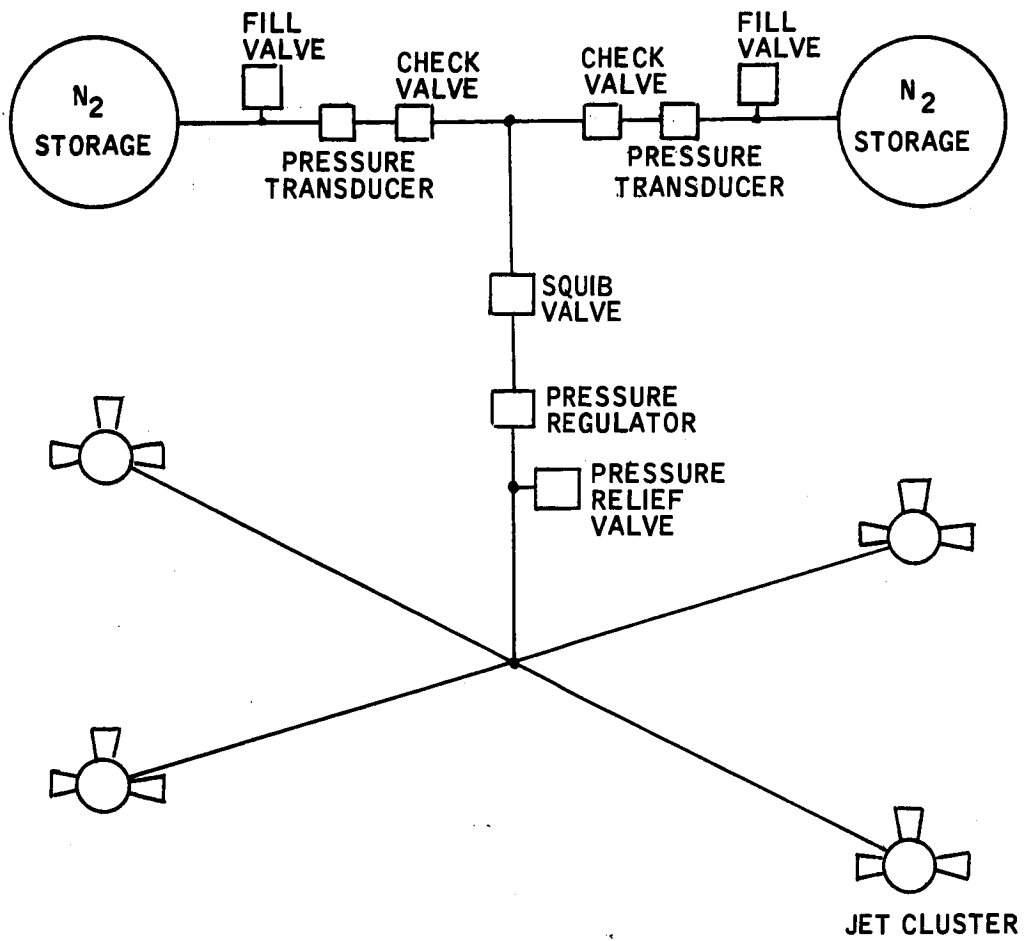
Figure 115 REACTION SYSTEM FUNCTIONAL DIAGRAM

k.   Gyro and control electronic packages.

1)   Electronics mechanization. Circuit concepts compatible with the requirements and design techniques used in microminiature circuit fabrication are developed wherever feasible throughout the gyro and control electronics.

The physical design for the active circuit elements, is based on the use of integrated circuits which should become available as standarized analog building blocks (functional electronic blocks) within the next two years. It is recognized that drawbacks such as limited accuracy still exist in the summing and feedback elements, within the integrated silicon block, and that any requirement for large capacitors in some shaping networks cannot be met now, or in the foreseeable future. To overcome these limitations, a marriage of thin-film techniques for the feedback and summing networks will be combined with the active microcircuit elements to form the complete system.

Present design status indicates that the required functional electronic blocks will be available in the necessary quantity by the end of 1965. However, in the event of an unforeseen lack of progress in semiconductor technology, the required active circuits could also be constructed using presently available pico semiconductor packages. Little overall effect on system size or power would result if the thin-film deposited circuit elements and pico-sized component versions of the active elements are used.

The major blocks of the gyro and control electronics are briefly described in the following paragraphs. At this time it is not practical to exactly define the circuits required for the SCS, but the circuits have been detailed to the extent necessary for realistic size, weight, power, and reliability estimates. The functional block diagrams for the control electronics and the gyro electronics packages are shown in figures 116 and 117, respectively.

2)   Control electronics. The control electronics provide the elements necessary to process the error input signals from the gyros or optical sensors and command the appropriate reaction jets when the preset deadband of the on-off level switch is exceeded. The phase of the error signal determines which polarity of jets is to be energized. The amplitude of the error signal determines when the deadband is exceeded. The mechanization chosen for the control electronics uses an ac (square wave) summing technique at the input to the switching amplifier. The conversion from dc to ac (square wave) is accomplished by simple, single half-wave chopper transistors which also function as mode control switches when energized continuously.

The following elements make up the control electronics: active lead-lag circuit; switching amplifier; peak reading half-wave voltage detector; low hysteresis switch (LHS); lag feedback circuit (for pseudo rate); jet solenoid driver; control electronics power supply; and mode command logic.

-306-
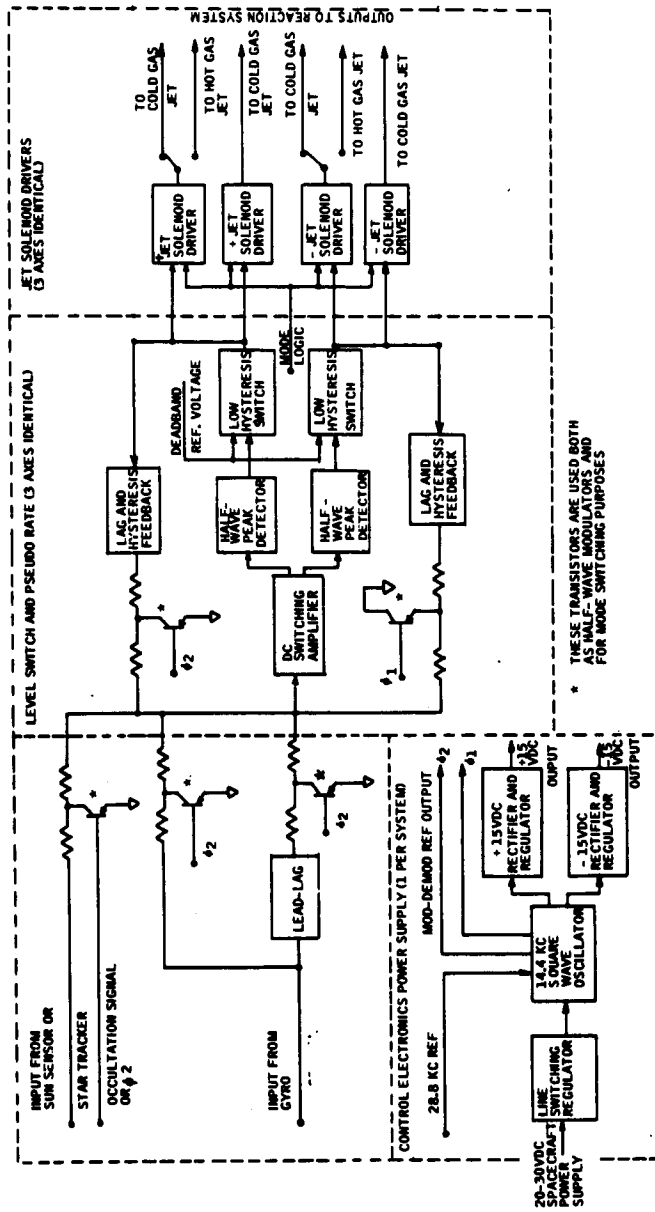
Figure 116 BLOCK DIAGRAM OF CONTROL ELECTRONICS PACKAGE

63-9301

-307-
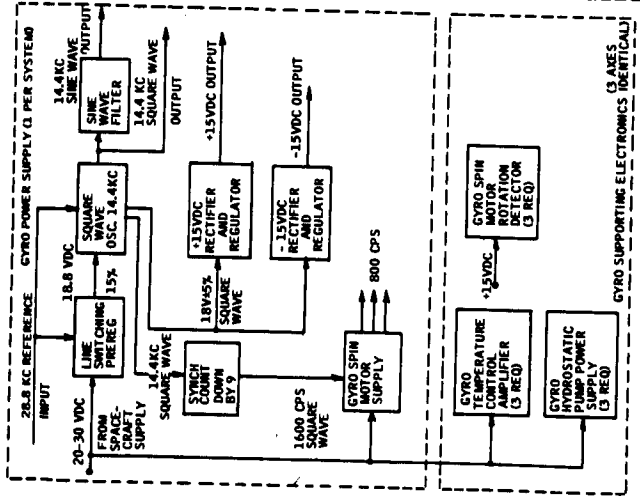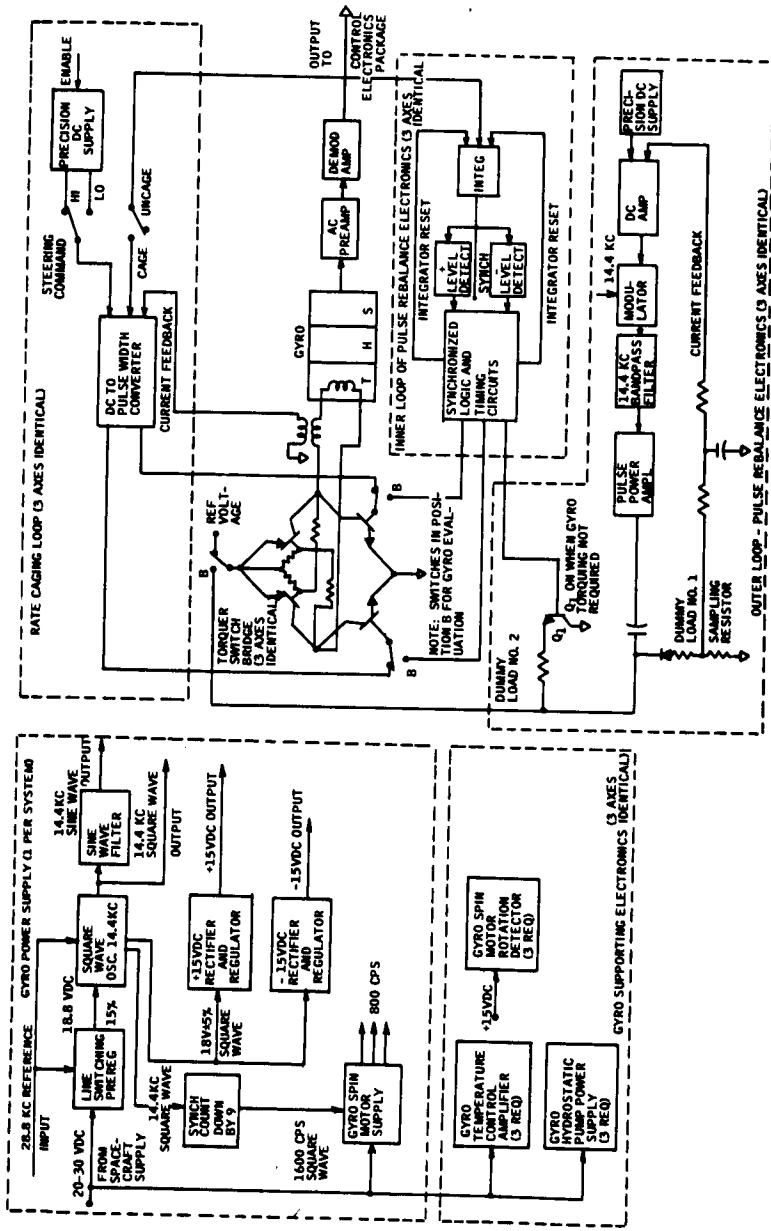
Figure 117 BLOCK DIAGRAM OF GYRO/ELECTRONICS PACKAGE

63-9302

-308-

3) <u>Gyro electronics.</u> The gyro electronics provide the elements necessary to control the gyros in the rate, attitude, and gyro evaluation configurations and to supply an output error signal to the control electronics. The mechanization of these circuits uses ac, dc, and pulse techniques to attain the required accuracy and interface with the DCU with a minimum of circuits.

The following elements shown in figure 117 make up the gyro electronics: rate caging electronics; pulse rebalance electronics; and gyro auxiliary electronics.

4) <u>Packaging.</u>

a) <u>Control electronics package.</u> The control electronics will be packaged as a separate unit. This unit is envisioned as a simple hard-mounted package with the electronics designed as plug-in subassemblies replaceable by function.

b) <u>Gyro electronics package.</u> The gyro electronics will be contained within the outlines of the gyro mounting block. Locating the gyro electronics on the mounting block creates a relatively stable temperature environment compatible with the use of integrated circuits. The electronics will be designed as plug-in subassemblies replaceable by function.

c) <u>Summary.</u> The gyro and control electronics package characteristics are summarized in table 32C.

<u>TABLE 32C</u>

GYRO AND CONTROL ELECTRONICS PACKAGE CHARACTERISTICS

Item	Volume (in^3)	Weight (lb)		Power Required (watts)	
				Steady-State	Peak
Control Electronics Package	125	3.0		2.5	
Gyro/Electronics Package	245	10.0		31.0	
Gyros (3)			3.00	9	
Casting (1)			1.25		
Harness and Mounting			0.50		
Power Supply (1)			1.25	1.0	
Caging Electronics (3)			1.00	2.0	
Pulse Rebalance Electronics (3)			2.00	10.0	
Temperature Control Electronics (3)			1.00	9.0	90*
Totals	470	13.0	10.00	33.5	31.0

*Gyro warmup power-twenty minutes maximum

1. Size, weight, and power characteristics. The SCS size, weight, and power characteristics are summarized below in table 32D for the system without redundancy.

TABLE 32D

SCS SIZE, WEIGHT AND POWER SUMMARY

Item	No.	Volume (in³)	Weight (lb.)	Power (watts)	
				Steady State	Peak
Gyro/Electronics Package	1	245	10.0	31.0	90*
Control Electronics Package	1	125	3.0	2.5	
Canopus Star Tracker	1	350	7.0	7.2	
Limit Cycle Sun Sensor	1	13	1.5	0.5	
Coarse Acquisition Sun Sensor	1	4	0.44	0.35	
Reaction System	1	2795	53.0		20**
Totals		3532	75.0	41.6	

*Gyro warmup power - 20 minutes maximum

**Reaction jet solenoids estimated at three watts each. Six jets could possibly be on simultaneously during initial acquisition for periods of one to two minutes. Otherwise jet operating duty cycle is so small as to make average power negligible.

3. Total impulse requirements. Table 33 lists the total impulse requirements resulting from the various SCS functions and external disturbances during the mission. The assumptions and calculations on which these figures were based appear in appendix I.

TABLE 33

MARS MISSION IMPULSE REQUIREMENTS

Item	Total Impulse (Pound-Seconds)
1. Initial Acquisition	58
2. Cruise Limit Cycling Plus Solar Pressure	52
3. Orientations	165
4. Payload Indexing	120
5. Gravity Gradient	97
6. Meteorites	164
7. Magnetic Field	0
Total	656

6.4 System Tradeoffs

A number of tradeoff studies were made in the process of defining the SCS proposed in this document. The five specific studies made and reported in this section are the following: 1. SCS configuration; 2. reaction systems; 3. onboard or ground switchover of redundant SCS circuits; 4. sun sensors; and 5. Canopus star trackers.

These studies are discussed in the following paragraphs.

1. **SCS configuration.** The SCS configuration tradeoffs concern choices pertaining to use of the DCU and to the selection of gyros. The DCU tradeoff involves an analog system which makes minimum use of the DCU as opposed to a digital system which makes maximum use of the DCU. The gyro tradeoff considered a digital system using either floated integrating gyros or electrically suspended gyros (ESG's). The tradeoff areas therefore involves the following three system configurations: an analog system using integrating gyros; a digital system using integrating gyros; and a digital system using ESG's. The tradeoff areas of the above system configurations are illustrated in figure 118.

The following criteria define the choice of an SCS: weight; size; power requirements; reliability; and development status. As is shown in the following study, the logical choice is the analog system using integrating gyros. This is the system chosen and detailed in this document.

a. **Digital versus analog SCS.** A comparison is made here of the digital and analog systems. Both systems use GG159 floated integrating gyros and optical sensors for obtaining vehicle rate information and attitude reference. The associated gyro electronics for each system, although functionally different, are comparable with respect to the criteria listed above.

The tradeoff areas, as shown in figure 118 are, optical sensor interface with the SCS, SCS loop stabilization, and jet control logic.

1) **Optical sensor interface.** In the analog version the inputs from the optical sensors are connected to on-off amplifier summing junctions. In the digital system, the sensors interface with the digital computer; therefore, an analog-to-digital converter is required in order to convert the sun sensor analog signal to a digital signal. In the present design, the Canopus tracker is provided with both digital and analog outputs; therefore, only the output failure rates enter into the tradeoff considerations. The output failure rates are nearly equal: 1.505 percent/1000 hours for the analog output and 1.535 percent/1000 hours for the digital readout.

2) **SCS loop stabilization.** Both versions of the SCS require vehicle angular rates for the SCS loop stabilization. In the analog system, these
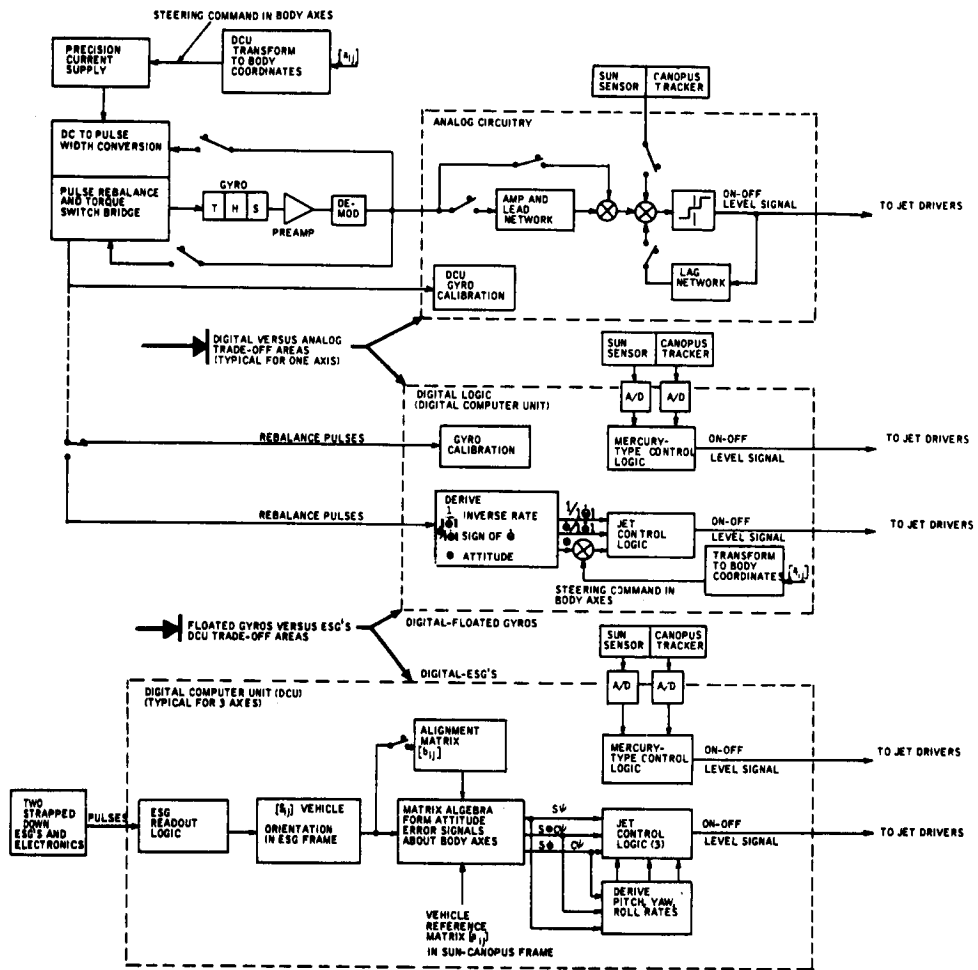
63-9303

Figure 118 SCS BLOCK DIAGRAM: DIGITAL VERSUS ANALOG VERSUS
ESG-DIGITAL SCS TRADEOFF AREAS

-312-

rates are obtained through active lead-lag networks when attitude reference is provided by the gyros. When the attitude reference is derived from the optical sensors, then the SCS loop stabilization is achieved by pseudo rates which are obtained through first-order lag networks connected in the feedback path of the on-off switching amplifiers.

In the digital version, if the attitude reference is provided by the gyros, the corresponding vehicle rates are derived by the DCU through differentiation of the attitude signals. With optical sensor inputs, the digital system requires only the type of control logic used in the Mercury spacecraft SCS. This method needs only the sign of the vehicle rate for stabilization, which is determined by the DCU.

     3) <u>Jet control logic.</u> In the analog version, the jet control logic is conveniently handled by the on-off switching amplifiers (one per axis). In the digital system, the jet control logic consists of two separate blocks of logic statements provided by Project Mercury-type control logic using attitude error and the sign of vehicle rate and conventional jet control logic using the sum of rate and attitude.

     4) <u>Tradeoff evaluation summary.</u> The three tradeoff areas discussed above were evaluated in terms of weight, size, power, reliability, and development status. The results are given in table 34, which shows that the analog SCS is superior to the digital SCS on a basis of weight, size, power, and reliability.

    b. <u>Electrically suspended gyros (ESG) versus integrating gyros.</u> The tradeoff areas between the SCS using ESG's and the SCS using integrating gyros are shown in figure 118. In general, the tradeoffs are the following: integrating gyro versus ESG and associated electronics; and comparison of the DCU computational requirements for the respective systems.

The tradeoffs in terms of size, power, weight, reliability, and development status appear in tables 35 and 36.

The ESG attitude reference approach warrants a tradeoff study because of the following advantages which ESG's offer over conventional floated integrating gyros: a strapped-down ESG has no attitude or rate limitations due to vehicle maneuvering; long life potential due to nonmechanical coupling of moving parts; high accuracy; and future ESG's may be able to add an acceleration measurement capability to their attitude reference function which would eliminate the accelerometer package and reduce the associated alignment problems. Present disadvantages of the ESG's are their size, weight, and power requirements.

TABLE 34

ANALOG VERSUS DIGITAL SCS TRADEOFF SUMMARY

Parameter	Analog SCS	Digital SCS
Parameter	3 on-off switching amplifiers 3 DC amplifiers and lead networks 3 Pseudo rate networks	DCU increase due to: 1 Sun sensor A/D, Jet control logic, Attitude signal processing
Weight (lb.)	0.08	1.0
Size (cu. in.)	1.56	45.0
Power (watts)	1.04	2.0
Reliability (percent failed per 1000 hours)	1.557[1]	1.965[2]
Development Status	Off-the-shelf equipment	Off-the-shelf integrated circuits

Note: Above is typical for three axes.

The DCU performs the sun sensor analog-to-digital function.

The jet control logic for the digital system is discussed in the section below.

[1]Includes Canopus tracker failure rate with analog readout.

[2]Includes Canopus tracker failure rate with digital output.

c. Tradeoff evaluation summary. From tables 35 and 36, the gyro requirements and the SCS are observed to be greater with the ESG's than with the analog approach using integrating gyros. The ESG approach also reduces computer and SCS reliability for this mission. Therefore, ESG's are not recommended.

2. Reaction systems.

a. Qualitative comparison of systems. In selecting the reaction system for Voyager an evaluation was made of the following approaches:

Mass Expulsion Systems	Momentum Transfer Systems
Cold gas jets	Reaction wheels
Sublimation jets	Control moment gyros
Hypergolic jets	Fluid flywheels
Monopropellant jets	Reaction spheres
Detonation jets	
Vapor jets	

To reduce the number to the most likely contenders in each of the above groups, a qualitative evaluation of all systems was made. This was done by itemizing advantages and disadvantages of each and making a selection based on this information. The advantages and disadvantages considered for each of the systems are given in the following paragraphs.

1) Mass expulsion systems.

a) Cold gas jets.

Good history of performance on other vehicle such as Mariner.

Most developed and proved system of those considered.

Components for the system are readily available.

Thrust range covers Voyager requirements.

High reliability since it is a simple system.

TABLE 35

GYRO COMPARISON: ESG'S VERSUS INTEGRATING GYROS

Parameter	Three GG1 59 Gyros and Associated Electronics	Two ESG's and Associated Electronics
Weight (pounds)	10	21
Size (in.^{3})	245	340
Power* (watts)	Warm up - 90	4
	Running - 31	
Reliability (percent failed per 1000 hours)	12.70**	83.0**
Development status	Off-the-shelf Equipment	The unit is in the study and development stage for space vehicle application

*Total mission power requirements are:
 	
   3 GG1 50 gyros - 122 kw-hr.
 	
   2 ESG's - 448 kw-hr.		

**These failure rates include no redundancy.

TABLE 36

DCU COMPARISON: ESG VERSUS INTEGRATING GYROS

Parameter	GG159 Gyros Including Gyro Calibration, Derive $\dot{\theta}$, $\dot{\theta}/|\dot{\theta}|$, $1/|\dot{\theta}|$ Transform $[a_{ij}]$ to body coordinates	ESG Including ESG Read Out Logic, Compute $[S_{ij}]$ Compute $[b_{ij}]$ Compute att. error about body axes; $[A_{ij}]$ Derive pitch, yaw, roll rates
Size (in. ^{3})	45	107
Weight (pounds)	1.0	4
Power (watts)	2.0	9 - 12
Reliability (percent failed per 1000 hours)	1.965*	2.721*
Development status	Off-the-shelf equipment	Off-the-shelf integrated circuits
Note: The numbers in the table are the increase in DCU requirements over those for the analog SCS. The DCU computational requirements for the ESG-SCS were determined from the mathematical functions which are discussed in the following section.		

*Includes Canopus tracker failure rate

Power is needed only for jet solenoids and this can be low (100 ma at 28 volts dc typically).

Highest weight system (by a factor of two or three) of those considered.

Approximate system weight = 7 lb + (0.034) x (total impulse).

Probably lowest cost system of those considered.

b) Sublimation jets

Not much actual operating history available at present.

There are systems operating in laboratory but none are yet flight-rated.

Thrust ranges satisfactory.

Should have excellent reliability since it is the least complex system considered.

Low power requirement, comparable to cold gas system.

Should weigh less than half of comparable cold gas system due to lower tankage weight and higher specific impulse.

Approximate system weight = 7 lb + (0.013) x (total impulse).

Cost probably somewhat higher than cold gas but should be less than others considered.

May require additional heaters during peak demand periods.

May present unusual pre-flight checkout problems.

c) Hypergolic bipropellant jets

Not recommended at the present time for thrust levels below about one pound due to orifice clogging problems.

Requires tankage, plumbing, valving, etc., for both fuel and oxidizer. Positive expulsion tanks necessary.

Reliability somewhat lower than cold gas or sublimation due to added complexity.

Combustion byproducts could be undesirable.

Volume and weight should be considerably lower than cold gas and somewhat lower than sublimation when based solely on total impulse requirements. Approximate system weight = 11 lb + (0.004) x (total impulse).

Nozzles would require heat transfer considerations due to heat of combustion.

d) Monopropellant jets.

Not recommended for extended missions due to possible chemical instability of monopropellants such as hydrazine and hydrogen peroxide.

May have catalyst and clogging problems, particularly on extended missions.

Thrust range satisfactory.

Weight probably slightly more than hypergolic system.

e) Detonation jets.

Present stage of development not adequate for detailed consideration.

System could have the required low thrust necessary.

Other characteristics would be similar to the hypergolic system.

f) Vapor jets.

Present state of development unsatisfactory.

Thrust range probably satisfactory. Weight comparable to a hypergolic system. May require the addition of heat to propellant.

2) <u>Momentum exchange systems</u>

    a)   <u>Reaction wheels.</u>

        Good history of performance on vehicles such as Nimbus, OGO, OAO.

        Proposed for use on OSO. Most developed and proven of those considered. Production units presently available.

        Characteristics such as torque, inertia, and power consumption may be varied rather widely.

        Reliability apparently very good due to reasonably low speeds, sealed units, over-design, etc. The failure rate estimate is 0.1 percent per 1000 hours for a typical Bendix unit.

    b)   Control moment gyros.

        Less history of performance and application data available than reaction wheels. Present availability questionable.

        Weight probably slightly higher than reaction wheel.

        Reliability lower than reaction wheel due primarily to higher wheel speeds. Torquer also degrades the reliability. Estimated failure rates are 10 to 20 percent per 1000 hours for ball bearing and 2 percent per 1000 hours for gas bearing units.

        Temperature control may be necessary.

        Cross-coupling effects can cause problems. Compensation for these effects could delete any advantages.

        Torque control power is very low, but gyro wheel power must remain on continuously. Average power consumption probably not much less than that for reaction wheels.

    e)   <u>Fluid flywheel.</u>

        Presently in laboratory development stage.

        Little application data available.

Weight probably higher than either reaction wheels or control moment gyros. Possible lower power consumption might balance this out so that over-all vehicle weight could be the same or less for fluid flywheel system. Reliability should be high as the fluid is the only moving part. Magnetic fields generated by the pump currents could be a problem.

Flexibility of location of the fluid loop could be an advantage.

d)   Reaction sphere.

Presently in laboratory development stage.

b.   Quantitative comparison of systems. From the preceding qualitative comparison the following conclusions were drawn: If a mass expulsion system is necessary, then the cold gas, the hypergolic bipropellant, and the sublimation systems are possibilities. If a momentum exchange system is necessary then the reaction wheels appear as the best choice.

Examination of the mission impulse requirements (appendix I) shows that a mass expulsion system is definitely necessary. The desirability of using a momentum exchange system in addition to the mass expulsion system must be based on the choice of mass expulsion system and further analysis.

The possible reaction system configurations for consideration then are: cold gas system without reaction wheels; cold gas system with reaction wheels; hypergolic system without reaction wheels; hypergolic system with reaction wheels; sublimation system without reaction sheels; and sublimation system with reaction wheels.

For a quantitative comparison of the above configurations, a weight comparison study was made. Table 37 summarizes the results. The data in the table are derived and discussed in the following paragraphs.

TABLE 37

REACTION SYSTEMS WEIGHT COMPARISON

System	Without Reaction Wheels (lbs)	With Reaction Wheels (lbs)
Cold Gas	53	48
Hypergolic	236	34
Sublimation	24	38

1) <u>Cold gas systems</u>

a) <u>Cold gas jet system without reaction wheels.</u> The following assumptions were used (see appendix I for more details): 12-jet system; 8.3-foot radius moment arms for jets; Nitrogen gas used (I_{sp} of 60 seconds); requires total impulse of 1330 pound-seconds (safety factor of two included) (see appendix I for derivation); 3/16-inch O.D. stainless tubing for both high and low pressure; 3000 psia gas storage; spherical titanium storage tanks; jet thrust of 0.03 pound per jet; and jet minimum impulse time of 0.01 second.

Characterisitcs of the cold gas jet system evolved from the above assumptions are summarized in table 38 below.

TABLE 38

COLD-GAS JET SYSTEM CHARACTERISTICS

Item	Number	Item Weight (lb)	System Weight (lb)	Item Volume (in^3)	System Volume (in^3)
Regulator	1	0.50	0.50	15	15
Plumbing		3.00	3.00		12
Valve, solenoid, and nozzle	12	0.25	3.00	2.75	33
Charge valve	2	0.09	0.18	2.5	5
Transducer	2	0.25	0.50	2.5	5
Check valve	2	0.25	0.50	2.5	5
Nitrogen		22	22	2580	
Tank	2	11.6	<u>23.20</u>	1360	<u>2720</u>
Totals			52.9		2795

b) <u>Cold gas jet system with reaction wheels.</u> The same assumptions hold except that total impulse now required is 818 pound-seconds (safety factor of 2 included). The cold gas jet system under these assumptions is summarized below in table 39.

TABLE 39

CHARACTERISTICS OF COLD-GAS JET SYSTEM WITH
REACTION WHEELS

Item	Number	Item Weight (lb)	System Weight (lb)	Item Volume (in^3)	System Volume (in^3)
Fixed Items			7.7		75
Nitrogen		13.6	13.6	1600	
Tank	2	7.2	14.4	843	1646
Totals			28.0		1761

The reaction wheels for this system are based on the following assumptions: wheels used in pitch and yaw only since the savings possible in the roll are small; wheels have a momentum capability of 1.2 ft-lb-sec[1]; wheels have a torque capability of 0.1 ft-lb; and Bendix reaction wheels used as a basis for size, weight, and power estimates.

Based on the above assumptions, the required reaction wheel would weigh about eight pounds and consume about 4.5 watts peak power. The complete reaction wheel system weight then is summarized in table 40.

c) <u>Cold gas jet system comparison.</u> The systems with and without reaction wheels weigh:

<table>
<tr><td><u>Cold Gas Jet System
without Reaction Wheels</u></td><td colspan="3"><u>Cold Gas Jet System
with Reaction Wheels</u></td></tr>
<tr><td>Jet system weight = 53 lbs</td><td>Jet system weight</td><td>=</td><td>28 lbs</td></tr>
<tr><td></td><td>Reaction wheel system</td><td>=</td><td>20 lbs</td></tr>
<tr><td></td><td>Total</td><td></td><td>48 lbs</td></tr>
</table>

---

[1]Derived in the reaction-wheel analysis which follows.

TABLE 40

COMPLETE REACTION WHEEL SYSTEM WEIGHT

Item	Number	Item Weight (lb)	System Weight (lb)
Wheel	2	8	16
Electronics (Wheel drives, unloading)		0.5	1
Fittings		0.5	1
Power Source[1]		1	2
Totals			20

[1]Assumes that approximately 0.25 pound of solar panels, etc., is added to the vehicle per watt required.

It is observed that using the reaction wheels results in no significant weight savings. Coupling this with the lower reliability and additional complexity entailed when adding reaction wheels, the decision is for a cold gas jet system without reaction wheels.

2) Reaction wheel analysis. The sizing of the reaction wheel torque and momentum capability is shown below:

a) Torque. As shown by table I-7 (appendix H), the major contributors to cyclic torques are the gravity gradient torque and the payload indexing torque. The maximum value of each torque is found below:

1 Gravity gradient peak cyclic torque. This occurs about the vehicle Y axis and is found from

$$T_{y_{max}} = \frac{3 g R_P^2}{R^3} (I_z - I_x) B_y$$

where

$$\frac{3 g R_P^2}{R^3} = 3 \omega_o^2 = 3 (3.6 \times 10^{-7}) \text{ rad}^2/\text{sec}^2$$

$$I_z - I_x = 479 \text{ slug-ft}^2$$

and

$$B_y = \frac{1}{2}[(\cos\psi \sin E \cos E)^2 + (\sin\psi \cos E)^2]^{1/2}$$

B_y = maximum cyclical torque component

letting

$\psi = \pi/8$ and $E = \pi/4$,

$B_y = 0.269$

then

$$T_{y_{max}} = 3(3.6 \times 10^{-7})(479)(0.269) = 1.4 \times 10^{-4} \text{ ft.-lb.}$$

2 Payload indexing peak cyclic torque.

Referring to the payload indexing section of appendix H, the peak disturbing torque from payload indexing is 3.52×10^{-3} ft-lb or over 25 times the peak gravity gradient torque. The payload indexing torque is therefore used for sizing the reaction wheels.

A reasonable value of 0.1 ft-lb for torque is assumed for the wheel torque capability. This places the wheel within the realm of commerically available wheels as far as torque is concerned, and at a level of one-fifth of the jet torque couple which is 0.5 ft-lb.

b) Momentum.

The cyclic momentum requirements for Voyager occur principally from the gravity gradient and payload indexing effects. For either case, the momentum for a half cycle must be absorbed by the reaction wheels, and is found from the general relationship: Momentum absorbed per half-cycle = (average torque per half-cycle) x (time per half-cycle).

1 Gravity gradients.

For gravity gradients, there are two nulls per Martian orbit, so the time for a half-cycle is one quarter of the Martian orbital period, or $\frac{26,600}{4}$ = 6625 seconds. The average torque per half cycle is:

$$T_{avg} = \begin{matrix}\text{max. torque for} \\ \text{a circular orbit}\end{matrix} \times \frac{\text{torque for elliptical orbit}}{\text{torque for circular orbit}} \times \frac{\text{average torque}}{\text{maximum torque}}$$

$$= (1.4 \times 10^{-4}) \times (0.223) \times (0.628) = 1.96 \times 10^{-5} \text{ ft-lb}$$

The momentum absorbed per half-cycle is then $T_{avg} \times$ time $= (1.96 \times 10^{-5})$ $\times (6.63 \times 10^3) = 0.130$ ft-lb-sec.

2   Payload Indexing. For payload indexing, the torque is constant at 3.52×10^{-3} ft-lb and a half cycle requires 263 seconds. The momentum absorbed per half-cycle is then:

$$T \times t = (3.52 \times 10^{-3}) \times (263)$$

$$= 0.925 \text{ ft-lb-sec}$$

The momentum absorbed from payload indexing is seen to exceed the momentum absorbed from gravity gradient by a factor of 7.1. The payload indexing momentum is therefore used to size the reaction wheel.

A value of 1.2 ft-lb-sec is assumed for the wheel momentum capabilities. This again is within the realm of commercially available wheels and provides a factor of safety of 1.3.

3)   Hypergolic systems. For the hypergolic jet system without reaction wheels, the following assumptions were made: 12-jet system; 8.3-foot radius moment arm for jets; total impulse of 56,280 pound-second is required (safety factor of 2 included) (derived in the hypergolic system weight analysis which follows); jet thrust of 1.0 pound per jet; jet minimum impulse time of 0.01 second; and specific impulse of 250 seconds.

The hypergolic jet system evolved from the above assumptions is summarized below.

Item	Weight (lb)
Fixed items (plumbing valves, solenoids, jets, etc.)	11
Tanks, fuel, and oxidizer	225
Total	236

This high weight is primarily due to the high propellant requirements. This, in turn, is due to the high thrust level (1.0 lb) required for reliable operation of a hypergolic engine. Lower thrust levels could lead to orifice clogging problems and should not be considered.

a) <u>Hypergolic jet system with reaction wheels.</u> The same assumptions hold except, total impulse now required is 818 pound-seconds (safety factor of 2.0 included) (see mission impulse requirements section for derivation). The hypergolic jet system under these assumptions is summarized below.

Item	Weight (lb)
Fixed items (plumbing, valves, solenoids, jets etc.)	11
Tanks, fuel and oxidizer	3.3
Total	14.3

The reaction wheels for this system would be identical to those previously assumed for the cold jet system. (Reaction wheel system total weight is 20 pounds.)

b) <u>Hypergolic jet system comparison.</u> The systems with and without reaction wheels have the following weights:

Hypergolic Jet System without Reaction Wheels	Hypergolic Jet System with Reaction Wheels	
Jet system weight = 236 lb.	Jet system weight	= 14.3 lb.
	Reaction wheel system	= 20 lb.
	Total	34.3 lb.

On the basis of weight alone, the hypergolic jet system with reaction wheels is by far superior to the hypergolic system without reaction wheels. However, the additional complexity and degraded reliability of the over-all system must be taken into account.

4) <u>Hypergolic system weight analysis.</u> To obtain the hypergolic system weight it is necessary to first obtain the total impulse required for the mission. In general, this will differ from that of the cold gas jet system in the limit cycle regime if different thrust jets are used, since the limit cycle rate and period will change. If the minimum jet on-time and jet torque arms are the same for both systems, then the limit cycle impulse required will vary as the square of the thrust ratios, hypergolic to cold gas.

For this analysis it is assumed that the hypergolic jet thrust level is one pound and the minimum on-time is 0.01 second. These assumptions are considered to be optimum for hypergolics at the present time. Lower thrusts could possibly present jet orifice clogging problems while shorter on-times require more complex drive circuits and also result in reductions in specific impulse. Further analysis of these areas was considered beyond the scope of this study.

For the above assumptions the impulse required for limit cycling becomes

$$\left[\text{impulse (cold gas)}\right] \quad \text{x} \left(\frac{\text{hypergolic jet thrust}}{\text{cold gas jet thrust}}\right)^2 = 25\ (33.3)^2$$

$$= \quad 27,500 \text{ pound-seconds}$$

and the total impulse required (including maneuvers and disturbances) becomes 27,500 + 630 = 28,130 lb-sec. Using a safety factor of 2, the total required impulse is 56,270 lb-sec.

The approximate system weight for a hypergolic system with an I_{sp} of 250 seconds is 11 lb + (0.004 x impulse required). Therefore the system weight is approximately 236 pounds.

Figure 119 indicates the trend in system weight as a function of jet thrust and minimum jet on-time for this system. Reduction in jet thrust and/or the minimum jet on-time will reduce the system weight.

5) Sublimation systems.

a) Sublimation jet system without reaction wheels. The following assumptions were made: 12-jet system; 8.3-foot radius moment arm for jets; total impulse of 1330 lb-sec required (safety factor of two included); jet thrust of 0.03 pound per jet; jet minimum on time of 0.01 second; and specific impulse of 85 seconds. The sublimation jet system weight based on the above assumptions is summarized below.

Item	Weight (lb)
Fixed items (plumbing, valves, solenoids, jets, etc.)	7
Tank and propellant	17[1]
Total	24 pounds

---

[1]Derived from manufacturer's data on a laboratory-tested sublimation system. Tank plus propellant weight is approximately equal to 0.013 × (required impulse).
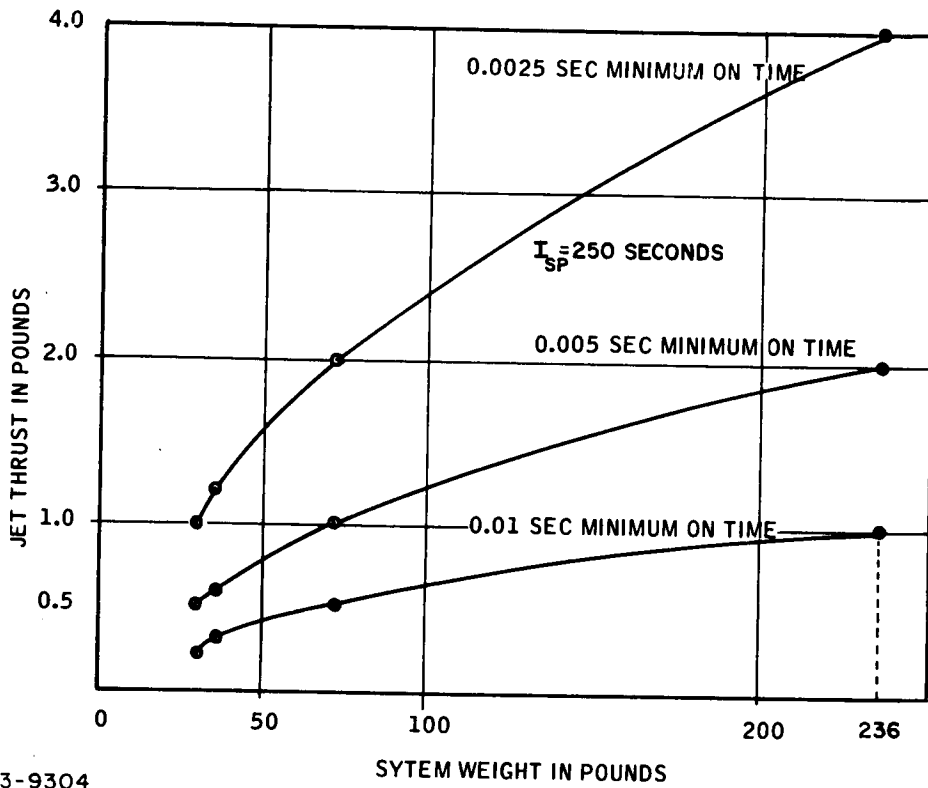
Figure 119   JET THRUST VERSUS SYSTEM WEIGHT FOR HYPERBOLIC SYSTEMS

63-9304

-328-

b) <u>Sublimation jet system with reaction wheels.</u> The same assumptions hold except that total impulse now required is 818 lb-sec (safety factor of two included). The sublimation jet system weight under these assumptions is summarized below.

Item	Weight (lb)
Fixed items (plumbing, valves, solenoids, jets, etc.)	7
Tank and propellant	<u>10.7</u>
Total	17.7 pounds

The reaction wheels for this system would be identical to those previously assumed for the cold gas jet system. (Reaction wheel system total weight is 20 pounds.)

c) <u>Sublimation jet system comparison.</u> The systems with and without reaction wheels have the following weights:

Sublimation Jet System without Reaction Wheels	Sublimation Jet System with Reaction Wheels	
Jet system weight = 24 lb.	Jet system weight	= 18 lb.
	Reaction Wheel system	= 20 lb.
	Total	38 lb.

The addition of reaction wheels with a sublimation system causes a weight penalty and was therefore not considered further.

6) <u>Summary.</u> For the six reaction systems described, the preceding analysis has narrowed down the choice to one of the following three:

Cold gas systems without reaction wheels (53 pounds)

Hypergolic system with reaction wheels (34 pounds)

Sublimation system without reaction wheels (24 pounds)

Additional points for future consideration are presented below and should be taken into account before a final decision is made.

a) <u>Cold gas jet system.</u> It is important to observe that future weight shaving on this system appears to be slight. Some improvement can be achieved by changing to other gases, but the gain is small.

The simplicity, reliability, availability, and operational history are firm selling points.

The ease of testing the entire system at pre-launch is an important factor for consideration.

b) <u>Hypergolic jet system with reaction wheels.</u> Important considerations are a weight saving of 19 pounds over the cold gas jet system can be achieved with this system (34 pounds instead of 53 pounds). However, the reduced reliability or probability of mission success due to added complexity of this dual system would have to be considered. Testing a hypergolic system presents many problems not present with a cold gas system.

c) <u>Sublimation jet system.</u> Note that lowest weight, simplicity and high reliability are this systems prime attractive points.

Lack of operational data is a serious drawback at present, but this may well be corrected by the time the Voyager system must be firm.

System operating pressure must be considered. A present manufacturer specifies a system propellant pressure of about one-half atmosphere. This pressure would cause serious test and prelaunch irritation, if not problems, since the system would require vacuum chambers for observation of propellant flow.

7) <u>Summary.</u> In view of the weight tradeoffs and all other pertinent factors, the decision is to presently consider a cold gas reaction jet system for Voyager.

3. <u>Onboard versus ground switching for failure correction.</u> At this point in the Voyager program it does not appear possible to show a preference for onboard or ground-based failure correction since the decision is so dependent on the over-all vehicle and its subsystem configuration. A few considerations involved in the decision are presented to briefly review what is involved.

The considerations involved in onboard versus ground-based switching for failure correction tie in very closely with possible telemetry configurations. If many signals are to be telemetered to Earth, then it may be possible to conduct performance and failure analyses on Earth and send switching commands back to the vehicle through the telemetry link. This concept would require carrying standby components, such as gyros, power supplies, rebalance electronics, etc., and switching them in by ground command in the event of failures.

The other alternative (if standby redundancy is necessary) is to carry standby components and monitor performance either within the SCS itself by monitor circuits or by having the DCU monitor performance. If the SCS does its own monitoring, then it could perform its own switching functions. If the DCU does the monitoring, then it could command switching. The Earth-based system has advantages of weight saving since the monitoring and analysis are not done on board. The weight of telemetry may very well be the same since it may be necessary to telemeter failure information to Earth regardless of whether monitoring and switching are done onboard or not. The disadvantage of the Earth-based system is the amount of telemetry necessary, the communication time delays, and the fact that telemetry reliability would enter into the series chain of SCS success probability.

The best system might be to have the DCU monitor and command on-board switching. Failure information could then be telemetered but telemetry would not be a series element in SCS success probability. The disadvantage is the additional requirements on DCU capabilities. Time sharing might help here since continuous monitoring probably is not necessary.

4. **Sun sensors.** Two separate coarse acquisition Sun sensor mechanizations were studied to provide acquisition without gimbals or complicated search maneuvers and accurate positioning of the vehicle along the sun line. This was done since the requirements necessitating large acquisition field of view, high accuracy about null, and long operating time in a hostile space environment are conflicting requirements.

The acquisition sun sensor described represents the simplest practical configuration resulting in acquisition signals over 4π steradians and requires very little tradeoff study due to the absence of stringent accuracy requirements.

The limit cycle sun sensor, however, was the object of more thorough analysis. In anticipation of use of the sun sensor output by the DCU, several digital mechanizations were investigated. Since a digital output is not required, the digital study is only briefly discussed here. Three types of digital mechanization were studied in an effort to determine complexity:

a. Use of a pulse code modulation detector arrangement in which the output is in binary form.

b. Use of a linear detector mosaic in which the output is analog but at discrete levels rather than continuous, and which would require conversion to binary form.

c. Proportional analog output requiring complete analog-to-digital conversion.

Examination showed that all three mechanizations require extremely complex detector configurations or signal processing electronics compared to that required for an analog output.

Two types of analog sensors were studied: One uses a detector bridge and shadow vane configuration similar to that of the sterilized sun sensor proposed for the Voyager lander. The other uses only a single detector, an internally reflecting prism, and vibrating-reed modulator to form proportional error signals. Each of these two types has distinct advantages and disadvantages. The detector bridge configuration is simpler by about a factor of two than the single detector configuration. However, the single detector is considerably more accurate since it is not dependent on critical bridge balancing parameters, notably slight variations in detector drift, and cover glass transmission with time and solar exposure. Since accuracy is a critical guidance requirement, the single detector configuration is recommended. However, as detector state-of-the-art continues to advance, a bridge configuration may become available that will maintain sufficient balance over the time and environment of Voyager. Should this come about, the bridge configuration would be adopted so as to realize a reduced failure rate.

The proposed sun sensor is a part of the extremely accurate Sun tracker to be used on the Advanced Orbiting Solar Observatory. The unit will have been fully developed, qualified, and flown prior to its use in the Voyager program. Ultimate accuracy of the device is much better than required by Voyager, being limited only by the alignment of the sensor to a known vehicle reference.

5. <u>Canopus star tracker.</u> The useful field of view of the Canopus tracker must be approximately ±18 degrees in the pitch plane to provide for apparent Canopus motion since Canopus is not a pole star, and in the roll plane must be sufficiently large to satisfy SCS requirements.

The relatively large pitch field of view can be achieved by either of two following methods: gimballing the optical axis of a small instantaneous field of view; or providing an instantaneous field of view of ± 18 degrees in pitch.

Operation without the use of gimbals is desired to maximize reliability. To achieve the large angular field requires the use of a large detector. The type and size of detector is a complicated function of detector sensitivity, optical parameters, available star light, and scanning techniques. The most likely and currently most popular method to achieve large field and reliable scanning is to utilize image dissector photomultiplier tubes which feature electronic scanning. These tubes have a large sensitive area compared to other types of available detectors which would also require some type of mechanical scanning. The angular field of the tube would be 36 degrees corresponding to a maximum tube sensitive area dimension of 0.6 inch. The current capability of determining star position on the tube face is about ± 0.002 inch resulting in

an angular resolution and accuracy of about ±8 minutes of arc. Assuming that future developments result in improving the capability of determining star position to ± 0.001 inch, the angular uncertainty is still about ± 4 minutes of arc. Further, assuming larger tubes become available with twice the active surface, the angular accuracy could be at best only ±2 arc minutes. This is in agreement with accuracy capabilities predicted by at least one other star tracker supplier for a nongimbaled image dissector tracker with the required field of view. However this accuracy does not satisfy the stringent guidance and navigation requirements for the Voyager mission. Consequently nongimbaled trackers were not further considered as being capable of satisfying both SCS and guidance requirements.

A star tracker utilizing a gimbaled mirror to provide sufficient field to track the apparent Canopus motion in pitch can be mechanized with accuracies approaching 10 seconds of arc. The major problem is satisfying the DCU requirement for a binary output and the SCS requirement for an analog error signal output. This problem was solved by feeding the components of the scan-generated error signal into both digital and analog signal processing electronics.

The digital output required by the DCU prompted the use of a digital rather than analog gimbal loop. A completely digital mechanization does away with the need for any complicated analog-to-digital or digital-to-analog conversion and further benefits are obtained.

A pulsed gimbal readout can be used and is achieved without additional gears or bearings. A collimated light beam is directed through a coded wheel rigidly attached to the mirror gimbal shaft and strikes a solid-state photo detector. A pulse amplifier consisting of only a few transistors and associated components form the remainder of the readout. The failure rates of all components are extremely low with the light source being the least likely to fail. The particular bulb selected has been estimated by the National Bureau of Standards to have a lifetime of one billion years. Prepackaged pulse readouts were discarded because they are generally heavier and less reliable than the method employed.

The digital mechanization lends itself readily to use as a bang-bang servo system with the stepper motor being energized only periodically to make corrections and then making the corrections by a fixed number of steps without the usual "hunting" in analog servo systems. Finally, the electronics available for use in digital mechanizations are more reliable than those available for analog mechanizations.

TABLE 41

SCS MISSION SUCCESS PROBABILITY

	Circuit Technique	System/Mission No. 1	System/Mission No. 2	System/Mission No. 3	System/Mission No. 4
Probability of reaching orbit around Mars	Conventional high reliability circuitry	0.712	0.712	0.782	0.892
	Integrated circuitry*	0.697	0.697	0.785	0.897
Probability of completing the entire mission	Conventional high reliability circuitry	0.417	0.520	0.658	0.803
	Integrated circuitry*	0.415	0.506	0.659	0.806
Comments		● Nonredundant SCS ● System weight = 75 pounds	● Nonredundant SCS ● Pitch and yaw gyros not required in orbit ● No gyro evaluation required in orbit ● System weight = 75 pounds	● Redundant electronics, self-monitoring and switching ● Pitch and yaw gyros not required in orbit ● No gyro evaluation required in orbit ● System weight = 81 pounds	● Redundant electronics, self-monitoring and switching ● Pitch and yaw gyros not required in orbit ● No gyro evaluation required in orbit Simplified Canopus Star Tracker with a passive standby ● System weight = 78 pounds (Star Tracker standby weight of 3 pounds not included)

*Used in computing the SCS weight, volume, and power requirements

6.5 Reliability

The approach selected in this analysis is to present system success probabilities for a number of variations in mission and system configuration. These results are presented in table 41. The over-all SCS functional reliability diagram is shown in figure 120. Failure rate data are shown in tables 42 and 43. A discussion of areas for future consideration for reliability improvement is given in the summary at the end of this section.

1. Mission success probabilities. A summary of mission success probabilities for various mission and system configurations is shown in table 41. The table is followed by paragraphs discussing the data for each entry in the table.

2. System/mission No. 1. The ground rules for this system/mission are as follows: no redundancy; and all gyros, electro-optical sensors, circuits, etc., must operate for the full mission for success. The reliability diagram for this system/mission is shown in figure 121.

For future analyses, a further breakdown of table 41 is shown below, with and without the electro-optical (E-O) sensors (Sun sensors and Canopus star tracker). The success probabilities for these cases are presented in table 42.

TABLE 42

SUCCESS PROBABILITIES

	Circuit Technique	With Electro-Optical Sensors	Without Electro-Optical Sensors
Probability of reaching orbit around Mars	Conventional high reliability circuitry	0.682	0.890
	Integrated circuitry	0.675	0.871
Probability of completing the entire mission	Conventional high reliability circuitry	0.396	0.589
	Integrated circuitry	0.399	0.586

Figure 120 SCS RELIABILITY DIAGRAM

Figure 121 RELIABILITY DIAGRAM OF SYSTEM/MISSION NO. 1

63-9306
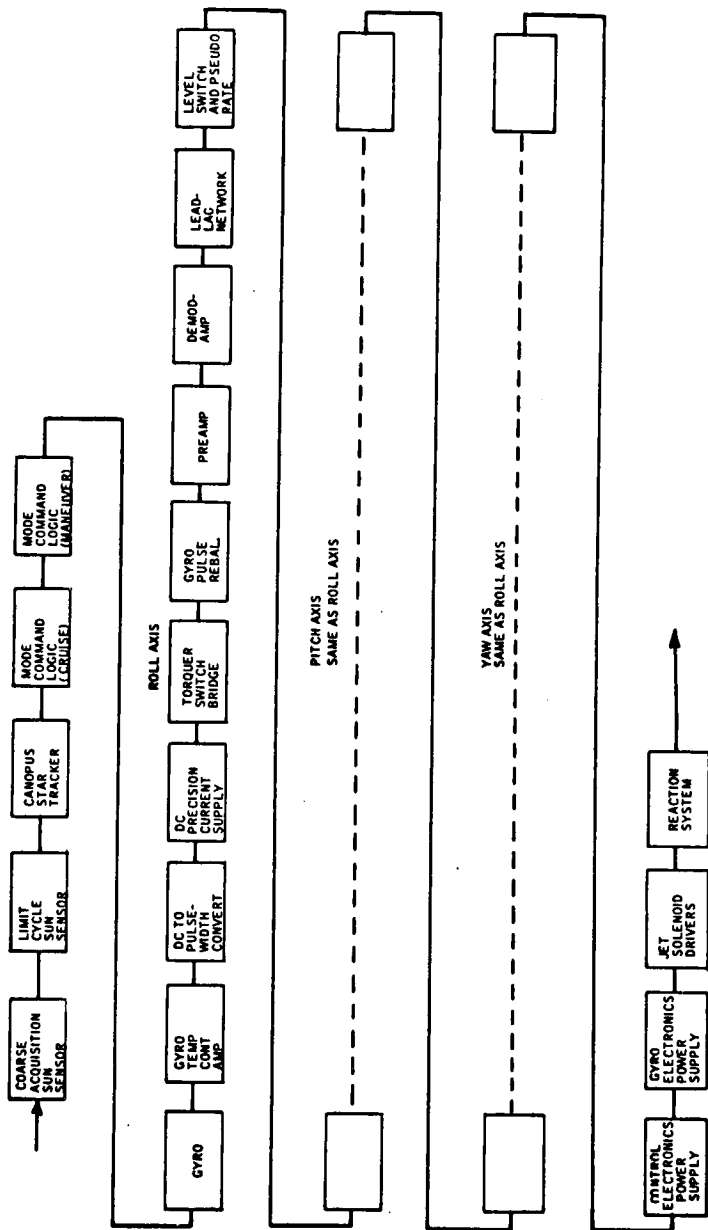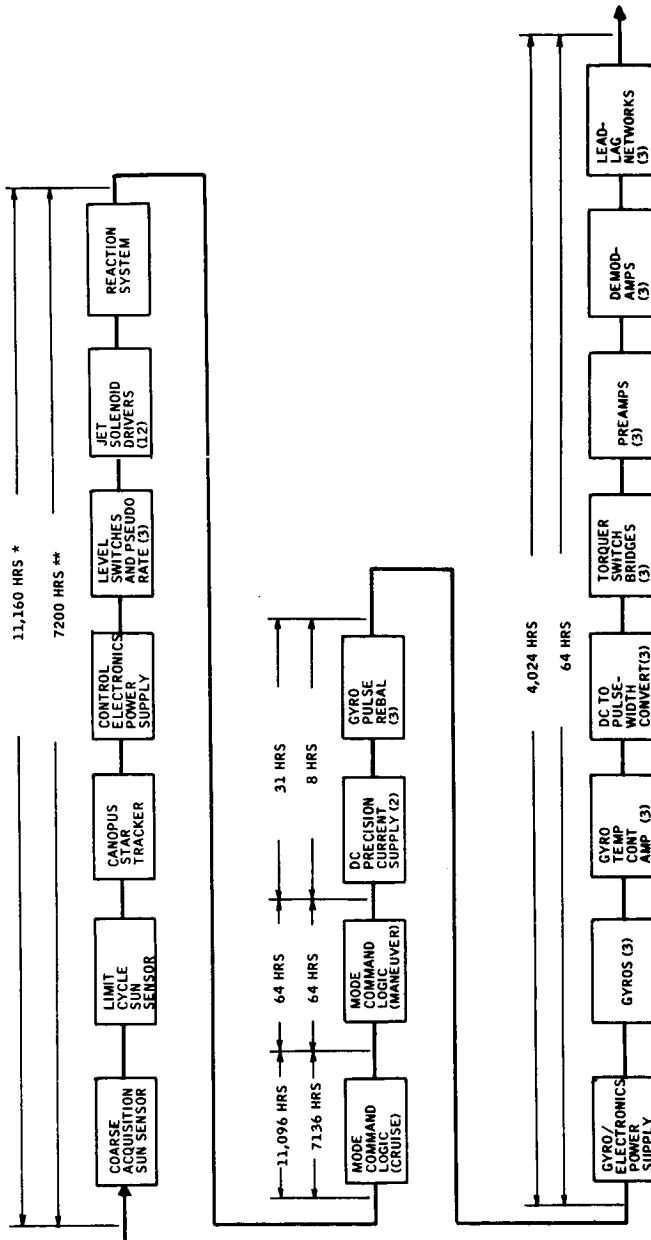
* OPERATING HOURS OF ITEMS FOR TOTAL MISSION SUCCESS (UPPER FIGURES)
** OPERATING HOURS OF ITEMS FOR ACHIEVING MARS ORBIT (LOWER FIGURES)

3. System/mission no. 2. The ground rules for this system/mission are
as follows:

No SCS redundancy.

No gyro evaluation required in orbit. It is assumed that there will be no
requirement for the vehicle to maneuver once in orbit around Mars and there-
fore there is no requirement for the DCU to store gyro drift information. The
small drift of the gyros during occultation will merely cause the vehicle to be
slightly off reference after occultation. With the gyros available as rate sources,
realignment to the Sun and Canopus following occultation should be completely
satisfactory.

The pitch and yaw gyros may fail to zero output in orbit without causing
mission failure. This assumption is based upon the fact that these gyros are
used only for attitude hold during Sun occultation in orbit. The periods of
occultation should not exceed approximately three hours, and, even if some
drift occurs, the sun sensors should be able to reacquire the Sun line within
a reasonable time. Since the rate damping during reacquire would be from
pseudo-rate only, the acquisition will not be as optimum as with gyros, but
should be adequate.

The reliability diagram for this system/mission is shown in figure 122.

For future analysis, a further breakdown of table 41 is shown below with
and without the electro-optical sensors. The success probabilities for these
cases are presented in table 43.

<u>TABLE 43</u>

OTHER SUCCESS PROBABILITIES

	Circuit Technique	With Electro-Optical Sensors	Without Electro-Optical Sensors
Probability of reaching orbit around Mars	Conventional high reliability circuitry	0.682	0.890
	Integrated circuitry	0.675	0.871
Probability of completing the entire mission	Conventional high reliability circuitry	0.493	0.734
	Integrated circuitry	0.487	0.716

```
                              11,600 HRS *
                              7,200 HRS **
```

| COARSE ACQUISITION SUN SENSOR | LIMIT CYCLE SUN SENSOR | CANOPUS STAR TRACKER | CONTROL ELECTRONICS POWER SUPPLY | LEVEL SWITCHES AND PSEUDO RATE (3) | JET SOLENOID DRIVERS (12) | REACTION SYSTEM |

```
   11,096 HRS      64 HRS              8 HRS          4,024 HRS
   7,136 HRS       64 HRS              8 HRS          64 HRS
```

| MODE COMMAND LOGIC (CRUISE) | MODE COMMAND LOGIC (MANEUVER) | DC PRECISION CURRENT SUPPLY (3) | GYRO PULSE REBAL (3) | GYRO/ ELECTRONICS POWER SUPPLY |

```
                              64 HRS
                              64 HRS
```

| GYRO TEMP CONTROL AMPS (3) | GYROS (3) | DC TO PULSE-WIDTH CONVERTER (3) | TORQUER SWITCH BRIDGES (3) | PREAMPS (3) | DEMOD-AMPS (3) | LEAD-LAG NETWORKS (3) |

```
                              3960 HRS
                              NOT USED
```

| ROLL GYRO TEMP CONTROL AMP | ROLL GYRO | ROLL DC TO PULSE-WIDTH CONVERTER | ROLL TORQUER SWITCH BRIDGES | ROLL PREAMP. | ROLL DEMOD-AMP. | ROLL LEAD-LAG NETWORK |

* OPERATING HOURS OF ITEMS FOR TOTAL MISSION SUCCESS (UPPER FIGURES)
** OPERATING HOURS OF ITEMS FOR ACHIEVING MARS ORBIT (LOWER FIGURES)

63-9307

Figure 122 RELIABILITY DIAGRAM OF SYSTEM/MISSION NO. 2

-339-

4. <u>System/mission no. 3</u> -- The ground rules for this system/mission are as follows:

Redundant electronics, self-monitoring and switching. Specifically the items which are paralleled with a passive standby are:

Control electronics package power supply

On-off level switch and pseudo rate in each axis

Gyros in each axis

Gyros temperature control amplifiers in each axis

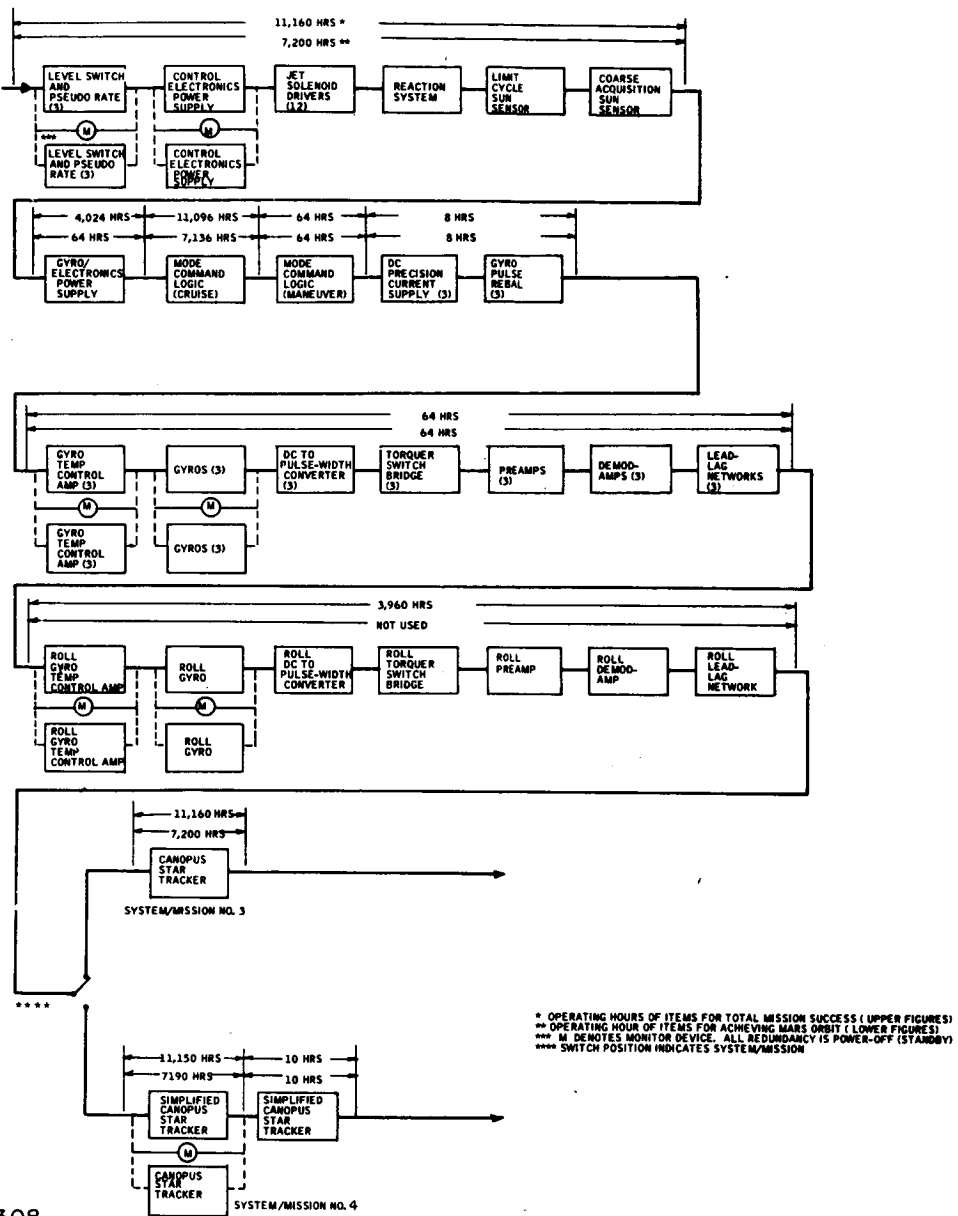No gyro evaluation required in orbit. Refer to system/mission no. 2 for discussion.

Pitch and yaw gyros may fail to zero output in orbit without causing mission failure. Refer to system/mission no. 2 for discussion.

The reliability diagram for this system/mission is shown in figure 123. For future analysis, a further breakdown of table 41 is shown below with and without the electro-optical sensors. The success probabilities for these cases are presented in table 44.

TABLE 44

SUCCESS PROBABILITIES (ELECTRO/OPTICAL)

	Circuit Technique	With Electro-Optical Sensors	Without Electro-Optical Sensors
Probability of reaching orbit around Mars	Conventional high reliability Circuitry	0.748	0.977
	Integrated Circuitry	0.760	0.982
Probability of completing the entire mission	Conventional high reliability Circuitry	0.624	0.929
	Integrated Circuitry	0.635	0.932

63-9308

Figure 123 RELIABILITY DIAGRAM OF SYSTEM/MISSIONS NOS. 3 AND 4

5. **System/mission no. 4.** -- The ground rules for this system/mission are as follows:

Redundant electronics, refer to system/mission no. 3.

No gyro evaluation required in orbit, refer to system/mission no. 2.

Pitch and yaw gyros may fail to zero output in orbit without causing mission failure, refer to system/mission no. 2.

Assume that two Canopus star trackers are employed, one a relatively simple analog device (with no gimbaling) for SCS use, and the other a more complex star tracker (as now used in the detailed system of this document for both guidance and control) would be used for guidance only. Since the guidance system requires the Canopus tracker for only a few hours during the entire mission for navigation sighting, it would be available at all other times as a passive backup unit to the SCS Canopus tracker. The SCS Canopus tracker would be used throughout the entire mission under these ground rules. This simplified SCS Canopus tracker is discussed briefly below.

The Canopus star tracker described in this document as a component of the SCS is a dual-purpose device which was designed to satisfy both guidance and control requirements. Consequently, it is more complex than a device designed to satisfy only the control requirements. A simpler, smaller, less accurate Canopus tracker could be designed which would satisfy SCS requirements and enhance reliability. The more accurate and complex Canopus tracker would be retained for guidance use and could be used as the SCS tracker backup.

The simplified SCS Canopus tracker would utilize an image dissector photomultiplier tube as a detector and short focal length optics to provide a large total field of view so that gimbals are not required. A large circular scanning aperture would be driven in a star-shaped scan pattern across the tube face to produce a pulse train output with the phase and pulse width containing the Canopus image information. This output would be filtered and synchronously demodulated to provide a dc roll error signal to the SCS. A presence signal would also be available indicating that Canopus is within the tube sensitive area.

The tube size and optics focal length would result in a total field of view of ± 18 degrees, sufficient to accommodate the apparent Canopus motion throughout the mission and small vehicle motions in both pitch and roll. The accuracy of determining star position on the tube face near null would be about ± 0.002 inch resulting in an angular accuracy near null of about ± 0.1 degree. The accuracy away from null would degrade to about ± 0.5 degree due to decreasing resolution of tube and optics near the edge of the field of view. Since the vehicle will be operating near the roll null position in limit cycle operation, roll accuracy should remain better than ± 0.2 degree during the mission.

SCS simplified Canopus Tracker characteristics:

Size   -   100 inch^3

Weight   -   3.5 pounds

Power   -   5 watts

Reliability - λ = 0.869 percent/1000 hours for high-reliability
                components

The reliability diagram for system/mission no. 4 is essentially identical to that of system/mission no. 3 except that the Canopus star tracker area would differ as discussed above. Since system no. 3 and no. 4 are identical except for star trackers, the probabilities of success without electro-optical sensors are the same and no breakdown in shown here.

6.   Reliability and redundancy analysis techniques.   The failure rates used in making SCS reliability analyses (tables 45 and 46) are those presently in use by Honeywell for the Apollo command module SCS project. These failure rates have been accepted by North American Aviation's Space and Information Systems Division and NASA. (Some modifications to these failure rates are presently being negotiated with North American Aviation and NASA in order to update them.)

The failure rate assigned to the proposed analog microelectronics integrated circuits (0.05 percent/1000 hours/circuit) was based on the current reliability growth of the semiconductor industry. It is felt that this projected failure rate (0.05 percent/1000 hours/circuit) is conservative and will be achievable by 1967 because of the following:

Texas Instruments has projected a failure rate of 0.01 percent/ 1000 hours in 1963 for digital microelectronics circuits. (1962 Texas Instruments Inc. Reliability Report - 1st quarter.)

Fairchild Semiconductor has demonstrated a failure rate of 0.028 percent/1000 hours at the 60 percent confidence level for their micrologic devices at the present time. (Micrologic Reliability Report - March 1963 - Fairchild Semiconductor.) Integrated circuits are relatively new and the reliability growth will probably be more rapid than that of the conventional parts because of increased awareness of and desire for high reliabilities, which was not present in the development of many of today's conventional components.

Active or power-on redundancy techniques were used only in the reaction jet subsystem. The pressure tank was made redundant (by use of two tanks) to ensure a supply of gas in the event a micrometeorite penetrated one tank. The jets were considered to be actively redundant due to the torque coupling arrangement that exists in the jets.

TABLE 45

SCS SUBASSEMBLY RELIABILITY*

Item	Failure Rate with Standard High Reliability Techniques	Failure Rate with Integrated Circuitry Techniques
Gyro (GG159)	2.0000	2.0000
Reaction system**	0.9997	0.9997
Canopus star tracker	1.5670	1.5670
Coarse acquisition sun sensor	0.4166	0.4166
Limit cycle sun sensor	0.7518	0.7518
Power supply, gyro electronics package	0.5754	0.5958
Power supply, control electronics package	0.5070	0.4362
Gyro temperature control amplifier	0.4974	0.1624
Mode command logic (cruise phase)	0.2720	0.2000
Mode command logic (maneuvering phase)	0.4280	0.0500
Preamplifier	0.0506	0.1024
Demodulator-amplifier	0.1152	0.1024
Pulse rebalance circuitry	0.7352	0.6640
DC to pulse-width converter	0.0626	0.0500
DC precision current supply	0.0740	0.0500
Torquer switch bridge	0.0316	0.0500
ON-OFF level switch and pseudo rate	0.2460	0.4002
Active lead-lag network	0.0122	0.0500
Jet solenoid driver**	0.9999	0.9999
Failure monitor	0.1286	0.1100

*Expressed as failure rate in percent per thousand hours.
**These items required a separate analysis due to inherent redundancy; therefore, only total mission reliability is shown.

TABLE 46

SCS INDIVIDUAL COMPONENT RELIABILITY*

Item	Failure Rate
Analog microcircuitry block	0.05
Resistor, metal film	0.006
Transistor, medium-signal	0.007
Diodes, general purpose	0.0022
Diodes, zener	0.02
Capacitors	0.0052
Coils	0.01
Transformers, signal	0.05
Transformers, power	0.10
Temperature sensor	0.33
Gyro heater	0.07
Gyro (MIG, gas bearing)	2.00
Tanks, pressure	0.013
Valve, check	0.50
Regulator, pressure	0.001
Jet solenoid and valve	0.301

* Expressed as failure rates in percent per 1000 hours.

Standby or power-off redundancy techniques were used in place of active redundancy techniques in the rest of the system where a need for redundancy was indicated or desirable because of increased reliability over active techniques and, in some cases, ease of design.

A second Canopus tracker which is not gimballed, but rather has a large field-of-view, may be used as an SCS roll reference. The elimination of gimbals would increase the trackers's reliability, and hence overall SCS reliability. The first (gimballed) Canopus tracker would then only be required for navigation sightings, and could serve as a back-up to the fixed-gimbal SCS Canopus tracker to further increase reliability.

Summary

It is obvious that for a mission of this duration and the pyramided complexity of ground equipment, launch equipment, boosters, vehicle subsystems, DSIF, etc., that reliability of each subsystem may well be the overriding design criterion. For these reasons, the approach of presenting mission system variations to show reliability improvement was selected. A reasonable amount of data has been presented to serve as a present design base and to show trends for future improvement. Other possibilities, not detailed here but subject for consideration, are:

Consider digital computer unit monitoring and switch-in of standby components in case of failures.

Consider telemetry of performance and failure data to Earth for analysis and switch-in of standby components by DSIF command. This was not explored in this study since telemetry considerations were unknown.

Consider mission phases where degraded accuracy or even sensor shutdown could be tolerated and analyze the system design accordingly.

Consider use of the auxiliary star tracker of the guidance system as the attitude reference in roll during Canopus occultation while in orbit about Mars rather than the roll gyro. This approach could discard the roll gyro completely in orbit or use the auxiliary star tracker as a backup in case of gyro failure.

This approach involves considerations of the geometry of the star used by the auxiliary star tracker and the complexity of resolving the various coordinate systems involved to determine if an over-all reliability gain could be achieved.

It may be desirable to hold a particular plane of the spacecraft in the spacecraft-ecliptic axis plane throughout the mission to simplify communication antenna pointing actuators. If this is the case and if somewhat

lower accuracy than present can be accepted, a simplified SCS Canopus tracker as described in system/mission no. 4 could be considered which would have a wide enough field-of-view to accommodate the apparent motion of Canopus while this orientation is maintained. This approach would enhance both SCS and communications system reliabilities if the attainable accuracies are acceptable.

REFERENCES

1. J. Amer. Phil. Soc., vol. 82, 339, 1940.

2. Glaser, R. R.: Let's Look at Venus. Microwaves, vol. 41, pp. 26-31, January 1963.

3. Chandra and Srivastava: Zeitschrift Fur Astrophysik, vol. 47, p. 127, 1959.

4. Jaffes and Rechtin: IRE trans, IT, p. 66, March 1955.

5. Frazier and Page: IRE Trans SET, p. 210, September 1962.

6. Viterbi: MRI Symp. on Active Networks and Feedback Systems (Book). p. 582, 1960.

7. Jaffe, R. and E. Rechtin: Design and Performance of Phase-Lock Circuits Capable of Near Optimum Performance over a Wide Range of Input Signal and Noise Levels. IRE Trans. on Information Theory, p. 66, March 1955.

8. James, H., et al: Theory of Servomechanisms. McGraw-Hill Radiation Laboratory Series.

9. Martin, B. D.: Threshold Improvement in an FM Subcarrier System. IRE Trans. on Space Electronics and Telemetry, March 1960.

10. Viterbi: JPL Tech. Report 32-527.

11. Weaver: IRE Trans. Set, p. 60, September 1961.

12. Viterbi: On Coded Phase-Coherent Communications. IRE Trans., p. 9, figure 8, for word error probability 5×10^{-3}.

13. Jaffee: Digilock Telemetry System. IRE Trans. Set, p. 48, figure 6, March 1962.

14. Mathison, R. P.: Jet Propulsion Laboratory, Tech. Report No. 32-284, 1 August 1962.

15. Jet Propulsion Laboratory, Space Programs Summary. No. 37-14, vol. 1, p. 75, 1 April 1962.

16. Baumert, I., et al: Coding Theory and Its Applications to Communications Systems. Jet Propulsion Laboratory, Tech. Report No. 32-67, 31 March 1961.

17. Jet Propulsion Laboratory, Technical Report 32-353.

18. Papas, C.H., and R. King: Radiation from Wide-Angle Conical Antennas Fed by a Coaxial Line. Proc. IRE, vol. 39, p. 1269, November 1949.

19. Kelleher, K.S.: Antenna Engineering Handbook. McGraw-Hill Book Company, Inc., 1st edition, pp. 12-6, 1961.

20. Silver, S.: Microwave Antenna Theory and Design. McGraw-Hill Book Company, Inc., N.Y., pp. 254, 1949.

21. Barber, T.A.: Voyager Satellite Orbit Determination Accuracy Using Earth-Based Doppler Radar-Part I: Classical Orbital Element and Position Accuracies. Technical Memorandum 312-306.

22. Barber, T.A.: Voyager Satellite Orbit Determination Accuracy Using Earth-Based Doppler Radar - Part II - Inertial Position and Velocity Accuracies, Technical Memorandum 312-312.

23. Wallace, Jr., R.R., V.R. Vinson, M. Kornhauser: Effects of Hypervelocity Particles on Shielded Structures. Paper presented at ARS Lifting Reentry Vehicles, Structures, Materials, and Design Conference, Palm Springs, Calif., 4 to 6 April 1961.

24. Nysmith, C.R. and J.L. Summers: Preliminary Investigations of Impact on Multiple-Sheet Structures and an Evaluation of the Meteoroid Hazard to Space Vehicles. NASA TN D-1039.

25. Pepitone, S.J. and B.W. Reynolds: Meteoroid Protection Systems for Space Vehicles. Paper presented at AIAA Launch and Space Vehicles Shell Structures Conference, Palm Springs, Calif., 1 to 3 April 1963.

26. Whipple, F.L.: On Meteroids and Penetration. Paper presented at the Ninth Annual American Astronautical Society Meeting, Los Angeles, Calif., 15 to 17 January 1963.

27. Space Materials Handbook. Lockheed Missiles and Space Co., C. G. Goetzel and J.B. Singletary, Eds., ASTIA AD284547.

28. Adanczack, R.L., R.J. Benzing, and H. Schwenker: Lubrication in Space Environments. ASD-TDR-62-541, June 1962.

29. Gaumer, R. E., and L. A. McKellar: Thermal Radiative Control Surfaces for Spacecraft. Lockheed Missiles and Space Division, TR No. LMSD-704014, ASTIA AD264127, 1 March 1961.

30. Goetzel, C. G. and J. B. Singletary: Space Materials Handbook. Lockheed Missiles and Space Division, ASTIA AD284547, January 1962.

31. Van Vliet, R. M.: Coatings for the Aerospace Environment. WADD TR 60-773, ASTIA AD267310, July 1961.

32. Jaffe, L. D.: Effects of Space Environment upon Plastics and Elastomers. from Applications of Plastic Materials in Aerospace, Chemical Engineering Progress Symposium, series 40, vol. 59, 1963.

33. Schmitt, R. G. and R. C. Hirt: Studies on the Protective Ultraviolet Absorbers in a High-Vacuum Environment II. WADD TR 60-704, February 1961.

34. Pigmented Surface Coatings for Use in the Space Environment. ASD-TDR-62-840, Part 1, January 1963.

35. Bovey, F. A.: Effects of Ionizing Radiation on Natural and Synthetic High Polymers. Interscience Publishers, New York, 1958.

35a. Reliability Stress and Failure Rate Data for Electronic Equipment. MIL HOBK-217, 8 August 1962.

35b. Fick, J.: Thermal Analyzer Network. LMSC.

35c. Bowe, J.: Envelopes and Lines of Constant Mach Number for Axially Symmetric Free Jet. Convair Astro. Rep. 25-7-054.

36. Laszlo, T. S., and R. E. Gannon: The Effect of Micrometeorite Impact on the Optical Properties of Metals. Being presented at the 6th National Symposium (SAMPE), Materials for Space Vehicle Use, Seattle, Wash., Nov. 18 to 20, 1963.

37. Whipple, F. L.: On Meteoroids and Penetration. AAS paper presented at Interplanetary Missions Conference, 9th Annual AAS Meeting, January 1963.

38. Dalton, C. C.: Meteoroid Hazard to Space Vehicles in Orbit Near the Earth - A Functional Interpretation of the Information for Design and Operations Decisions. NASA, TM X-789, December 1962.

39. Loeffler, Lieblein, and Clough: Meteoroid Protection for Space Radiators. ARS Paper No. 2543-62, ARS Space Power Systems Conference, 25 to 28 September, 1962.

40. Summers, J. L., Investigation of High-Speed Impact: Regions of Impact At Oblique Angles, NASA TN D-94, October 1959.

41. Hermann and Jones: Survey of Hypervelocity Impact Information. A. S. R. L. Report No. 99-1 (MIT), September 1961.

42. Esgar, J. B.: Fuel Tanks for Spacecraft: The Difficulties. Mech. Eng., 85, No. 4, pp. 44-47. April 1963.

43. Pipitone and Reynolds: Meteoroid Protection System for Space Vehicles. AIAA paper No. 2895-63 April 1963.